Energy Efficiency in Buildings

Estimating and decoupling the Heat Loss Coefficient of in-use buildings into its Transmission (UA) and Infiltration and/or Ventilation (C_V) heat loss coefficients through basic monitoring and modelling

University of the Basque Country

2021

Irati Uriarte Perez de Nanclares

Supervisors: Dr. Aitor Erkoreka Gonzalez - Dr. Koldobika Martín Escudero

Irati Uriarte Perez de Nanclares

DOCTORAL PROGRAM

Energy efficiency and sustainability in engineering and architecture

DOCTORAL THESIS

Estimating and decoupling the Heat Loss Coefficient of in-use buildings into its Transmission (UA) and Infiltration and/or Ventilation (C_v) heat loss coefficients through basic monitoring and modelling

DIRECTED BY

Dr. Aitor Erkoreka Gonzalez

Dr. Koldobika Martin Escudero

Acknowledgements (in Basque)

Lerro hauen bidez nire esker ona adierazi nahiko nieke proiektu hau aurrera eramaten lagundu didaten pertsona guztiei.

Lehenik eta behin, Aitor Erkoreka eta Koldo Martin, tesi honen zuzendari eta zuzendari ordea eskertu nahiko nituzke, haien laguntza eta konfiantzagatik. Tesi honen garapenerako haien eskarmentua eta orientazioa ezinbestekoa izan baita.

Danimarkan egondako bi egonaldietan jaso dudan laguntza ere aditzera eraman nahi dut. Bi egonaldiak Technical University of Denmarken (DTU) izan dira Pr. Henrik Madsenen gainbegirapean. Hori dela eta, Henrik Madsen eta bere lan taldeari eskerrak eman nahiko nizkieke, nire ezagutzaren garapenaren parte izateagatik.

IEA-EBC "Annex 71- Building energy performance assessment based on in-situ measurements" aditu bilerako kide guztiak eskertu behar ditut bertan parte hartzeko eta haien datuen analisia egiteko aukera bermatzeagatik. Bereziki, bertako partaide diren Dynastee taldeko kideak aipatu nahiko nituzke, "Summer School- Dynamic Calculation Methods for Building Energy Performance Assessment" udako kurtsoetako lan taldean onartzeagatik eta niregan jarri duten konfiantza guztiagatik.

Maria Jose Jimenezi, erraztu dizkidan datu guztiengatik eta eskaini didan dedikazio guztiagatik. Baita Vigoko Unibertsitateko Pablo Eguia eta Enrique Granada, elkarrekin egindako kolaborazio guztiengatik.

Ezin ahaztu Bilboko unibertsitateko lagun eta tesiko lankide guztiak: Ana, Naiara, Erik, Catalina eta Nikko, bulegoko eta kanpoko momentu ahaztezinengatik. Hauetaz aparte departamentuko gainontzeko lankideak kafe eta bazkalorduetako solasaldiengatik. Aipatu beharrean nago Danimarkako egonaldietan ondoan izandako lagunak; Eder, Henning eta Marijana.

Azkenik, nire familia osoari eskerrik beroenak eman nahiko nizkieke. Batez ere ama, aita eta Olatz, zuei esker honaino iritsi naizelako. Nire bikoteari, animo eta laguntza izateagatik momentu oro. Kuadrillako eta Zumaiako lagunak beti hor egoteagatik.

Eskerrak ere Eusko Jaurlaritzari Tesia aurrera eramateko emandako laguntza ekonomikoagatik (PRE_2017_1_0122 beka).

Abstract

There still exists a considerable difference when comparing the design energy consumption in buildings with the real consumption. The actual building energy performance essentially depends on the building occupant's behaviour, the real performance of the installed energy systems and the in-use performance of the building envelope. The thermal performance characterization of in-use building envelopes, based on monitored data, represents a crucial step towards bridging the gap between the designed and as-built energy performance of buildings. The main performance indicator to analyse the performance gap of building envelopes is the Heat Loss Coefficient (HLC); when measured, it commonly shows considerable differences when compared to the design value. Therefore, this research goes further and proposes a method, based on monitored data from in-use buildings, for the estimation and decoupling of the HLC of in-use buildings into its transmission (UA) and infiltration and/or ventilation (C_v) heat loss coefficients, in order to identify the origin of the heat losses. Achieving this will facilitate our understanding of the performance gap.

Although there exists a wide range of methods to estimate the HLC in in-use buildings, they are still far from being considered a general method. Therefore, this work further develops an existing 'average method' by fully developing it from the energy conservation principle applied to a generic in-use building. Furthermore, the uncertainty sources are identified and limited through the mathematical development of the method. An innovative solution to the problem of multizone buildings is also demonstrated, where HLC values should be calculated for different floors and then aggregated to obtain the entire building's HLC. Furthermore, all these can be done without the need for a detailed model of the building. The method's applicability is tested in three different case studies: A simple test box, two in-use residential buildings showing completely different characteristics, and a rehabilitated four-storey occupied office building. All these case studies have been widely monitored.

However, despite the fact that the developed average method to estimate the HLC value in in-use buildings considers the effect of solar gains entering through the windows, the solar gains through the opaque walls are completely ignored . However, for some HLC estimation methods, disregarding the solar gains through the opaque walls can lead to an

underestimation of the estimated HLC value. Therefore, in order to demonstrate that this effect is negligible in the developed average method, a detailed analysis of the effect of solar radiation on the inner surface heat flux of opaque elements has been performed. Therefore, a fully monitored simple test box is used for this analysis, due to its extensive solar radiation and inner surface heat flux data measured for each wall of the test box. Different resistance-capacitance models are fitted for each opaque wall of the test box in different periods. Then, the results are validated with the measured data and the known thermal characteristics. Thus, the solar radiation is removed from the models and the hypothetical inner surface heat flux is estimated without it. Therefore, the weight the solar radiation has on the inner surface heat flux is mathematically quantified. This effect is later transmitted to the HLC estimation in methods where the solar gains through opaque walls are not considered, such as the average method developed before.

Having tested and demonstrated the fact that the developed average method is able to estimate reliable HLC values of in-use buildings, it is possible to carry out the last step of the work: the decoupling process. Therefore, only the multi-storey occupied office building data has been used, since it is the only case study providing the necessary air quality data for this analysis. The in-use HLC values for each floor, and for the whole building, have already been estimated using the average method in the first part of this Thesis. Then, based on the ASTM D6245-18 Standard, the decay method of the metabolic CO_2 of the building´s occupants has been applied in this work to obtain the Air Change per Hour (ACH_{decay}) rates. These ACH_{decay} values have been used to decouple the estimated HLC values into their transmission and infiltration and/or ventilation parts. Then, as commented before, the origin of the heat losses is identified and this facilitates our understanding of the performance gap and possible future optimal retrofitting solutions.

List of contents

Abbreviations

ABBREVIATION	DESCRIPTION	UNIT
A_W	Inner surface area of each wall of the Round Robin Box	m^2
A_1	Aperture of the wall for the inner surface heat flux	-
α or A_5	Solar absorptivity of the corresponding wall	-
ACH	Air Changes per Hour, or air change renovation rate of the considered volume	h^{-1}
$ACH_{building}$	The Air Change per Hour of the whole building	h^{-1} or s^{-1}
ACH_{decay}	The Air Change per Hour estimated using the CO_2 tracer gas decay method of the considered volume	h^{-1}
$ACH_{Fi,j}$	The corresponding Air Change per Hour of the i^{th} zone of the j^{th} floor	h^{-1} or s^{-1}
ACH_{Fi,j_decay}	The corresponding Air Change per Hour estimated using the CO_2 tracer gas decay method of the i^{th} zone of the j^{th} floor	h^{-1} or s^{-1}
ACH_{decay_aver}	The entire floor average Air Change per Hour estimated using the CO_2 tracer gas decay method for the whole considered testing period	h^{-1}
$ACH_{decay\_aver\_Vi}$	The average Air Change per Hour estimated using the CO_2 tracer gas decay method of the whole considered testing period associated with each 'i' volume portion of F0 and F2, respectively	h^{-1}
ACH_{decay_Vi}	The daily Air Change per Hour estimated using the CO_2 tracer gas decay method of the whole considered testing period associated with each of the 'i' volume portions of F0 and F2, respectively	h^{-1}
AQ	Air quality of the building	ppm CO_2
$ARMAX$	Autoregressive-moving-average models	-
ARX	Autoregressive with exogenous terms model	-
B	Parameter used in order to estimate the equation of time, depending on the day of the year	°
β	The corresponding slope of the wall, the angle between the plane surface and the horizontal	°
C	Effective heat capacity	MJ/m^2K or MJ/K
C_F	Final indoor to outdoor concentration difference	ppm, $\frac{mol_{CO2}}{mol_{air}}$, $\frac{m^3_{CO2}}{m^3_{air}}$
$C_{F\,building}$	Final indoor to outdoor concentration difference for the whole building	ppm, $\frac{mol_{CO2}}{mol_{air}}$, $\frac{m^3_{CO2}}{m^3_{air}}$
$C_{F\,Fi,j}$	Final indoor to outdoor concentration difference of the i^{th} zone of the j^{th} floor	ppm, $\frac{mol_{CO2}}{mol_{air}}$, $\frac{m^3_{CO2}}{m^3_{air}}$
c_i	Specific heat of the i^{th} incompressible material	kJ/kgK
C_I	Initial indoor to outdoor concentration difference	ppm, $\frac{mol_{CO2}}{mol_{air}}$, $\frac{m^3_{CO2}}{m^3_{air}}$
$C_{I\,building}$	Initial indoor to outdoor concentration difference for the whole building	ppm, $\frac{mol_{CO2}}{mol_{air}}$, $\frac{m^3_{CO2}}{m^3_{air}}$
$C_{I\,Fi,j}$	Initial indoor to outdoor concentration difference of the i^{th} zone of the j^{th} floor	ppm, $\frac{mol_{CO2}}{mol_{air}}$, $\frac{m^3_{CO2}}{m^3_{air}}$
CO_2	Carbon dioxide	-
CO_{2aver_Fn}	Carbon dioxide concentration in each floor of the analysed building	ppm
cp_{air}	Constant pressure specific heat of the air at the average indoor temperature	kJ/kgK
C_v	Infiltration and/or ventilation heat loss coefficient	kW/K or W/K

ABBREVIATION	DESCRIPTION	UNIT
C_{v_aver}	The entire floor average infiltration and/or ventilation heat loss coefficient for the whole considered testing period	kW/K
$C_{v\ Fi,j\text{-}out}$	Considers the envelope infiltration and/or ventilation heat loss coefficient going from the i^{th} zone of the j^{th} floor to the exterior	kW/K
$C_{v\text{-}inf}$	Infiltration heat loss coefficient	kW/K or W/K
$C_{v\text{-}vent}$	Ventilation heat loss coefficient	kW/K or W/K
c_w	Specific heat of the water at the average flow and return temperatures	kJ/kgK
δ *(Solar declination angle)*	The angular position of the sun at solar noon with respect of the equator plane	°
ΔT	Temperature difference between the T_{in} and the T_{out}	K
Δt	Time frequency at which each discrete measurement is done	h
ΔR	The difference between long-wave radiation incidence on surface from sky and surroundings and radiation emitted by a blackbody at outdoor air temperature	W/m²
DHW	Domestic hot water	m³
D_{sol} *(Diffuse solar radiation)*	The global solar radiation part that enters the Earth's surface and is altered and disturbed	W/m²
E	The equation of time	minutes
E_{cv}	Total energy of the system	kJ
ε	The corresponding emissivity of the wall	-
E_{sol}	Vertical east global solar radiation	W/m²
η	Efficiency of the recovery system installed in the ventilation system	-
Fi,j	The i^{th} zone of the j^{th} floor in a building	-
Fn	Corresponding floor of the analysed building (F0 (ground floor), F1 (first floor), F2 (second floor) and F3 (third floor))	-
g	Gravity	m/s²
g-value or solar factor	Percentage of solar radiation incidence on a window or façade that is transmitted to the interior of the building	-
γ	Surface azimuth angle, the angle between the normal to the surface and the local longitude meridian	°
G_{gr_1}	Ground reflected solar radiation	W/m²
GMT timeframe	Greenwich Mean Time (Longitude 0° 0' 0")	-
G_{sol}	Global solar radiation	W/m²
H	Thermal conductance of the corresponding wall layer. If there is more than one layer in the wall, H is presented as the thermal conductance between two nodes. Then, it is called $H_{n\text{-}1\ -\ n}$	W/m²K
h	Enthalpy of the fluid in the inlet (subscript 'i') or in the exit (subscript 'e') of the system	kJ/kg
h_{ae}	Enthalpy of the returned air from the Control Volume	kJ/kg
h_{ai}	Enthalpy of the supplied air to the Control Volume	kJ/kg
h_{comb}	Combined heat transfer coefficient of the air (h_{conv}+ h_{rad})	W/m²K
h_{conv}	Convective heat transfer coefficient of the air	W/m²K
HLC (Heat Loss Coefficient)	Considers the building transmission heat losses through envelope plus ventilation and/or infiltration per degree difference between indoor and outdoor temperatures. HLC = UA + C_v	kW/K or W/K
$HLC_{building}$	Heat Loss Coefficient calculated as a whole unique building	kW/K or W/K
$HLC_{Fi,j}$	Heat Loss Coefficient of the i^{th} zone of the j^{th} floor	kW/K
HLC_{simple}	Heat Loss Coefficient calculated without considering the solar gains	kW/K or W/K
$HLC_{simple\_Fi,j}$	Heat Loss Coefficient without considering the solar gains of the i^{th} zone of the j^{th} floor	kW/K

ABBREVIATION	DESCRIPTION	UNIT
HLC_{sum}	Heat Loss Coefficient calculated as the sum of each individual thermal zone HLC	kW/K or W/K
H_{LW} *(Horizontal long wave radiation)*	Long wave radiation emitted from the sky and the Earth's surface incident in the horizontal plane	W/m^2
h_{rad}	Radiation heat transfer coefficient	W/m^{2}K
H_{sol}	Horizontal global solar radiation	W/m^2
HVAC	Heating, ventilation, and air conditioning technology	-
H_W	The total thermal conductance of the wall surface-to-surface	W/m^{2}K
h_{we}	Enthalpy of the returned water from Control Volume	kJ/kg
h_{wi}	Enthalpy of the supplied water to the Control Volume	kJ/kg
I_{in}	Illuminance of the building	lux
K	All the other heat gains inside the building excluding solar gains (S_aV_{sol}) and all heating system gains (Q). $K = K_{electricity} + K_{occupancy}$.	kW or W
k	Thermal conductivity of the wall's layer material	W/m K
KE	Kinetic energy of the system. The energy of an object owing to its movement.	kJ
$K_{electricity}$	Heat gains inside the building due to electricity consumed within the building envelope	kW or W
$K_{Fi,j}$	All the other heat gains inside the ith zone of the jth floor excluding solar gains (S_aV_{sol}) and all heating system gains (Q)	kW
$K_{lighting}$	Heat gains inside the building due to light consumed within the building envelope	kW or W
$K_{occupancy}$	Heat gains inside the building due to metabolic generation of the occupants	kW or W
KPI	Key Performance Indicator, in this work referring to HLC, S_a (or gA), S_aV_{sol}, UA and C_v.	-
l	Determines the thickness of each of the wall's layers	m
L_{loc}	Longitude in the location	°
LORD	Software for the modelling and calculation of thermal systems. LOgical R–Determination (LORD)	-
L_{st}	*S*tandard meridian for the local time, in this case the reference meridian is Greenwich (Longitude 0° 0' 0")	°
m_i	The different mass types within the building	kg
$\dot{m}$	Mass flow rate of the fluid in the inlet (subscript 'i') or in the exit (subscript 'e') of the system	kg/s
$\dot{m}_{air}$	Air mass flow rate	kg/s
$\dot{m}_{Fi,j-Fi,j}$	Mass flow rate of the air going from the ith zone of the jth floor to other ith zone of the same or a different jth floor	kg/s
$\dot{m}_{Fi,j-out}$	Mass flow rate of the air going from the ith zone of the jth floor to the exterior. In the case the air goes from the exterior to the ith zone of the jth floor, it will be named as $\dot{m}_{out-Fi,j}$	kg/s
$\dot{m}_{water}$	Water mass flow rate within the heating system circuit	kg/s
n	Number of day of the year	-
n_{air}	The total number of moles of air within the whole building	mol
$n_{CO2,F,building}$	The total number of moles of CO_2 within the whole building at the end of the decay analysis period (t = t [s])	mol
$n_{CO2,I,building}$	The total number of moles of CO_2 within the whole building at the beginning of the decay analysis period (t = 0 [s])	mol
PE	Potential energy of the system. There are several types of potential energy. In this work we refer to the gravitational potential energy	kJ
Φ	Latitude of the location, an angle that ranges from the Equator (0°) to the poles (90°)	°

ABBREVIATION	DESCRIPTION	UNIT
ω *(Hour angle)*	The hour angle defines the angular distance between the observer's meridian and the hour circle on which lie some celestial bodies	°
P_{in}	Pressure inside the building	bar
P_{out}	Pressure outside the building	bar
Q *or* $Q_{heating}$	All heating systems' energy inputs inside the building	kW or W
$\dot{q}$	Inner surface heat flux when considering the solar radiation effect	W/m^2
$\dot{q}'$	Hypothetical inner surface heat flux when not considering the solar radiation effect	W/m^2
$\dot{Q}_{cv}$	The heat exchanged through the Control Volume	kW or W
Q_{DHW}	Gas used to heat the Domestic Hot Water	W
$\dot{q}_{dif}$	Inner surface heat flux difference between the heat flux considering the solar radiation and the heat flux without considering the solar radiation	W/m^2
$\bar{q}_{dif}$	Period averaged inner surface heat flux difference between the inner surface heat flux when not considering the solar radiation effect and the inner surface heat flux when considering the solar radiation effect	W/m^2
$Q_{Fi,j}$	All heating systems' energy inputs inside the ith zone of the jth floor	kW
$Q_{infiltration}$	Heat losses of the building due to infiltrations	kW or W
$Q_{inf+vent}$	Sum of $Q_{infiltration}$ and $Q_{ventilation}$	kW or W
$Q_{recovery}$	Heat exchanged between flow and return streams in a ventilation system's heat recovery system	kW or W
Q_{Tot}	Sum of the gas used to heat the Domestic Hot Water and the space heating	W
$Q_{transmission}$	Heat losses of the building due to transmission	kW or W
$Q_{ventilation}$	Heat losses of the building due to ventilation system	kW or W
R	Thermal resistances of the envelope element, in this case R_{comb} ($R_{convenction}$+ $R_{radiation}$) and R_{cond} ($R_{conduction}$)	m^2 K/W
R_b *(Beam radiation ratio)*	Relation between corresponding tilted surface and the horizontal surface	-
RC models	Resistance-capacitance models	-
RH	Relative humidity of the building	%
RMSE (Root Mean Square Error)	A measure of the error between two data sets, the measured data and the model estimated data	-
RN	Rain in the exterior of the building	yes/no
ROLBS	Randomly Ordered Logarithmic Binary Sequence	-
R_{si}	Thermal resistance in the inner surface of the wall	m^{2}K/W
R_T	Total thermal resistance of the wall surface-to-air	m^{2}K/W
R_W	Total thermal resistance of the wall surface-to-surface	m^{2}K/W
ρ_{air}	Density of the air at the building average indoor temperature and pressure	kg/m^3
ρ_{CO2}	Density of the CO_2 at the building average indoor temperature and pressure	kg/m^3
S_a *or gA (solar aperture)*	Equivalent surface of the building that allows the same solar energy as to the whole building to enter	m^2
S_aV_{sol}	Corresponding solar gains of the building	kW or W
$(S_aV_{sol})_{Fi,j}$	Corresponding solar gains of the ith zone of the jth floor	kW
$(S_aV_{sol})_{walls}$	Corresponding solar gains of the building through the opaque envelope elements	kW or W
$(S_aV_{sol})_{windows}$	Corresponding solar gains of the building through the windows	kW or W
SF_6	Sulphur hexafluoride	-
σ	Stefan–Boltzmann constant (5.67×10^{-8})	W/m^{2}K^4
Solar time	The solar time is based on the current motion of the sun	minutes

ABBREVIATION	DESCRIPTION	UNIT
Standard time	A fixed time for places that share approximately the same longitude	minutes
t	Time, any variable with a '(t)' is a time dependant variable	s
t_1	Time period's first hour	h
T_{exh}	Temperature of the exhausted air after crossing the heat recovery system	K or °C
$T_{Fi,j}$	Indoor temperature of the ith zone of the jth floor	K or °C
T_{ground}	Ground temperature	K or °C
θz	The zenith angle, the angle between the zenith and the sun position	°
T_{in}	Indoor air temperature	K or °C
$T_{in\text{-}bed}$	Indoor air temperature in the bedroom	K or °C
T_{in_down}	Indoor air temperature measured in the lowest part of the Round Robin Box (1/3 height of the box)	K or °C
$T_{in\text{-}lounge}$	Indoor air temperature in the lounge	K or °C
T_{in_up}	Indoor air temperature measured in the highest part of the Round Robin Box (2/3 height of the box)	K or °C
t_N	Time period's last hour	h
T_{out}	Outdoor air temperature	K or °C
T_{out_down}	Outdoor air temperature measured below the Round Robin Box	K or °C
T_{out_middle}	Outdoor air temperature measured at the same height of the middle of the Round Robin Box	K or °C
t_p	Duration of the CO_2 concentration decay analysis	h
T_{Sin}	Inner surface temperature	K or °C
T_{sky}	Sky temperature	K or °C
T_{Sout}	Outer surface temperature	K or °C
$T_{Sout,nosolar}$	Hypothetical outer surface temperature without considering solar radiation effect	K or °C
T_{sup}	Temperature of the supply air after crossing the heat recovery system	K or °C
T_{surr}	Surrounding air temperature	K or °C
T_w	Temperature of the water in the inlet (subscript 'i') or in the exit (subscript 'e') of the system	K or °C
U or U-value	Building envelope element transmittance	W/m^{2}K
UA or UA value	Considered building envelope transmission heat loss coefficient	kW/K or W/K
$UA_{Fi,j\text{-}ground}$	Considers the envelope transmission heat loss coefficient going from the ith zone of the jth floor to the ground	kW/K
$UA_{Fi,j\text{-}Fi,j}$	Considers the envelope transmission heat loss coefficient going from the ith zone of the jth floor to other ith zone of the same or a different jth floor	kW/K
$UA_{Fi,j\text{-}out}$	Considers the envelope transmission heat loss coefficient going from the ith zone of the jth floor to the exterior	kW/K
U_{IE}	Internal energy of the system. It considers the energy gains and losses inside the system as a result of the changes that take place in the internal state	kJ
v	Velocity of the fluid in the inlet (subscript 'i') or in the exit (subscript 'e') of the system	m/s
$\dot{V}$ *or* $\dot{V}_{air(total)}$	Volumetric airflow rate	m^3/h
$\dot{V}_{air(exh)}$	Exhausted air volumetric air flow rate after crossing the heat recovery system	m^3/h
$\dot{V}_{air(inf)}$	Infiltration volumetric air flow rate	m^3/h
$\dot{V}_{air(sup)}$	Supply air volumetric air flow rate after crossing the heat recovery system	m^3/h
$\dot{V}_{air(vent)}$	Ventilation volumetric air flow rate	m^3/h

ABBREVIATION	DESCRIPTION	UNIT
$\dot{V}_{building}$	Total volumetric air flow rate of the whole building	m^3/h or m^3/s
$\dot{V}_{Fi,j}$	The volumetric air flow rate of the i^{th} zone of the j^{th} floor	m^3/h or m^3/s
$\dot{V}_{Fi,j\_decay}$	The volumetric air flow rate estimated using the CO_2 tracer gas decay method of the i^{th} zone of the j^{th} floor	m^3/h or m^3/s
$\dot{V}_{Fi,j-Fi,j}$	Volumetric air flow rate going from the i^{th} zone of the j^{th} floor to other i^{th} zone of the same or a different j^{th} floor	m^3/h or m^3/s
$\dot{V}_{Fi,j-out}$	Volumetric air flow rate going from the i^{th} zone of the j^{th} floor to the exterior. In the case the air goes from the exterior to the i^{th} zone of the j^{th} floor, it will be named as $\dot{V}_{out-Fi,j}$	m^3/h or m^3/s
VIP	Vacuum Insulated Panels	-
V_{LW} *(Vertical south long wave radiation)*	Long wave radiation emitted from the sky and the Earth's surface incident on a south vertical plane	W/m^2
V_{n_sol}	Vertical north global solar radiation	W/m^2
$V_{ol\_building}$	The total volume of the building	m^3
$V_{ol\_Fi,j}$	The volume of the i^{th} zone of the j^{th} floor	m^3
V_{ol_floor}	The volume of each floor	m^3
V_{ol_i}	The volume portion of each floor	m^3
V_{sol}	Vertical south global solar radiation	W/m^2
WB	West block	-
$\dot{W}_{cv}$	The work exchanged through the Control Volume	kW or W
$W_{HLC\%}$	The weight in percentage of the effect the solar radiation has on the inner surface heat flux of the building envelope opaque elements with respect to the HLC term	%
WS	Wind speed	m/s
$W_{S_aV_{sol}\%}$	The weight in percentage of the effect the solar radiation has on the inner surface heat flux of the building envelope opaque elements, regarding the solar gains through the semi-transparent elements of the building envelope	%
W_{sol}	Vertical west global solar radiation	W/m^2
z	Elevation of the fluid in the inlet (subscript 'i') or in the exit (subscript 'e') of the system	m

General index of figures

APPENDIX A

APPENDIX B

APPENDIX C

APPENDIX E

APPENDIX F

General index of tables

APPENDIX D

AIM AND STRUCTURE OF THE THESIS

AIM AND STRUCTURE OF THE THESIS

One of the main problems found when working with buildings is that there still exists a considerable performance gap between the real energy consumption and the design energy consumption. This performance gap is a result of several sources affecting the building performance, such as the performance of the systems installed inside the dwelling, the effect of the behaviour of the occupants inside the dwelling, and finally, the building envelope's in-use performance. However, the in-use performance of the building envelope is the key source affecting the performance gap. Through the estimation of a Key Performance Indicator (KPI), such as the Heat Loss Coefficient (HLC), it is possible to perform a proper building envelope energy performance characterization.

Therefore, the main objective of this Thesis is to develop a method that can estimate a reliable HLC value for in-use buildings based on monitored data. This method must consider all the uncertainty sources affecting the in-use HLC value and analyse their effect in detail. Once this HLC has been accurately estimated, it will then be possible to carry out the decoupling of the in-use HLC value into the transmission heat loss coefficient through the envelope (UA [kW/K]) and the ventilation and/or infiltration heat loss coefficient (C_v [kW/K]). Once both coefficients are known, it will be possible to analyse them separately and study which of them is the most significant in the in-use building's energy performance. Thus, the real origin of the heat losses can be identified and the performance gap of the in-use building can be understood.

In order to develop this Thesis, several objectives have been fixed during the analysis:

- To mathematically develop a measured data-based average method, following the energy conservation principle applied to a generic in-use building. There, the identification and limitation of the uncertainty sources of the method will be justified so as to obtain reliable HLC values for in-use buildings.
- To demonstrate a solution for the doubtful multizone building problem. It will be proven that it is possible to estimate the total in-use HLC of the whole building by estimating the HLC of each floor and adding them all, even if they have different indoor air temperatures.

- To estimate the uncertainty created by the sensors in the HLC value by an error propagation method, since the rest of the errors have already been considered when limiting the uncertainty sources.
- To test the robustness of the developed average method by testing it in different types of widely monitored "buildings". First, the method is applied to a simple test box named the Round Robin Box. Having tested the simplest case, it is then tested in two completely different in-use residential buildings; the first being a well-insulated dwelling and the second, a poorly-insulated residential building. Finally, it will be applied to a four storey occupied office building, before and after being retrofitted.
- To analyse in detail the effect of the solar gains, one of the main uncertainty sources, on the in-use HLC value. The developed average method used to estimate the HLC value of in-use buildings only considers the effect of the solar gains entering through the windows of the building. However, the effect that solar gains through opaque walls have on the HLC estimated with different methods, such as the average method, where the solar gains through opaque walls are not considered, is also studied. Thus, it is possible to determine if their effect is negligible or not when estimating the HLC value using the developed average method.
- Finally, once the reliability of the method has been tested and demonstrated, some of the estimated in-use HLC values are decoupled, using the decay method, from the metabolic CO_2 of the building´s occupants. Therefore, the Air Change per Hour (ACH_{decay}) rates are estimated due to infiltrations and/or ventilation in the building. Once these ACH_{decay} values have been obtained, they are used to estimate the corresponding C_v values. The estimated HLCs are then decoupled into their transmission and infiltration and/or ventilation parts (UA and C_v values). Thus, the origin of the heat losses can be identified, and this allows the energy performance to be understood better and, consequently, the performance gap of the in-use building.

The structure followed throughout the Thesis is explained below:

The introduction of the Thesis is outlined in chapter 1. This chapter describes one of the main problems that exist when working with real in-use buildings, the performance

gap. The current concern about this performance problem is demonstrated and the Heat Loss Coefficient is presented as the main key performance indicator in carrying out the in-use building envelope energy performance characterization. It is also shown that, although there is a wide range of methods to estimate this HLC in in-use buildings, none of them are considered to be a general method. Moreover, as far as the authors are concerned, none of the existing methods for the HLC estimation in occupied buildings have been developed further in order to perform the decoupling of the HLC. Therefore, the average method that is developed during this work is presented. Moreover, the HLC decoupling process used in this work to identify the main origin of the heat losses in order to understand the energy performance gap is also presented.

Chapter 2 develops all the methodologies used to achieve the final objective, the estimation and decoupling of the in-use HLC into the transmission heat loss coefficient (UA) and the ventilation and/or infiltration heat loss coefficient (C_v). Therefore, the development of the average method used to estimate the HLC of an in-use building based on monitored data is first presented. Then, since the solar gains through opaque walls have not been considered during the average method development, a detailed analysis of this variable has also been carried out. The weight that not considering this variable has in the HLC estimate is also estimated through this analysis. The latter analysis has been carried out using a simulation programme named LORD. Finally, the in-use HLC decoupling methodology used is presented.

Chapter 3 presents all the case studies where the presented methodologies have been applied. This chapter starts by presenting the Round Robin Box (a small scale building). Then, the two in-use residential buildings studied are presented, showing completely different characteristics; the house located in Gainsborough being a well-insulated dwelling and the house located in Loughborough a poorly-insulated residential building. Finally, the in-use Rectorate office building of the University of the Basque Country is presented, where the data before and after the retrofitting have been analysed. Moreover, their monitorisation systems and the data provided have also been presented and analysed.

All the results are reported in chapter 4 and a discussion is developed for each of the case studies in order to compare the results.

Finally, chapter 5 presents all the conclusions taken from the previously shown results and future work is proposed.

CHAPTER 1: INTRODUCTION

1. INTRODUCTION

1.1- Background of the building energy efficiency

Climate change is one of the biggest challenges our society has to deal with. Global warming due to greenhouse gas emissions is one of the major causes of its existence. Therefore, in order to reduce these emissions, the Kyoto protocol [1] was adopted by the governments of the most developed countries in 1997. However, it was not entered into force until 2005. This protocol established targets in order to reduce emissions by 5 % compared to 1990 levels between the years 2008 and 2012. However, a second commitment period was adopted in 2012, the Doha Amendment to the Kyoto Protocol, which was extended from 2013 to 2020. Meanwhile, the Conference of Climate (COP21) was celebrated in Paris in 2015. The Paris Agreement [2] established aims to limit the global ambient temperature to be below 2 °C in order to avoid dangerous global warming. One of the strategies of the European Union (EU) to achieve the objectives of the Paris Agreement is the energy efficiency improvement.

According to H2020 Energy Efficient Buildings (EeB) [3], buildings are responsible for 40 % of energy consumption and 36 % of CO_2 emissions in the EU. In order to solve this problem, the European Union commitment to energy efficiency can be clearly seen in the directives and objectives proposed for the years 2020, 2030 and 2050. The most recent directive related to the energy performance in buildings is the Directive 2018/844 [4] of "Energy Performance Building Directive" which was recast on 30 May 2018 modifying Directive 2010/31/EU [5] on the energy performance of buildings and Directive 2012/27/EU [6] on energy efficiency. Nowadays, the energy saving and the energy efficiency when constructing or rehabilitating a building are one of the main aims.

The first thermal regulation for buildings was introduced in Europe in the 1970s [7]. Since millions of buildings in Europe were constructed before then, in general, energy efficiency was not considered a main issue in any of those buildings [7, 8]. Hence, a wide range of buildings in Europe is energetically inefficient. Therefore, Buildings Performance Institute Europe (BPIE) [9] has specified some principles in order to achieve a realistic and sustainable net zero consumption. There can be found the promotion of the

application of renewable energies, the maximum limit of energy demand and the limit on the emissions and use of the primary energies.

Moreover, in order to solve the current energy efficiency problems in the building sector, the International Energy Agency IEA-EBC Programme [10] has been developed. This programme involves energy research and innovation in buildings with collaboration from several countries.

1.2- Energy performance gap of buildings

Achieving an energy efficient building is not a simple task. Following one of the requirements of directive [4], several countries in the European Union have developed different energy performance estimation methods, where they use whole building simulation software with thermal models [11]. These methods are commonly used for the implementation of building energy certification schemes. However, energy saving methods should be based on empirical methods instead of model estimations [12]. In general, these models assume standard operation conditions and consequently, the occupation and real heat requirements are not considered in these simulations. Therefore, unless fed with monitored occupation and HVAC system data, simulation models tend to overestimate the energy demand of old buildings and to underestimate it in new buildings [12].

Several buildings designed to obtain a considerable reduction in energy consumption have failed during this process. This is because an important “performance gap” [13, 14] is observed when designed or simulated energy consumptions are compared to real ones. A considerable number of studies have shown that the real energy consumption can be up to two to five times higher than the predicted energy consumption [15, 16]. Therefore, in order to address this “performance gap”, the in-situ measurements are considered essential.

The energy performance difference, commonly known as the “performance gap”, has numerous different causes. Some are due to such factors as the construction or operation [13]; others derive from such data uncertainties as the climate conditions affecting the building. Several analyses have been carried out to study how a specific climate can affect the energy behaviour of the building [17]. Moreover, the shape of the building is also

linked to its energy efficiency [18]. Hemsath and Bandhosseini [19] and Montazeri et al. [20] have done research into how the relation between the height and the width of a building can affect the heat transfer and energy consumption. However, there are three main sources affecting the energy performance gap: The behaviour of the occupants [21, 22], the building systems [23, 24] and the building envelope [25, 26] (see Figure 1). However, they are all correlated. If the efficiency of the building envelope is improved, it would directly affect the two other sources, reducing considerably their energy consumption. In other word, if the building envelope efficiency is high, the energy consumption of the systems inside the building would be considerably reduced, since less energy would be necessary to provide the same indoor comfort conditions in the building. Moreover, if the systems of the building are performing correctly and the heat losses through the envelope are reduced, the comfort inside the buildings increases and the impact generated by the occupants behaviour in the energy consumption of the building is generally reduced. Then, it can be concluded that the building envelope is the key source in order to reduce the energy consumption and therefore, the main source for this performance gap. Therefore, in order to accurately characterise the building envelope energy performance using in-situ measurements, it is necessary to use Key Performance Indicators (KPI).

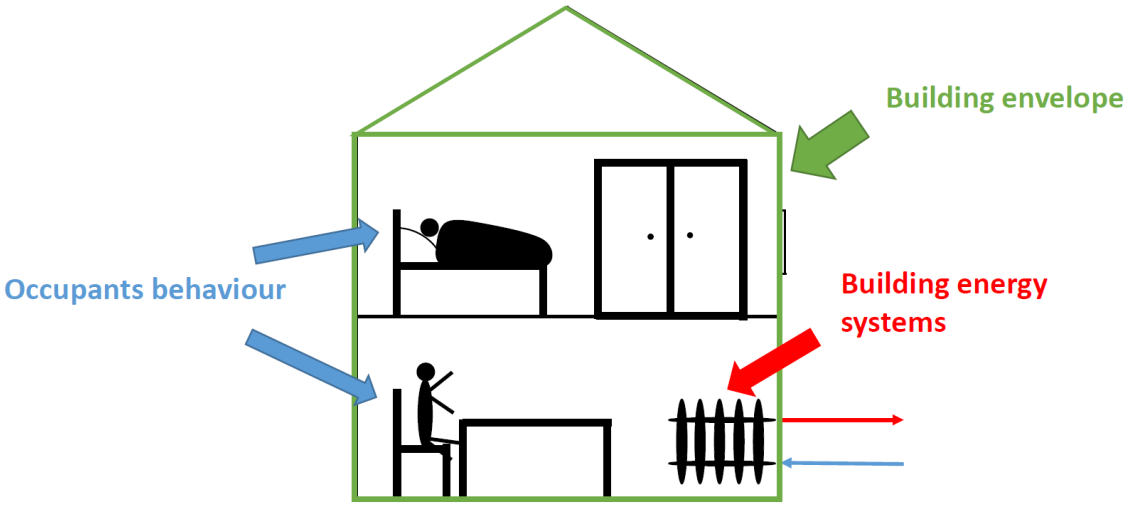

Figure 1. The three main sources affecting the performance gap: The behaviour of the occupants, the building systems and the building envelope.

1.3- Building envelope energy performance characterization

The most commonly used Key Performance Indicators for the building envelope energy performance characterization are the Heat Loss Coefficient (HLC [kW/K or W/K]) and the solar gains (S_aV_{sol} [W/day])[27]. However not all the measurement based methods used to characterize the building envelopes are able to estimate the solar gains. Then, it can be said that the HLC is the most commonly estimated KPI.

On the one hand, the Heat Loss Coefficient is the sum of two heat loss coefficients representing two phenomena occurring through the envelope of the building; the transmission and the infiltration and/or ventilation heat loss coefficient [28]. The first coefficient is the transmission heat loss coefficient (UA), which considers the heat transmission occurring through the envelope of the building. The transmission heat loss coefficient is mainly dependent on the thermal conductivity and thickness of the building envelope materials. It can be measured in-situ for such components as windows, walls, roofs…[29, 30], as the U-value can be estimated by measuring the inner surface heat flux and the outdoor and indoor temperatures. Despite the UA value can be slightly dependent to the average temperature of the insulation layer, unless the building envelope is damaged or deteriorated, it can be assumed to be constant after the building construction. However, the proper and accurate in-situ measurement of the UA value for a complete building envelope can be time consuming and quite expensive if the aforementioned method is used [31].

The second coefficient that makes up the total heat loss coefficient is the infiltration and/or ventilation heat loss coefficient (C_v), which depends on the airtightness and ventilation system performance of the corresponding building. Infiltrations can be defined as the uncontrolled air movements across the building through unintentional openings or cracks, while ventilation is an intentional renovation of the indoor air through outdoor airflows entering the building in order to improve the indoor air quality. The ventilation can be natural (through window opening) and driven by the weather conditions or mechanical ventilation (through a ventilation system) [32-34]. Therefore, infiltrations are a consequence of the air pressure difference between the interior and exterior, dependent on such climatic conditions as wind speed and temperature difference between the interior and exterior [35]; while the behavior of the occupants,

such as window and door opening and/or the performance of the ventilation system, will be directly related to the ventilation part [36, 37]. The estimation of this heat loss coefficient can be carried out by multiplying the volumetric airflow rate ($\dot{V}$) by the air ρ_{air} and Cp_{air} (the density and constant pressure specific heat of the air at the average indoor temperature). This volumetric airflow rate is the multiplication of the Air Change per Hour (ACH) and the volume of the analysed room or building [38, 39]. Note that, when ventilation systems with heat recovery are present, the heat recovery efficiency must be considered when calculating the ventilation part of the infiltration and/or ventilation heat loss coefficient.

On the other hand, the building envelope's solar aperture, as [40] explains, is "the heat flow rate transmitted through the building envelope to the internal environment under steady state conditions, caused by solar radiation incident at the outside surface, divided by the intensity of incident solar radiation in the plane of the building". The solar gains are estimated by multiplying the solar aperture by the corresponding solar radiation incident on the wall or window. However, although the global solar radiation can be accurately measured, the solar aperture is not an easy parameter to estimate. The latter can also be defined as the multiplication between the surface area hit by the solar radiation and the solar factor (g-value). This solar factor represents the proportion of incident solar radiation on a window or façade that is transmitted to the interior of the building [41]. This factor varies depending on the orientation of the building and the position of the sun [42], which complicates considerably its estimation due to the obstacles and shading that the sun can face before striking the building façades and windows. Therefore, some researchers have tested different methods where a variable solar aperture is considered and estimated over time, in order to study whether it improves the accuracy of the results. From them can be concluded that, when the building characteristics are well known, it is possible to perform suitable building characterizations using just a constant gA value, been included as an unknown and identifiable parameter in the models [29, 43].

Despite a wide range of methods exist in order to estimate the Heat Loss Coefficient based on measurements, not all of them are able to estimate the solar gains. The main methods used in order to estimate this HLC can be separated in two main groups: the

dynamic or statistical methods used to estimate the stationary and dynamic thermal properties of the building and the stationary or physical methods used in order to estimate the stationary thermal properties of the building.

On the one hand, the most commonly used dynamic methods should be mentioned. There can be found advanced mathematical modelling techniques, such as ARMAX [44-46] (ARX) and Grey Box modelling (Stochastic state space models) [47-49]. These methods have been used by different authors to identify the real energy behaviour of building envelopes or building components based on measurements [50]. Some of those methods even identify such building characteristics as U-values, thermal resistances and thermal capacitances. They are also able to estimate the solar aperture using an unknown identifiable constant value. Due to the limitations of installing sensors in in-use buildings, the advanced mathematical modelling techniques, where physical–statistical approaches are used, have become common [51].

When working with state space models, it is important to obtain some previous physical knowledge of the building. The analysis consists of fitting several models, starting from the simplest and going on to the most complex, comparing their log likelihood values and residuals. Therefore, it is very important to obtain accurate results on the diffusion term in order to verify the quality of the model [49, 50]. On the other hand, when working with ARMAX models, single and multi-output models [44, 45] can be developed. Comparing with the state space equation, the ARMAX models do not need previous physical knowledge. Unfortunately, since the ARMAX models do not identify steady state physical parameters, the results obtained are estimated by comparing the ARMAX model and the steady state energy balance equation [50]. Unfortunately, these two methods tend to work with complex models, which sometimes can complicate the process of the HLC estimation considerably.

On the other hand, among the measured data based stationary methods, the most known are the simple or multiple linear regression methods [27, 52, 53] and the averaging method [54].

The most commonly used stationary methods are the regression methods. Among this method, the well known co-heating method can be found [27, 52, 55]. The original co-heating method introduces an electric heater, which provides a constant temperature of

25 °C during a period that lasts between 1 and 3 weeks inside the dwelling (see an example of the configuration in Figure 2). By measuring the amount of electrical energy that is required to maintain the elevated mean indoor temperature each day, the daily heat input (W) to the dwelling can be determined. The heat loss coefficient for the dwelling can then be calculated by plotting the daily heat input against the daily difference in temperature between the inside and outside of the dwelling (ΔT). The resulting slope of the plot gives the Heat Loss Coefficient in W/K. This method is named as Siviour method. This test is applied in unoccupied dwellings where effects of users ($K_{occupancy}$) are avoided. As a result, only the heat supplied by the electrical heaters is going to be transmitted through the walls of the dwelling plus infiltration losses. In order to calculate the solar radiation [25] or the wind effects on the walls, extra calculations must be done. Then, unfortunately, this method is not prepared for working in in-use buildings and the experiment takes a long time to be performed, which means that the building needs to be unoccupied during all the time.

Figure 2. Example of a typical co-heating configuration. [27]

However, unlike the original co-heating method, the average method can be used for the HLC estimation of in-use whole buildings [54]. Note that, due to the method applicability in in-use buildings, apart from the heat losses transmitted through the walls of the dwelling due to transmission and infiltration heat losses, also the ventilation heat losses are considered within the estimated HLC value. To apply the average method

accurately, cold and cloudy periods of at least three days in a row are required. In this short and cloudy periods it is possible to ensure high indoor to outdoor temperature difference (low uncertainty in the indoor to outdoor air temperature measurement), high heating consumption (high weight of the accurately measurable heat gains due to heating in the total heat gains) and low solar gains (low weight of the not accurately measurable heat gains due to solar radiation). Considering the period mean of the total heat gains inside the building and dividing them by the mean indoor and outdoor temperature difference, it is possible to obtain the building average HLC value. Within the mentioned total heat gains inside the building, the space heating consumption of the building, the total electricity consumption within the building and the solar heat gains of the building are considered. The majority of this variables are usually measured using simple monitoring system of actual in-use buildings. Unfortunately, this method is not able to estimate the solar gains of the building. Therefore, it is necessary to fix an equivalent solar aperture in order to obtain the solar gains of the corresponding building by multiplying this solar aperture by the measured global solar radiation. Note that in cloudy periods the solar radiation can be considered purely diffuse and similar in all the orientations of the building, making possible to make reasonable accurate estimations of solar gains in those cloudy periods where, furthermore, solar gains are very low in comparison with the space heating accurately measurable heat gains.

Hence, despite the wide range of existing methods to estimate the HLC using measurements, and also some of them able to estimate the corresponding solar gains using an unknown identifiable constant parameter, they are still far from been a general method. Unfortunately, in order to work with statistical methods such as the grey box models or the ARMAX, it is necessary to have some previous knowledge about advanced mathematical modelling techniques. If this knowledge is not acquired, the application of the method can become complicate and time consuming. Therefore, the adaptation of a stationary method would be the best solution in order to obtain a reliable simple and accurate in-situ HLC estimation method for analysing in–use buildings. Thus, it would be possible to continuously evaluate the building in its in-use conditions. Moreover, the developed adapted method should be able to estimate accurate HLC results without the need of an extensive monitoring system. Furthermore, this method should try to consider and understand the main uncertainty sources existing in building physics in order to carry

out a reliable energy characterization of an occupied building envelope. However, due to the numerous knowledge gaps found in the estimation process of an accurate in-use Heat Loss Coefficient value of the building envelope, it is a complex task.

1.4- Uncertainty sources affecting the Heat Loss Coefficient estimation

There are several uncertainty sources that must be considered and understood when trying to obtain a reliable and simple HLC estimation method for in-use buildings. However, one of the main sources creating a considerable uncertainty when estimating the in-use HLC value are the previously presented solar gains.

Despite the majority of variables needed in order to estimate the HLC in in-use buildings can be accurately measured, such as the space heating, the electrical consumption and the indoor and outdoor temperatures, other heat gains affecting this HLC estimation such as the solar gains cannot. Due to its difficulties to be accurately estimated in in-use buildings, the solar gains are one of the main uncertainty sources when estimating in-use HLC values [56]. It must be remarked that the solar radiation can enter buildings through the windows and the opaque walls. In the case of the windows, a part of the solar radiation incident to the glass part will be transmitted to the interior of the building. Nevertheless, the solar radiation hitting the opaque elements will heat up the outer surface and block the heat flux going to the exterior [57]. Depending on the opaque wall's thermal characteristics and the incident solar radiation, if the inner surface temperature is lower than the outer, it is also possible to transmit heat flux through the wall in the opposite direction (from the exterior to the interior). In some cases, the solar gains through the opaque walls are negligible and are not considered in the building characterization. In other cases, it is of the same importance and thus both must be considered, since the building heat losses can be affected by both solar gains [58]. In these cases, a sufficiently good building characterization can be done through an unknown identifiable constant solar gain, where both the solar gains through windows and opaque walls are considered. There are several studies where an unknown identifiable constant solar gain value is considered. Among these studies, such research works as [45, 59] have compiled a set of case studies that consider this parameter in order to characterize components. Moreover, it has been dealt with in several building characterizations that apply steady-state methods [29, 60, 61] and dynamic parameter identification methods

[30, 48, 62, 63], where some methods presented in section 1.3 can be found. So this coefficient enables a proper estimation of the HLC despite the solar gains are considerable through the opaque walls. For example, several co-heating tests are described in [60] considering the solar gains effect. Although some of them consider the solar gains as an unknown identifiable constant parameter, one of the co-heating tests used considers a fixed value of the solar gain coefficient obtained from the window area and the transmittance of the glass. As done in this co-heating test, in simple methods that are not prepared for estimating the solar gains such as the average method, it is assumed that a rough estimate of the solar aperture of the building can be done considering only the window area and its corresponding g-value or transmittance of the glass. Then, using this rough estimate of the window solar aperture, it is possible to estimate the solar gains only coming through the window of the building [64]. Due to the difficulties to roughly estimating the solar gains through the opaque elements, they are commonly neglected in this kind of methods. Then, when using these kinds of methods; if there were solar gains through opaque walls, they would not be considered within the HLC estimation calculations and thus, the HLC value would be underestimated. However, as far as the authors are concerned, a method to quantify this error in the HLC value has not been developed yet.

Moreover, it must be remarked that the majority of the authors using an unknown identifiable constant solar gain value only focuses on the estimation of the U-value and g-value (see some examples of this value estimations of [64] in Figure 3). It is proven that the obtained g-values are extremely low, as compared to the g-values commonly obtained in the windows. Moreover, these results are justified with the visual checking of the inner surface temperature and the U-value estimation, also detailed in [29], where no improvement is found in the U-value estimation when the solar radiation is included in the models. Therefore, the researchers conclude that the corresponding effect would be negligible in the energy balance of the surface. However, as far as the authors know, no one has carried out a deeper analysis of the solar radiation effect on inner surface heat flux. If the inner surface heat flux is analysed, it is possible to quantify the inner surface heat flux blocked from going to the exterior. Thus, it is possible to quantify the effect the solar radiation has in the inner surface heat flux and then, to estimate the corresponding

weight it would have respect with the HLC value estimated using simple methods without considering an unknown identifiable constant solar gains value.

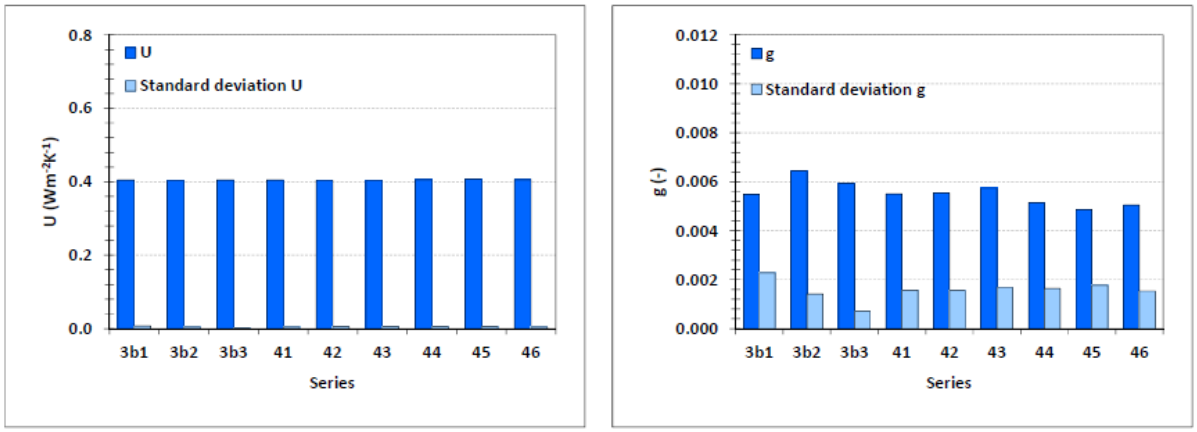

Figure 3. Some estimated average U and g values for opaque wall during the Annex 58 project. [64]

Therefore, in the way to estimate a reliable and simple HLC estimation method for in-use buildings, it is important to know the weight the solar gains through the opaque walls would have respect with the HLC value estimated without using an unknown identifiable constant solar gain value. It must be verified that for methods applied during periods where the solar gains are high through opaque elements, the avoidance of the estimation of the solar gains through opaque walls could have a considerable weight in the error of the HLC value. Therefore, in order to avoid this underestimation in the HLC results, the solar gains uncertainty source, together with other uncertainty sources such as the metabolic heat generation effect, heat accumulation term effect, ground temperature effect and the indoor temperature variability effect, must be considered and limited through several requirements stablished when developing the method. Unfortunately, when a real in-use HLC value based on measured data is estimated from an in-use HLC estimation method, due to the building's "performance gap", this estimated value usually shows a considerable difference when compared with the design HLC value.

1.5- Gap between the real estimated and the design HLC values

When estimated, there commonly exist a considerable difference between the design and real estimated HLC results. In [25], an analysis is carries out where the HLC of 25 houses located in the UK are estimated. There, the comparison of the predicted HLC (using design values) is done against the real HLC (using in-situ measured data) values estimated

using a co-heating method. The results of the article show that in every analysed house, the real HLC value estimated by the co-heating method exceeds the predicted HLC value (see Figure 4). Moreover, it is also proven that the difference between the HLC can vary between 6 and 140 %, which in some cases means a considerable difference.

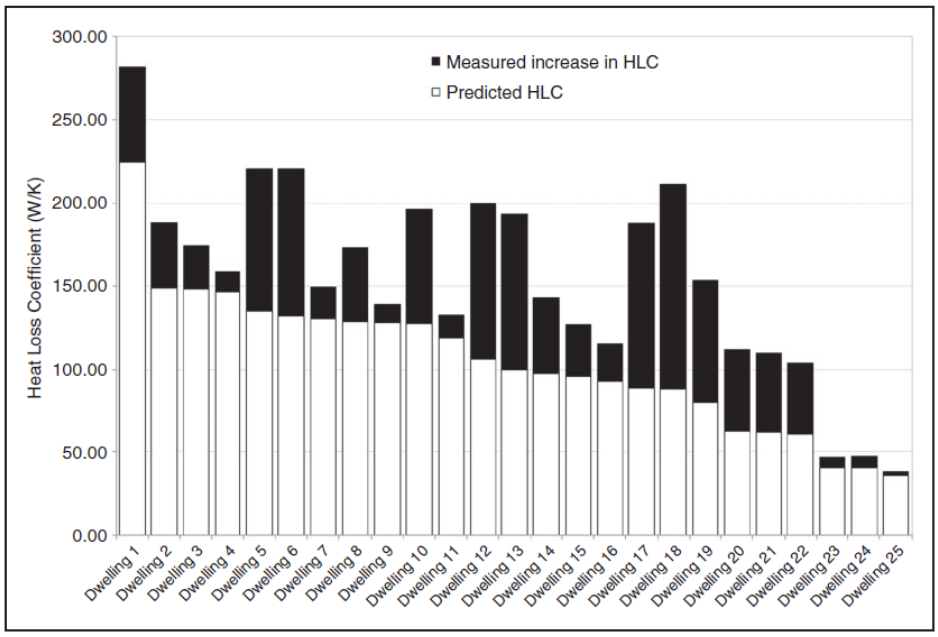

Figure 4. Comparison between the predicted HLC against the real HLC values estimated using the co-heating method. [25]

As commented in section 1.3, the Heat Loss Coefficient is the sum of the transmission and infiltration and/or ventilation heat loss coefficient. As remarked there, the infiltration and/or ventilation heat loss coefficient can be estimated using the Air Change per Hour (ACH). The ACH is commonly studied by the researchers working in the Indoor Air Quality field. The ACH [33] represents the total rate of outdoor air entering the building, normally considering both the ventilation and the infiltration air rates. There are two main techniques to estimate the ACH values of a building. Tracer gas techniques are based on the mass conservation of a tracer gas, which is injected into the studied zone or building and uniformly mixed. The injection method defines the tracer gas techniques, which are concentration decay [65-67], constant injection and constant concentration techniques [68]. Despite some analysis tent to compare the methods with each other [69-71], the most commonly used method individually is the concentration decay method, since it needs less tracer gas and is the easiest to perform. Moreover, the gases used for this analysis are usually inert. The most commonly used gases are sulphur hexafluoride (SF_6) [68, 70, 71] or carbon dioxide (CO_2) [69, 72, 73]. However, CO_2 is the cheapest and most

easily measurable tracer gas for in-use buildings, since it is also generated by the occupants [65, 74].

The ACH measured using tracer gas techniques is the actual value in an enclosure for a given set of conditions during the test: air infiltration characteristics, climatic influences, ventilation system operation, etc. Therefore, when those conditions change, the ACH value will also change. To overcome this drawback, one approach is to measure ACH under different boundary conditions trying to cover a wide range of conditions; another approach is to build a ventilation model.

The blower door test [32, 75, 76] does not measure the ACH in actual boundary conditions of the enclosure, the ACH is measured for several indoor/outdoor pressure differences of the building. The aim is to characterise the air permeability of the enclosure envelope, and thus, to measure the airtightness of the building envelope, as done in [77] to improve it after the rehabilitation. By the data obtained from the test and defining the behaviour of the ventilation system, it is possible to build a ventilation model and, once validated, to analyse the ACH under different sets of conditions.

Although the ACH and the HLC [46, 78-80] are two parameters which have been widely analysed separately, as far as the authors know, they have not yet been related to decouple the HLC into its transmission (UA) and infiltration and/or ventilation (C_v) parts using in-situ measurements on in-use buildings by means of basic monitoring systems. Thus, knowing the corresponding heat loss value of each coefficient would be helpful for the understanding of the main origin of the performance gap.

1.6- Aim of the Thesis

The main aim of the Thesis is to identify the real origin of the heat losses, in order to make possible to understand as much as possible the HLC performance gap between the real and the design value in in-use buildings. However, several indispensable steps need to be followed in the process. The first step to follow is the obtaining of a simple and reliable method in order to estimate the in-situ HLC value of in-use buildings.

Therefore, although there are some research works that estimate this Heat Loss Coefficient in monitored in-use buildings, they are still far from being a general method. Of the presented methods in section 1.3 to estimate the building envelope Heat Loss

Coefficient, the co-heating method is the most developed. However, this method is no able to work in in-use buildings. Therefore, due to its simplicity and its applicability without the necessity of an extensive monitoring system and a considerable advanced mathematical technique knowledge, the average method is further developed in order to estimate the HLC of in-use buildings in this work. The whole mathematical demonstration, starting from the energy conservation equation, is developed in order to enable comprehension of the limits the method has when applied to in-use buildings. Thus, the period selection criteria for reliable HLC estimation by the average method has been defined in detail, for minimizing the HLC estimate uncertainty. In other word, the method has been developed in detailed step by step in order to understand and limit the main uncertainty sources found when estimating the HLC. Within these main sources affecting the HLC result in in-use buildings, the metabolic heat generation effect, the weather data effect, the heat accumulated effect in the building, the effect of the uniformity of the indoor temperature within the building, the ground temperature effect and the solar gains effect can be found. Therefore, some requirements have been stablished in the method in order to control the effect of the mentioned uncertainty sources.

This method does not require to build a detailed physical model of the building to estimate its in-use HLC. Thus, it could be used within Building Management System's programing in a general way, with the only need to be fed by the total window area of the building, the scheduled occupancy data and the already widespread energy monitoring data. The Thesis also focuses on the innovative demonstration of the summation properties of the HLC values when estimated floor by floor. Therefore, a multizone building is presented and the detailed heat and mass exchanges between the zones or volumes and adjacent surroundings are analysed to prove the HLC summation properties. Note that the reliable in-use HLC estimation should be achievable by analysing the data sets obtained by already widespread building monitoring systems simply made up of indoor and outdoor temperatures, heating system energy inputs to the building, electricity consumption and weather data.

Furthermore, despite the average method is developed for a multi-storey office building, the work studies the applicability of the average method in three different case studies: a simple test box, two in-use residential buildings and a pre and post-

rehabilitated occupied office building. The simple test analysis is based on the study of the Round Robin Box, a widely monitored experimental box. However, the second test case considers two in-use residential buildings, being one of them a very well insulated building and the other a poorly insulated building. The final building is a rehabilitated occupied four-storey office building, where both, the HLC results before and after the rehabilitation are estimated. Since every case study presents completely different characteristics and behaviour, and considering that the average method has been developed for an office building, very interesting HLC results and conclusions will be obtained from this work.

As commented before, the developed average method studies and limits a wide range of uncertainty sources. Within them, the limitation of the solar gains effect through the windows is considered. However, the effect the solar gains through opaque walls have in the HLC value in in-use buildings is completely ignored. Nevertheless, as highlighted in section 1.4, for methods where the solar gains through opaque walls are not considered, the HLC value could be underestimated. Hence, the second part of the Thesis proposes an experimental method for the analysis of the effect of the solar radiation affecting each of the opaque faces of the Round Robin Experiment box [64] based on the analysis of the inner surface heat flux using real in-situ measured data. Each opaque face of the Round Robin Box is analysed one by one, considering how the solar radiation is affecting each of the inner surface heat flux measurements. Since the Round Robin Box was monitored in detail, it has been possible to obtain a very detailed dataset for each of the faces. Then, apart from the inner surface heat flux and the wide solar radiation data, such variables as the wind speed and the long wave radiation were also measured, which helped considerably to increase the accuracy of the models. Moreover, all the thermal characteristics of the Round Robin Box layers were also known, so a very exhaustive theoretical analysis of the Round Robin Box envelope could be done. Once the solar radiation effect on the inner surface heat flux of each face has been quantified, the analysis is developed further in order to estimate how the solar radiation through opaque faces affects the HLC value, when applying methods where an unknown identifiable constant solar gain value is not used, such as the average method developed in this work.

Thus, the aim of the analysis is to study the weight the solar radiation has on the inner surface heat flux coming through the opaque walls of the Round Robin Box using in-situ measured data. Once this weight has been estimated, it is transmitted to the estimation of the HLC in methods where the solar gains through opaque walls are not estimated, as the average method developed over this work. Through this analysis, the blockage that this solar radiation creates in the opaque walls can be estimated. Therefore, based on RC models, an estimation of the best representative models has been carried out using the LORD software [81, 82]. A wide range of candidate models has been proposed where several combinations of variables were fixed, considering in detail different physical phenomena. From these candidate models, the real physical parameters are estimated in order to compare them with the buildings' physical values and see which model's values most closely approaches reality. Moreover, the residuals of the models are analysed. Once the best fits are found, the effect of the solar radiation is removed in order to estimate the real weight it has in the inner surface heat flux through the estimation of the hypothetical inner surface heat flux. Then, once the weight the solar radiation has in the inner surface heat flux had been quantified, it has also been possible to quantify the percentage weight the solar radiation through opaque walls would have with respect to the HLC estimation, when methods without an unknown identifiable constant solar gain value are used. Finally, constant g-values have also been estimated for each of the walls; using the difference between the inner surface heat fluxes from estimating it mathematically and directly from the LORD software. Then, the analysis has been performed using two different datasets, one in winter and one in summer, in order to the see the differences in the results. Through the analysis of the winter dataset, where only cloudy and cold days have been considered, the percentage weight the solar radiation through opaque walls would have respect to the HLC estimated using the developed average method can be estimated. However, when developing this average method, due to the requirements fixed to limit the solar gains coming through the windows, it is assumed that this requirement would also limit the solar gains effect through the opaque walls. Therefore, it is also assumed that they would not have a considerable effect in the HLC value uncertainty and they are considered negligible. Then, through this work, their negligibility will be demonstrated. Nevertheless, through the analysis of the summer period, the percentage weight the solar radiation through opaque walls would have respect to the HLC estimated

using applicable method during sunny and warm periods is estimated, in order to estimate the error their avoidance could generate in the HLC value.

Unfortunately, when considering uncertainty sources such as the solar gains and other uncertainty sources presented before in the development of the in-use building reliable HLC estimation average method, the obtained HLC results usually show a considerable difference when compared with the design HLC values. As remarked in section 1.5, it is common in measurement based HLC estimation methods. Therefore, this research goes further and proposes a method, based on in-use buildings monitored data, for the decoupling of the HLC of in-use buildings into its transmission (UA) and infiltration and/or ventilation (C_v) heat loss coefficients in order to identify the origin of the heat losses. Moreover, in the cases where the design values are provided, it would also be possible to understand the disagreement with these two design values.

Thus, this Thesis is focussed on developing a new decoupling method that could be implemented in real world scenarios through the use of simple sensors for monitoring in-use buildings. Metabolic CO_2 will be used as a tracer gas to estimate air infiltration and/or ventilation rates by means of CO_2 decay analysis. The CO_2 concentration can be easily and accurately measured by simple air quality sensors. This work is based on the requirements described in the ASTM D6245-18 'Standard Guide for Using Indoor Carbon Dioxide Concentrations to Evaluate Indoor Air Quality and Ventilation' [83]. Although the objective of this Standard is not to decouple the HLC, one of its by-products is the estimation of the Air Change per Hour (ACH) of the analysed volume (usually a thermal zone of a building). This ACH value can be used to estimate the infiltration and/or ventilation heat loss coefficient (C_v) of the studied volume. Since HLC = UA + C_v, if HLC and C_v are estimated, then the HLC may be decoupled into its transmission (UA) and infiltration and/or ventilation (C_v) parts.

The application of the proposed decoupling method requires the estimation of the HLCs of the different thermal zones or volumes to be analysed, where corresponding C_v values will also be estimated. In this work, the volumes will be the four floors of the rehabilitated office building mentioned before. The HLC values estimated by applying the average method mentioned before will be used to decouple those already estimated HLC values into the C_v and UA values.

Thus, the final objective of this Thesis is to apply and test the proposed CO_2 concentration decay method to decouple the in-use HLC into its UA and C_v values of an in-use office building by means of monitored data. The decoupling of the HLC would allow a clear identification of the main origin of the heat losses. In other words, it would be possible to estimate which of the heat losses are higher; the transmission heat losses or the infiltration and/or ventilation heat losses.

Moreover, it must be remarked that the HLC values of the in-use building are estimated for two different periods, one before the building was rehabilitated and the other, after been rehabilitated. Before rehabilitation, there was no ventilation system installed in the building. So, the C_v values obtained during the pre-retrofitting winters will only consider the infiltration heat losses of the building. However, after the rehabilitation, a ventilation system was installed on each of the floors. Thus, the obtained C_v during the post-retrofitting winter periods should consider both the infiltration and ventilation heat losses.

To sum up, through this Thesis, it has been possible to develop an accurate method based on measured data in order to estimate reliable HLC results for in-use buildings, which later are decoupled into the transmission and infiltration and/or ventilation heat loss coefficient. Thus, the work will help to identify the heat losses origin in order to better understand the building energy performance gap.

CHAPTER 2: METHODOLOGY

2. METHODOLOGY

This section describes all the methods and procedures carried out in order to obtain the objective of the Thesis. The simulation programs used during the work are also mentioned.

First of all, the methodology used to reliably estimate the HLC in in-use buildings is explained. Therefore, the origin of the used average method has been deeply analysed and described in section 2.1.1 and thus, the origin of the method requirements is detailed. This section is followed by the analysis of the HLC properties in relation to a multizone building in section 2.1.2. There, the cancelation of the internal heat and mass transfer effects between the adjacent thermal zones is proven. Moreover, the used error propagation method in order to estimate the uncertainties created by the sensors is also included in section 2.1.3.

Once the average method is studied in detail, it has been identified that one of the main parameters creating uncertainties in the HLC value are the solar gains. However, during the development of the average method in section 2.1.1, only the effect of the solar gains through the windows has been studied and limited. Then, the effect of the solar gains through the opaque elements has been completely ignored. Therefore, a method for a deeper analysis of this effect is presented in section 2.2. Section 2.2.1 contains the theoretical quantification of the solar factor and the effect the solar radiation has on the inner surface heat flux of opaque walls under steady-state conditions. During the Thesis, the theoretically presented method is applied to the measured data using different models in the software LORD. Since not always the corresponding solar radiation data of each orientation is measured, it has been necessary to estimate it. Therefore, section 2.2.2 also includes the method followed in order to estimate the missing solar radiation data. So, as commented before, once all the necessary data is estimated, it is possible to analyse the solar gains effect on the inner surface heat flux using several different models in LORD. Therefore, the structure and the theoretical thermal characteristics of all the models tested are presented in section 2.2.3. The identified best models used to estimate the solar gains effect on the inner surface heat flux and the procedure followed for obtaining these values are also presented in section 2.2.4. Also the estimation of the g-values is included in section 2.2.5. Finally, the effect the solar gains have through the opaque walls is

transmitted to the HLC estimation method. Therefore, the theoretical procedure followed in order to estimate the weight the not consideration of the solar gains through opaque walls would have with respect to HLC value when estimated using HLC estimation method such as the average method is also introduced in section 2.3.

Finally, once tested that all the main uncertainty sources are considered in the average method development, and therefore, the obtained HLC results from this method are considered reliable enough, it is possible to present and apply the last part of the work. This is the decoupling of the in-use HLC value, which consist on separating the HLC into its transmission and infiltration and/or ventilation heat loss coefficient. Thus, the procedure performed for this decoupling is extendedly explained in section 2.4. Since the studied building has been analysed before and after its rehabilitation, and during the rehabilitation of the building, a mechanical ventilation system was installed, the method has been adapted for both situations. Therefore, section 2.4.3 shows the method used in order to estimate the infiltration heat loss coefficient before the rehabilitation of the building and section 2.4.4 shows the method used in order to estimate the infiltration and ventilation heat loss coefficient after the rehabilitation of the building.

2.1- Methodology for the HLC estimation

This section presents the development of an average method for the estimation of an accurate in-situ HLC value of in-use buildings. The method development has been based on a multi-storey occupied office building described later in section 3.3.

2.1.1- Origin of the average method

The origin of the method has been studied in detail in order to understand the method's limits when used in dynamic problems such as an in-use building. Figure 5 shows the system to be analysed from the Thermodynamics Open System viewpoint. As can be seen in Figure 5, the building's envelope is the Control Volume or the boundary of the system through which heat and mass can be exchanged with the surroundings and the ground. Eq. 1 states the energy conservation principle of a generic Thermodynamic Open System [84].

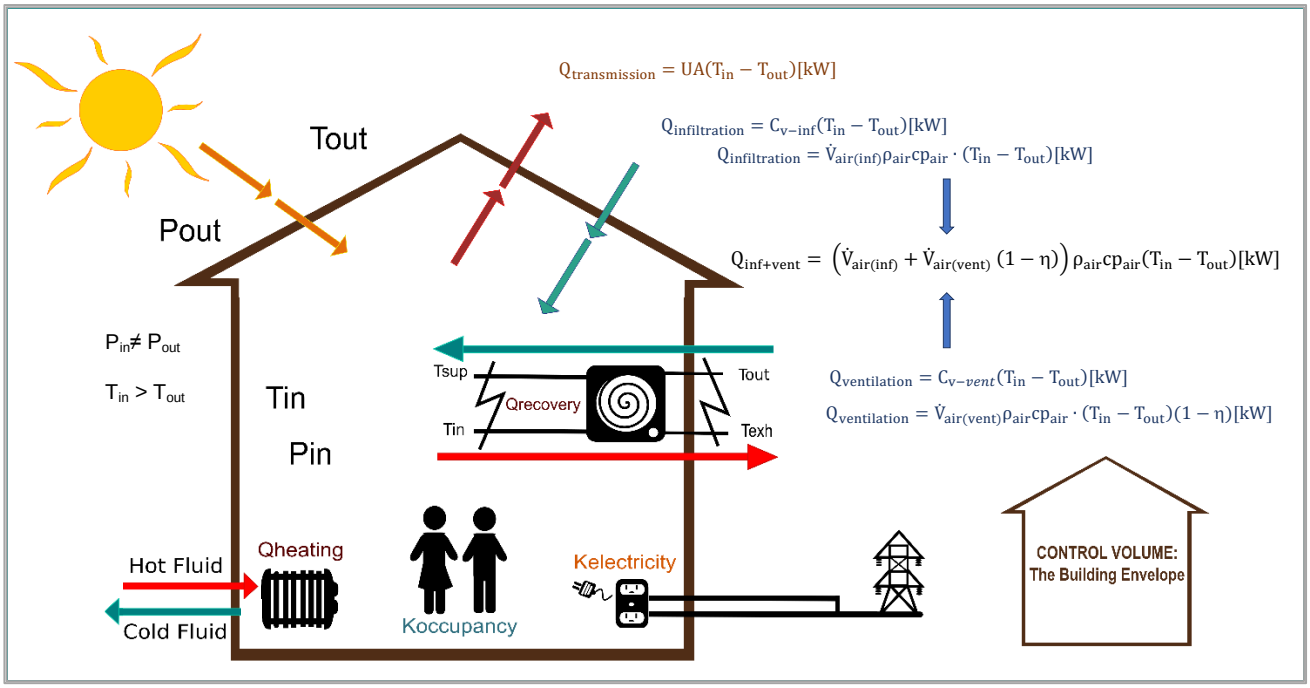

Figure 5. Schematic of all energy and mass exchanges through the control volume defined by the building envelope. [85]

$$\left\{\begin{matrix}\text{Time rate of change}\\ \text{of the energy contained}\\ \text{within the control volume}\end{matrix}\right\} = \left\{\begin{matrix}\text{net rate at which energy}\\ \text{is being transferred in}\\ \text{by heat transfer at time t}\end{matrix}\right\} - \left\{\begin{matrix}\text{net rate at which energy}\\ \text{is being transferred out}\\ \text{by work transfer at time t}\end{matrix}\right\} + \left\{\begin{matrix}\text{net rate at which energy}\\ \text{transfer into the}\\ \text{control volume}\\ \text{accompanying mass flow}\end{matrix}\right\}$$

$$\frac{dE_{cv}}{dt} = \dot{Q}_{cv} - \dot{W}_{cv} + \sum_i \dot{m}_i \left(h_i + \frac{V_i^2}{2} + gz_i\right) - \sum_e \dot{m}_e \left(h_e + \frac{V_e^2}{2} + gz_e\right) \text{ [W or kW]} \quad \text{Eq. 1}$$

Each term of Eq. 1 is developed separately. So the first term represents the energy accumulation in the system, including the Internal Energy (U_{IE}), the Kinetic Energy (KE) and the Potential Energy (PE). Since these last two terms are usually constant in a building, their derivative over time will be zero. Therefore, only the Internal Energy is relevant when estimating the energy accumulation term:

$$\frac{dE_{cv}}{dt} = \frac{dU_{IE}}{dt} + \frac{dKE}{dt} + \frac{dPE}{dt} = \frac{dU_{IE}}{dt} \text{ [W or kW]} \quad \text{Eq. 2}$$

On the other hand, the second term in Eq. 1 takes into account all the pure heat exchanges occurring through the Control Volume boundary (the building envelope). In this case, the heat gained through the solar radiation entering the building and the metabolic heat generated by the occupants of the building are considered to be inputs. Nevertheless, the added negative inputs are transmission heat losses through the envelope of the building.

$$\dot{Q}_{CV} = S_a V_{sol} + K_{occupancy} - UA(T_{in} - T_{out}) \quad \text{[W or kW]} \qquad \text{Eq. 3}$$

The next term, $\dot{W}_{cv}$, considers the pure work exchanged through the Control Volume. In this case, the consumed electricity is considered as work. However, as the electricity is converted into heat within the system, the considered negative work is presented as positive heat gain:

$$-\dot{W}_{CV} = K_{electricity} \ \text{[W or kW]} \qquad \text{Eq. 4}$$

Finally, the last two terms in Eq. 1 consider the net energy exchanged by the system due to the mass flow rates of the water (it could be other Heat Transfer Fluid) in the heating system and the air mass flow rates of the ventilation and/or infiltration air exchanges. Here, the heat provided by the heating system is considered in the energy balance equation as flow and return hot water of the heating system circuit (Eq. 5). The hot water for the heating system could be produced by different technologies. If electrical heating is present, this would be considered in the Eq. 4 term.

If we have buildings with a ventilation system without heat recovery, then the terms $\dot{V}_{air(vent)}\rho_{air}cp_{air}(T_{in} - T_{out}) + \dot{V}_{air(\text{inf})}\rho_{air}cp_{air}(T_{in} - T_{out})$ represents the heat exchanged by the building with the outdoor ambient due to ventilation plus infiltration. If no ventilation system is present in the building, the ventilation term disappears. Then, the ventilation and/or infiltration heat losses can be calculated using the specific heat at constant pressure of the air, cp_{air}, and the indoor to outdoor temperatures (Eq. 5). Kinetic and potential energy variations of both flows can be neglected.

$$\begin{aligned}&\textstyle\sum_i \dot{m}_i \left(h_i + \frac{V_i^2}{2} + gz_i\right) - \sum_e \dot{m}_e \left(h_e + \frac{V_e^2}{2} + gz_e\right) = \dot{m}_{water}(h_{wi} - h_{we}) + \dot{m}_{air}(h_{ai} - h_{ae}) = \\ &\dot{m}_{water}c_w(T_{wi} - T_{we}) - \dot{V}_{air(vent)}\rho_{air}cp_{air}(T_{in} - T_{out}) - \dot{V}_{air(\text{inf})}\rho_{air}cp_{air}(T_{in} - T_{out}) = \\ &\dot{m}_{water}c_w(T_{wi} - T_{we}) - Cv(T_{in} - T_{out}) = Q_{heating} - Q_{inf+vent} \ \text{[W or kW]}\end{aligned} \qquad \text{Eq. 5}$$

However, if the building is working on a ventilation system with heat recovery, the term $\dot{V}_{air(vent)}\rho_{air}cp_{air}(T_{in} - T_{out})$ of Eq. 5 should be calculated considering the heat recovery system efficiency. In order to check how the recovery system affects our calculations, it is necessary to develop the following equations. Figure 5 shows the

schematic of the different temperatures involved in a generic heat recovery system for a ventilation system.

The heat recovery system works with four main temperatures: The outdoor or ambient temperature (T_{out}), the renewed or supply temperature (T_{sup}), the indoor temperature (T_{in}) and the exhaust temperature (T_{exh}). The supplied and exhaust temperatures are those obtained after crossing the recovery system by both, the flow and return of the air flows. The supply temperature is that obtained after the outdoor temperature crosses the recovery system. In winter, this temperature will increase. Considering an adiabatic heat exchanger and the same volumetric flow rates for supply and exhaust flows ($\dot{V}_{air(sup)} = \dot{V}_{air(exh)} = \dot{V}_{air(vent)}$), the heat from the exhaust stream will be used to heat up the cold inlet stream. Thus, the temperature drop of the exhaust stream should be equal to the inlet stream temperature increase across the heat exchanger. Therefore, the percentage of heat recovered would be defined as in Eq. 6:

$$\eta = \frac{T_{sup} - T_{out}}{T_{in} - T_{out}} \quad \text{Eq. 6}$$

Eq. 7 represents the heat exchanged inside the heat exchanger, while Eq. 8 represents the heat that the ventilation system will require for the building's heating system.

$$Q_{recovery} = \dot{V}_{air(vent)}\rho_{air}cp_{air} \cdot (T_{in} - T_{exh}) = \dot{V}_{air(vent)}\rho_{air}cp_{air} \cdot (T_{sup} - T_{out}) \quad \text{Eq. 7}$$

[W or kW]

$$Q_{ventilation} = \dot{V}_{air(vent)}\rho_{air}cp_{air} \cdot (T_{in} - T_{sup}) \text{ [W or kW]} \quad \text{Eq. 8}$$

Developing Eq. 6, a relation between T_{sup}, T_{in}, T_{out} and η can be obtained. Then, combining Eq. 8 and Eq. 9, Eq. 10 would be obtain.

$$T_{sup} = (1 - \eta) \cdot T_{out} + \eta \cdot T_{in} \text{ [°C]} \quad \text{Eq. 9}$$

$$Q_{ventilation} = \dot{V}_{air(vent)}\rho_{air}cp_{air}((1 - \eta) \cdot T_{out} + \eta \cdot T_{in} - T_{out}) \text{ [W or kW]} \quad \text{Eq. 10}$$

Then, $Q_{ventilation}$ can also be presented as:

$$Q_{ventilation} = \dot{V}_{air(vent)}\rho_{air}cp_{air}(1 - \eta)(T_{in} - T_{out}) \text{ [W or kW]} \quad \text{Eq. 11}$$

Therefore, if the compensated ventilation system with heat recovery system is added to the building, the previously presented Eq. 5 is converted into Eq. 13, where:

$$C_v = \dot{V}_{air(vent)}\rho_{air}cp_{air} \cdot (1-\eta) + \dot{V}_{air(\text{inf})}\rho_{air}cp_{air} \text{ [W/K or kW/K]} \quad \text{Eq. 12}$$

$$\sum_i \dot{m}_i\left(h_i + \frac{V_i^2}{2} + gz_i\right) - \sum_e \dot{m}_e\left(h_e + \frac{V_e^2}{2} + gz_e\right) = \dot{m}_{water}(h_{wi} - h_{we}) + \dot{m}_{air}(h_{ai} - h_{ae})\eta = \dot{m}_{water}c_w(T_{wi} - T_{we}) - \dot{V}_{air(vent)}\rho_{air}cp_{air}(T_{in} - T_{out})(1-\eta) - \dot{V}_{air(\text{inf})}\rho_{air}cp_{air}(T_{in} - T_{out}) = \dot{m}_{water}c_w(T_{wi} - T_{we}) - Cv\,(T_{in} - T_{out}) = Q_{heating} - Q_{inf+vent} \text{ [W or kW]} \quad \text{Eq. 13}$$

However, if the ventilation system is not compensated, and the supply volumetric flow rate $\dot{V}_{air(sup)}$ is different to the exhaust volumetric flow rate $\dot{V}_{air(exh)}$, then it can be proven, that Eq. 11 will have the form of Eq. 14. Then it will be necessary to measure in the ventilation system at least the supply and return volumetric flow rates and the supply (T_{sup}) and indoor (T_{in}) temperatures (See Figure 5). For those cases, the C_v value would be estimated as in Eq. 15.

$$Q_{ventilation} = \frac{\left(\dot{V}_{air(exh)}\rho_{air}cp_{air}T_{in} - \dot{V}_{air(sup)}\rho_{air}cp_{air}T_{sup}\right)}{(T_{in} - T_{out})}(T_{in} - T_{out}) \text{ [W or kW]} \quad \text{Eq. 14}$$

$$C_v = \frac{\left(\dot{V}_{air(exh)}\rho_{air}cp_{air}T_{in} - \dot{V}_{air(sup)}\rho_{air}cp_{air}T_{sup}\right)}{(T_{in} - T_{out})} + \dot{V}_{air(\text{inf})}\rho_{air}cp_{air} \text{ [W/K or kW/K]} \quad \text{Eq. 15}$$

Then, Eq. 13 is converted into Eq. 16:

$$\sum_i \dot{m}_i\left(h_i + \frac{V_i^2}{2} + gz_i\right) - \sum_e \dot{m}_e\left(h_e + \frac{V_e^2}{2} + gz_e\right) = \dot{m}_{water}(h_{wi} - h_{we}) + \dot{m}_{air}(h_{ai} - h_{ae})\eta = \dot{m}_{water}c_w(T_{wi} - T_{we}) - \frac{\left(\dot{V}_{air(exh)}\rho_{air}cp_{air}T_{in} - \dot{V}_{air(sup)}\rho_{air}cp_{air}T_{sup}\right)}{(T_{in} - T_{out})}(T_{in} - T_{out}) - \dot{V}_{air(\text{inf})}\rho_{air}cp_{air}(T_{in} - T_{out}) = \dot{m}_{water}c_w(T_{wi} - T_{we}) - Cv\,(T_{in} - T_{out}) = Q_{heating} - Q_{inf+vent} \text{ [W or kW]} \quad \text{Eq. 16}$$

If we put together all the terms developed in Eq. 1, we then obtain the Eq. 17 expression for the complete energy balance of the building at the time instant t. In this work, the heat losses to the ground have been considered within the HLC value, as if they were working against (T_{in} – T_{out}). Note that the long wave radiative heat exchange occurring in the building envelope is again considered within the HLC value, as if they were working against (T_{in} – T_{out}). These last two assumptions are also made in the original co-heating method [27], where the UA and C_v values are also considered to be constant.

$$\frac{dU_{IE}(t)}{dt} = S_a V_{sol}(t) + K_{occupancy}(t) - UA(T_{in} - T_{out})(t) + K_{electricity}(t) + Q_{heating}(t) - Cv\,(T_{in} - T_{out})(t) \text{ [W or kW]}$$
$$\frac{dU_{IE}(t)}{dt} = S_a V_{sol}(t) + Q_{heating}(t) + K_{electricity}(t) + K_{occupancy}(t) - (UA + Cv)(T_{in} - T_{out})(t) \text{ [W or kW]} \quad \text{Eq. 17}$$

If C_v is defined as in Eq. 5, Eq. 13 or as in Eq. 15, then Eq. 17 is valid for any type of ventilation system of a building and the HLC can be estimated by:

$$HLC = (UA + C_v) \text{ [W/K or kW/K]} \quad \text{Eq. 18}$$

$$\frac{dU_{IE}(t)}{dt} = S_a V_{sol}(t) + Q_{heating}(t) + K_{electricity}(t) + K_{occupancy}(t) - HLC(T_{in} - T_{out})(t) \text{ [W or kW]} \quad \text{Eq. 19}$$

Analysing Eq. 19, it could be said that if the building's HLC is to be estimated by means of measurements, it would be necessary to make an instantaneous measurement of the energy rate being stored in the building ($\frac{dU_{IE}(t)}{dt}$), the exact solar gains at the same instant ($S_a V_{sol}(t)$), the exact instantaneous heating gains ($Q_{heating}(t)$), the exact instantaneous internal gains due to occupants and electricity consumption ($K_{electricity}(t) + K_{occupancy}(t)$) and the exact indoor to outdoor temperature difference $(T_{in} - T_{out})(t)$. Obviously, the instantaneous accumulation term is nearly impossible to measure accurately and the exact instantaneous solar gains are also difficult to measure in an in-use building. The rest of the terms can be measured accurately and instantaneously.

If $Q(t) = Q_{heating}(t)$ and $K(t)$ as in Eq. 20, then reordering Eq. 19, we obtain the Eq. 21:

$$K(t) = K_{electricity}(t) + K_{occupancy}(t) \text{ [W or kW]} \quad \text{Eq. 20}$$

$$-\frac{dU_{IE}(t)}{dt} + Q(t) + K(t) = HLC(T_{in} - T_{out})(t) - S_a V_{sol}(t) \text{ [W or kW]} \quad \text{Eq. 21}$$

Since the internal energy is a property of the system and we consider the HLC to be constant, making the integer over a period of time considered between t_1 and t_N, we can convert Eq. 21 into:

$$-\int_{u_1}^{u_N} dU_{IE}(t) + \int_{t_1}^{t_N} Q(t)dt + \int_{t_1}^{t_N} K(t)dt = HLC \int_{t_1}^{t_N} (T_{in} - T_{out})(t)dt - \int_{t_1}^{t_N} S_a V_{sol}(t)dt \text{ [J or kJ]} \quad \text{Eq. 22}$$

$$-\sum_{i=1}^{z} m_i(u_{IE_i}(t_N) - u_{IE_i}(t_1)) + \int_{t_1}^{t_N} Q(t)dt + \int_{t_1}^{t_N} K(t)dt = HLC \int_{t_1}^{t_N}(T_{in} - T_{out})(t)dt - \int_{t_1}^{t_N} S_a V_{sol}(t)dt \quad \text{[J or kJ]}$$

$$\sum_{i=1}^{z} m_i c_i(T_i(t_1) - T_i(t_N)) + \int_{t_1}^{t_N} Q(t)dt + \int_{t_1}^{t_N} K(t)dt = HLC \int_{t_1}^{t_N}(T_{in} - T_{out})(t)dt - \int_{t_1}^{t_N} S_a V_{sol}(t)dt \text{ [J or kJ]}$$

where m_i are the different mass types within the building (the analysed system), such as concrete, bricks, furniture, wood (the sum goes up to z different types of masses present within the building), which might change their temperatures (and thus their internal energy) when going from time instant t_1 to t_N. The c_i represents the different specific heats of the different masses within the system. For the air within the building, the specific heat at constant volume should be used. Since monitoring systems make discrete measurements every Δt, the integers of Eq. 22, would be converted into sums from k =1 (at t_1) to k = N (at t_N):

$$\sum_{i=1}^{z} m_i c_i(T_i(t_1) - T_i(t_N)) + \sum_{k=1}^{N} Q_k \Delta t + \sum_{k=1}^{N} K_k \Delta t = HLC \sum_{k=1}^{N}(T_{in,k} - T_{out,k})\Delta t - \sum_{k=1}^{N}(S_a V_{sol})_k \Delta t \quad \text{[J or kJ]} \qquad \text{Eq. 23}$$

Thus, if the thermal level is not equal at the start and end of the analysis period from Eq. 23, we could solve for HLC as in Eq. 24. Note that Δt cannot be cancelled because the thermal storage is a property that depends solely on the initial and final thermal level of the building and not on the time dependant path as are the rest of the variables of the equation:

$$HLC = \frac{\sum_{i=1}^{z} m_i c_i(T_i(t_1) - T_i(t_N)) + \sum_{k=1}^{N}(Q_k + K_k + (S_a V_{sol})_k)\Delta t}{\sum_{k=1}^{N}(T_{in,k} - T_{out,k})\Delta t} \text{ [W/K or kW/K]} \qquad \text{Eq. 24}$$

In Eq. 24, it can be seen that the longer the considered period is, the smaller the impact of the difference in thermal level of the building on the HLC estimate. Since the internal energy of the building is a property, it only depends on the initial and final states of the building. While the denominator increases, the longer the period is. The accumulation term is very hard to estimate accurately. The proposed average method is formed by selected periods, where the initial indoor and outdoor temperatures (at t_1) and final indoor and outdoor temperatures (at t_N) are equal. In other words, both indoor and outdoor temperatures must be equal at the start and end of the periods. Thus, the average temperature between the indoor and outdoor temperature will also be equal at t_1 and t_N.

If this is fulfilled, it can be assumed that there will be no accumulated heat in the building, since the start and end points of the analysed period will have a similar thermal level. Then, the energy accumulation inside the building will be negligible between these two time instants and it will be possible to ensure similar conditions as in the stationary stage for the selected period. Since the longer the period is, the smaller the impact of the accumulation term, as proved in Eq. 24; if the period fulfils the same initial and final thermal level conditions, applying the method to periods of at least 72 hours (three days), the accumulation term effect on the HLC, by Eq. 28, will be negligible. Therefore, if it can be assumed that $T(t_1) = T(t_N)$ for a period, then Eq. 22 can be rewritten as:

$$\sum_{i=1}^{z} m_i c_i(0) + \int_{t_1}^{t_N} Q(t)dt + \int_{t_1}^{t_N} K(t)dt = HLC \int_{t_1}^{t_N} (T_{in} - T_{out})(t)dt - \int_{t_1}^{t_N} S_a V_{sol}(t)dt \quad \text{[J or kJ]}$$

$$\int_{t_1}^{t_N} Q(t)dt + \int_{t_1}^{t_N} K(t)dt = HLC \int_{t_1}^{t_N} (T_{in} - T_{out})(t)dt - \int_{t_1}^{t_N} S_a V_{sol}(t)dt \quad \text{[J or kJ]} \qquad \text{Eq. 25}$$

Since monitoring systems make discrete measurements every Δt, the integers of Eq. 25 would be converted into sums from k =1 (at t_1) to k = N (at t_N):

$$\sum_{k=1}^{N} Q_k \Delta t + \sum_{k=1}^{N} K_k \Delta t = HLC \sum_{k=1}^{N} (T_{in,k} - T_{out,k})\Delta t - \sum_{k=1}^{N} (S_a V_{sol})_k \Delta t \quad \text{[J or kJ]} \qquad \text{Eq. 26}$$

Taking Δt as a common factor and cancelling it:

$$\sum_{k=1}^{N} Q_k + \sum_{k=1}^{N} K_k = HLC \sum_{k=1}^{N} (T_{in,k} - T_{out,k}) - \sum_{k=1}^{N} (S_a V_{sol})_k \quad \text{[W or kW]} \qquad \text{Eq. 27}$$

and, finally, reordering Eq. 27, we obtain Eq. 28:

$$HLC = \frac{\sum_{k=1}^{N} (Q_k + K_k + (S_a V_{sol})_k)}{\sum_{k=1}^{N} (T_{in,k} - T_{out,k})} \quad \text{[W/K or kW/K]} \qquad \text{Eq. 28}$$

The second term introducing uncertainties in the method application are the solar gains of Eq. 28. The method proposes using periods, not only with the same initial and final temperature of the building, but also with cold and cloudy periods where solar radiation is very low and could thus be considered purely diffuse [86]. For cloudy periods, where the radiation can be considered purely diffuse, any orientation global radiation measurement can be used since any of these measurements will be similar to a diffuse solar radiation measurement. These periods can be easily found in countries or areas where cloudy and cold days are common in winter. It must be possible to ensure that the

solar heat gains for those periods compared to the rest of the heat gains (heating (Q) + all internal gains excluding solar radiation (K)) of the building are less than 10 %. Then, if these roughly estimated solar gains have an uncertainty as large as 100 %, their effect on the HLC estimation would only be 10 %. Accurately measuring heating and internal gains is possible, while measuring solar gains accurately is a hard task. However, if only cloudy days are present in the studied period and it can be considered that only diffuse solar radiation is affecting the whole building envelope, then it is possible to make a rough estimate of the solar gains.

To make a rough estimate of the solar gains, it can be considered that multiplying the total window area of the building envelope by a g-value of 0.5 [87], a rough estimation of the solar aperture regarding the diffuse radiation can be obtained. Since diffuse radiation can be considered to be similar in all orientations, if this value is multiplied by the solar aperture, the internal gains created by the solar radiation can be estimated. Therefore, it is reasonably easy to make rough estimates of the S_aV_{sol} term in cloudy periods. Hence, due to the similarity between the results of S_aV_{sol} and S_aH_{sol} in cloudy periods, the method could be applied using any of them indistinctly.

If the period is also cold, the weight of the solar gains in the energy balance is small and enables us to make accurate estimates of the HLC, even though the solar gains are roughly calculated. This work considers a period to be cold if the average indoor to outdoor temperature difference is 10 °C or bigger. Thus, the uncertainty associated with the indoor to outdoor temperature difference is limited. For example, a 0.5 °C uncertainty in the indoor to outdoor temperature difference will only represent a 5 % error in the indoor to outdoor temperature difference. Furthermore, the method also proposes calculating the HLC, assuming the S_aV_{sol} term to be zero, as shown in Eq. 29. Thus, the effect of the solar gains of the period on the HLC can be analysed.

$$HLC_{simple} = \frac{\sum_{k=1}^{N}(Q_k+K_k)}{\sum_{k=1}^{N}(T_{in,k}-T_{out,k})} \text{ [W/K or kW/K]} \qquad \text{Eq. 29}$$

Eq. 29 introduces errors up to 10-15 % in the estimated HLCs in the considered periods of very low solar radiation, as compared to Eq. 28. However, Eq. 29, although slightly underestimated, makes it simple to obtain quite a reliable HLC value of a building. From

now on, the HLC of Eq. 28 will be named HLC, while the HLC of Eq. 29 will be named HLC_{simple}.

This proposed average method has some similar characteristics regarding the mathematical estimation method used by the ISO 9869-1 method [88] for obtaining in-situ U-values of walls. The method described by the ISO 9869-1 requires plotting the accumulated average U-value during the periods considered valid for the estimation. On those plots, a stabilization band of ±2 % of the final estimate during the last 24 hours of the testing period is required. Based on the mathematical development carried out in this work for the whole building in-use HLC estimation method, due to the complexity of a whole building when compared to a single wall analysis and considering the uncertainty limits imposed, this band will be expanded to ±10 %. In other words, the proposed average method will also perform the HLC accumulated average plots for the selected periods and should be able to provide stable HLC values within a ±10 % during the last 24 hours in order to ensure a reliable HLC estimation. Some examples of HLC accumulated average plots can be seen in Appendix A, B and C.

2.1.2- HLC application to a multizone building through the energy balance

In this section, the properties of the HLC estimation related to a multizone building are analysed. As shown in section 2.1.1, several heat gains and losses have been considered when estimating the Heat Loss Coefficient for a whole building enclosed in a control volume. However, the demonstration only considers the HLC estimation for a whole building with homogeneous indoor temperature. Section 2.1.2 explains how different thermal zones next to each other, or on different storeys located above or under each other, behave when considering the whole building HLC. It is proved how the internal heat and mass transfer effects passing from one room to another can be cancelled out through the following simple case:

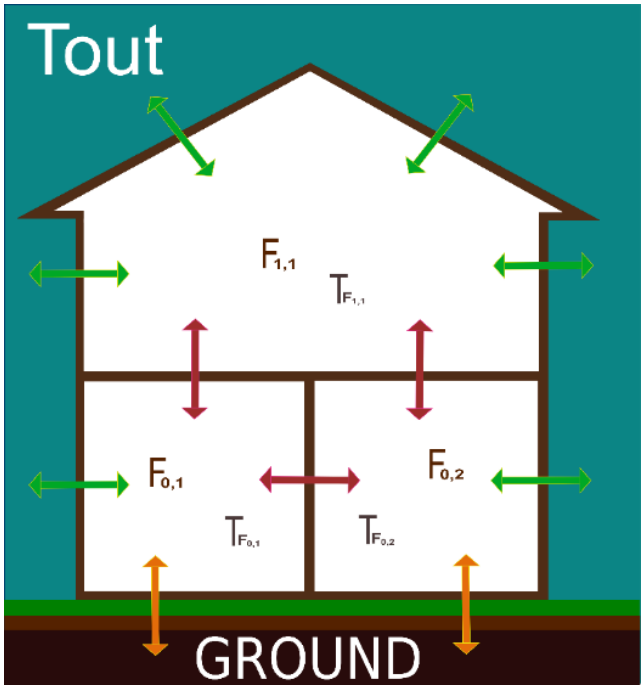

Figure 6. Schematic of all heat and mass exchanges through the multizone building. [85]

Figure 6 shows the proposed simple toy model for a multizone building. Three different zones, distributed on two floors (F0 and F1), form the building. Each zone is affected by different heat and mass exchanges, coming either from other zones, the ground or the exterior. Thus, we aim to prove that for a building with L floors and M thermal zones per floor, the building's total Heat Loss Coefficient can be estimated by applying the following formula:

$$HLC_{sum} = \sum_{i=1}^{L} \sum_{j=1}^{M} HLC_{Fi,j} \quad \text{Eq. 30}$$

$$HLC_{sum} = HLC_{F0,1} + HLC_{F0,2} + HLC_{F1,1} \text{ [W/K or kW/K]} \quad \text{Eq. 31}$$

where each zone HLC can be estimated by applying Eq. 28 directly to each zone as if they were only affected by $(T_{Fi,j} - T_{out})$. For clarity, the sum from k = 1 to k = N is not shown in this section developments. The sum is only presented in the generalized equations Eq. 44 and Eq. 49.

$$HLC_{F0,1} = \frac{[Q_{F0,1} + K_{F0,1} + (S_a V_{sol})_{F0,1}]}{(T_{F0,1} - T_{out})} \text{ [W/K or kW/K]} \quad \text{Eq. 32}$$

$$HLC_{F0,2} = \frac{[Q_{F0,2} + K_{F0,2} + (S_a V_{sol})_{F0,2}]}{(T_{F0,2} - T_{out})} \text{ [W/K or kW/K]} \quad \text{Eq. 33}$$

$$HLC_{F1,1} = \frac{[Q_{F1,1} + K_{F1,1} + (S_a V_{sol})_{F1,1}]}{(T_{F1,1} - T_{out})} \text{ [W/K or kW/K]} \quad \text{Eq. 34}$$

In this example, two zones are on the ground floor and another one on the first floor. Thus, the whole energy balance of each zone (Eq. 35 to Eq. 37) is presented considering all transmission and infiltration exchanges for each of them:

Ground floor (zone F0,1):

$$Q_{F0,1} + K_{F0,1} + (S_a V_{sol})_{F0,1} = UA_{F0,1-ground}(T_{F0,1} - T_{ground}) + UA_{F0,1-F0,2}(T_{F0,1} - T_{F0,2}) + UA_{F0,1-F1,1}(T_{F0,1} - T_{F1,1}) + UA_{F0,1-out}(T_{F0,1} - T_{out}) + \dot{V}_{F0,1-F0,2}\rho_{air}cp_{air}(T_{F0,1} - T_{F0,2}) + \dot{V}_{F0,1-F1,1}\rho_{air}cp_{air}(T_{F0,1} - T_{F1,1}) + C_{v\,F0,1-out}(T_{F0,1} - T_{out})\ \text{[W or kW]} \quad \text{Eq. 35}$$

Ground floor (zone F0,2):

$$Q_{F0,2} + K_{F0,2} + (S_a V_{sol})_{F0,2} = UA_{F0,2-ground}(T_{F0,2} - T_{ground}) + UA_{F0,2-F0,1}(T_{F0,2} - T_{F0,1}) + UA_{F0,2-F1,1}(T_{F0,2} - T_{F1,1}) + UA_{F0,2-out}(T_{F0,2} - T_{out}) + \dot{V}_{F0,2-F0,1}\rho_{air}cp_{air}(T_{F0,2} - T_{F0,1}) + \dot{V}_{F0,2-F1,1}\rho_{air}cp_{air}(T_{F0,2} - T_{F1,1}) + C_{v\,F0,2-out}(T_{F0,2} - T_{out})\ \text{[W or kW]} \quad \text{Eq. 36}$$

First floor (zone F1,1):

$$Q_{F1,1} + K_{F1,1} + (S_a V_{sol})_{F1,1} = UA_{F1,1-F0,2}(T_{F1,1} - T_{F0,2}) + UA_{F1,1-F0,1}(T_{F1,1} - T_{F0,1}) + UA_{F1,1-out}(T_{F1,1} - T_{out}) + \dot{V}_{F1,1-F0,2}\rho_{air}cp_{air}(T_{F1,1} - T_{F0,2}) + \dot{V}_{F1,1-F0,1}\rho_{air}cp_{air}(T_{F1,1} - T_{F0,1}) + C_{v\,F1,1-out}(T_{F1,1} - T_{out})\ \text{[W or kW]} \quad \text{Eq. 37}$$

Since the average method considers periods with negligible energy accumulation within the building, when Eq. 35 to Eq. 37 are summed, the energy transfers through internal walls due to transmission and infiltration between the considered zones are cancelled out. Then, only heat and mass transfers between indoor and outdoor air and heat transfer between floor 0 zones and ground remain.

$$[Q_{F0,1} + K_{F0,1} + (S_a V_{sol})_{F0,1}] + [Q_{F0,2} + K_{F0,2} + (S_a V_{sol})_{F0,2}] + [Q_{F1,1} + K_{F1,1} + (S_a V_{sol})_{F1,1}] = UA_{F0,1-ground}(T_{F0,1} - T_{ground}) + UA_{F0,1-out}(T_{F0,1} - T_{out}) + C_{v\,F0,1-out}(T_{F0,1} - T_{out}) + UA_{F0,2-ground}(T_{F0,2} - T_{ground}) + UA_{F0,2-out}(T_{F0,2} - T_{out}) + C_{v\,F0,2-out}(T_{F0,2} - T_{out}) + UA_{F1,1-out}(T_{F1,1} - T_{out}) + C_{v\,F1,1-out}(T_{F1,1} - T_{out})\ \text{[W or kW]} \quad \text{Eq. 38}$$

Taking $\left(T_{F_{i,j}} - T_{out}\right)$ as the common factor for each zone:

$$[Q_{F0,1} + K_{F0,1} + (S_a V_{sol})_{F0,1}] + [Q_{F0,2} + K_{F0,2} + (S_a V_{sol})_{F0,2}] + [Q_{F1,1} + K_{F1,1} + (S_a V_{sol})_{F1,1}] = \left(UA_{F0,1-ground}\frac{(T_{F0,1}-T_{ground})}{(T_{F0,1}-T_{out})} + UA_{F0,1-out} + C_{v\,F0,1-out}\right)(T_{F0,1} - T_{out}) + \left(UA_{F0,2-ground}\frac{(T_{F0,2}-T_{ground})}{(T_{F0,2}-T_{out})} + UA_{F0,2-out} + C_{v\,F0,2-out}\right)(T_{F0,2} - T_{out}) + \left(UA_{F1,1-out} + C_{v\,F1,1-out}\right)(T_{F1,1} - T_{out})\ \text{[W or kW]} \quad \text{Eq. 39}$$

Since $HLC_{Fi,j} = UA_{Fi,j-out} + C_{v\,Fi,j-out}$, and reordering Eq. 39, we obtain Eq. 40:

$$[Q_{F0,1} + K_{F0,1} + (S_a V_{sol})_{F0,1}] + [Q_{F0,2} + K_{F0,2} + (S_a V_{sol})_{F0,2}] + [Q_{F1,1} + K_{F1,1} + (S_a V_{sol})_{F1,1}] = HLC_{F0,1}\left(T_{F0,1} - T_{out}\right) + HLC_{F0,2}\left(T_{F0,2} - T_{out}\right) + HLC_{F1,1}\left(T_{F1,1} - T_{out}\right) \quad \text{Eq. 40}$$

[W or kW]

Eq. 40 proves that the only valid solution for any $T_{Fi,j}$ is the one provided by Eq. 32 to Eq. 34 for each of the $HLC_{Fi,j}$ of Eq. 40, where each $HLC_{Fi,j}$ has only the indoor to outdoor $UA_{Fi,j-out}$ and $C_{v\,Fi,j-out}$ values within it. Remember that the $HLC_{F0,j}$ of the ground floor also includes the UA value against the ground multiplied by the factor $\frac{(T_{F0,j}-T_{ground})}{(T_{F0,j}-T_{out})}$.

Thus, it has been proven that the whole building Heat Loss Coefficient can be estimated by the sum of the individual zones $HLC_{Fi,j}$ as if they were only exchanging heat and mass with the outdoor air:

$$HLC_{sum} = \frac{[Q_{F0,1}+K_{F0,1}+(S_a V_{sol})_{F0,1}]}{(T_{F0,1}-T_{out})} + \frac{[Q_{F0,2}+K_{F0,2}+(S_a V_{sol})_{F0,2}]}{(T_{F0,2}-T_{out})} + \frac{[Q_{F1,1}+K_{F1,1}+(S_a V_{sol})_{F1,1}]}{(T_{F1,1}-T_{out})} = HLC_{F0,1} + HLC_{F0,2} + HLC_{F1,1}\ \text{[W/K or kW/K]} \quad \text{Eq. 41}$$

Where the generic equation of each zone (or floor) can be presented as Eq. 42 for the simple HLC and Eq. 43 for the HLC:

$$HLC_{simple\_Fi,j} = \frac{(Q_{Fi,j}+K_{Fi,j})}{(T_{Fi,j}-T_{out})}\ \text{[W/K or kW/K]} \quad \text{Eq. 42}$$

$$HLC_{Fi,j} = \frac{(Q_{Fi,j}+K_{Fi,j}+(S_a V_{sol})_{Fi,j})}{(T_{Fi,j}-T_{out})}\ \text{[W/K or kW/K]} \quad \text{Eq. 43}$$

Hence, generalizing the example to a building with L floors and M zones per floor, Eq. 41 can be written as Eq. 44. Considering Eq. 28 of section 2.1.1, it can be written as the sum of N time step measurements for the period k =1 (at t_1) to k = N (at t_N):

$$HLC_{sum} = \sum_{i=1}^{L}\sum_{j=1}^{M} HLC_{Fi,j} = \sum_{i=1}^{L}\sum_{j=1}^{M}\sum_{k=1}^{N} \frac{(Q_{i,j,k}+K_{i,j,k}+(S_aV_{sol})_{i,j,k})}{(T_{i,j,k}-T_{out,k})} \text{ [W/K or kW/K]} \quad \text{Eq. 44}$$

From the previous analysis, it can be concluded that it is possible to develop a precise estimation of the whole building HLC estimating the Heat Loss Coefficients for each thermal zone and summing them, since the transmissions and infiltration through the walls between the zones are cancelled out in this overall summation process. Moreover, it must be commented that there is no physical meaning when measuring the HLCs of each zone independently, since this parameter considers the heat transmitted from one room to another. Those effects are only cancelled when all individual HLCs are summed for the whole building. The individual HLC of each zone will only be physically meaningful when the same indoor temperature is found in all the building's zones. Only there, each zone HLC will be representing the HLC regarding the indoor to outdoor exchange effects. For this specific case, where all $T_{Fi,j}$=T_{in}, then Eq. 41 becomes Eq. 45:

$$HLC_{sum} = \frac{[Q_{F0,1}+K_{F0,1}+(S_aV_{sol})_{F0,1}]+[Q_{F0,2}+K_{F0,2}+(S_aV_{sol})_{F0,2}]+[Q_{F1,1}+K_{F1,1}+(S_aV_{sol})_{F1,1}]}{(T_{in}-T_{out})} =$$

$$HLC_{F0,1} + HLC_{F0,2} + HLC_{F1,1} \text{ [W/K or kW/K]} \quad \text{Eq. 45}$$

However, the proposed zone-by-zone development for the HLC estimation, as far as concerned, has not been used in order to estimate the HLC of a whole building. Instead of the HLC_{sum}, in previous works, the $HLC_{building}$ has usually been estimated considering the whole building is a unique thermal zone.

In order to estimate the $HLC_{building}$, Eq. 48 must be used, here, the sum of all the input parameters must be introduced (heating system's heat, occupancy and solar gains) for the whole building. Moreover, the indoor temperature must be calculated as a unique indoor temperature. Usually two different methods are used: the average temperature method (Eq. 46) and the volume weighted average temperature method (Eq. 47).

$$T_{in} = \frac{T_{F0,1}+T_{F0,2}+T_{F1,1}}{3} \text{ [K or °C]} \quad \text{Eq. 46}$$

$$T_{in} = \frac{T_{F0,1}*V_{F0,1}+T_{F0,2}*V_{F0,2}+T_{F1,1}*V_{F1,1}}{V_{F0,1}+V_{F0,2}+V_{F1,1}} \text{ [K or °C]} \quad \text{Eq. 47}$$

Using the simple average temperature method, the formula in order to obtain the Figure 6 example building $HLC_{building}$ is the following:

$$HLC_{building} = \frac{[Q_{F0,1}+Q_{F0,2}+Q_{F1,1}]+[K_{F0,1}+K_{F0,2}+K_{F1,1}]+[(S_aV_{sol})_{F0,1}+(S_aV_{sol})_{F0,2}+(S_aV_{sol})_{F1,1}]}{\left(\frac{[T_{F0,1}+T_{F0,2}+T_{F1,1}]}{3}-T_{out}\right)} =$$

$$\frac{[Q_{F0,1}+Q_{F0,2}+Q_{F1,1}]+[K_{F0,1}+K_{F0,2}+K_{F1,1}]+[(S_aV_{sol})_{F0,1}+(S_aV_{sol})_{F0,2}+(S_aV_{sol})_{F1,1}]}{(T_{in}-T_{out})} \text{ [W/K or kW/K]} \quad \text{Eq. 48}$$

Generalizing Eq. 48 to a building with L floors and M zones per floor, $HLC_{building}$ can be written as Eq. 49. Once again, considering Eq. 28 of section 2.1.1, it can be written as the sum of N time step measurements for the period k =1 (at t_1) to k = N (at t_N):

$$HLC_{building} = \sum_{k=1}^{N} \frac{[\sum_{i=1}^{L}\sum_{j=1}^{M} Q_{i,j}+\sum_{i=1}^{L}\sum_{j=1}^{M} K_{i,j}+\sum_{i=1}^{L}\sum_{j=1}^{M}(S_aV_{sol})_{i,j}]_k}{(T_{in,k}-T_{out,k})} \text{ [W/K or kW/K]} \quad \text{Eq. 49}$$

The estimation of an average unique indoor temperature can affect considerably the final $HLC_{building}$ estimation regarding the HLC_{sum} estimation value. Information is lost due to the indoor temperature averaging process. Therefore, the Eq. 44 should provide more accurate results since each thermal zone has been analysed individually.

2.1.3- Error propagation

The existence of uncertainty due to measurements will be analysed in this section, since uncertainty sources due to modelling have already been detected and limited in section 2.1.1. In this section, all uncertainties, excluding the one related to the disregarding of the accumulation term, are propagated to the estimation of the HLC. The effect of the accumulation term on the HLC estimate is assumed to be close to zero, considering the length of the period and the same thermal level condition to be established at the start and end of the valid data periods, as described in section 2.1.1.

The error propagation method used in this section is based on the book [89]. The propagation of errors has been applied to the already presented Eq. 28 Heat Loss Coefficient formula, but using the period averaged values for all the variables:

$$HLC = \frac{\sum_{k=1}^{N}(Q_k+K_k+(S_aV_{sol})_k)}{\sum_{k=1}^{N}(T_{in,k}-T_{out,k})} = \frac{\frac{\sum_{k=1}^{N}(Q_k+K_k+(S_aV_{sol})_k)}{N}}{\frac{\sum_{k=1}^{N}(T_{in,k}-T_{out,k})}{N}} = \frac{\bar{Q}+\bar{K}+\overline{S_aV_{sol}}}{\overline{T_{in}}-\overline{T_{out}}} \text{ [W/K or kW/K]} \quad \text{Eq. 50}$$

The propagation of error for the addition and subtraction in Eq. 50 should be estimated first:

$$HLC = \frac{(\bar{Q}\pm\delta\bar{Q}) + (\bar{K}\pm\delta\bar{K}) + (\overline{S_aV_{sol}}\pm\delta\overline{S_aV_{sol}})}{(\overline{T_{in}}\pm\delta\overline{T_{in}}) - (\overline{T_{out}}\pm\delta\overline{T_{out}})} = \frac{(\bar{Q}+\bar{K}+\overline{S_aV_{sol}}) \pm (\delta\bar{Q}+\delta\bar{K}+\delta\overline{S_aV_{sol}})}{(\overline{T_{in}}-\overline{T_{out}})\pm(\delta\overline{T_{in}}+\delta\overline{T_{out}})} \text{ [W/K or kW/K]} \quad \text{Eq. 51}$$

In Eq. 51, all terms' uncertainties are considered, including that of the roughly estimated solar gains. Finally, the propagation error for the division in Eq. 51 must be calculated in order to estimate the error propagation when estimating the HLC of the building or of a thermal zone within the building:

$$HLC = \frac{(\bar{Q}+\bar{K}+\overline{S_aV_{sol}}) \pm (\delta\bar{Q}+\delta\bar{K}+\delta\overline{S_aV_{sol}})}{(\overline{T_{in}}-\overline{T_{out}})\pm(\delta\overline{T_{in}}+\delta\overline{T_{out}})} =$$

$$\frac{(\bar{Q}+\bar{K}+\overline{S_aV_{sol}})}{(\overline{T_{in}}-\overline{T_{out}})} \pm \left|\frac{(\bar{Q}+\bar{K}+\overline{S_aV_{sol}})}{(\overline{T_{in}}-\overline{T_{out}})}\right| \cdot \left(\frac{(\delta\bar{Q}+\delta\bar{K}+\delta\overline{S_aV_{sol}})}{|\bar{Q}+\bar{K}+\overline{S_aV_{sol}}|} + \frac{(\delta\overline{T_{in}}+\delta\overline{T_{out}})}{|\overline{T_{in}}-\overline{T_{out}}|}\right) \text{ [W/K or kW/K]} \quad \text{Eq. 52}$$

2.2- Methodology to estimate the effect of the solar gains through opaque walls in buildings

During the development of the average method in section 2.1.1 for a proper estimation of the HLC in in-use buildings, the importance of the solar gains has been remarked. Therefore, a specific requirement has been established for its weight when estimating the HLC for in use-buildings. In order to reduce the uncertainties created by this parameter, the method has established that the selected period should only consider cold and cloudy periods where the effect of the solar radiation entering through the windows is considerably low.

However, as commented in section 2.1.1, only the solar radiation entering through the windows has been considered for the average method developed. However, it is important to consider also the impact the solar gains though the opaque walls of the building could have in the HLC results, since not considering them could create a considerable error in the estimates. Despite it is assumed that the fixed requirement regarding only considering cold and cloudy periods would also reduce the weight of the solar gains through the opaque walls in the HLC value, it has not been demonstrated yet.

Therefore, the description of the deep analysis performed in order to estimate the effect the corresponding solar radiation has in the inner surface heat flux of each individual opaque wall is presented in this section. Despite the methodology is applicable for any opaque building envelope element facing solar radiation, the methodology has been carried out based on the opaque walls of the well monitored Round Robin Box (a small scale well monitored building, see Figure 7) presented later in section 3.1.

Figure 7. The small scale "building" named Round Robin Box.

2.2.1- Theoretical quantification of the solar factor and the effect of the solar radiation on the inner surface heat flux of opaque walls under steady-state conditions

Due to the heating effect of the solar radiation on the outer surface of opaque walls, the inner surface heat flux going outwards through opaque walls is reduced. This effect is mathematically quantified for a general opaque wall presented in Figure 8 under steady-state assumptions. This mathematical development is also valid for any other opaque building envelope element facing solar radiation. Finally, this inner surface heat flux reduction effect is transferred to the estimation techniques of the Heat Loss Coefficient of in-use buildings where an unknown identifiable constant solar gain value is not used, as the average method developed in section 2.1.

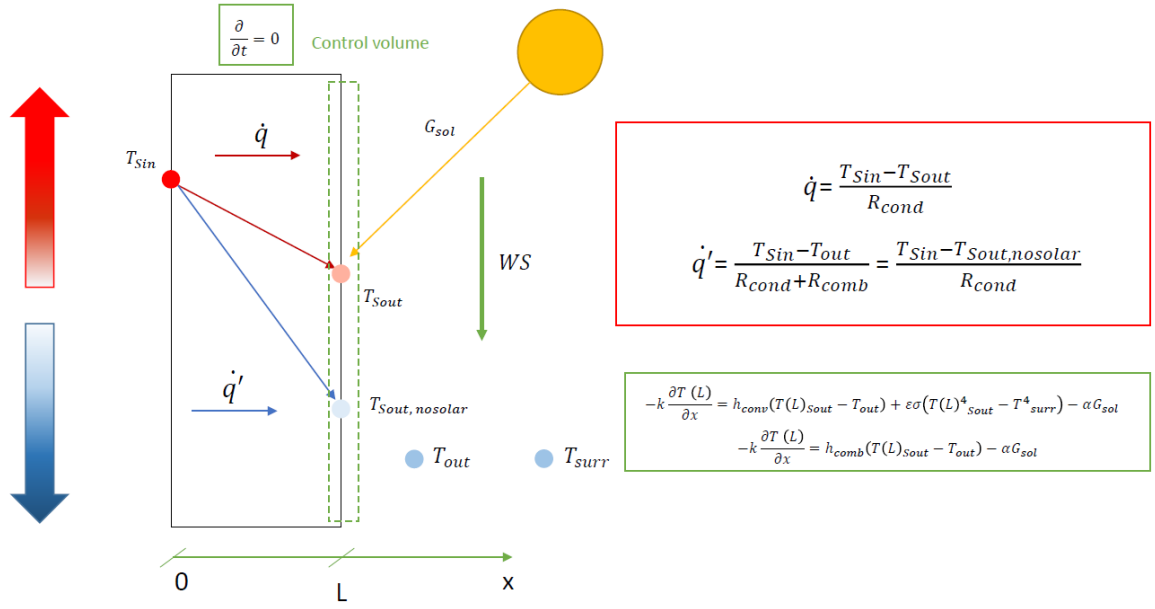

Figure 8. Energy balance representation in a massless control volume representing the outer surface of an opaque wall.

Even if the opaque elements of building envelopes are subjected to a dynamic behaviour, since they operate for very long periods of time, doing a steady-state analysis can give very valuable results. For example, the Heating Degree Days method permits us to obtain the annual heating demand of a building based on steady-state assumptions [90]. However, depending on the thermal mass and level of insulation of the element, the solar radiation effect on its outer surface will take more or less time to affect the inner surface heat flux; so, for a long period analysis, the dynamic effects become negligible and thus a steady-state analysis will be performed. Of course, the higher the insulation level of the building element, the lower will the effect of the solar radiation be on the inner surface heat flux.

In Figure 8, two inner surface heat fluxes are represented, the $\dot{q}$, which is the real inner surface heat flux considering the solar radiation effect, and $\dot{q}'$, which is the hypothetical inner surface heat flux without considering the solar radiation effect. The aim of this mathematical development is to relate $\dot{q}$ with $\dot{q}'$, based on the typical physical knowledge on common opaque building envelope elements. Of course, since this development assumes the steady-state assumption, the conduction heat flux will be the same in any other position within the opaque wall, including the outer surface. Then, applying the energy balance to the massless control volume representing the outer surface of the wall, we obtain Eq. 53.

$$\dot{q} = -k\frac{\partial T\,(L)}{\partial x} = h_{conv}(T_{Sout} - T_{out}) + \varepsilon\sigma({T^4}_{Sout} - {T^4}_{surr}) - \alpha G_{sol} \text{ [W/m}^2\text{]} \quad \text{Eq. 53}$$

Eq. 53 shows the three main terms related with three important phenomena that may affect the outer surface of the wall. The solar radiation is one of them. The effect of this phenomena is considered in the last term of the formula (αG_{sol}), where α represents the outer surface solar absorptivity and G_{sol} represents the global solar radiation incident on the outer surface of the wall.

The middle term, $\varepsilon\sigma({T^4}_{Sout} - {T^4}_{surr})$, considers the heat exchange due to the long wave radiation on the outer surface of the wall. T_{Sout} is the real outer surface temperature of the wall, considering the solar radiation effect (see Figure 8). Furthermore, the parameters ε and σ represent the emissivity of the wall's outer surface and the Stefan Boltzmann constant (5.67 x 10^{-8} [W/m^{2}K^4]), respectively. However, the temperature of the surroundings T_{surr} will vary, depending on the wall. As shown in Eq. 53, for the vertical walls, T_{surr} must be used. Nevertheless, for the ceiling and the floor, T_{sky} and T_{ground}, respectively, must be used. In this research, the surrounding temperature and the sky temperature can be obtained thanks to the available measurements of the vertical south (V_{LW}) and the horizontal (H_{LW}) long wave radiation.

$$T_{surr} = \sqrt[4]{\frac{(V_{LW})^2}{\sigma}} \text{ [K]} \quad \text{Eq. 54}$$

$$T_{sky} = \sqrt[4]{\frac{(H_{LW})^2}{\sigma}} \text{ [K]} \quad \text{Eq. 55}$$

However, since no long wave radiation measurement is available for the ground temperature estimation, a good approximation of the ground temperature is obtained, assuming the ground temperature tends to the sol-air temperature defined in ASHRAE [91]. Then, Eq. 56 is taken from ASHRAE [91] to estimate the ground temperature.

$$T_{ground} = T_{out} + \frac{\alpha \times G_{sol}}{h_{comb}} + \frac{\varepsilon \times \Delta R}{h_{comb}} \text{ [K]} \quad \text{Eq. 56}$$

where T_{out} is the outdoor air temperature [°C], α is the absorptance of the ground surface for the solar radiation [-], G_{sol} is the global solar radiation incident on the ground surface [W/m^2], h_{comb} is the combined coefficient of heat transfer by long wave radiation and convection at ground surface [W/m^{2}K], Ɛ is the hemispherical emittance of the

ground surface [-], and ΔR is the difference between the long-wave radiation incident on the surface from the sky and surroundings and the radiation emitted by a blackbody at outdoor air temperature [W/m^2]. Thus, Eq. 56 should provide very similar results to the real temperature of the ground surface.

However, the use of these temperatures complicates the mathematical development considerably. ASHRAE [91] remarked that for vertical walls, in common practice, it is assumed that the $\varepsilon\Delta R$ term is 0. Then, the correction factor between the surrounding temperature and outdoor air temperature equals 0. In conclusion, it can be assumed that $T_{surr} \approx T_{out}$. In the case of the horizontal surfaces, the $\varepsilon\Delta R$ correction term is close to 4 °C. However, due to the difficulties in estimating the horizontal long wave radiation and, consequently, the sky temperature, it is common to assume that $T_{sky} \approx T_{out}$. The same assumption is made for the floor case ($T_{ground} \approx T_{out}$). Despite the fact that these assumptions are considered for the development of this mathematical development section, the calculations carried out in section 2.2.3 are done using the measured surrounding (Eq. 54) and sky (Eq. 55) temperatures and the estimated ground (Eq. 56) temperature.

Finally, the last term ($h_{conv}(T_{Sout} - T_{out})$) can be used to introduce the effect of the wind speed on the inner surface heat flux estimation. Therefore, a correlation between the wind speed and the convection heat transfer coefficient (h_{conv}) should be found and fixed. However, the convection heat transfer coefficient can also be estimated without considering the effect of the wind speed.

All the phenomena that are going to be studied in detail have been presented. Thus, linearizing the radiation heat exchange term of Eq. 53 as done in [92], Eq. 58 is obtained. Finally, combining the convection heat transfer coefficient (h_{conv}) with the linearized radiation heat transfer coefficient (h_{rad}), the combined convection-radiation heat transfer coefficient ($h_{comb} = h_{conv} + h_{rad}$) can be obtained, as represented in Eq. 59.

$$\dot{q} = -k\frac{\partial T\,(L)}{\partial x} = h_{conv}(T_{Sout} - T_{out}) + \varepsilon\sigma({T^4}_{Sout} - {T^4}_{out}) - \alpha G_{sol}\ [\mathrm{W/m^2}] \qquad \text{Eq. 57}$$

$$\dot{q} = -k\frac{\partial T\,(L)}{\partial x} = h_{conv}(T_{Sout} - T_{out}) + h_{rad}(T_{Sout} - T_{out}) - \alpha G_{sol}\ [\mathrm{W/m^2}] \qquad \text{Eq. 58}$$

$$\dot{q} = -k\frac{\partial T\,(L)}{\partial x} = h_{comb}(T_{Sout} - T_{out}) - \alpha G_{sol}\ [\mathrm{W/m^2}] \qquad \text{Eq. 59}$$

Since we assume the steady-state conditions, $\dot{q}$ can also be calculated from the inner surface temperature to outdoor surface temperature by means of Eq. 60. R_{cond} represents the sum of all the conduction resistances of the opaque wall, represented in Figure 8. Note that the analysis could also be performed from the indoor air temperature by also considering the inner surface convection-radiation heat transfer coefficient added to the R_{cond}. As the models developed further; in order to avoid uncertainties associated to the inner surface convection-radiation heat transfer coefficient, the equations consider the inner surface as their boundary. Then, this mathematical development has been performed from the inner surface instead of from the indoor air.

$$\dot{q} = -k\frac{\partial T\,(L)}{\partial x} = \left(\frac{T_{Sin}-T_{Sout}}{R_{cond}}\right)\ [\mathrm{W/m^2}] \qquad \text{Eq. 60}$$

Combining Eq. 59 and Eq. 60, we can solve for T_{Sout} as done in Eq. 61.

$$\begin{gathered}\left(\frac{T_{Sin}-T_{Sout}}{R_{cond}}\right) = \frac{1}{R_{comb}}\left(T_{Sout} - T_{out}\right) - \alpha G_{sol}\\ 0 = -\frac{T_{Sin}}{R_{cond}} + \frac{T_{Sout}}{R_{cond}} + \frac{T_{Sout}}{R_{comb}} - \frac{T_{out}}{R_{comb}} - \alpha G_{sol}\\ T_{Sout}\left(\frac{1}{R_{cond}} + \frac{1}{R_{comb}}\right) = \frac{T_{Sin}}{R_{cond}} + \frac{T_{out}}{R_{comb}} + \alpha G_{sol}\end{gathered} \qquad \text{Eq. 61}$$

$$T_{Sout} = \frac{\frac{T_{Sin}}{R_{cond}}+\frac{T_{out}}{R_{comb}}+\alpha G_{sol}}{\left(\frac{1}{R_{cond}}+\frac{1}{R_{comb}}\right)} = \frac{T_{Sin}R_{comb}+T_{out}\,R_{cond}+\alpha G_{sol}R_{cond}\,R_{comb}}{R_{cond}+R_{comb}}\ [°\mathrm{C}]$$

With Eq. 61, a mathematical expression of the real outer surface temperature has been obtained, based on the inner surface temperature, the outdoor air temperature, the global solar radiation incident on the outermost surface of the opaque wall and the typical physical parameters known for a general opaque wall. Now, the real heat flux $\dot{q}$, that considers the solar radiation incident on the outermost surface of the wall, and the hypothetical heat flux $\dot{q}'$, that would occur in the absence of solar radiation on the outermost surface of the opaque wall, are related. The form the hypothetical heat flux $\dot{q}'$ would have in the absence of solar radiation is shown in Eq. 62.

$$\dot{q}' = \left(\frac{T_{Sin}-T_{out}}{R_{cond}+R_{comb}}\right)\ [\mathrm{W/m^2}] \qquad \text{Eq. 62}$$

If the T_{Sout} expression of Eq. 61 is introduced in the expression of Eq. 60, the right-hand term of Eq. 62 must be searched for in the development. Once this term is found, it is known that the rest of the terms that are not the right-hand term of Eq. 62 represent the effect the solar radiation has on the inner surface heat flux of the analysed wall.

$$\dot{q} = \frac{T_{Sin} - \left(\frac{T_{Sin}R_{comb} + T_{out}\,R_{cond} + \alpha G_{sol}R_{cond}\,R_{comb}}{R_{cond}\;+\;R_{comb}}\right)}{R_{cond}} =$$

$$= \frac{T_{Sin}(R_{cond}\;+\;R_{comb}) - T_{Sin}R_{comb} - T_{out}\,R_{cond} - \alpha G_{sol}R_{cond}\,R_{comb}}{R_{cond}\,(R_{cond}\;+\;R_{comb})} = \quad \text{Eq. 63}$$

$$= \frac{T_{Sin}R_{cond} - T_{out}\,R_{cond} + T_{Sin}R_{comb} - T_{Sin}R_{comb} - \alpha G_{sol}R_{cond}\,R_{comb}}{R_{cond}\,(R_{cond} + R_{comb})} \ [\mathrm{W/m^2}]$$

$$\dot{q} = \frac{T_{Sin} - T_{out}}{(R_{cond} + R_{comb})} - \frac{\alpha G_{sol}\,R_{comb}}{(R_{cond} + R_{comb})} = \dot{q}' - \frac{\alpha G_{sol}\,R_{comb}}{(R_{cond} + R_{comb})} \ [\mathrm{W/m^2}]$$

Analysing Eq. 63, it is found that the real heat flux on the inner surface of the wall $\dot{q}$ is equal to the hypothetical heat flux $\dot{q}'$ as if there was no solar radiation, minus the term $\frac{\alpha G_{sol}\,R_{comb}}{(R_{cond} + R_{comb})}$, which represents the reduction effect of the global solar radiation on the inner surface heat flux. Thus, the theoretical quantification of the effect of the solar radiation on the inner surface heat flux of opaque walls under steady-state conditions can be obtained by means of Eq. 64.

$$\dot{q}_{dif} = \dot{q}' - \dot{q} = \frac{\alpha G_{sol}\,R_{comb}}{(R_{cond} + R_{comb})} \ [\mathrm{W/m^2}] \quad \text{Eq. 64}$$

If this term is big enough, it can make the inner surface heat flux negative; remember that a negative inner surface heat flux is actually a heat gain to the interior of the building.

Note that, if the temperature simplification had not been done in Eq. 57, the h_{comb} could not be obtained, since Eq. 58 would be as follows:

$$\dot{q} = -k\frac{\partial T\,(L)}{\partial x} = h_{conv}(T_{Sout} - T_{out}) + h_{rad}(T_{Sout} - T_{surr}) - \alpha G_{sol} \ [\mathrm{W/m^2}] \quad \text{Eq. 65}$$

Then, the corresponding Eq. 63, obtained from this Eq. 65, would be Eq. 66:

$$\dot{q} = \frac{T_{Sin}(R_{conv}+1+R_{rad}-R_{conv}R_{rad}) - T_{out}R_{rad}}{(R_{cond} + R_{rad}+R_{conv})} - \frac{T_{surr}R_{conv}}{(R_{cond} + R_{rad}+R_{conv})} - \frac{\alpha G_{sol}\,R_{rad}R_{conv}}{(R_{cond} + R_{rad}+R_{conv})} \ [\mathrm{W/m^2}] \quad \text{Eq. 66}$$

However, since this form does not permit the analytical solution, the form developed in Eq. 63 will be used to show the relationship of the solar radiation effect on the inner surface with the g-value. However, in the calculation carried out in section 2.2.3, the real temperatures (T_{surr}, T_{sky} and T_{ground}) are considered.

Then, making a parallelism with the solar factor (g-value) concept for windows, the solar factor of an opaque wall under steady-state conditions would have the following expression:

$$g - value = \frac{\frac{\alpha G_{sol} R_{comb}}{(R_{cond} + R_{comb})}}{G_{sol}} = \frac{\alpha R_{comb}}{(R_{cond} + R_{comb})} \text{ [-]} \quad \text{Eq. 67}$$

Of course, another way of obtaining the solar factor of the opaque walls would be the use of Eq. 64 in Eq. 67, as shown in Eq. 68.

$$g - value = \frac{\dot{q}\prime - \dot{q}}{G_{sol}} \text{ [-]} \quad \text{Eq. 68}$$

It is important to have both Eq. 67 and Eq. 68, since Eq. 67 permits us to estimate the solar factor of an opaque element based solely on physical parameters of the wall or roof. The use of Eq. 67 has a problem; although R_{cond} can be obtained with a high accuracy based on the typical construction material properties, the solar absorptivity (α) values of the outermost surfaces of the building components are not always known with a high accuracy and, in real life, the combined convection-radiation heat transfer coefficient (R_{comb}) is time dependent. Many standards fix this R_{comb} at 0.04 m^2K/W [93].

Nevertheless, Eq. 68 would permit us to obtain the solar factor of the opaque element based on in-situ measurements of the inner surface heat flux ($\dot{q}$), the estimation of the hypothetical inner surface heat flux ($\dot{q}'$) in the absence of solar radiation and the incident global solar radiation measurement on the outer surface of the opaque element. The use of Eq. 68 has two problems; the first is the impossibility of measuring the hypothetical inner surface heat flux ($\dot{q}'$), since it is not real. This problem can be overcome by means of fitting a model of the opaque building envelope using measured data and system identification techniques. Once the model parameters have been identified, they can be fixed and the inner surface heat flux estimated by running the fitted model without considering the solar radiation on the outermost surface of the opaque element. Thus, the hypothetical inner surface heat flux ($\dot{q}'$) would be obtained.

The second problem is the lack of steady-state conditions on in-situ opaque elements in real life. The latter can be overcome by using sufficiently long period averaged values for $\dot{q}$, $\dot{q}'$ and G_{sol} [29]. That is, instead of using Eq. 68 with instantaneous values, periods of several days should be analysed and the period averaged $\bar{\dot{q}}$, $\bar{\dot{q}}'$ and $\overline{G_{sol}}$ values should be used, as in Eq. 69.

$$g - value = \frac{\bar{\dot{q}}\prime - \bar{\dot{q}}}{\overline{G_{sol}}} \text{ [-]} \quad \text{Eq. 69}$$

Finally, for long enough periods where the heat accumulation term within the wall becomes negligible in comparison with the rest of heat exchanges within the wall, it is also possible to check the period averaged effect the solar radiation has on the inner surface heat flux of opaque building elements by using the period averaged form of Eq. 64 presented in Eq. 70.

$$\bar{\dot{q}}' - \bar{\dot{q}} = \frac{\alpha \overline{G_{sol}} R_{comb}}{(R_{cond} + R_{comb})} \text{ [W/m}^2\text{]} \qquad \text{Eq. 70}$$

If the period averaged $\frac{\alpha \overline{G_{sol}} R_{comb}}{(R_{cond} + R_{comb})}$ term is significant, neglecting the blocking effect (or even inversion effects on the inner surface heat flux) created by the solar radiation, it should be considered in the different techniques where whole building envelope Heat Loss Coefficients are estimated.

Thus, the main aim of this research is to prove, on a practical basis, the validity of Eq. 69 and Eq. 70 by means of a real case. This real case is the Round Robin Box test (see section 3.1), where a detailed monitoring has been carried out on the east, west, and north opaque walls, as well as on the roof and ceiling of the Round Robin Box. All the monitoring data used for the analysis is later presented in Table 3 of section 3.1.2. It shows that even if many global solar radiation measurements are available for different orientations of the Round Robin Box test; the east and west walls did not have measurements of the global solar radiation incident on them. Thus, before presenting the method that will be used to validate Eq. 69 and Eq. 70, the next section presents the method used to estimate those vertical global solar radiations based on the available measurements.

2.2.2- Estimation of incident global solar radiation

During the Round Robin Box experiment, several solar radiation measurements incident on the walls of the Round Robin Box have been measured. Among them, the horizontal global solar radiation, the vertical south global solar radiation, the vertical north global solar radiation, the ground reflected solar radiation and the diffuse solar radiation have all been found. Using these values, it is possible to estimate the missing solar radiation data for the walls, such as the vertical east global solar radiation and the vertical west global solar radiation.

In order to carry out the estimation of the missing solar radiation values, the beam radiation ratio method has been used [86]. It must be remarked, that despite in this case, the vertical west and east global solar radiation data is estimated, the method presented in section 2.2.2.1 is valid for the estimation of any global solar radiation in any orientation. In other words, if the horizontal global (the most commonly measured solar radiation) and the diffuse solar radiation are measured, it is possible to estimate the solar radiation data for any orientation of the building (or box in this case). Finally, in order to check the reliability of the method, the vertical south global solar radiation has been estimated using the beam radiation ratio method and then, it has been compared against the measured vertical south global solar radiation.

2.2.2.1- Estimation of the global solar radiation with the beam radiation ratio method

In order to estimate any of the global solar radiation values using the beam radiation ratio method [86], it is indispensable to correct the solar angle. The measured data is given in GMT timeframe so, it is necessary to convert it into the current local time of the area. The corresponding local time of Almeria is GMT+01:00 for winter and GMT+02:00 in summer, as corresponds to Central European Time.

Then, the first step needed in order to estimate the global solar radiation in a specific orientation is to fix the number of the day of the year (1 < n < 365 days) that the first value of the dataset represents. In this case, the first day for summer dataset was the 31st of May, so it corresponds to the day number 151 of the year. The first parameter that needs to be estimated is B. This parameter is estimated using Eq. 71 and it is indispensable in order to estimate the equation of time (in minutes) E (Eq. 72).

$$B = (n-1)\frac{360}{365}\ [°] \qquad \text{Eq. 71}$$

$$\mathrm{E} = 229.2\ (0.000075 + 0.001868\cos B - 0.032077\ \sin B - 0.014615\ \cos 2\mathrm{B} - 0.04089\ \sin 2\mathrm{B})\ [\text{minutes}] \qquad \text{Eq. 72}$$

Once E is estimated, it is possible to estimate the solar time, where the solar noon is the time the sun crosses the meridian of the observer. Since the sun takes 4 minutes to transverse 1° of longitude, the difference between the solar time and the standard time is estimated using Eq. 73:

$$\text{Solar time} - \text{standard time} = 4\,(L_{st} - L_{loc}) + E \text{ [minutes]} \quad \text{Eq. 73}$$

Where the L_{st} is the standard meridian for the local time and the L_{loc} is the longitude of the location (2.35° West).

After this, the distance (in minutes) from each of the hours to the midday must be estimated (solar time-midday time). Thus, it has been possible to estimate the hour angle (ω) since it is known that this angle displaces 15° every hour. Then, multiplying the minute difference value between solar time and midday time by 15° and dividing it by 60 minutes (1 hour), the solar hour value can be estimated.

Apart from this parameter, also the solar declination angle must be estimated in order to be able to obtain the beam radiation ratio. The solar declination angle is calculated using Eq. 74:

$$\delta = 23.45 \sin(360 \frac{284+n}{365}) \text{ [°]} \quad \text{Eq. 74}$$

The solar declination angle shows the angular position of the sun at solar noon with respect of the equator plane, providing values between -23.45°$\leq \delta \leq$23.45. Then, once all these parameters are estimated, it is possible to estimate the beam radiation ratio (R_b). Eq. 75 shows the formula in order to estimate this parameter:

$$R_b = \frac{\cos\theta}{\cos\theta_z} \text{ [-]} \quad \text{Eq. 75}$$

Where $\cos\theta$ is

$$\cos\theta = \sin\delta \sin\Phi \cos\beta - \sin\delta \cos\Phi \sin\beta \cos\gamma + \cos\delta \cos\Phi \cos\beta \cos\omega + \cos\delta \sin\Phi \sin\beta \cos\gamma \cos\omega + \cos\delta \sin\beta \sin\gamma \sin\omega \text{ [°]} \quad \text{Eq. 76}$$

Where β [°] is the slope of the wall, γ [°] is the surface azimuth angle and Φ [°] is the latitude of the area. Eq. 76 is used to determine both parameters $\cos\theta$ and $\cos\theta_z$, since $\cos\theta$ represents the tilted surface of the object and $\cos\theta_z$, the horizontal surface. Then, Table 1 shows the slope and surface azimuth angle each wall or ceiling has:

SIDE OF THE WALL	SLOPE (β)	SURFACE AZIMUTH ANGLE (γ)
Horizontal surface	0°	0°
South vertical surface	90°	0°
East vertical surface	90°	-90°
West vertical surface	90°	90°
North vertical surface	90°	180°

Table 1. Slope and surface azimuth angle results for each of surfaces.

If the estimated beam solar radiation ratio is multiplied by the estimated beam solar radiation for the horizontal plane, the real beam solar radiation incident on the selected surface will be estimated. The beam solar radiation of the horizontal surface can be estimated by resting the measured diffuse solar radiation to the measured horizontal global solar radiation. Once the beam radiation incident on the selected surface is estimated, the diffuse radiation is summed in order to estimate the final global solar radiation incident on the surface.

2.2.2.2- Validation of the proposed beam radiation ratio method

Since the vertical west and east global solar radiations have not been measured, they have been estimated using the method presented on the section 2.2.2.1. In order to ensure the methods reliability, an estimation of the vertical south global solar radiation has been done using the method and then, it has been compared against the measured values. In this way, it is ensured that the obtained vertical west and east global solar radiations are reliable. Figure 9 and Figure 10 show the obtained results using the method compared to the real vertical south global solar radiation.

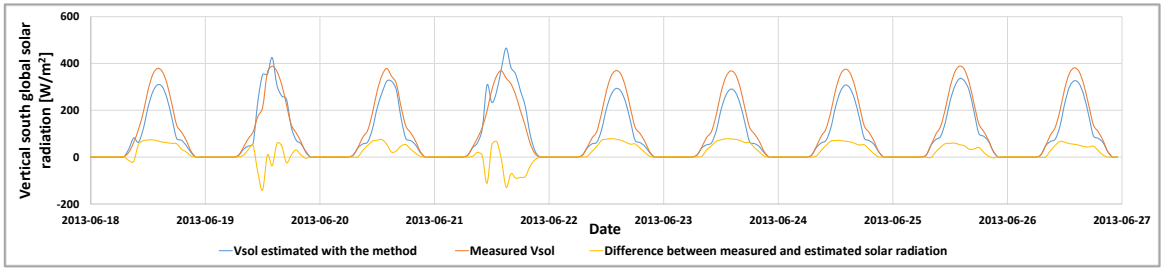

Figure 9. Vertical south global solar radiation during period 1 (summer).

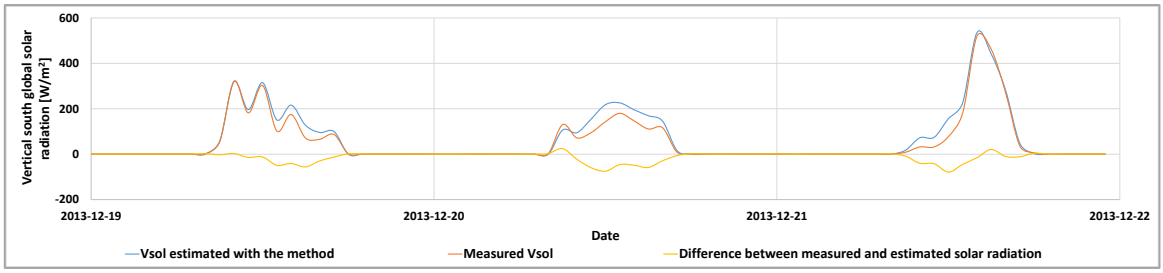

Figure 10. Vertical south global solar radiation during period 2 (winter).

From Figure 9 and Figure 10 can be assumed that the method is able to obtain a close approximation of the measured vertical south global solar radiation despite there still exist a difference mainly when obtaining the highest values of solar radiation at midday. The Root Mean Square Error (RMSE) value of this difference in summer is 40.2 W/m^2 with a standard deviation of 37.4 W/m^2 while RMSE value in winter is 23.7 W/m^2 with a standard deviation of 35.6 W/m^2. Then, since the obtained vertical south global solar radiation results within this method seem quite similar to the measured values, it will be used in order to estimate the vertical east and west global solar radiation results.

2.2.3- Fit and validation of the models

Once all the global solar radiation data have been made available for all the Round Robin Box walls, roof and floor, the corresponding solar factor of each of these elements must be estimated using the LORD software [81]. Since LORD is an estimation software based on parameter identification in RC models, it is able to estimate the U-value and the g-value of the wall drawing on the provided input data. Before developing the proposed method, the provided data have been analysed in order to identify the missing values and irregularities, as commented in section 3.1.3. Once the data has been checked and all the variables have been identified, the data to be used has been selected. A part of this data has been measured and it has been included in Table 3 of section 3.1.2 while the rest of the data has been estimated. In this case, the variables selected to develop the analysis are the inner surface temperature (T_{Sin}), the inner surface heat flux ($\dot{q}$), the outer surface temperature (T_{Sout}), the outdoor air temperature (T_{out}), the wind speed (WS), the surrounding, sky or ground temperature (T_{surr}, T_{sky} and T_{ground}) and the corresponding global solar radiation (G_{sol}) in each surface. The inner surface heat flux has been chosen as the output parameter in all the models.

2.2.3.1- Fit of the opaque walls, roof and floor models

Once all data has been checked and divided into smaller periods, the different models can be tested using the LORD software by estimating the models' parameters. These models will consider every phenomenon mentioned in section 2.2.1. In order to make the models behave as close to reality as possible, several limitations have been fixed from the beginning for the models' parameter estimations.

The first case to be fitted is the simplest, the surface to surface case (Model 1, M1), shown in Figure 11(a). The only variables introduced in this model are the temperatures in both surfaces (inner and outer) and the inner surface heat flux. The first node represents the inner node, including the inner surface temperature and the inner surface heat flux. The A_1 value represents the aperture of the heat flux in this node, which in this case, for all the models, corresponds to one, since the total heat flux on the inner surface of the wall is actually measured and it is known that 100 % of it crosses the wall's inner surface. However, node five represents the outermost surface and is linked to the outer surface temperature. In conclusion, this model represents the wall, without considering any phenomena occurring in the internal and external environments.

As the thermal characteristics of the materials forming the wall are previously known, it was easy to calculate the theoretical effective heat capacity (C_i) and thermal conductance (H_i) of the total wall. Moreover, as justified in section 2.2.1, the outermost surface node is assumed to be a massless node where the energy balance is carried out in the outer surface. Thus, it is considered that the thermal capacitance at this node is equal to 0 (C_5=0). Following physical laws, it must be fulfilled that the closest thermal resistance ($R_{4\text{-}5}$) to this node should also be very small. In other words, the higher the thermal resistance $R_{4\text{-}5}$ value is, the wider the layer of wall considered by this thermal resistance should be. Then, the wider the $R_{4\text{-}5}$ is, the higher the capacity C_5 this layer should have associated. Therefore, in order to limit $R_{4\text{-}5}$ low enough to carry out the proposed energy balance in node 5, this value has been limited to be 1 %, or lower than the total thermal resistance of the wall (R_w), where the surface to surface R_w =1.93 $\frac{m^2K}{W}$ (estimated in section 2.2.3.2). Therefore, the thermal resistance $R_{4\text{-}5}$ should not exceed the value of 0.0193 $\frac{m^2K}{W}$. The LORD software estimates thermal conductance (this is the inverse of the

thermal resistance ($R_W = {}^{1}/_{H_W}$)), which means that the thermal conductance should be high for $H_{4\text{-}5}$. Then, this parameter will be limited, fixing $51.8\ \frac{W}{m^2K}$ as the lowest limit. For the rest of the model conductances, a wide range has been imposed for their identification, the lower limit being set as the theoretical thermal conductance of the whole wall. The Model 1 fits the parameters under these conditions.

Once the surface to surface model provides reliable parameters (thermal capacitance and conductance) and a proper fit of the inner surface heat flux, it is possible to start working with new models, including the external phenomena affecting the outermost surface. It is therefore necessary to include an extra node in the model, as shown in Figure 11(b), to include the external effects. This model (Model 2, M2) represents the case without considering any of the outer environmental phenomena in detail. In other words, the convection and the long wave radiation are considered as a constant conductance, while the solar radiation is not considered at all.

This Model 2 shows six nodes. The first node is maintained as in the surface to surface model. However, the link to the outer surface temperature is removed from node five and the outdoor air temperature is included in node six. The thermal conductance and capacitances obtained in the surface to surface model are fixed between nodes one and five, since they should not vary depending on the external environment influence and they already represent a proper approximation of the theoretical thermal properties of the wall. Then, the only new parameter to be estimated is $H_{5\text{-}6}$, the combined heat transfer coefficient of the wall (named h_{comb} in section 2.2.1). This parameter has also been estimated based on the ASHRAE [91] where a theoretical value is obtained for this parameter. Thus, a reasonable range of limits is provided for the estimation of this parameter in LORD, following this standard value. Then, it is ready for model fitting.

The third model that has been tested is the one considering the influence of the solar radiation on the outer surface (Model 3, M3). The only difference between this Figure 11(c), compared with the previously mentioned Figure 11(b), is the incorporation of the global solar radiation (G_{sol}) in node five. Together with this variable, the software also includes an extra parameter named A_5. This parameter represents the absorptivity of the outer surface wall, which also needs to be estimated. Then, the only two parameters that

need to be estimated in this Model 3 are the previously mentioned $H_{5\text{-}6}$ combined conductance (fixing the limits of this parameter following the ASHRAE standard value) and the solar absorptivity (A_5). This solar absorptivity has been limited to between 0 and 1, always checking after the identification that the estimate has not gone to one of the limits.

The next phenomenon analysed in detail is the wind speed. Therefore, the same model structure as in Figure 11(c) is taken. However, in this case, instead of using the ASHRAE fixed standard limits for the estimation of $H_{5\text{-}6}$ (or h_{comb}), a function section provided by LORD software is used. The wind speed analysis is performed in two different manners; as in Model 4 (M4, see Figure 11(d)), where $H_{5\text{-}6}$ is estimated using a specific correlation function representing solely the convection coefficient when there exist wind speed (h_{conv}) (see Eq. 77, taken from [94]) or as in Model 5 (M5, see Figure 11(e)), where $H_{5\text{-}6}$ is estimated using an identifiable correlation function ($h_{comb} = x + y \times WS$), where during the model fit, within the identifiable x and y parameters the long wave radiation and convective effects (h_{comb}) can be considered.

$$h_{conv} = 2.8 + 3 \times WS \ \text{[W/m}^2\text{K]} \qquad \text{Eq. 77}$$

Thus, in case of M4, since a pure convective coefficient is used, and there is not any identifiable parameter for the $H_{5\text{-}6}$ estimation, only the heat transfer due to convection (h_{conv}) has been considered in $H_{5\text{-}6}$, avoiding the heat transfer due to long wave radiation. However, in M5, part of the long wave radiation effect will be considered within the x and y parameters during their identification. During the analysis, both cases (M4 and M5) have been tested and compared. Then, since for M4 only the solar absorptivity (A_5) is estimated, it is possible that the model estimates the effect of the long wave radiation in this parameter. However, as commented before, since in M5, apart from the solar absorptivity (A_5), also the parameters of the correlation function are estimated, the long wave radiation effect can be reflected in this x and y parameters. Thus, it has been possible to estimate which case was providing better parameters (closer to the theoretical values) and the best fit.

The next model (Model 6, M6) tested also considers the effect of the long wave radiation together with the solar radiation and the convection. So a new branch has been

included in Figure 11(c) as shown in Figure 11(f), where there is an extra branch between the node 5 and the node 7 in the model. The surrounding temperature is included in node 7, which has been estimated using Eq. 54 as explained in section 2.2.1. Therefore, the parameters estimated by the software when testing this model are the convective thermal conductance (instead of the combined thermal conductance of Figure 11(c) between nodes 5 and 6 ($H_{5\text{-}6}$), the long wave radiation thermal conductance between nodes 5 and 7 ($H_{5\text{-}7}$) and the solar absorptivity (A_5). The thermal conductance $H_{5\text{-}6}$ and the solar absorptivity are limited, as in the model in Figure 11(c). The conductance $H_{5\text{-}7}$ corresponds to the previously presented radiation heat transfer coefficient h_{rad} in section 2.2.1. This h_{rad} could be estimated using the following Eq. 78.

$$h_{rad} = \varepsilon\sigma({T_{sout}}^2 + {T_{surr}}^2)(T_{sout} + T_{surr}) \text{ [W/m}^2\text{K]} \quad \text{Eq. 78}$$

The emissivity (ε) of the wall must also be fixed between 0 and 1. Therefore, the lowest h_{rad} value that can be obtained would be 0. However, the highest value would depend on the measured variables. In this case, ε would be one. Since the Stefan Boltzmann value (σ) is a constant value, the maximum h_{rad} would depend on the surface temperature and the surrounding temperature. In order to estimate this maximum value, the h_{rad} value of each hourly data of the total selected dataset is estimated. Thus, the highest limit of this $H_{5\text{-}7}$ will be different for each of the walls, since it depends on their surface and surrounding temperature. In the case of the ceiling and the floor, the same procedure will be followed, but instead of using the T_{surr}, the corresponding temperature (T_{sky} or T_{ground}) will be used.

Once all the outer environmental phenomena have been presented in detail in the previous models, two new models (Model 7, M7 and Model 8, M8) are proposed and analysed, considering all the detailed phenomena together. The structure of the model used for this case is the same as that used in Figure 11(f). However, instead of limiting the convective thermal conductance $H_{5\text{-}6}$ using the ASHRAE standard values, the effect of the wind speed is introduced within the convection coefficient using the fixed correlation (M7) of Eq. 77, or leaving the parameters of the correlation free (M8). Both cases will again be analysed, but in this case together with the solar radiation and the long wave radiation affecting the outer surface of the corresponding wall, as shown in Figure 11(g) and Figure 11(h). Therefore, the common parameters estimated by LORD for these two models will be the solar absorptivity (A_5) and the conductance $H_{5\text{-}7}$, limited in the same

way as done in Model 6. Once again, if the model leaves the parameters free to estimate the influence of the wind speed in the model, these parameters would also be estimated by LORD.

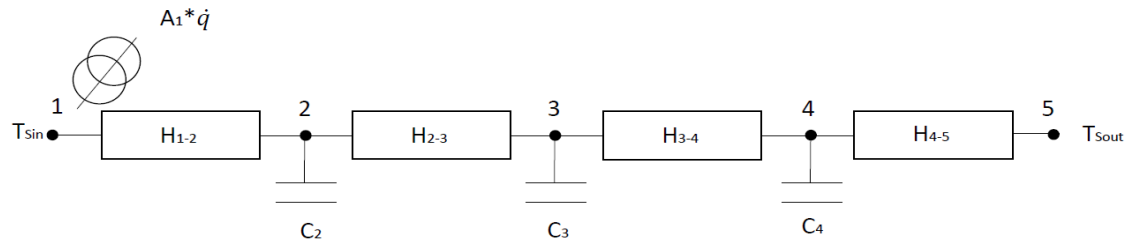

(a)

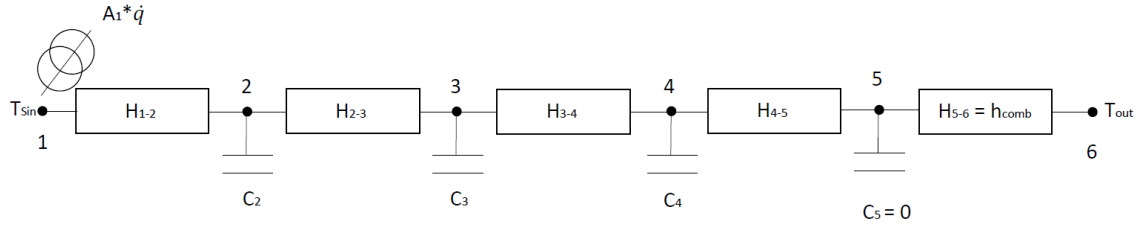

(b)

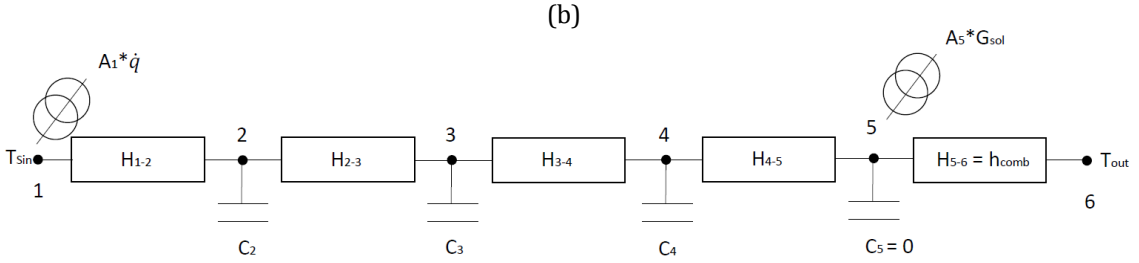

(c)

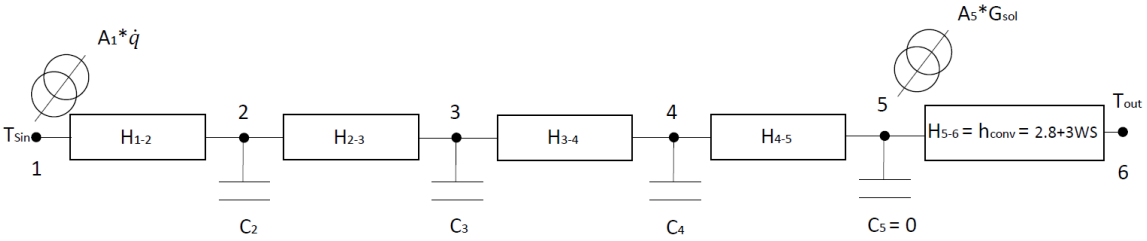

(d)

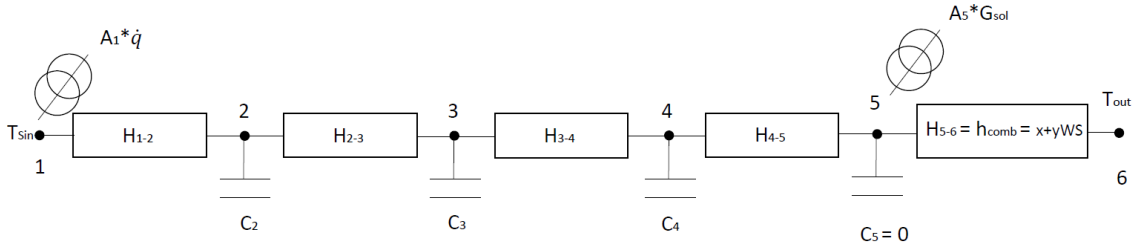

(e)

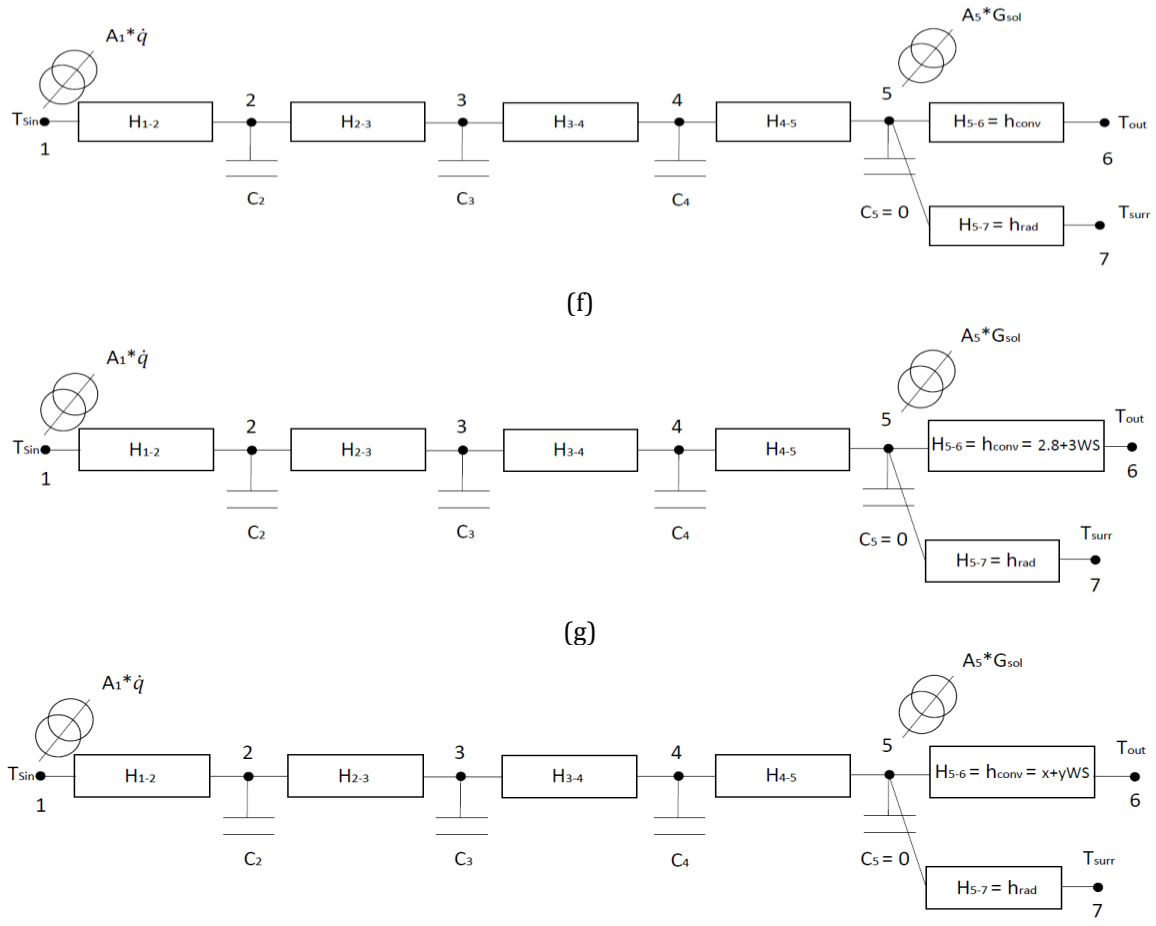

Figure 11. All the candidate models: (a) Model 1, (b) Model 2, (c) Model 3, (d) Model 4, (e) Model 5, (f) Model 6, (g) Model 7 and (h) Model 8.

It must be said that, in the development of section 2.2.1, the h_{conv} and the h_{rad} have been considered together as h_{comb} in order to simplify the calculation. However, as shown in this section, when implementing the models, each heat transfer coefficient has been considered and estimated individually against their respective temperatures.

Finally, all the estimated parameters in each of the models are compared with the theoretical values, as explained in the next section, and the best fits are selected by comparing the estimated and measured inner surface heat flux values. The best-fit selection is carried out using the Root Mean Square Error (RMSE). Thus, it is possible to estimate the model that best represents the reality of the wall's outermost surface and it will be used for the inner surface heat flux analysis in section 2.2.4. This procedure has been repeated for two periods (one in winter and one in summer).

2.2.3.2- Validation of the fitted models

As commented in the previous section, in order to develop a proper validation of the obtained model results, the thermal and geometrical properties of the Round Robin Box have been used. Thus, it is possible to estimate the design transmittance (U-value) of the walls, roof and ceiling. The information of the walls, roof and ceiling is detailed in [50]. Then, the U-value is estimated using the following formula:

$$U = \frac{1}{R_{si}+\sum\frac{l_i}{k_i}+R_{comb}} = \frac{1}{R_{si}+R_W+R_{comb}} \text{ [W/m}^2\text{K]} \qquad \text{Eq. 79}$$

where l_i and k_i are the thickness and thermal conductivity of the layers that form the wall. Then, the thermal resistance of the whole wall is calculated using the sum of the thermal resistance of each of the wall layers: $R_W=\sum_{i=1}^{N}(l_i/k_i)=(l_1/k_1)+(l_2/k_2)+(l_3/k_3)+\ldots+(l_N/k_N)\left[\frac{m^2K}{W}\right]$. The variable i is the sum index to which an initial value of 1 is given as the lowest limit and this will make up the range of all the integer values until the upper limit N is reached. This N value will vary depending on the layer quantity forming the wall. However, R_{si} and R_{comb} (which in [50] are presented as R_{se}) are, respectively, the inner and outer surface thermal resistances of the wall. The R_{si} and R_{comb} (R_{conv} and R_{rad} in parallel) values are standard constant values taken from [93]. The obtained U-value from Eq. 79 is 0.48 $\frac{W}{m^2K}$. The fact that, in the tested basic model M1 considered in section 2.2.3.1, the internal first node is considered to be the inner surface instead of the indoor air must be taken into account. Then, the estimated value from Eq. 79 will be an air to air value, while the value obtained from M1 is a surface to surface or a surface to air value from the models M2 to M8 presented hereafter.

However, since LORD is able to provide the value of each of the thermal conductances of the model, it is possible to calculate the thermal resistance (R_W) of the wall (since $R_W = {}^1/_{H_W} = {}^1/_{H_{1-2}} + {}^1/_{H_{2-3}} + {}^1/_{H_{3-4}} + \cdots + {}^1/_{H_{N-1-N}} \left[\frac{m^2K}{W}\right]$), again using the sum of each of the layers' thermal resistance from i=1-2 to i=N-1 – N, and comparing the results of these thermal resistances with the design values. Then, the wall design thermal resistance surface to surface can be calculated as in Eq. 80:

$$R_W = \sum \frac{l_i}{k_i} \text{ [m²K/W]} \quad \text{Eq. 80}$$

From Eq. 80, the theoretical value of the thermal resistance of the wall can be calculated, since the thicknesses and the thermal conductivities of all the walls' materials are known. Then, using the sum of the thermal resistance of each of the wall layers, as done for Eq. 80, it is possible to estimate the total wall thermal resistance. The estimated R_w result is 1.93 $\frac{m^2K}{W}$. This value should be compared with the total thermal resistance value obtained from Model 1 (M1) of section 2.2.3.1.

However, it is also possible to estimate the total thermal resistance of the best model tested in section 2.2.3.1 theoretically, since the outer surface thermal resistance of the wall is also known, as discussed previously. Therefore, Eq. 81 is used:

$$R_T = \sum \frac{l_i}{k_i} + R_{comb} \text{ [m²K/W]} \quad \text{Eq. 81}$$

Thus, the design R_T value for this case would be 1.97 $\frac{m^2K}{W}$, since the R_{comb} value is taken from [93] and its value is 0.04 $\frac{m^2K}{W}$. Then, the best estimated model, from all the models presented in section 2.2.3.1, should be able to estimate a similar R_T result to the theoretical R_T value. However, since R_{comb} is a standard value, the estimations of LORD could differ from the theoretical values.

The next sections will show that M7 and M8 are the models showing the best results. As discussed previously, in the models, the convective and radiation heat transfer coefficients have been estimated independently. In this case, unlike the rest of the conductance inside the wall, these two conductances (h_{conv} and h_{rad}) are in parallel, as shown in Figure 11(g) and Figure 11(h). Thus, in this case, both conductance values obtained from LORD can be summed directly to estimate the h_{comb} (h_{comb}= $H_{5\text{-}6}$+$H_{5\text{-}7}$), and the total R_{comb} is obtained as the inverse of this value. Thus, summing this R_{comb} to the previously estimated R_W, the total thermal resistance can be estimated.

Finally, it must be said that the rest of the physical parameters, such as the solar absorptivity, have also been useful in the validation process of the models.

2.2.4- Estimation of the hypothetical inner surface heat flux without considering solar radiation

The estimation of the hypothetical inner surface heat flux will be carried out based on the previous model fits (section 2.2.3.1) and the proper validation of the models (section 2.2.3.2). Following a deep analysis of the models presented in section 2.2.3.1, one of them will be selected as the best at representing the reality for each of the walls. As shown in section 4.1.2.2, Models 7 and 8 are the best for almost every wall. Then, these two models will be used for the estimation of the solar radiation effect in the inner surface heat flux. Thus, Figure 12(a) (the Figure 11(g) presented in section 2.2.3.1) and Figure 12(b) (the Figure 11(h) presented in section 2.2.3.1) represent the new model (Model 9, M9 and Model 10, M10) structures to estimate the inner surface heat flux without considering the solar radiation.

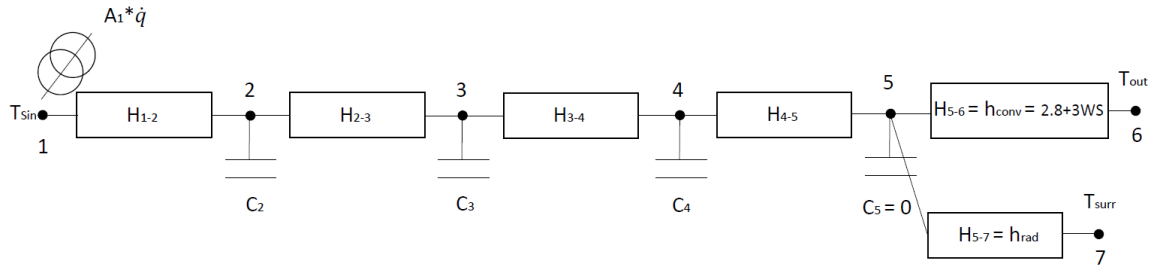

(a)

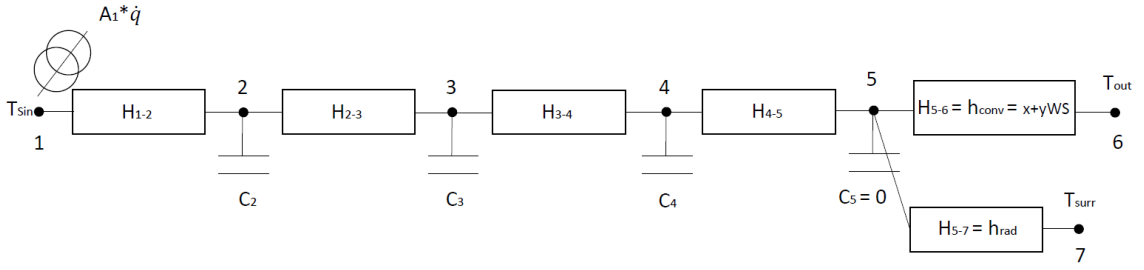

(b)

Figure 12. Best identified models modified for inner surface heat flux estimation without the solar radiation effect: (a) Model 9 and (b) Model 10.

Only these two models have been tested without the effect of the solar radiation, since they were the best in all the tested cases. Figure 12(a) and Figure 12(b) show the same number of nodes, respectively, as the M7 and M8 of section 2.2.3.1. Moreover, the same H_i and C_i values estimated during the fit of these models will be used for each of them. The rest of the parameters will also be fixed during the simulation. The only difference between the models M9 and M10, as compared to the models M7 and M8 in section 2.2.3.1,

is the lack of the solar radiation signal on node 5. Then, if solar radiation is not provided for the model, it will be able to estimate the hypothetical inner surface heat flux ($\dot{\bar{q}}'$) for the wall when subjected to the same inner surface temperature, the same outdoor air temperature, the same surrounding/sky/ground temperature and the same wind speed, but without solar radiation striking the outermost surface of the wall.

Finally, once both the inner surface heat fluxes have been estimated, the inner surface heat flux considering the solar radiation ($\dot{q}$) and the hypothetical inner surface heat flux without considering the solar radiation ($\dot{q}'$), it is possible to estimate the effect of the solar radiation on the inner surface heat flux using Eq. 70. Moreover, the effect of the solar radiation has also been quantified as a percentage using Eq. 82.

$$\dot{q}_{\%} = \frac{\dot{q}' - \dot{q}}{\dot{q}} \times 100 \ [\%] \qquad \text{Eq. 82}$$

The results for both equations are shown in section 4.1.2.3.

2.2.5- Solar factor (g-value) estimation

The estimation of the g-value has been performed in two different manners; the simplest case was using LORD, which automatically provides the g-value when fitting the model. Then, the g-value obtained from the selected best model for each of the walls is presented.

Then, the value estimated by LORD is compared with the g-value estimated using Eq. 69 for each corresponding wall. Therefore, the heat flux difference estimated in section 2.2.4 must be used.

2.3- Methodology to estimate the effect of the solar gains through opaque walls in the HLC estimation

As shown in section 2.2, it is possible to quantify the effect of the solar radiation on the inner surface heat flux of opaque walls. Then, it is also possible to quantify the percentage weight the solar radiation through opaque walls would have respect to the HLC estimation when methods without an unknown identifiable constant solar gain value are used such as the average method developed in section 2.1.1, where the solar gains effect though opaque walls are neglected.

The fact that the solar radiation effect in opaque walls is not considered can create an error in the estimation of the HLC for some estimation methods. For HLC estimation methods where an unknown identifiable constant value for estimating the solar gains is not used and the solar gains through opaque walls could have a considerable weight, the HLC value tends to be underestimated. In order to understand this effect, the HLC equation Eq. 50 (now called Eq. 83) achieved in section 2.1.3 must be observed.

$$HLC = \frac{\sum_{k=1}^{N}(Q_k + K_k + (S_a V_{sol})_k)}{\sum_{k=1}^{N}(T_{in,k} - T_{out,k})} = \frac{\frac{\sum_{k=1}^{N}(Q_k + K_k + (S_a V_{sol})_k)}{N}}{\frac{\sum_{k=1}^{N}(T_{in,k} - T_{out,k})}{N}} = \frac{\bar{Q} + \bar{K} + \overline{S_a V_{sol}}}{\overline{T_{in}} - \overline{T_{out}}} \text{ [W]} \quad \text{Eq. 83}$$

This Eq. 83, as explained in section 2.1, is obtained by applying the energy conservation principle to a monitored in-use building during a 3 to 5 day cold and cloudy period. This energy conservation equation analysis allows the HLC and the period averaged solar gains ($\overline{S_a V_{sol}}$) to be related to the measurable variables. These variables are the period averaged heating system energy supply ($\bar{Q}$), all internal gains due to occupant metabolic heat generation and electrical device consumption within the building envelope ($\bar{K}$) and the indoor to outdoor temperature difference ($\overline{T_{in}} - \overline{T_{out}}$). In cold and cloudy periods, the period averaged $\bar{Q}$ and ($\overline{T_{in}} - \overline{T_{out}}$) are usually high, so their measurement uncertainty is minimum. On the other hand, in such cold and cloudy periods, the uncertain in-use solar gains ($\overline{S_a V_{sol}}$) are low compared to the accurately measurable ($\bar{Q} + \bar{K}$).

When the outermost surface of the opaque elements of a building are heated by solar radiation, the heating system would need to provide less heat inside the building ($\bar{Q}$) to maintain the same temperature. However, if the solar gains term ($\overline{S_a V_{sol}}$) in Eq. 83 does not consider the effect of the solar gains through the opaque walls, the term of the heat gains inside the term ($\bar{Q} + \bar{K} + \overline{S_a V_{sol}}$) would be lower than it is in reality. Therefore, the HLC obtained by Eq. 83 would be underestimated. Since the solar gains term is the sum of the solar gains through the semi-transparent envelope elements (windows) plus the solar gains through the opaque envelope elements (walls, roof…) ($S_a V_{sol} = (S_a V_{sol})_{windows} + (S_a V_{sol})_{walls}$), the underestimation of the HLC due to not considering the $(S_a V_{sol})_{walls}$ would be equal to $\frac{\overline{(S_a V_{sol})_{walls}}}{(\overline{T_{in}} - \overline{T_{out}})}$.

In this research work, the effect of the solar radiation on the inner surface heat flux has already been estimated for the Round Robin Box opaque envelope, as explained in section 2.2.4 and the HLC of the Round Robin Box has also been estimated using the methodology of section 2.1. Then, it is possible to analyse, on a practical basis, the weight the term $\frac{(\overline{S_a V_{sol}})_{walls}}{(\overline{T_{in}}-\overline{T_{out}})}$ has with respect to the Round Robin Box HLC. It is also interesting to analyse the weight that the solar gains through the opaque envelope have with respect to the solar gains through the window. To do so, Eq. 84 provides the weight in percentage that the effect of the solar radiation has on the inner surface heat flux of the building envelope opaque elements of the estimated HLC when estimated by means of Eq. 83. On the other hand, Eq. 85 provides the weight in percentage that the effect of the solar radiation has on the inner surface heat flux of the building envelope opaque elements regarding the solar gains through the semi-transparent elements of the building envelope.

$$W_{HLC\%} = \frac{\frac{(\overline{S_a V_{sol}})_{walls}}{(\overline{T_{in}}-\overline{T_{out}})}}{HLC} \times 100 = \frac{\left(\frac{\sum(\bar{q}_{dif} \times A_W)}{(\overline{T_{in}}-\overline{T_{out}})}\right)}{HLC} \times 100 \ [\%] \qquad \text{Eq. 84}$$

$$W_{S_a V_{sol}\%} = \frac{(\overline{S_a V_{sol}})_{walls}}{(S_a V_{sol})_{windows}} \times 100 = \frac{\sum(\bar{q}_{dif} \times A_W)}{(S_a V_{sol})_{windows}} \times 100 \ [\%] \qquad \text{Eq. 85}$$

Then, considering the HLC and the window solar aperture (S_a) values estimated using the average method of the Round Robin Box during the winter period, and using the mean values of ($\overline{T_{in}} - \overline{T_{out}}$) and the $\overline{V_{sol}}$ for each studied period, it is possible to estimate the weight of the $\frac{\sum(\bar{q}_{dif} \times A_W)}{(\overline{T_{in}}-\overline{T_{out}})}$ term with respect to the HLC (using Eq. 84)) and the $(S_a V_{sol})_{windows}$ (using Eq. 85) terms. The same procedure can also be performed using the theoretical HLC and window solar aperture (S_a) values of the Round Robin Box, provided in [64]. The estimated HLC value for the winter period of the Round Robin Box is 4.1 W/K (very similar to the theoretical value 4.08 W/K) and the S_a value for the window estimated based on the average method requirements is 0.135 m^2 (also close to the theoretical value 0.162 m^2), as remarked in section 3.1.1. Since the average method can only be applied in cold and cloudy periods, it has been impossible to estimate the HLC value for the summer period. Then, in this case, the $\frac{\sum(\bar{q}_{dif} \times A_W)}{(\overline{T_{in}}-\overline{T_{out}})}$ terms' weight estimation would be done respect to the theoretical values. Moreover, each wall $\bar{q}_{dif}$ value for each period must be multiplied by the inner surface area of each of the walls (A_w), 96x96 cm^2 in this case, and

then, all of them must be summed to get the total difference for the whole Round Robin Box in W. Note that the solar gains through the thermal bridges are not considered.

Through this analysis, it is possible to analyse the reliability of the developed average method in section 2.1. In other words, since the method is not considering the effect of the solar gains through the opaque walls in the HLC estimation, it is possible to obtain underestimated HLC results. However, due to the requirements fixed in order to limit the solar gains effect through the windows, also the solar gains through the opaque walls are affected. Then, it must be proved that since the solar radiations affecting the opaque walls can be considered almost purely diffuse in all orientation in cold and cloudy periods, its percentage weight respect to the HLC estimation when estimated with the average method is considerably low. In this case, its effect could be considered negligible. If this percentage weight would be considerable, it should be considered when developing a reliable HLC estimation method. Once the reliability of the developed average method is tested and demonstrated, it is possible to present and apply the last methodology of the Thesis, the decoupling process. As commented in section 1.6, through this process, it would be possible to identify the origin of the heat losses in order to better understand the performance gap.

2.4- Methodology for the HLC decoupling

Once an accurate and reliable HLC estimation method has been developed for in-use buildings, it is possible to implement the methodology in order to carry out the HLC decoupling process. The developed average method is able to estimate the in-use floor-by-floor Heat Loss Coefficients, as already shown in section 2.1, their sum being the HLC of the whole building. Since this decoupling methodology will be implemented in the same multi-storey rehabilitated office building, the HLC values are necessary in order to perform the HLC decoupling process of this section. As described later in section 3.3, after the rehabilitation, a ventilation system with heat recovery was installed in each of the floors of the building. So this section describes the metabolic CO_2 decay method applied to estimate thermal zone's Air Change per Hour (ACH), and then the infiltration (before rehabilitation, without ventilation system installed) or infiltration and/or ventilation (after rehabilitation, with ventilation system installed) heat loss coefficient (C_v). Therefore, the methodology is detailed for the case of a complex building with multiple

thermal zones and the consideration of the infiltration and ventilation heat losses are included. Finally, considering the HLC estimated previously and the C_v estimated during this study, the HLC decoupling method used is also described in detail. Then, although in this case the methodology has been implemented for a multi-storey rehabilitated office building, it is also applicable to any building that fulfils the fixed requirements of the method.

2.4.1- Mass balance equation applied to in-use buildings with multiple thermal zones

The strict metabolic CO_2 concentration homogeneity requirements presented in section 2.4.2 to obtain the infiltration/ventilation heat loss coefficient, makes it nearly impossible to obtain them in a whole building basis. Thus, it is needed to obtain them in a thermal zone basis. Of course, there might be heat and mass transfer between thermal zones within a building. This is why, in this subsection, since the key aspects regarding the heat exchanges between thermal zones of the building have already been the analysed in section 2.1.2, the key aspects regarding the mass exchanges between thermal zones within a building are related to the HLC estimation and decoupling.

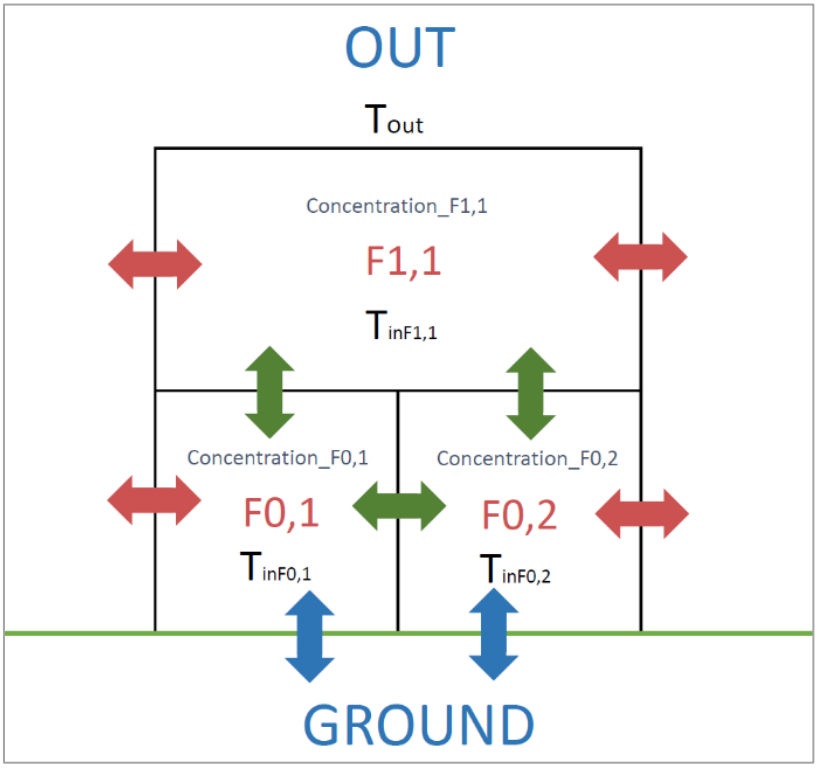

Figure 13. Schematic of all energy and/or mass exchanges in a building composed of multiple thermal zones.

The demonstration presented in section 2.1.2 is crucial for the proposed HLC decoupling method feasibility since it gives a powerful tool to deal with the huge variations on internal temperature that might occur within a multi-storey occupied building where important temperature variations within the different building thermal zones are usual. Now a similar development will be performed using the same toy model presented again in Figure 13 to prove that the building's total infiltration plus ventilation rates can be estimated by applying the following formula, where the Air Change per Hour (ACH) values of each thermal zone are obtained directly from the analysis of the decay curve of the anthropogenic CO_2 in each of those thermal zones:

$$\dot{V}_{building} = \dot{V}_{F0,1\_decay} + \dot{V}_{F0,2\_decay} + \dot{V}_{F1,1\_decay} \rightarrow$$
$$ACH_{building} V_{ol\_building} = ACH_{F0,1\_decay} V_{ol\_F0,1} + ACH_{F0,2\_decay} V_{ol\_F0,2} + ACH_{F1,1\_decay} V_{ol\_F1,1} \quad [m^3/s] \qquad \text{Eq. 86}$$

To prove Eq. 86, it is necessary to start applying the mass balance to the three thermal zones represented in Figure 13. The accumulation of the mass within a building or a thermal zone within a building can be considered negligible. Otherwise, if even a small amount of air would be accumulated within a thermal zone of a building, its pressure would change considerably.

Ground floor (volume $F_{0,1}$):

$$0 = \left(\dot{m}_{out-F0,1} + \dot{m}_{F1,1-F0,1} + \dot{m}_{F0,2-F0,1}\right) - \left(\dot{m}_{F0,1-out} + \dot{m}_{F0,1-F0,2} + \dot{m}_{F0,1-F1,1}\right) \quad [kg/s] \qquad \text{Eq. 87}$$

Ground floor (volume $F_{0,2}$):

$$0 = \left(\dot{m}_{out-F0,2} + \dot{m}_{F1,1-F0,2} + \dot{m}_{F0,1-F0,2}\right) - \left(\dot{m}_{F0,2-out} + \dot{m}_{F0,2-F0,1} + \dot{m}_{F0,2-F1,1}\right) \quad [kg/s] \qquad \text{Eq. 88}$$

First floor (volume ($F_{1,1}$)):

$$0 = \left(\dot{m}_{out-F1,1} + \dot{m}_{F0,2-F1,1} + \dot{m}_{F0,1-F1,1}\right) - \left(\dot{m}_{F1,1-out} + \dot{m}_{F1,1-F0,1} + \dot{m}_{F1,1-F0,2}\right) \quad [kg/s] \qquad \text{Eq. 89}$$

Furthermore, in the building sector, the pressure within the building and the temperature within the building is usually quite homogeneous regarding their possible effect on the variation of the density of the air within a building, thus the air density can

be considered constant. Note that for the HLC estimation a 5 °C variation between thermal zones is an important variation since the indoor to outdoor temperatures used for HLC estimation usually range between 10 °C to 20 °C. Otherwise, a 5 °C variation on the air produces a negligible variation on its density. Then, since $\dot{m}_{air} = \dot{V}\rho_{air}$ and the density of the air (ρ_{air}) can be considered as a constant value, Eq. 87 to Eq. 89 are converted into:

$$0 = \left(\dot{V}_{out-F0,1}+\dot{V}_{F1,1-F0,1}+\dot{V}_{F0,2-F0,1}\right) - \left(\dot{V}_{F0,1-out}+\dot{V}_{F0,1-F0,2}+\dot{V}_{F0,1-F1,1}\right) \ [m^3/s] \quad \text{Eq. 90}$$

$$0 = \left(\dot{V}_{out-F0,2}+\dot{V}_{F1,1-F0,2}+\dot{V}_{F0,1-F0,2}\right) - \left(\dot{V}_{F0,2-out}+\dot{V}_{F0,2-F0,1}+\dot{V}_{F0,2-F1,1}\right) [m^3/s] \quad \text{Eq. 91}$$

$$0 = \left(\dot{V}_{out-F1,1}+\dot{V}_{F0,1-F1,1}+\dot{V}_{F0,2-F1,1}\right) - \left(\dot{V}_{F1,1-out}+\dot{V}_{F1,1-F0,2}+\dot{V}_{F1,1-F0,1}\right) [m^3/s] \quad \text{Eq. 92}$$

Analysing Eq. 90 to Eq. 92, we can relate the total infiltration/ventilation rates of each thermal zone with its corresponding total ACH as follows:

$$ACH_{F0,1}V_{ol\_F0,1} = \dot{V}_{F0,1} = \left(\dot{V}_{out-F0,1}+\dot{V}_{F1,1-F0,1}+\dot{V}_{F0,2-F0,1}\right) = \left(\dot{V}_{F0,1-out}+\dot{V}_{F0,1-F0,2}+\dot{V}_{F0,1-F1,1}\right) \ [m^3/s] \quad \text{Eq. 93}$$

$$ACH_{F0,2}V_{ol\_F0,2} = \dot{V}_{F0,2} = \left(\dot{V}_{out-F0,2}+\dot{V}_{F1,1-F0,2}+\dot{V}_{F0,1-F0,2}\right) = \left(\dot{V}_{F0,2-out}+\dot{V}_{F0,2-F0,1}+\dot{V}_{F0,2-F1,1}\right) \ [m^3/s] \quad \text{Eq. 94}$$

$$ACH_{F1,1}V_{ol\_F1,1} = \dot{V}_{F1,1} = \left(\dot{V}_{out-F1,1}+\dot{V}_{F0,1-F1,1}+\dot{V}_{F0,2-F1,1}\right) = \left(\dot{V}_{F1,1-out}+\dot{V}_{F1,1-F0,2}+\dot{V}_{F1,1-F0,1}\right) \ [m^3/s] \quad \text{Eq. 95}$$

Applying the mass conservation principle (assuming (ρ_{air}) as a constant value) to the control volume enclosing the whole building we get:

$$0 = \left(\dot{V}_{out-F0,1}+\dot{V}_{out-F0,2}+\dot{V}_{out-F1,1}\right) - \left(\dot{V}_{F0,1-out}+\dot{V}_{F0,2-out}+\dot{V}_{F1,1-out}\right) \ [m^3/s] \quad \text{Eq. 96}$$

$$ACH_{building}V_{ol\_building} = \left(\dot{V}_{out-F0,1}+\dot{V}_{out-F0,2}+\dot{V}_{out-F1,1}\right) = \left(\dot{V}_{F0,1-out}+\dot{V}_{F0,2-out}+\dot{V}_{F1,1-out}\right) \ [m^3/s] \quad \text{Eq. 97}$$

Making the sum Eq. 90 to Eq. 92, reordering and applying the equivalences of Eq. 93 to Eq. 97, the following expression is obtained:

$$ACH_{building}V_{ol\_building} = ACH_{F0,1}V_{ol\_F0,1} + ACH_{F0,2}V_{ol\_F0,2} + ACH_{F1,1}V_{ol\_F1,1} \ [m^3/s] \quad \text{Eq. 98}$$

Unless the thermal zones within a building are completely airtight between them, the $ACH_{F0,1\_decay}$ of Eq. 86 will not be equal to the $ACH_{F0,1}$ of Eq. 98. However, the application of the HLC decoupling method only requires to prove that the $ACH_{building}V_{ol\_building}$ of Eq. 86 and the $ACH_{building}V_{ol\_building}$ of Eq. 98 are equal. For that, the following demonstration is done. As detailed in section 2.4.2, when applying the ASTM D6245-18 to a thermal zone of a building, the measured final concentration of CO_2 (C_F) of a thermal zone is related to the measured initial concentration (C_I) and to the ACH_{decay} with the following formula:

$$C_F = C_I e^{-ACH_{decay}\, t_p} \; [ppm_{CO2}, \frac{mol_{CO2}}{mol_{air}}, \frac{m^3_{CO2}}{m^3_{air}}] \qquad \text{Eq. 99}$$

If there are mass interactions between thermal zones with different CO_2 concentrations together with mass interactions with the outdoors ambient, the ACH_{decay} will be different to the ACH values as calculated in Eq. 93 to Eq. 95. However, when the mass balance of CO_2 is done for the whole building of Figure 13 during a decay analysis period between t = 0 [s] to t = t [s], we get the following equation:

$$\begin{gathered}
\left(C_{I_{F0,1}} - C_{F_{F0,1}}\right)V_{ol_F0,1}\,\rho_{CO2} + \left(C_{I_{F0,2}} - C_{F_{F0,2}}\right)V_{ol_F0,2}\;\rho_{CO2} + \left(C_{I_{F1,1}} - C_{F_{F1,1}}\right)V_{ol_F1,1}\,\rho_{CO2} = \\
\left(\frac{n_{CO2,I,building}}{n_{air}} - \frac{n_{CO2,F,building}}{n_{air}}\right)V_{ol_building}\,\rho_{CO2} = \left(C_{I_{building}} - C_{F_{building}}\right)V_{ol_building}\,\rho_{CO2} \quad [\text{kg}] \\
\left(C_{I_{F0,1}} - C_{F_{F0,1}}\right)V_{ol_F0,1} + \left(C_{I_{F0,2}} - C_{F_{F0,2}}\right)V_{ol_F0,2} + \left(C_{I_{F1,1}} - C_{F_{F1,1}}\right)V_{ol_F1,1} = \\
\left(\frac{n_{CO2,I,building}}{n_{air}} - \frac{n_{CO2,F,building}}{n_{air}}\right)V_{ol_building} = \left(C_{I_{building}} - C_{F_{building}}\right)V_{ol_building} \quad [\text{m}^3]
\end{gathered} \qquad \text{Eq. 100}$$

Note that assuming Amagat Model [92] using the molar fraction or the volume fraction is equivalent to express the concentration. The Amagat Model assumes that the total volume of a mixture of ideal gases, is the sum of the partial volumes of each of the components of the mixture as if they were at the same total pressure and temperature as the mixture. Those partial volumes are proportional to the molar fraction its species has in the gas mixture. Assuming the total volume is the building volume and that the building indoor air total pressure and temperature have small variations regarding the density calculation of each of those partial volumes, the CO_2 density associated to the partial volume occupied by the CO_2 at the beginning of the decay period analysis and at the end of the decay period analysis can be considered constant. Thus, the mass balance, the molar balance and the volume balance of the CO_2 are equivalent in Eq. 100. This is a valid model

when the working gas behaves as an ideal gas, and the air, in usual building indoor conditions, behaves as an ideal gas. In Eq. 100 $n_{CO2,I,building}$ and $n_{CO2,F,building}$ are the total number of moles of CO_2 within the whole building at t = 0 [s] and at t = t [s], respectively. While n_{air} are the total number of moles of air within the whole building (it can be considered constant during the decay method application period unless huge temperature and/or pressure variations occur within the building). Thus, the term $\left(C_{I_{building}} - C_{F_{building}}\right) V_{ol\_building}$ represents the net amount of CO_2 that has been transferred from the building to the exterior during the decay period.

The decay method only considers the measured $C_{I_{Fi,j}}$ and the measured $C_{F_{Fi,j}}$ to estimate the corresponding thermal zone ACH_{Fi,j_decay}. Obviously, unless the thermal zones are completely airtight between them, the ACH_{Fi,j_decay} in general will be different to the $ACH_{Fi,j}$ calculated as in Eq. 93 to Eq. 95. For example, if F0,1 has the same indoor concentration as F0,2, even if there are infiltration exchanges between F0,1 and F0,2, the decrease on the concentration of F0,1, will only be due to the mass exchange of the F0,1 with the outdoors air. Then, in this case, even if the $ACH_{Fi,j}$ considers both mass exchanges (with the outdoor air and with F0,2), the decay analysis will only identify the part of the mass exchange that generates a concentration variation, this is, the exchange with the outdoors represented by ACH_{Fi,j_decay}.

Including Eq. 99 into Eq. 100 the following expression is obtained:

$$\left(C_{I_{F0,1}} - C_{I_{F0,1}} e^{-ACH_{F0,1\_decay}\, t_p}\right) V_{ol\_F0,1} + \left(C_{I_{F0,2}} - C_{I_{F0,2}} e^{-ACH_{F0,2\_decay}\, t_p}\right) V_{ol\_F0,2} + \left(C_{I_{F1,1}} - C_{I_{F1,1}} e^{-ACH_{F1,1\_decay}\, t_p}\right) V_{ol\_F1,1} = \left(C_{I_{building}} - C_{I_{building}} e^{-ACH_{building}\, t_p}\right) V_{ol\_building} \quad \text{Eq. 101}$$

[m³]

Since Eq. 101 fulfils the net CO_2 mass balance during a decay analysis test for the whole building, the Eq. 86 must also fulfil the air balance on the whole building basis. Of course, when the infiltration exchanges between thermal zones tend to zero, the individual ACH_{Fi,j_decay} values of Eq. 86 will tend to be equal to the $ACH_{Fi,j}$ of Eq. 98.

Resuming, when all the thermal zones of a building have the same indoor air temperature, if the HLC of those thermal zones is estimated, they will represent the HLC

value of those thermal zones regarding the outdoors air. Thus they will be meaningful in the sense that they do not consider energy exchanges with other thermal zones within the building. If the thermal zones have different temperatures, then the individual HLCs of the thermal zones will not represent the HLC of those thermal zones with the outdoors air. But even if individually they are not meaningful, when we aggregate all the HLCs of all the thermal zones, they represent the total HLC of the whole building envelope.

On the other hand, when the infiltration plus ventilation mass flow rates are estimated by means of the ACH_{decay} values obtained by means of the anthropogenic CO_2 decay analysis, they will only represent the total air flow exchange of the analysed thermal zone when the occupied thermal zones are completely airtight between them. In those cases, they will represent the mass exchange with the outdoors. However, if we sum all the infiltration plus ventilation rates of all the thermal zones of a building estimated by means of the ACH_{decay} values, the total building infiltration plus ventilation rates with the outdoors are obtained even if the thermal zones are not airtight between them.

In other words, only when all the building thermal zones have the same indoor air temperature and are completely airtight between them, the individual HLCs have physical meaning and could be decoupled maintaining the physical meaning with the estimated ACH_{decay} values.

Nevertheless, due to the similarity of the measured indoor temperatures in the different floors of the analysed four storey office building, the obtained individual thermal zones HLC results are meaningful. Furthermore, the thermal zones considered in the analysed building are separated by continuous concrete slabs, thus, the considered thermal zones are assumed to be airtight between them.

After the above demonstration regarding the infiltration and ventilation estimations, in order to develop further the estimation of the HLC done in section 2.1 using the average method, the next section describes the metabolic CO_2 decay method applied to estimate the thermal zone's Air Change per Hour (ACH_{decay}) and then the infiltration and/or ventilation heat loss coefficient estimation method (C_v). Finally, considering the HLC estimated previously, and the C_v estimated during this study, the decoupling method used is also described in detail.

2.4.2- Air Change per Hour (ACH_{decay}) estimation method by means of metabolic CO_2 decay analysis

The metabolic CO_2 of the building's occupants has been used as tracer gas to estimate air infiltration and/or ventilation rates by means of CO_2 concentration decay analysis. This is shortly how the concentration decay method works [95]: if a fixed quantity of tracer gas is uniformly distributed into a space, its concentration will reach a peak level. Subsequently, as the seeded air becomes diluted with incoming air, the concentration of tracer gas will gradually decay. The decay in tracer gas concentration is logarithmic, with the air exchange rate being directly related to the decay gradient. Therefore, the air change rate is given by the logarithmic gradient of the tracer gas decay concentration curve. This could be readily determined by plotting the tracer gas concentration decay over time on logarithmic paper.

The use of CO_2 generated from occupants as a tracer gas to determine air change rates in buildings is described in ASTM D6245-18, the 'Standard Guide for Using Indoor Carbon Dioxide Concentrations to Evaluate Indoor Air Quality and Ventilation' [83]. According to this guide, and together with the ASTM E741-11 Method [96], air change rates (or Air Changes per Hour, ACH in [h^{-1}]) can be estimated using the tracer gas decay technique in which occupant-generated CO_2 is used as a tracer gas if the measurements are conducted after the occupants leave the building.

These are the requirements established by the ASTM D6245-18 guide affecting to the in-use office building analysed in this Thesis:

- Section 9.3.1 of the guide: The decay technique is based on the assumption that there is no source of tracer gas in the building, which in the case of CO_2 means that the building is no longer occupied. In practice, an occupancy density of one person per 1000 m^2 or less will not impact the measurement results. To fulfil this requirement in the analysed office building, data from 18:00 to 20:00 hours has been used, shortly after the end of the working day.
- Section 9.3.2.: The tracer gas decay technique, as described in the Test Method ASTM E741-11, assumes that the outdoor tracer gas concentration is zero, which is not the case with CO_2. However, if the outdoor concentration is constant during the decay measurement, then the tracer gas decay technique can be used by substituting the

difference between the indoor and outdoor concentrations for the indoor concentration in the analysis contained in the Test Method. Analysing the data sets and having Figure 14 as an example, it can be stated that the background CO_2 concentration changes very little. The variation is within 3-5 ppm (minimum individual measurement 395 ppm), thus the background or outdoor concentration is considered constant as 400 ppm.

- Section 9.3.3.: The concentration measurement uncertainty must be better than ±5 % during the decay analysis period. When using CO_2 as a tracer gas, this precision requirement must be applied to the difference between the indoor to outdoor CO_2 concentrations. As shown in the experimental set-up section of this study, the monitoring system used in this study fulfils this requirement if the 350 ppm condition established in section 9.3.4 is fulfilled.
- Section 9.3.4.: The indoor CO_2 concentration when the building is finally unoccupied depends on the concentration in the building when the occupants start leaving, the amount of time it takes them to leave, and the air change rate of the building. Depending on the values of these parameters, the indoor CO_2 concentration may be too low once the building is unoccupied to perform a reliable tracer gas decay measurement. It is proposed an initial minimum acceptable value of the decay should be 350 ppm (the difference between the indoor and outdoor concentrations) to avoid low concentration values at the end of the measurements that could reduce the reliability of the measurements. This minimum initial value permits the section 9.3.3 uncertainty requirement to be fulfilled at the end of all the periods analysed in this work. This minimum value has been fixed following a procedure that permits the ±5 % accuracy stated in section 9.3.3 to be complied with, even at the end of the decay curve. The previously mentioned Eq. 99 (now Eq. 102) can be used to estimate the final indoor to outdoor concentration difference:

$$C_F = C_I e^{-ACH_{decay}\, t_p} \; [ppm_{CO2}, \frac{mol_{CO2}}{mol_{air}}, \frac{m^3_{CO2}}{m^3_{air}}] \qquad \text{Eq. 102}$$

where C_F is the final indoor to outdoor concentration difference [ppm], C_I is the initial indoor to outdoor concentration difference [ppm] (350 ppm is assumed to be the initial minimum possible value), ACH_{decay} is the Air Change per Hour [h^{-1}] and t_p is the time [h] (2 hours in our analysis). Then, fixing the initial minimum indoor to

outdoor concentration difference C_I and considering the maximum ACH_{decay} value obtained for all the identified valid days for analysis, it is possible to check whether the selected C_I value is high enough to fulfil the 9.3.3 uncertainty requirement for all the estimated C_F values. Therefore, Eq. 103 is used to check if the lowest estimated C_F value provided by Eq. 102 fulfils the ±5 % accuracy stated in section 9.3.3:

$$Relative\ error = \frac{Total\ measurement\ error}{C_F} \times 100 = < 5\ \% \qquad \text{Eq. 103}$$

where the "Total measurement error" is the ((C_F + 400ppm) x error of the sensor (1 % in this case)). Then, if this lowest possible C_F is lower than 5 %, it would be possible to fulfil the section 9.3.3 uncertainty requirement for all the measurements carried out in this work. Then, the selected minimum of 350 ppm for the C_I value would be a proper initial indoor to outdoor concentration difference for all cases.

- Section 9.3.5.: The Test Method ASTM E741-11 requires that the indoor tracer gas concentration at multiple points (at least three) within the analysed thermal zone (a floor of the analysed in-use building in this case) differs by less than 10 % of the average concentration in the floor (at least at the beginning and end of the sampling period). When using CO_2, this concentration uniformity requirement should be applied to the difference between the indoor to outdoor concentrations.

Due to the different spatial distributions of the ground floor and the second floor (F0 and F2) of the office building presented in section 3.3.3, the last requirement has never been fulfilled for these two floors for any of the days of the analysed period. Since these floors are formed by smaller office rooms, it is impossible to homogenise the CO_2 in the whole floor. Therefore, for these two floors, the last requirement has been substituted by the following proposed extra-requirement to ensure acceptable results for some days of the analysed period:

- To ensure no windows are opened, the maximum acceptable value of outdoor daily average temperature has been established at 10 °C, assuming the building's users will not open windows with such low outdoor temperatures. In fact, the not opening of windows is only required for the period 18:00 to 20:00, when the decay analysis is applied. If a window is opened, for example from 16:00 to 17:00, there will be a sudden drop of the CO_2 and it will make it more difficult to fulfil the 9.3.4 and 9.3.5

criteria in the subsequent period 18:00 to 20:00. In this work, the decay analysis has been done manually for each of the daily regressions. The opening of windows has been detected visually in the monitored data by representing the CO_2 ppm over time, as in Figure 14, where the sensor 'S3' has a sudden drop from 16:00 to 17:30 on the first day (9th February 2015). This is a clear window opening of the office where the sensor 'S3' is installed. If this type of disturbance were present in any of the floor sensors between 18:00 to 20:00, the data of the corresponding day would have been discarded. In any case, on cold days, the opening of windows was not detected after 18:00. It is thus possible to ensure similar window opening behaviour in all the different compartmentalised offices. Thus, measuring only CO_2 concentrations in a few of them would be sufficient, since the infiltration behaviour can be assumed to be similar for all of them. On hotter days, it is possible to have different window opening behaviours between compartmentalised offices and, thus, measuring CO_2 in a few of them will lead to erroneous results. Although this time the window opening check has been done visually, it seems feasible to be able to automatically detect window openings by analysing the CO_2 concentrations over time, as discussed above.

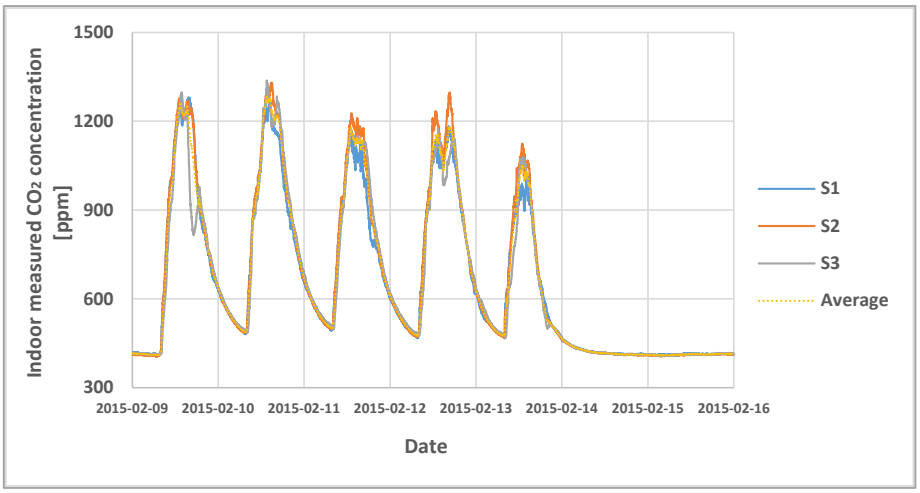

Figure 14. Minute by minute measured air quality data of each sensor of the first floor (F1) from 9th to 15th of February 2015 over time.

After the rehabilitation, as later explained in section 3.3.3, a ventilation system with recovery was installed in the building. Due to the ventilation system, the CO_2 concentration inside the building will be considerably lower than the CO_2 concentration without it (see Figure 15). Figure 15 shows the measured CO_2 data for a week in February

as analysed in Figure 14, but after the rehabilitation. There can be seen, as compared with Figure 14, that the maximum indoor CO_2 concentration inside the first floor is considerably lower than before. Then, it would be more complicated to find days where all the requirements of ASTM D6245-18 are fulfilled, especially section 9.3.4.

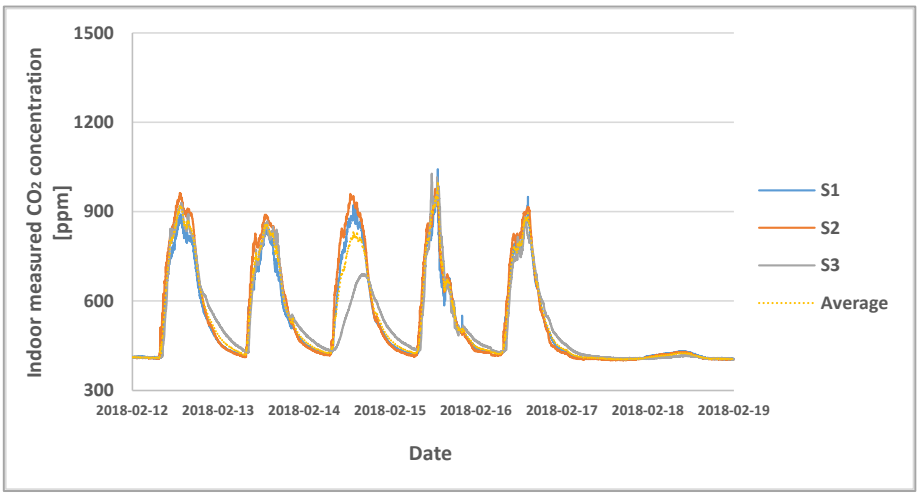

Figure 15. Minute by minute measured air quality data of each sensor of the first floor (F1) from 12th to 18th of February 2018 over time.

The Air Changes per Hour (ACH_{decay} in [h^{-1}]) of each day fulfilling the above requirements have been estimated for each floor, using the available minute CO_2 concentration data in [ppm] before and after the rehabilitation. The average ACH_{decay_aver} of each floor for each considered winter period is therefore the average of the ACH_{decay} values for those days that meet all the above requirements within the analysed winter. Then, for each analysed winter period, the ACH_{decay_aver} of each floor is used for the estimation of the floor-by-floor infiltration (before rehabilitation) or infiltration and/or ventilation (after rehabilitation) heat loss coefficient (C_v).

2.4.3- Air infiltration heat loss coefficient (C_v) estimation method before rehabilitation

When analysing the data of the considered winters before the rehabilitation, no ventilation heat losses need to be considered, since there was no ventilation system installed in the building during these winter periods. Then, based on the ACH_{decay} values estimated using the section 2.4.2 methodology, it is possible to estimate the air infiltration heat loss coefficient ((C_v) in [kW/K]) of each analysed floor using Eq. 104.

$$C_v = C_{v-inf} = V_{ol\_floor} ACH_{decay\_aver} \rho_{air} Cp_{air} \text{ [kW/K]} \quad \text{Eq. 104}$$

where V_{ol_floor} is the volume of each floor [m^3], ACH_{decay_aver} is the floor average Air Change per Hour for the whole considered testing period in [h^{-1}], ρ_{air} [kg/m^3] and Cp_{air} [kJ/kg°C] are the density and the constant pressure specific heat of the air at the average indoor temperature, respectively. Note that, in this equation, it is necessary to convert ACH_{decay_aver} to [s^{-1}] to obtain the C_v in [kW/K].

For the ground and second floors, an extra calculation has been made to guarantee appropriate results. Taking into account the distribution of these two floors and the location of the air quality sensors, each sensor has been assigned a portion of the total volume of each floor (see Figure 44), and the C_v of the ground floor and second floor have been estimated using both Eq. 104 and Eq. 105. The results obtained by Eq. 104 and Eq. 105 have then been compared.

$$C_v = C_{v-inf} = \sum_{i=1}^{N}(V_{ol\_i} \times ACH_{decay\_aver\_Vi})\rho_{air}Cp_{air} \quad [kW/K] \qquad \text{Eq. 105}$$

where V_{ol_i} and $ACH_{decay\_aver\_Vi}$ are the volume portions and the average Air Change per Hour of the considered period associated with each volume portion, respectively, and N is the number of divisions made in the total volume of each floor (see Figure 44).

2.4.4- Air infiltration and ventilation heat loss coefficient (C_v) estimation method after rehabilitation

During the rehabilitation carried out, the building was dotted with a ventilation system together with its recovery system in each of the floors. Therefore, unlike in section 2.4.3, section 2.4.4 must consider the effect of the ventilation losses in the building. Then, based on the ACH_{decay} values estimated using the methodology presented in section 2.4.2 for the period after rehabilitation, it is possible to estimate the air infiltration and ventilation heat loss coefficient ((C_v) in [kW/K]) of each floor. Therefore, it is necessary to have a proper measurement of the volumetric airflow rate of the ventilation system for each of the floors. Moreover, it is possible to estimate the average total volumetric airflow rate of each floor ($\dot{V}_{air\ (total)}$) of the building by the multiplication between the average ACH_{decay_aver} estimated using the methodology of section 2.4.2 for data after the rehabilitation for each of the floors and the volume of each floor as shown in Eq. 106:

$$\dot{V}_{air\ (total)} = V_{ol\_floor}ACH_{decay\_aver} \ [m^3/h] \qquad \text{Eq. 106}$$

where V_{ol_floor} is the volume of each floor [m^3] and ACH_{decay_aver} is the floor average Air Change per Hour for the whole considered testing period in [h^{-1}].

Then, if the average total volumetric airflow rate is calculatedo estimate the average infiltration volumetric airflow rate ($\dot{V}_{air\ (inf)}$). It can be estimated using Eq. 107:

$$\dot{V}_{\text{air(inf)}} = \dot{V}_{air(total)} - \dot{V}_{air(vent)} \ [\text{m}^3/\text{h}] \qquad \text{Eq. 107}$$

Once the average ventilation volumetric airflow rate and the average infiltration volumetric airflow rate are known, it is possible to estimate the corresponding ventilation and infiltration heat loss coefficients. In order to estimate these two coefficients, Eq. 108 and Eq. 109 need to be applied.

$$C_{v-vent} = \dot{V}_{air(vent)}\rho_{air}cp_{air} \cdot (1-\eta) \ [\text{kW/K}] \qquad \text{Eq. 108}$$

$$C_{v-inf} = \dot{V}_{air(inf)}\rho_{air}cp_{air} \ [\text{kW/K}] \qquad \text{Eq. 109}$$

where, $\dot{V}_{air(vent)}$ and $\dot{V}_{air(inf)}$ are the average ventilation and infiltration volumetric airflow rates respectively [m^3/s], ρ_{air} [kg/m^3] and Cp_{air} [kJ/kgK] are the density and the constant pressure specific heat of the air at the average indoor temperature respectively. For estimating the ventilation heat loss coefficient, it is necessary to consider the efficiency (η) of the recovery system installed in the ventilation system. Note that it is necessary to convert ACH_{decay_aver} to [s^{-1}] to obtain C_v in [kW/K]. Eq. 108 and Eq. 109 are valid for compensated ventilation systems where supply and exhausted volumetric flow rates are equal.

Finally, both heat loss coefficients are summed in order to estimate the infiltration and ventilation heat loss coefficient (C_v) as shown in Eq. 110:

$$C_v = C_{v-vent} + C_{v-inf} \ [\text{kW/K}] \qquad \text{Eq. 110}$$

2.4.5- Estimation of the transmission heat loss coefficient (UA) before and after the rehabilitation

Section 2.4.2, 2.4.3 and 2.4.4 have already described the method used, based on the ASTM D6245-18 guide, to estimate the infiltration and infiltration/ventilation heat loss coefficient of the analysed in-use office building. However, in order to achieve the aim of

this work, it is necessary to use these results together with the previously estimated HLC values using the methodology presented in section 2.1 to estimate the transmission heat loss coefficient for winters before and after rehabilitation. Thus, it would be possible to know which of the coefficients, the transmission heat loss coefficient or the infiltration or infiltration/ventilation heat loss coefficient, is the main responsible factor for the energy losses regarding the building envelope. Therefore, the average floor-by-floor infiltration and/or ventilation heat loss coefficient value for each of the winters is subtracted from each floor HLC value of the corresponding winter. The same is done with the sum of all the floors in order to estimate the total results for the whole building. This procedure is carried out using Eq. 111.

$$\mathrm{UA} = \mathrm{HLC} - C_v \ \text{[kW/K]} \qquad \text{Eq. 111}$$

CHAPTER 3: CASE STUDIES

3. CASE STUDIES

This chapter presents three different case studies, each of them providing different input data and different characteristics. Despite that, and although the average method was developed based on the multi-storey occupied office building, all the cases will be tested in order to estimate their HLC, since all of them provide input data that enables its estimation. However, depending on the rest of the measured variables they provide, each of the case studies will be used in order to demonstrate the validity of the rest of the methodologies presented in section 2. For instance, due to the wide range of solar radiation data measured in the Round Robin Box, it is perfect for the application of the methodology presented in section 2.2. However, only the measurements of the air quality data inside the office building presented in section 3.3 enable the application of the HLC decoupling methodology presented in section 2.4.

In order to justify the application of each methodology for each case study, their characteristics and their monitoring systems are detailed in this section. The three case studies used in the Thesis are, the Round Robin Box, two in-use residential buildings and a rehabilitated multi-storey occupied office building.

3.1- The Round Robin Box

3.1.1- Description of the Round Robin Box

Unlike common study cases, when applying the energy characterization in buildings, the proposed analysis is not carried out in a real building, but in a test box representing a building in miniature. This Round Robin Box has been built by KU Leuven and shipped to different countries in order to test its behaviour under different climate conditions. The Round Robin Box has been monitored by several participants in different countries and the obtained data has been distributed to different members taking part in the International Energy Agency (IEA) Annex 58 project [50].

The test box has an exterior volume of 120x120x120 cm^3 and all the walls, floor and ceiling have the same thickness of 12 cm. Thus, the dimensions of the inner surface of the Round Robin Box are 96x96x96 cm^3. There is a wooden window of 71x71 cm^2 located in one side of the Round Robin Box with a glazed part of 52x52 cm^2. Moreover, the Round

Robin Box is not in contact with the floor in order to avoid the effects of the ground on the Round Robin Box's behaviour. The test box can be seen in Figure 16, located in CIEMAT's Solar Plataform in Almeria (Spain).

Figure 16. The Round Robin Box during its experiment in Almeria.

Moreover, the theoretical values for the HLC and the S_a of the window were also calculated in [64]. Then, the theoretical HLC value is 4.08 W/K and the theoretical S_a for the window is 0.162 m^2.

3.1.2- Monitoring system of the Round Robin Box

As introduced in section 3.1.1, the Round Robin Box experiment has been carried out in several locations in Europe. However, only the data regarding the tests carried out at CIEMAT's Solar Plataform in Tabernas (lat. 37.09°, long. -2.35°), Almeria (Spain), has been analysed during this study due to the availability of multiple extra sensors included in the experimental set up. Moreover, Almeria receives a high solar radiation during both summer and winter, so the obtained solar radiation measurements are valid for carrying out the proposed study.

During the Round Robin Box test, a wide range of variables were measured. On the one hand, there is enough data for the estimation of the HLC using the average method. All the measured values used for the estimation of this performance indicator are shown in the following Table 2:

SENSOR	MEASUREMENT	DESCRIPTION	UNIT	UNCERTAINTY
Temperature	Indoor air temperature (T_{in}) *PT100, 1/10 DIN, 4 wire connection*	Indoor temperature measured in the lower part of the Round Robin Box (1/3 height of the box) and in the higher part of the Round Robin Box (2/3 height of the box).	°C	0.1 °C
	Outdoor air temperature (T_{out}) *PT100, 1/10 DIN, 4 wire connection*	Outdoor temperature measured below the Round Robin Box and at the same height as the middle of the Round Robin Box.	°C	0.1 °C
Heating system	Heating power (Q) *Power transducer, model SINEAX DME 440 manufactured by Camille Bauer Ltd.*	Heating power in the Round Robin Box	W	0.25 %
Solar radiation	Vertical south global solar radiation (plane of the glazing) (V_{sol}) *Pyranometers, model CM11 manufactured by Kipp and Zonen.*	Vertical south global solar radiation (plane of the glazing)	W/m^2	3 %

Table 2. Sensors used for measuring the variables required for the HLC estimation.

For the estimation of the HLC, in order to make a rough estimate of the solar gains entering through the window of the Round Robin Box, the vertical south global solar radiation has been multiplied by the solar aperture of the window of the Round Robin Box. The Round Robin Box only have one window, which has been orientated to the south during the analysed period. Therefore, it can be assumed that the vertical south global solar radiation is the main responsible of the solar gains entering through the window. Then, the window solar aperture has been roughly estimated by multiplying the window area and a 0.5 g-value proposed in section 2.1.1. Then, the obtained window solar aperture was 0.135 m^2. Moreover, it must be commented, that there have not been considered any electrical heat gains or metabolic heat gains apart from the heating power in the HLC estimation since the Round Robin Box was unoccupied.

Furthermore, Table 2 also shows the accuracy of each of the used sensors. This information is provided since the propagation of the uncertainty of the sensors has been considered when estimating the HLC error bands as explained in section 2.1.3. It must be

remembered that the other uncertainty sources related to the assumptions made by the method are not propagated to the HLC estimations carried out in this work. Despite the solar aperture is considered unknown, the error estimated for this value was a 10 %. Since the accuracy of the pyranometer measuring the vertical south global solar radiation was of 3 %, the total uncertainty considered for the solar gains was 13 %.

On the other hand, the Round Robin Box is also used to perform the solar gains analysis through the opaque walls. Therefore, in order to carry out a deeper analysis of the solar gains through the Round Robin Box's different opaque faces (east, north and west walls, roof and ceiling), each of the faces was analysed individually. The Round Robin Box walls are named as follows: the glazing wall (the one with the window and orientated to the south), the east wall (the opaque wall orientated to the east), the west wall (the opaque wall orientated to the west), the north wall (the opaque wall orientated to the north), the ceiling wall (the opaque wall orientated to the sky) and the floor wall (the opaque wall orientated to the ground). However, the glazing wall is excluded from the analysis, since only the effect of the solar radiation in opaque walls is analysed. Among the several measurements carried out during the Almeria Round Robin Box test, Table 3 shows only the variables measured within the Round Robin Box experiment that will be used during the proposed analysis of the solar gains through the opaque walls of the Round Robin Box. A full description of the experiment set up is included in the final report of Annex 58 [64].

NAME	MEASUREMENT	DESCRIPTION	UNIT	ACCURACY
Temperature	Indoor air temperature (T_{in}) *PT100, 1/10 DIN, 4 wire connection*	Indoor temperature measured in the lower part of the Round Robin Box (1/3 height of the box) and in the higher part of the Round Robin Box (2/3 height of the box).	°C	0.1 °C
	Outdoor air temperature (T_{out}) *PT100, 1/10 DIN, 4 wire connection*	Outdoor temperature measured below the Round Robin Box and at the same height as the middle of the Round Robin Box.	°C	0.1 °C
	Inner surface temperature (T_{Sin}) *Analogous sensors and connections as those used for air temperature, embedded in the corresponding surface.*	Inner surface temperature measured in the centre of each of the walls	°C	0.1 °C
	Outer surface temperature (T_{Sout}) *Analogous sensors and connections as those used for air temperature, embedded in the corresponding surface.*	Outer surface temperature measured in the centre of each of the walls	°C	0.1 °C
Heat flux	Heat flux in the inner surface ($\dot{q}$) *HFP01 manufactured by Hukseflux, voltage measured directly by differential connection.*	The heat flux measured in the centre of each of the walls, gluing the sensor in the centre of each inner face and covered with the same colour type.	W/m^2	5 %
Solar radiation	Vertical south global solar radiation (plane of the glazing) (V_{sol}) *Pyranometers, model CM11 manufactured by Kipp and Zonen.*	Vertical south global solar radiation (plane of the glazing)	W/m^2	3 %
	Horizontal global solar radiation (H_{sol}) *Pyranometers, model CM11 manufactured by Kipp and Zonen*	Horizontal global solar radiation	W/m^2	3 %
	Diffuse solar radiation (D_{sol}) *Pyranometers, model CM11 manufactured by Kipp and Zonen.*	Diffuse solar radiation	W/m^2	3 %
	Ground reflected solar radiation (G_{gr_1}) *Pyranometers, model CM11 manufactured by Kipp and Zonen*	Ground reflected solar radiation	W/m^2	3 %
	Vertical north global solar radiation (V_{n_sol}) *Pyranometers, model CM11 manufactured by Kipp and Zonen*	Vertical north global solar radiation	W/m^2	3 %
	Horizontal long wave radiation (H_{LW}) *Pyrgeometers, model CGR-4 manufactured by Kipp and Zonen.*	Horizontal long wave radiation	W/m^2	2 %
	Vertical south long wave radiation (V_{LW}) *Pyrgeometers, model CGR-4 manufactured by Kipp and Zonen.*	Vertical south long wave radiation	W/m^2	2 %
Wind	Wind speed (WS) *WindSonic manufactured by GILL INSTRUMENTS LTD*	Wind speed	m/s	2 %

Table 3. Sensors used for measuring the variables required for the solar gains analysis through opaque walls.

Table 3 shows only the sensors used for this second part of the Round Robin Box analysis. As shown, some of the variables used in Table 2 for the HLC estimation are also used for the solar gains analysis in opaque walls. Due to the comprehensive set of solar radiation measurements performed in the Round Robin Test in Almeria, it has been considered a perfect candidate to perform the proposed analysis. However, two of the solar radiations needed for this analysis are not measured by sensors. They are the vertical west (W_{sol}) and east (E_{sol}) global solar radiation, which are estimates as detailed in section 2.2.2.1.

The experiment in Almeria was conducted over eight months; including a first period under summer conditions and a second period under winter conditions. The summer dataset considers the period from 31st May 2013 until 2nd July 2013. During the summer period, two different tests were performed: constant indoor air temperature set point and Randomly Ordered Logarithmic Binary Sequence (ROLBS) power sequence [97]. This dataset has been divided in 5 different series. The measurements of the first three series (from 31st May 2013 to 17th June 2013) were considered reliable but the test conditions were not completely optimized. However, the two last series (from 18th June 2013 to 2nd July 2013) were fully optimized. From 18th June 2013 to 26th June 2013, a controlled 100 W incandescent lamp was used as heating power. During that series, a set point of 40 °C was fixed for the indoor air temperature, with a dead band of 0.8 °C for the first day and 0.5 °C for the rest of the days. The series from 28th June 2013 to 2nd July 2013 corresponds to ROLBS power sequence where a 60 W incandescent lamp was used as heating power. However, the winter dataset considers the period from 6th December 2013 until 7th January 2014. During this winter period, three different tests were performed: two co-heatings with constant indoor air temperature set point and a ROLBS power sequence. There, during the first series from 6th December 2013 to 17th December 2013, the ROLBS power sequence test was performed where a 100 W incandescent lamp was used as heating power. However, in the other two series the co-heating test was performed with a set point and a dead band for the indoor temperature. In the case of the second series (from 18th December 2013 to 26th December 2013) a set point of 35 °C and a dead band of 0.5 °C were fixed. Moreover, in the case of the third series (from 27th December 2013 until 7th January 2014) a set point of 21 °C and a dead band of 0.8 °C were fixed. For both cases, a 100 W incandescent lamp was used as heating power. Then, once both datasets

had been individually analysed by plotting each of the measured data and comparing them in order to find any irregularity, as done in section 3.1.3, summer and winter datasets were divided into shorter periods for analysis. Due to the requirements stablished in section 2.1.1, the average method is only applicable in cold and cloudy winter periods. Therefore, for that analysis, only the winter data will be used. Despite the analysis of the solar gains through opaque walls is also applied to the winter data in order to test whether the HLC already estimated using the average method without considering them has a negligible uncertainty, also the summer data has been analysed. Thus, a comparison between two extreme cases will be performed in order to test these solar gains weight in the HLC value for both situations.

3.1.3- Representation of the useful input data of the Round Robin Box

In order to ensure a proper analysis when working with measured data, the visual checking of the input data is an indispensable first step of the process. Therefore, the analysis of the estimation of the HLC is not an exception. Then, this section shows graphically represented all the input data used for the proper estimation of the HLC and also, the input data used for the estimation of the solar gains effect in opaque walls.

As commented is section 3.1.2, all the useful data needed for the HLC estimation provided for this case study is shown in Table 2 and plotted in the following Figure 17, Figure 18, Figure 19 and Figure 20. Despite a winter and a summer dataset are provided for the Round Robin Box test, the heat loss coefficient estimation analysis, due to the requirements stablished in section 2.1.1, can only be carried out during the winter period, between the 6th December 2013 and the 7th January 2014.

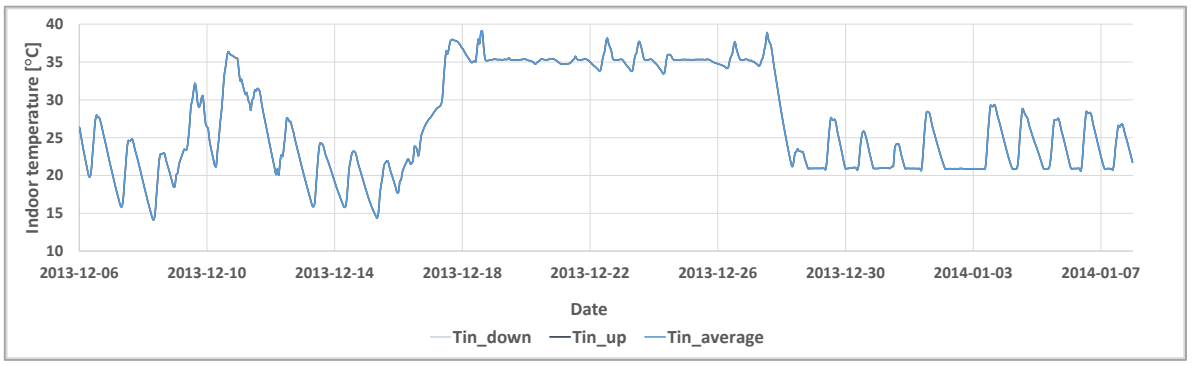

Figure 17. Indoor air temperature measured in the lower part (T_{in_down}) of the Round Robin Box (1/3 height of the box), in the higher part (T_{in_up}) of the Round Robin Box (2/3 height of the box) and the average ($T_{in\_average}$) of both of the winter period. Note: The two measured temperatures, and of course, the average temperature value, overlap perfectly during the whole winter period.

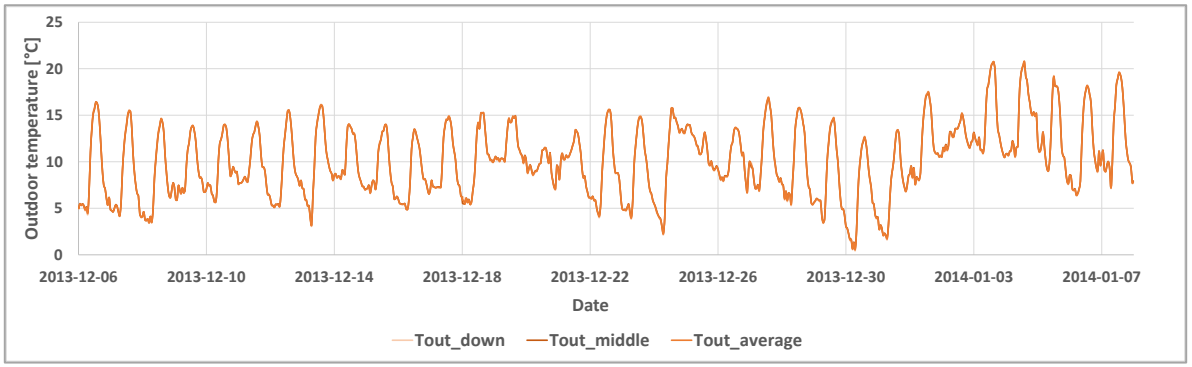

Figure 18. Outdoor air temperature measured below (T_{out_down}) the Round Robin Box and as the same height of the middle (T_{out_middle}) of the Round Robin Box and the average ($T_{out\_average}$) of both of the winter period. Note: The two measured temperatures, and of course, the average temperature value, overlap perfectly during the whole winter period.

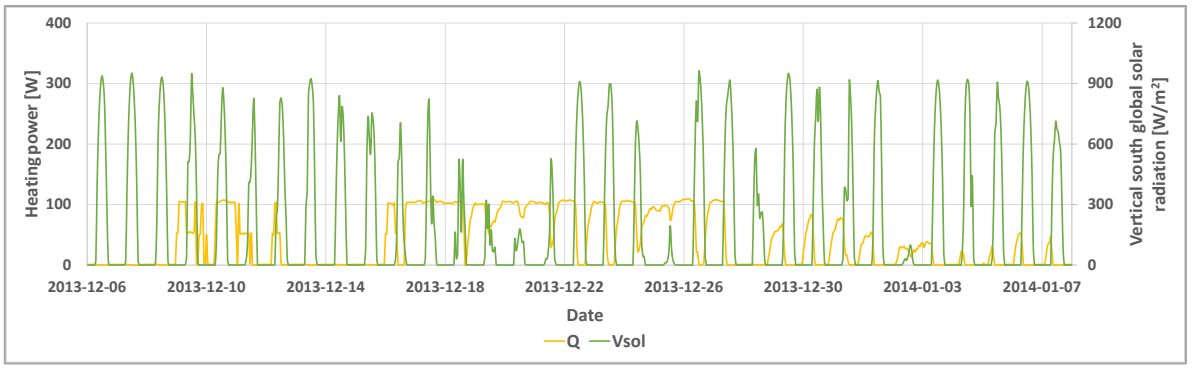

Figure 19. Heating power and vertical south global solar radiation (plane of the glazing) of the winter period.

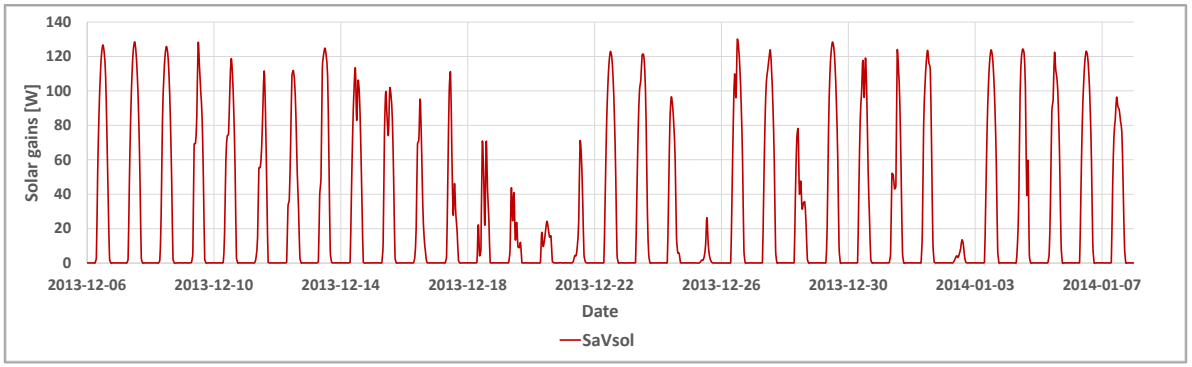

Figure 20. Estimated solar gains through the window of the winter period.

From this figures, it is possible to take a considerable amount of initial conclusions. First of all, it is possible to find the missing data and check if the measured data makes sense. Moreover, the visual checking enables the possibility to find periods that fulfil the requirements of section 2.1.1 such as the one related with the solar radiation or the minimum indoor to outdoor temperatures difference. An example of this can be seen in Figure 21 and Figure 22, where the period 1 of section 4.1.1 later analysed is marked fulfilling all these requirements.

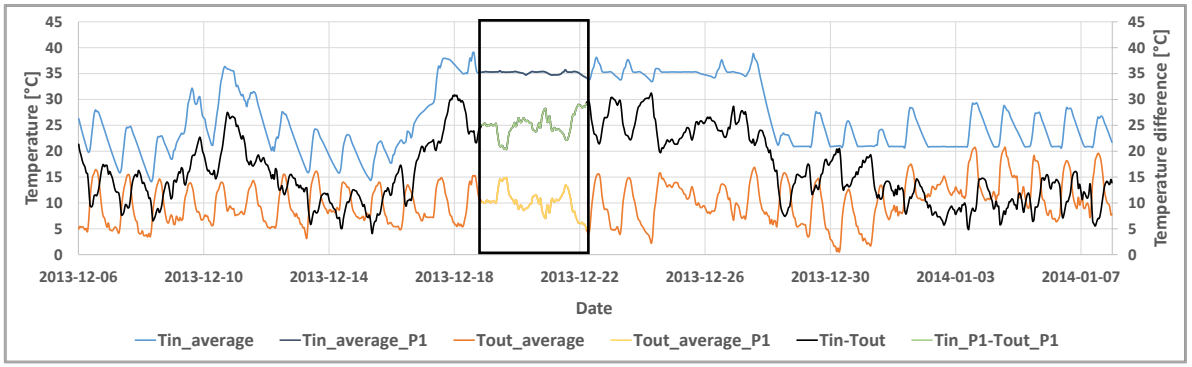

(a)

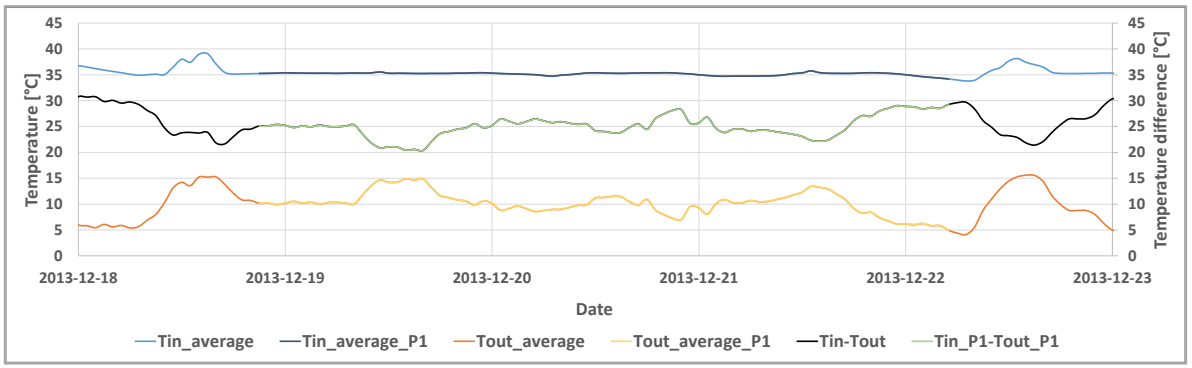

(b)

Figure 21. Indoor air temperature ($T_{in\_average\_P1}$), outdoor air temperature ($T_{out\_average\_P1}$) and air temperature difference (T_{in_P1}- T_{out_P1}), (a) for the whole winter dataset, (b) for period 1.

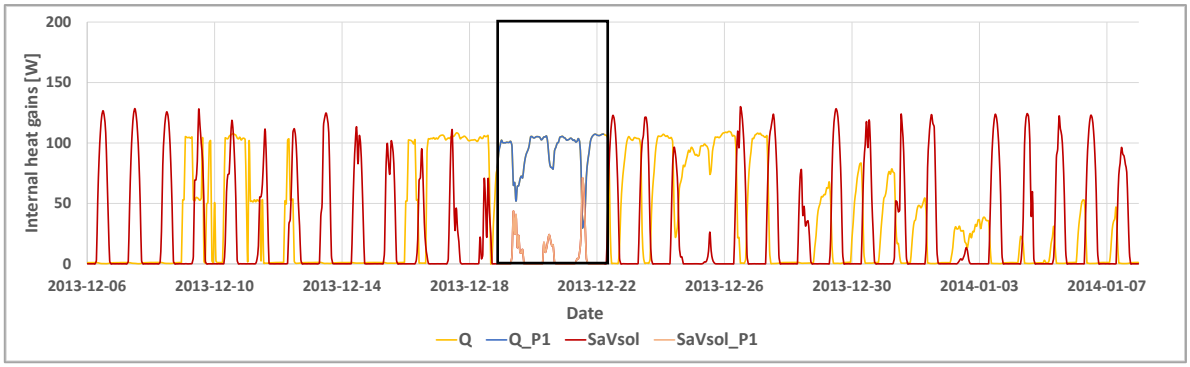

(a)

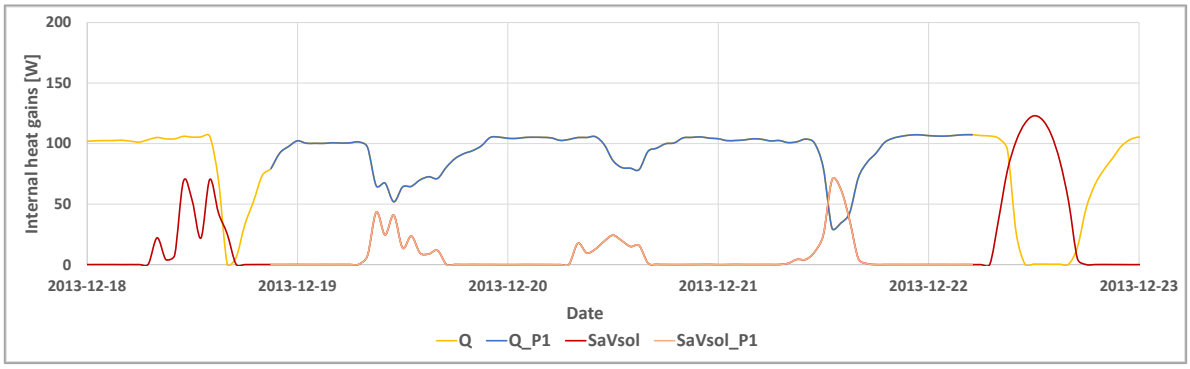

(b)

Figure 22. Space-heating systems' heat input (Q_{P1}) and vertical south global solar radiation (V_{sol_P1}), (a) for the whole winter dataset, (b) for period 1.

As said before, it can be normally easy to identify or to take an idea of where the useful periods for HLC estimation by means of the average method could be by visual checking. For example, in this case, it is possible to identify in Figure 21 that the useful period could be between the 18th of December and the 27th of December, since the temperature difference is quite high there. If also the solar gain requirement is considered in Figure 22, it is obvious that the lowest solar gains are obtained between the 18th of December and the 22nd of December, which coincides with the period selected as the one with the highest temperature difference. Then, it must be numerically analysed and the rest of the requirements fulfilment must be also ensured. However, this first steps considerably helps in the period selection process.

However, in order to carry out the solar gains analysis in opaque walls, it is necessary to analyse other input data also shown in Table 3 of section 3.1.2. Moreover, as explained in section 2.2.1, some other data must be also calculated such as the sky, the surrounding and the ground temperature shown in Figure 27 and Figure 33 using some input data presented in Table 3. These values will be also useful for the later solar gains analysis

through the Round Robin Box opaque walls. All this data (the measured and the calculated) is plotted in the following Figure 23 to Figure 34 where both, summer (from 31st May 2013 until the 2nd July 2013) and winter (from 6th December 2013 until the 7th January 2014) periods are shown.

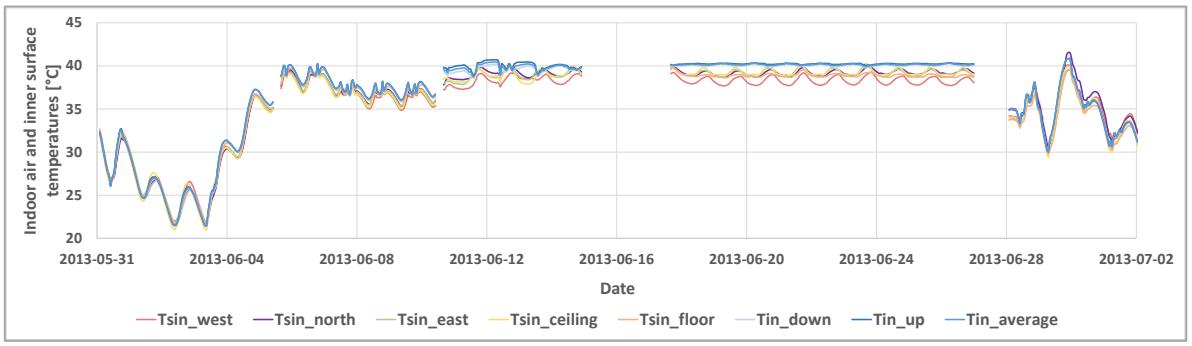

Figure 23. Inner surface temperature in the west (T_{Sin_west}), north (T_{Sin_north}), east (T_{Sin_east}), ceiling ($T_{Sin\_ceiling}$) and floor (T_{Sin_floor}) of the Round Robin Box and indoor air temperature measured in the lower part (T_{in_down}) of the Round Robin Box (1/3 height of the box), in the higher part (T_{in_up}) of the Round Robin Box (2/3 height of the box) and the average ($T_{in\_average}$) of both of the summer period.

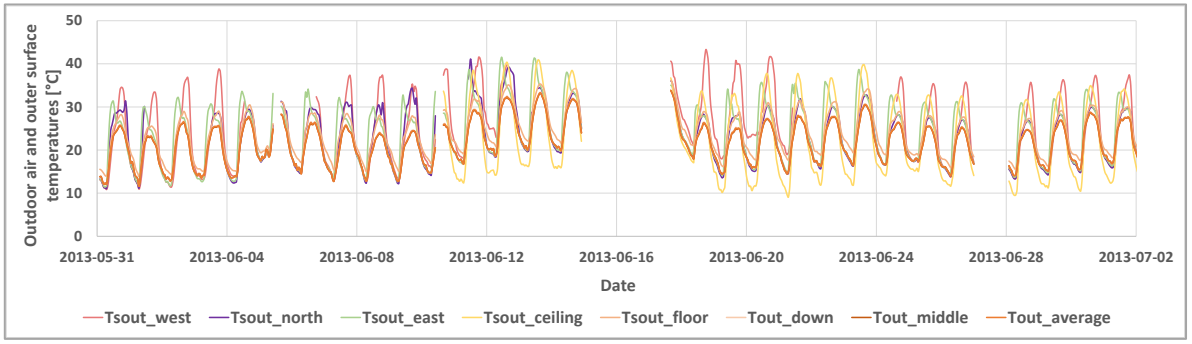

Figure 24. Outer surface temperature in the west (T_{Sout_west}), north (T_{Sout_north}), east (T_{Sout_east}), ceiling ($T_{Sout\_ceiling}$) and floor (T_{Sout_floor}) of the Round Robin Box and outdoor air temperature measured below (T_{out_down}) the Round Robin Box (1/3 height of the box), at the same height of the middle (T_{out_middle}) of the Round Robin Box and the average ($T_{out\_average}$) of both of the summer period.

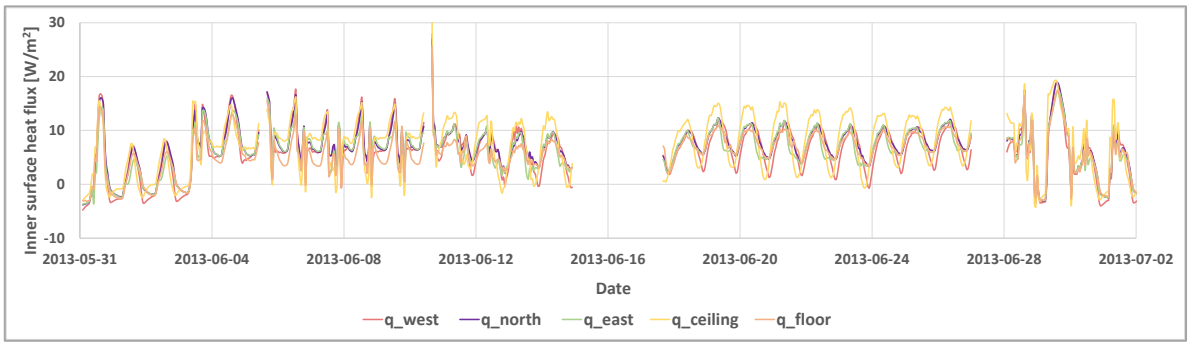

Figure 25. Inner surface heat flux in the west ($\dot{q}_{\_west}$), north ($\dot{q}_{\_north}$), east ($\dot{q}_{\_east}$), ceiling ($\dot{q}_{\_ceiling}$) and floor ($\dot{q}_{\_floor}$) of the Round Robin Box in the summer period.

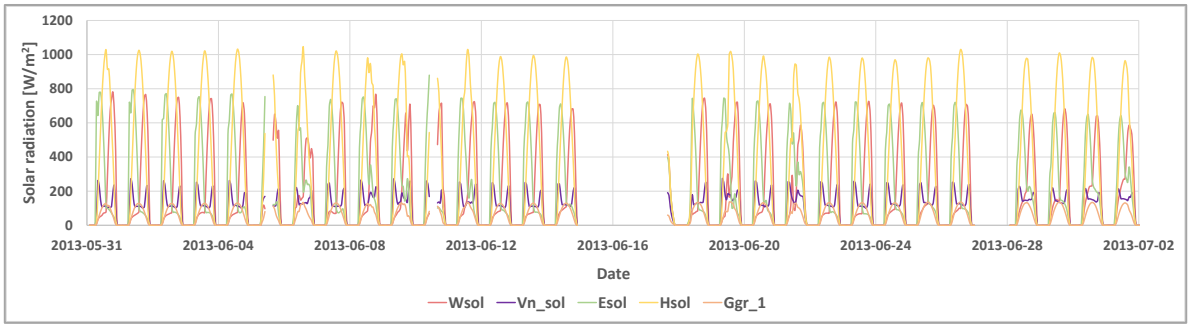

Figure 26. Solar radiation on the west (W_{sol}), north (V_{n_sol}), east (E_{sol}), ceiling (H_{sol}) and floor (G_{gr_1}) of the Round Robin Box in the summer period.

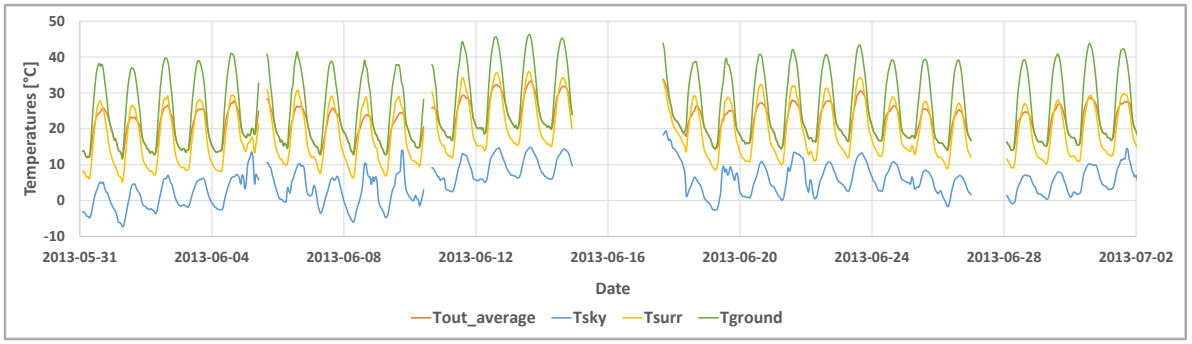

Figure 27. The outdoor average ($T_{out\_average}$) air temperature, the sky temperature (T_{sky}), the surrounding temperature (T_{surr}) and the ground temperature (T_{ground}) for the summer period.

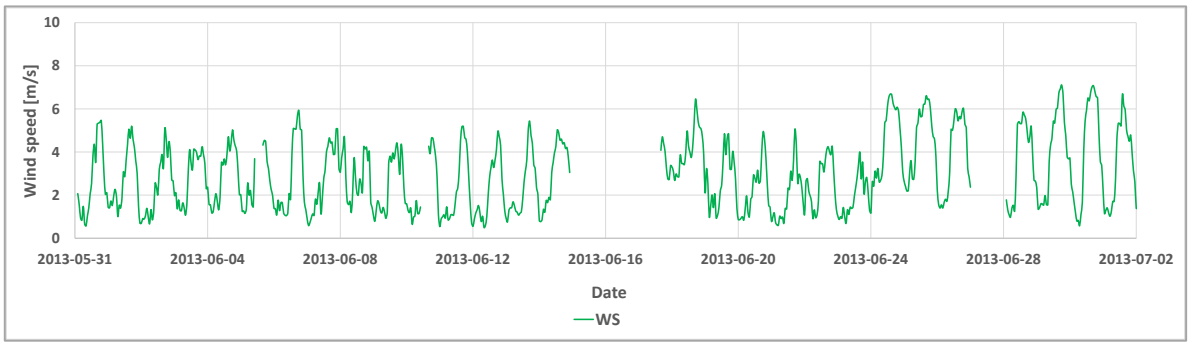

Figure 28. Wind speed (WS) for the summer period.

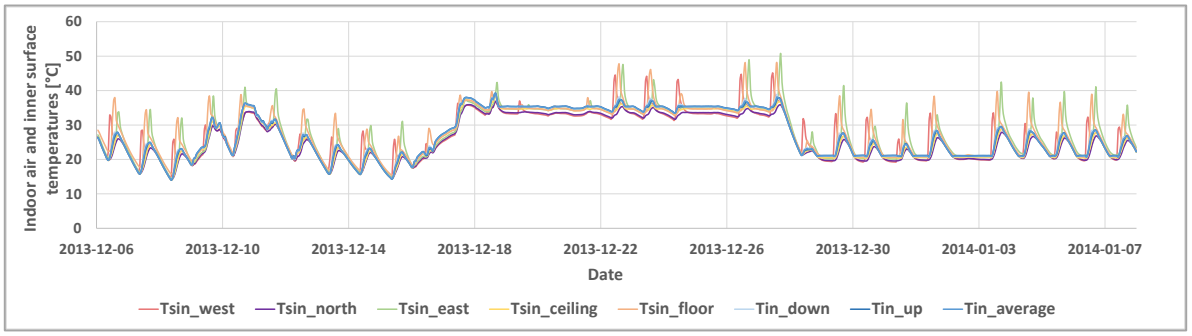

Figure 29. Inner surface temperature in the west (T_{Sin_west}), north (T_{Sin_north}), east (T_{Sin_east}), ceiling ($T_{Sin\_ceiling}$) and floor (T_{Sin_floor}) of the Round Robin Box and indoor air temperature measured in the lower part (T_{in_down}) of the Round Robin Box (1/3 height of the box), in the higher part (T_{in_up}) of the Round Robin Box (2/3 height of the box) and the average ($T_{in\_average}$) of both of the winter period.

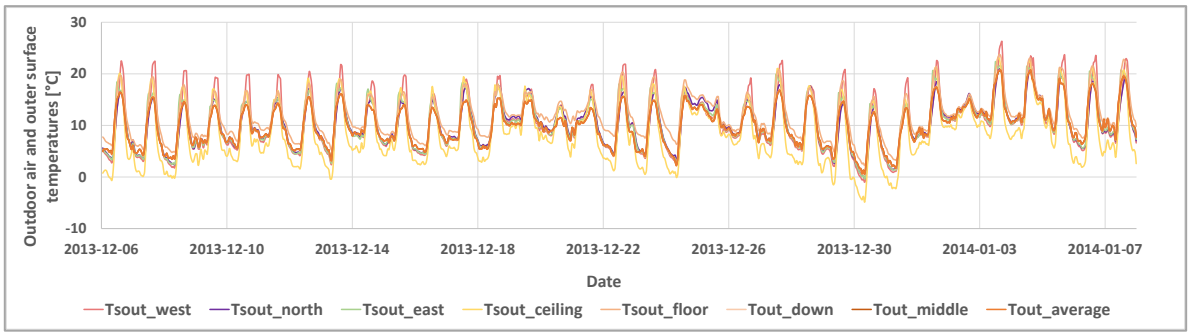

Figure 30. Outer surface temperature in the west (T_{Sout_west}), north (T_{Sout_north}), east (T_{Sout_east}), ceiling ($T_{Sout\_ceiling}$) and floor (T_{Sout_floor}) of the Round Robin Box and outdoor air temperature measured below (T_{out_down}) the Round Robin Box (1/3 height of the box), as the same height of the middle (T_{out_middle}) of the Round Robin Box and the average ($T_{out\_average}$) of both of the winter period.

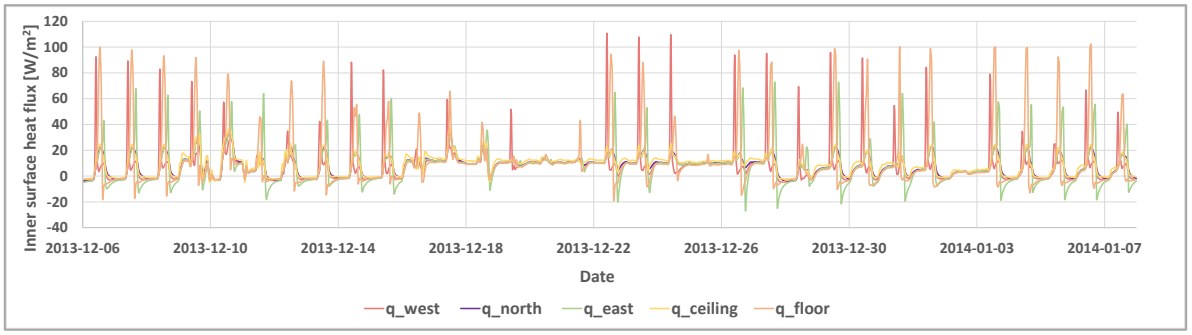

Figure 31. Inner surface heat flux in the west ($\dot{q}_{\_west}$), north ($\dot{q}_{\_north}$), east ($\dot{q}_{\_east}$), ceiling ($\dot{q}_{\_ceiling}$) and floor ($\dot{q}_{\_floor}$) of the Round Robin Box in the winter period.

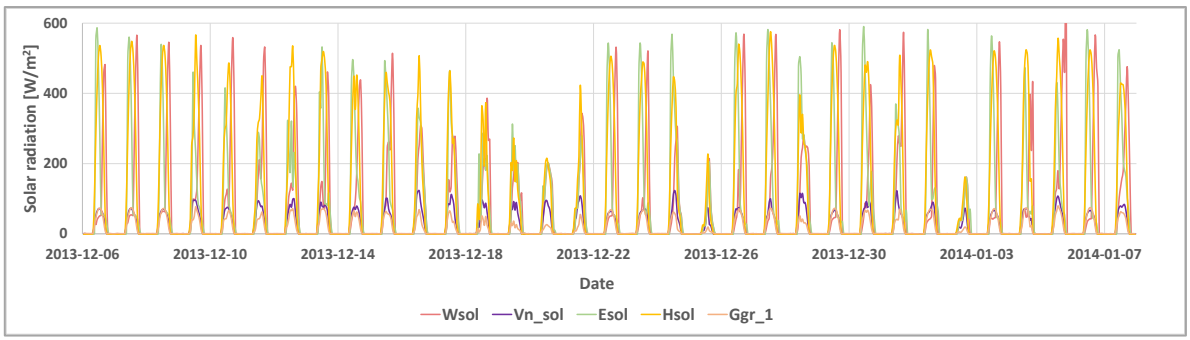

Figure 32. Solar radiation on the west (W_{sol}), north (V_{n_sol}), east (E_{sol}), ceiling (H_{sol}) and floor (G_{gr_1}) of the Round Robin Box in the winter period.

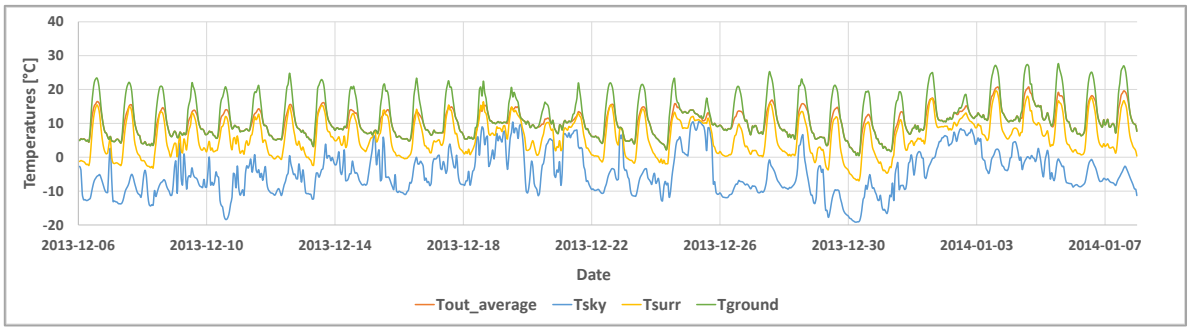

Figure 33. The outdoor average ($T_{out\_average}$) air temperature, the sky temperature (T_{sky}), the surrounding temperature (T_{surr}) and the ground temperature (T_{ground}) for the winter period.

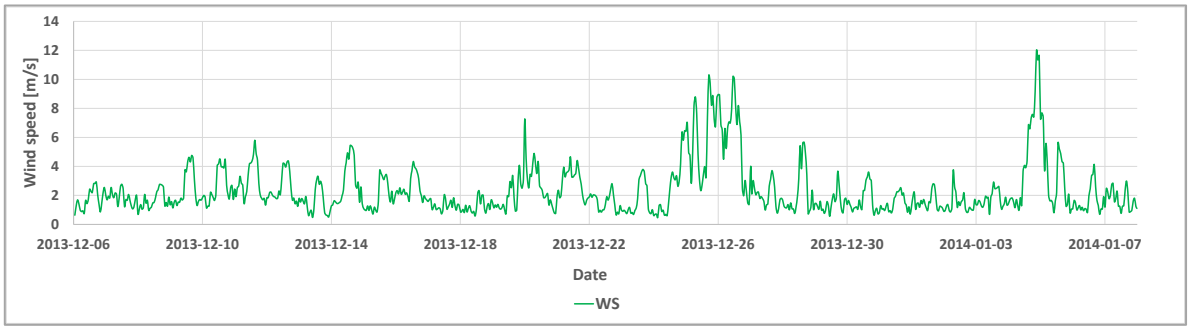

Figure 34. Wind speed (WS) for the winter period.

It is very important to check one by one the variables that are going to be used later in the models. Then, the first step is to find periods where the data is missing. If these values are not removed from the datasets, the software might provide problems. Moreover, in order to identify periods where the models could provide the best fits, the correlation between the variables and the alterations these variables could suffer must be analysed. In this case, since the inner surface heat flux is the used output variable, it is the first

variable that must be studied. Then, if the inner surface heat flux for summer is analysed in Figure 25, it can be seen that the period where this variable remains more stable during a long period of time is between the 18th and the 26th of June. Then, the selected period would probably be within this period. However, since the period in winter is consciously selected to have the lowest solar radiation in a row, the data of Figure 32 must be carefully analysed first. Since the winter period has already been analysed for the HLC estimation, the period with the lowest solar radiation in a row has already been selected. Then, this period will be also used for the solar gains analysis in order to test the relevance of the solar gains through opaque walls in the HLC when estimating this parameter using the average method presented above. Then, the inner surface heat flux and the rest of the parameters must be analysed one by one for both selected periods.

Moreover, as commented previously, the data plotted in Figure 27 and Figure 33 has been calculated using the measured long wave radiation data of Table 3 as presented in section 2.2.1. Since the average outdoor air temperature and the average surrounding temperature commonly show similar values, it is common to use the outdoor air temperature instead of the surrounding temperature in order to avoid complex calculations without a considerable accuracy improvement. However, despite the development of section 2.2.1 also considers that the sky temperature and the ground temperature can be replaced by the outdoor air temperature in order to avoid complex calculation, these graphs show that it is important to consider the corresponding sky temperatures when implementing the models. In the case of the ground temperature, it is considerably higher than the outdoor air temperature during the day. However, at night, it is similar to the outdoor air temperature. Then, it is important to consider this ground temperature effect in the models mainly during the day hours in order to obtain the most accurate model representations considering all the heat transfers effects. Nevertheless, the most notorious difference is observed when the outdoor air temperature and the sky temperature are compared. In general, the sky temperature shows considerably lower values than the rest of the measured or estimated temperatures. During the day, the effect of this sky temperature might not affect considerably the Round Robin Box outer surface temperature due to the high effect of the horizontal global solar radiation. However, during the night, there is no solar radiation influence, so the effect of this sky temperature would affect considerably the outermost surface temperature of the Round Robin Box.

Then, the heat exchanges due to long wave radiation are important to be estimated during the night period mainly in the ceiling models in order to obtain the most accurate fits. Therefore, mainly for the ceiling case, it is important to consider both, the convection and the radiation heat transfer when estimating the best model fits.

3.2- Residential buildings

After the test box, the HLC estimation experiment goes further with the analysis of two residential buildings located in Gainsborough and Loughborough in the UK (Figure 35). In this case, the data from the residential buildings is provided by the International Energy Agency-Energy in Buildings and Communities (IEA-EBC) Annex 71 [98] project called "Building Energy Performance Assessment Based on In-situ Measurements". This Annex is the step that follows the previously developed IEA-EBC Annex 58 titled "Reliable building energy performance characterization based on full scale dynamic measurements", where the Round Robin Box test was developed.

In this case, the buildings monitored where located in the UK. It must be remarked, that the summers in this area of the UK are commonly cloudy, short and comfortable while the winters are considerably long, very cold, windy and mostly cloudy. These are perfect characteristics for the average method application. Moreover, these two buildings show very different characteristics due to their insulation level and building behaviors. Thus, these two cases are considered suitable for this Thesis, since they represent the extreme opposite situations for testing the average method in the residential building level.

(a) (b)

Figure 35. (a) North side of Gainsborough house [99] (b) Front side of Loughborough house [100].

The monitoring systems of each given building measured different parameters. A combination of smart meters and dedicated sensors were used in both buildings to monitor each of the parameters in Table 4 with at least a 5 min frequency. The monitoring system of Gainsborough is described in detail in [99], while the monitoring system of Loughborough is described in detail in [100]. However, the input data provided were filtered in order to obtain common input parameters for both houses, as shown in Table 4 of section 3.2.3. The filtering procedures were not the same due to the different characteristics of the monitoring systems.

3.2.1- Highly insulated residential building

3.2.1.1- Description of the building

The first residential building is located in Gainsborough (UK) (see Figure 35(a)) and is a well-insulated, occupied building. It is one of the four social houses monitored in [99] and the HLC 'theoretical value' given by the Annex 71 is 49.9 W/K. The latter value is estimated based on the building design characteristics. The Gainsborough case represents a not very detailed monitoring system of a real in-use house, but with a very long monitoring period of three years.

3.2.1.2- Input data and monitoring system of the building

For the Gainsborough house, only the total gas consumed by the boiler was provided. However, the mains water consumption of the house was also provided. The boiler was providing heat for both the space heating and the DHW (Domestic Hot Water). The Gainsborough boiler is a Potterton Promax combination boiler with an efficiency of 91 % regarding the SAP procedure, according to the manufacturer [101]. Like most conventional boilers, it does not produce DHW in parallel with space heating. Thus, when DHW is required, the boiler stops the space heating supply and all the heat produced by the boiler is used for DHW production. In order to estimate the gas consumed by the space heating from the total gas consumption, the following assumption was considered: If there was gas consumption at the same time as there was mains water consumption, all this consumed gas was considered as gas consumption solely for DHW. In other words, only the gas consumption while no mains water was consumed was considered as space heating. This filter was applied on a five minute basis.

Moreover, for the Gainsborough building, only the electricity consumption was considered when estimating the internal gains (K). The occupancy heat created by the occupants' metabolic generation was neglected (part of K), as not enough information was provided to make an estimation. Different occupants lived in this building over the three winters of the data provided. Due to this, achieving occupancy patterns of the inhabitants to estimate the metabolic heat gain they produced was very complicated.

3.2.2- Poorly insulated residential building

3.2.2.1- Description of the building

The second residential building is located in Loughborough (UK) (see Figure 35(b)) and it is inhabited by synthetic occupants. Moreover, it is a traditional uninsulated semidetached residential building. This house has already been tested through the co-heating method in [100] and the HLC 'theoretical value' is 382 W/K. The dataset used for the house analysed in Loughborough can be found in [100], where the house 1 (HT1) files were studied. The Loughborough case represents a very detailed monitoring system of a synthetic occupants' in-use house, but with a short monitoring period of one month.

3.2.2.2- Input data and monitoring system of the building

The Loughborough house is a traditional uninsulated building occupied by monitored synthetic occupants. This means that the house behaves as if real people were living inside. Thus, the metabolic heat gain produced by these synthetic users was also considered as a heat gain. All the internal heat gains, including the metabolic generation of the synthetic occupants, were measured by means of several watt meters that measured all the electrical consumptions occurring within the building. Moreover, for the Loughborough house, the heat output of the boiler to the space heating system was directly measured. In other words, it was not necessary to use the boiler efficiency or split the space heating and the DHW consumptions. Moreover, accurately measured synthetic profiles were added to simulate the occupants' behaviour. Therefore, all heat gains (Q + K), as well as the thermostat settings, were accurately known.

3.2.3- Common input data and monitoring system of the buildings

Despite the different monitoring systems used in each of the houses, there are also some common variables. One common variable used for both houses analysis is the solar radiation, which has been obtained from the Waddington weather station. In order to obtain a rough estimate of the solar aperture, a g-value of 0.5 could be multiplied to the total window area of the building, as specified in section 2.1.1. The corresponding measured total window area of Gainsborough is 15.66 m^2 and Loughborough 20.70 m^2. Then, this roughly estimated solar aperture must be multiplied by the corresponding solar radiation in order to estimate the solar gains of the building. Once this roughly estimated solar gains are obtained for both buildings, they can then be compared to the averaged (Q + K) value of the selected periods to see whether the averaged period solar gains are below 10 % as compared to the averaged period (Q + K). Then, the HLC estimate would mainly be dependent on the measured Q and K that can be accurately measured when compared to solar gains.

Then, it has been possible to filter all the input data from section 3.2.1.2 and section 3.2.2.2 and achieve common input variables for both buildings as shown in Table 4:

SENSOR	MEASUREMENT	DESCRIPTION	UNIT
Temperature	Indoor air temperature (T_{in})	Measured in different rooms of the house. In order to achieve a unique temperature for the building, a non-weighted average temperature has been estimated using the following formula: $T_{in} = \frac{T_{in,1} + T_{in,2} + \cdots + T_{in,n}}{n}$	°C
	Outdoor air temperature (T_{out})	On-site outdoor air temperature	°C
Heating system	Boiler heat output $Q_{heating}$	When required, the gas consumption has been converted by boiler efficiencies to space heating system kWh supply. Hot water energy supply is not considered in this term.	kWh
	Total electricity consumption $K_{electricity}$	Measured for the whole building or in each of the rooms of the house.	kWh
Solar radiation	Solar radiation (horizontal global solar irradiance) H_{sol}	Obtained from the Waddington weather station. In order to apply the average method, it has been converted into vertical south global solar radiation (V_{sol}) applying the method of section 2.2.2.1.	W/m^2

Table 4. List of input parameters for applying the average method. [102]

In Table 4, due to the high homogeneity of indoor temperatures during the analysed periods, the indoor temperature is considered as the non-weighted average of all the measured indoor temperatures. A full development of the properties of the HLC, regarding its estimation in buildings comprising different thermal zones with different indoor temperature set points, is mathematically developed and demonstrated in section 2.1.2. There, the requirements to be able to estimate the whole building HLC by means of the sum of the zone HLCs are described. Such needs are basically to know individually each zone heat gain ($Q + K + S_aV_{sol}$) and each zone T_{in}. In both of the one family residential buildings analysed in this work, it was only possible to consider one thermal zone, as the internal heat gains ($Q + K + S_aV_{sol}$) could not be accurately split between the different rooms that make up the dwelling. Most of the internal gains were measured only on the whole building level. Furthermore, for each individual temperature measurement, the period averaged value has been compared to the period average of the non-weighted average indoor temperature. For all the analysed periods, the indoor temperature homogeneity of the buildings has been so high that the difference between the period averaged values of individual indoor temperatures and the non-weighted indoor temperatures have been within the sensor error band.

Moreover, the propagation of the uncertainty of the sensors was also considered when estimating the HLC error bands. The provided sensor accuracy for the monitoring systems of the two houses can be seen in Table 5. Note that, as detailed in section 2.1.3, other uncertainty sources related to the assumptions made by the method are not propagated to the HLC estimations carried out in this work. In the case of the solar gains uncertainty, apart from the accuracy of the pyranometer (considered 5 % for this analysis), the solar aperture uncertainty was also considered. Despite the solar aperture (S_a) being unknown, a 10 % error was considered for the latter. Thus, the total uncertainty considered for the solar gains of both buildings was 15 %.

Measurement	Gainsborough uncertainty	Loughborough uncertainty
Indoor temperature	+/-0.25 °C	+/-0.2 °C
Outdoor temperature	+/-0.5 °C	+/-0.2 °C
Gas meter	+/-2 %	+/-2 %
Electricity consumption	+/-2 %	Not provided (+/-2 % assumed)

Table 5. List of measurements and provided uncertainty for applying the average method. [102]

Finally, it must be commented that the data monitorization period of the two houses was different. While the houses in Gainsborough was monitored for three winter periods (1st November 2012 until 30th April 2015), the house in Loughborough was only monitored for a month (16th February 2014 to 15th March 2014).

3.2.4- Representation of the useful input data of the two houses

Once all the monitored data is listed in the tables, it is very important to perform a visual checking analysis of the measured data. Therefore, each of the useful variables presented in Table 4 are plotted in different graphs in order to understand their behaviour and compare them between both houses.

Therefore, the following Figure 36, Figure 37, Figure 38 and Figure 39 show the indoor and outdoor air temperatures, the boiler heat output, total electricity consumption and the solar gains for both houses, Gainsborough and Loughborough.

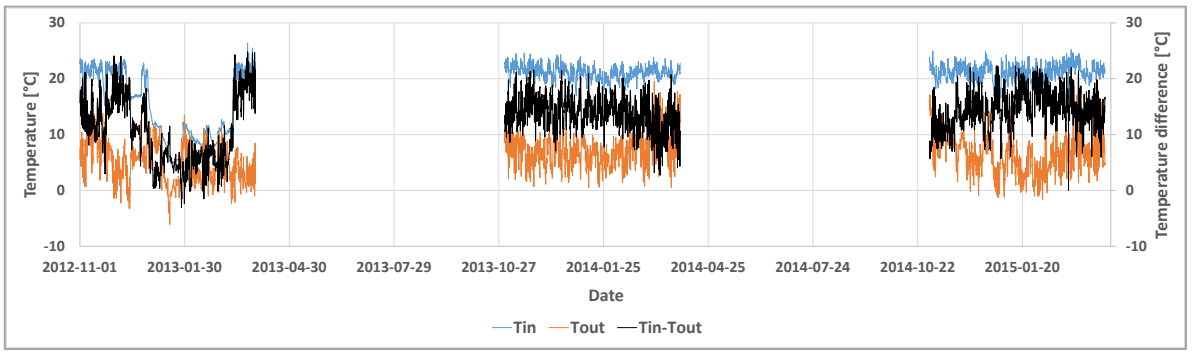

Figure 36. Indoor air temperature (T_{in}), outdoor air temperature (T_{out}) and air temperature difference (T_{in}-T_{out}) for Gainsborough.

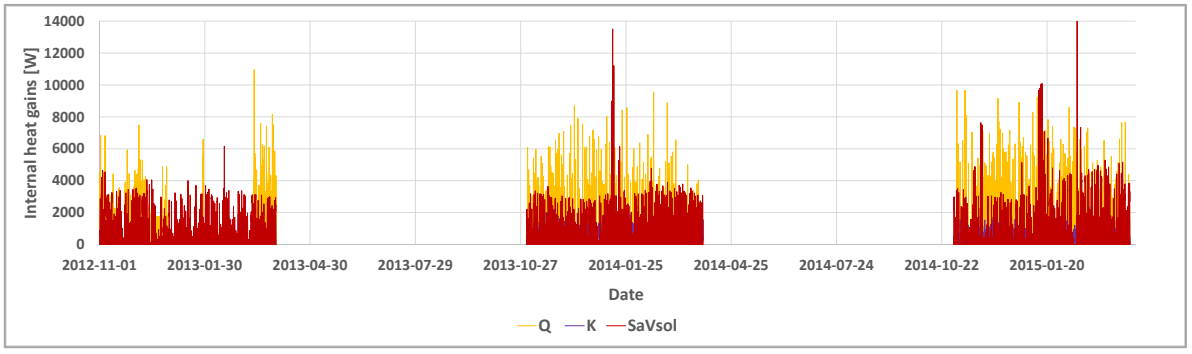

Figure 37. Space-heating systems' heat input (Q), total electricity consumption (K) and solar gains (S_aV_{sol}) in Gainsborough.

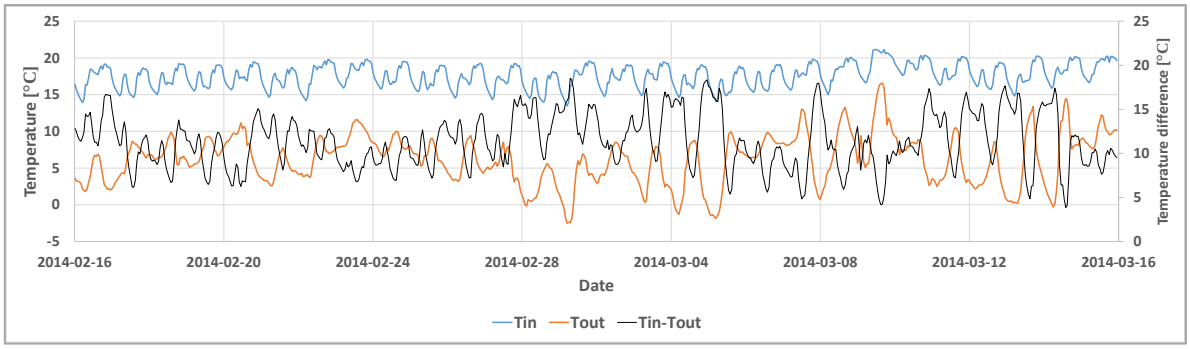

Figure 38. Indoor air temperature (T_{in}), outdoor air temperature (T_{out}) and air temperature difference (T_{in}-T_{out}) for Loughborough.

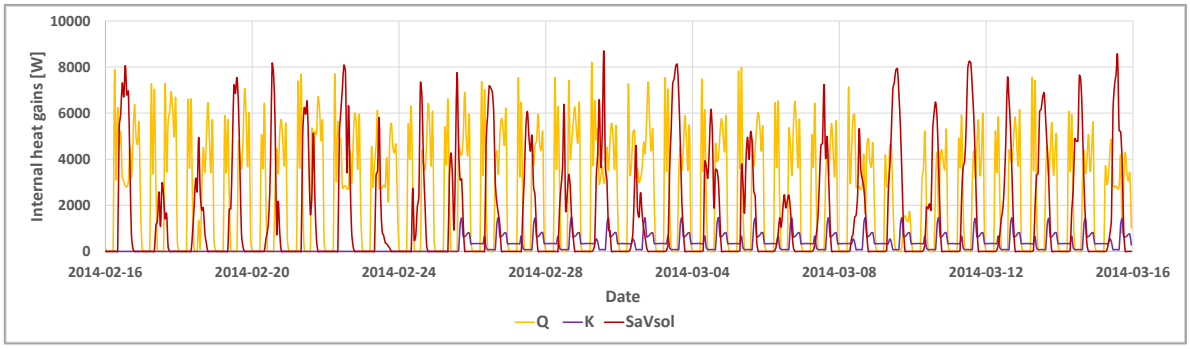

Figure 39. Space-heating systems' heat input (Q), total electricity consumption, including synthetic occupants' generation (K), and solar gains (S_aV_{sol}), for Loughborough.

As commented in section 3.2.3 and shown in Figure 36 to Figure 39, the dataset of Gainsborough is much longer than the dataset of Loughborough. Thus, it can be concluded that probably, it will be easier to find suitable periods to estimate the HLC that fulfil the average method requirements. Moreover, a first analysis of the temperature difference can be also done for both of the buildings in Figure 36 and Figure 38. Moreover, from Figure 37 and Figure 39, it is possible to make an idea of the solar gains effect in the building and how their effect can be compared with the space heating system consumption and the rest of the internal gains in the building.

Finally, considering all the data presented before, an example of a selected period in order to apply the average method is shown. Figure 38 shows the evolution over one month of the indoor and outdoor air temperatures for the Loughborough building. There, the temperature difference between the interior and the exterior is also plotted. From this Figure 38, it can be concluded that the temperature difference between the exterior and interior is considerably high during the selected period shown in the new Figure 40(a). A zoom-in of period 1, used later to apply the average method, is also presented in Figure 40(b). Figure 39 shows the evolution of the solar gains (S_aV_{sol}), the space heating systems'

heat input (Q) and the total electricity consumption, including the synthetic occupants' generation (K) for the Loughborough building, again including Figure 41(a) with a zoom-in on period 1 in Figure 41(b). If Figure 41(a) is analysed, it can be seen that it is not possible to find a three day period where the solar gains remain below 10 % when compared to the rest of the measurable heat gains (Q + K). Finally, as an example, Figure 42 shows the accumulated average plot of the HLC for period 1 in Loughborough. It can be seen how the accumulated average of the HLC value stabilises along the duration of the period and remains within the 10 % bands over the last 24 hours.

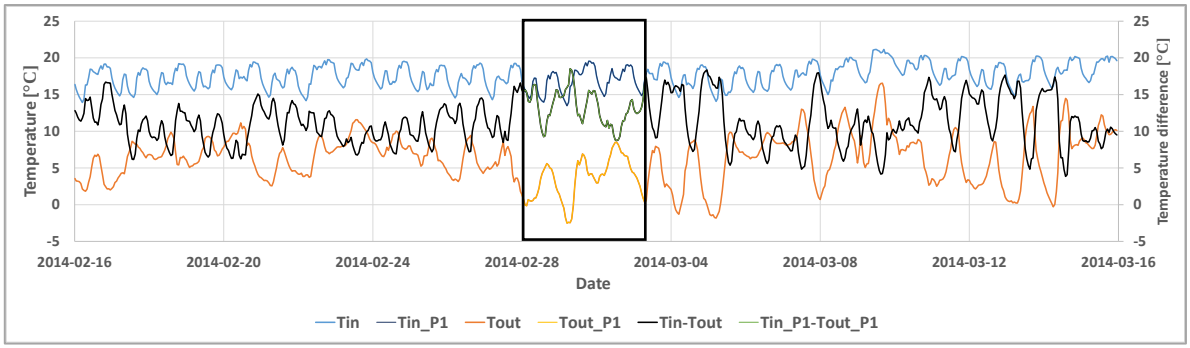

(a)

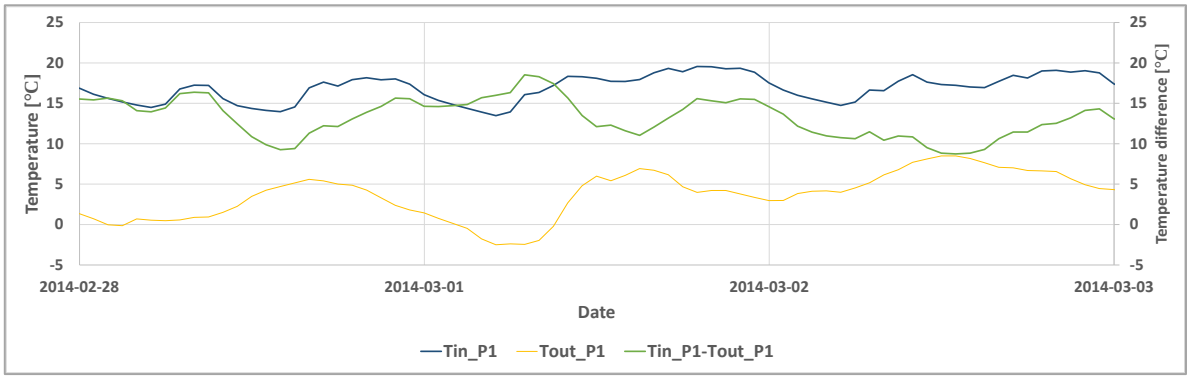

(b)

Figure 40. Indoor temperature (T_{in}), outdoor temperature (T_{out}) and temperature difference (T_{in}-T_{out}): (a) for the whole dataset in Loughborough, (b) for period 1 in Loughborough. [102]

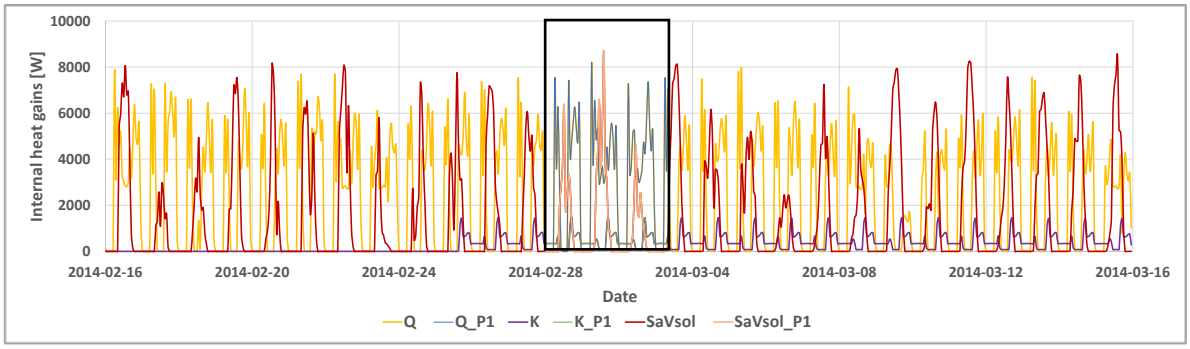

(a)

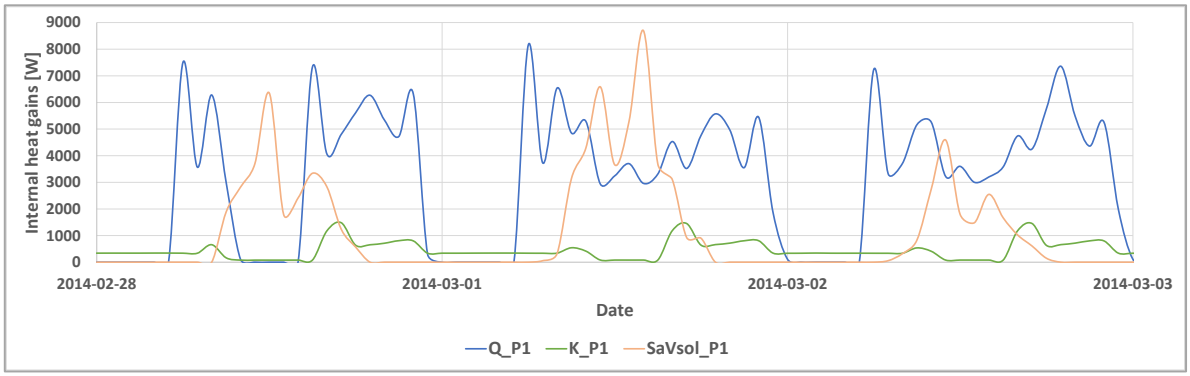

(b)

Figure 41. Space-heating systems' heat input (Q), total electricity consumption, including synthetic occupants' generation (K) and solar gains (S_aV_{sol}): (a) for the whole dataset in Loughborough, (b) for period 1 in Loughborough. [102]

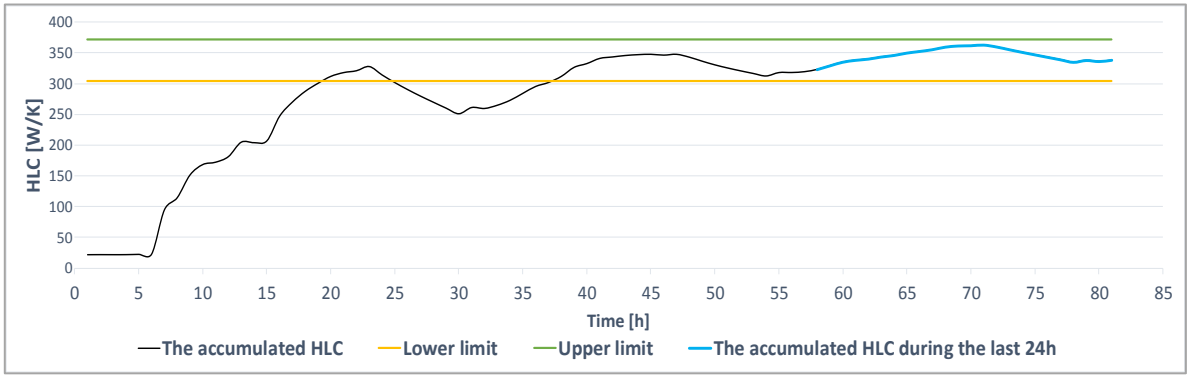

Figure 42. Evolution of the accumulated average of the Heat Loss Coefficient for period 1 in Loughborough. [102]

3.3- Rectorate in-use office building

The last HLC estimation analysis and its decoupling process is performed in a public building of the University of the Basque Country. The building is located on the Leioa University Campus, close to Bilbao, in the north of Spain.

For the analysis of the building HLC, it is indispensable to know about the climate of the area. Leioa has a humid oceanic climate with a predominance of the westerly winds, which softens the temperatures and favours a temperate time throughout the year. Due to the proximity to the sea, the climate is mild, however, it contrasts with the very marked temperature difference between seasons: 8 °C of average temperature in winter and 20 °C in summer. Hence, while the summers are comfortable, the winters are long, cold, wet and windy and it is partly cloudy all year round.

3.3.1- Description of the building before retrofitting

The building presents a complex geometry, with an irregular façade and projecting parts on different levels. The building is formed by three different blocks, but only the west block (WB) has been considered in the energy characterization. Since the WB thermal zones are separated by “always closed” fire doors, the air mass exchanges with the central block can be considered negligible. Furthermore, both blocks have similar indoor temperature settings, so the energy exchange between blocks can also be considered insignificant. Thus, the west block has been treated as if it was completely isolated from the central block. Moreover, the whole building has the same heating system. The west block has four storeys and has a narrow layout with a structure of concrete pillars and grid concrete slabs. The distribution of the floor is different for each of them (see Figure 44), where the first floor (F1) and the third floor (F3) are mainly large, open offices, while different smaller rooms and offices make up the ground floor (F0) and the second floor (F2). The building has a centralized heating system, but before retrofitting, it did not have ventilation or air conditioning facilities. The structure of the floors is important when it comes to the heat loss coefficients estimation.

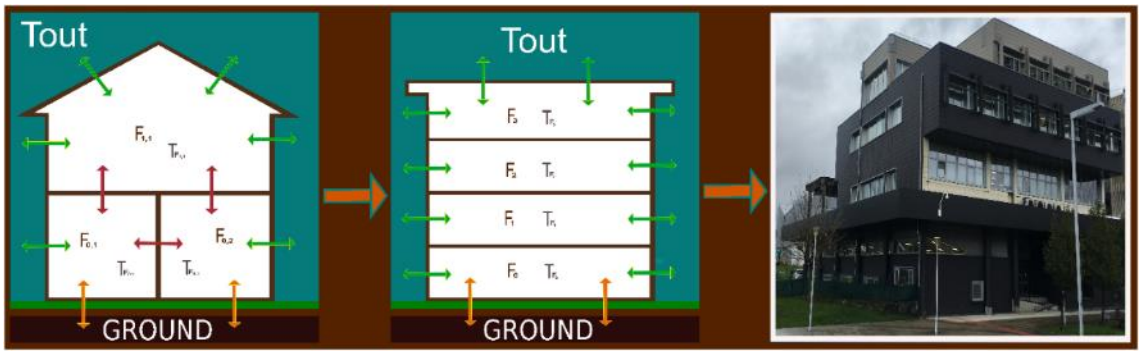

Figure 43. Left: generic building schematic used for method demonstration. Centre: from the generic building schematic to the schematic of the studied building. Right: photo of the studied building after retrofitting. [85]

The building was constructed in the 1970s without insulation. During its life, it has been modified several times. Regarding the opaque walls, the majority of the façade was built with precast concrete panels without an air gap. There were three kinds of window in the building; wooden frame and single glazed windows, aluminium frame (without thermal break) and double glazed windows and, finally, aluminium frame (with thermal break) and double glazed windows. Some of the windows had concrete-sunshades to reduce solar gains during summer. Moreover, the roof was partially insulated.

Section 2.1.2 and section 2.4.1 demonstrate that the HLC and C_v estimation of the whole building can be done as if each of the analysed thermal zones are exchanging heat and mass only with the outdoors. This sections demonstrate that the heat and mass exchange between the internal walls and ceilings are cancelled out when calculating the sum of all the floors heat loss coefficients. Then, the considered energy exchange schema of the presented building is shown in Figure 43(centre). Therefore, four HLC and C_v values will be calculated, one for each floor of the building.

3.3.2- Description of the building after retrofitting

The retrofitting works were designed during the year 2015, and the works were started in summer 2016. However, the majority of the works where carried out during summer 2017. A monitoring study was carried out before these works in order to make a diagnosis of the building and this was taken into account to define the optimal retrofitting actions.

The main objective of the retrofitting was to decrease the building's energy consumption. Therefore, the first step carried out to achieve this aim was to reduce the

energy demand through the reduction of the building's envelope energy losses. Furthermore, improvements in the energy systems of the building were also considered.

Thus, several actions were carried out to reduce the energy consumption and CO_2 emissions of the building. The first action developed was the retrofitting of the façade, which has been insulated by adding vacuum insulated panels (VIPs) within a ventilated façade. Moreover, a new lighting system has been installed, where natural and LED lights were combined as well as a control system for it. Some windows have also been replaced by a new type of reversible window and others by market available high performance windows with different solar behaviour, depending on the orientation.

In addition, a ventilation system with recovery has been installed for each floor, with its control system and thermostatic control valves on the hot water radiators in order to improve the control capacities.

3.3.3- Monitoring system of the building

Different types of sensors have been located all around the building, depending on the distribution of each plant (see Table 7). Three different types of monitoring systems have been installed: sensors measuring the outdoor conditions, sensors measuring the indoor conditions and, finally, sensors measuring the building's energy consumption. The outdoor measurements include the brightness level on the roof, temperature (two sensors), relative humidity (two sensors), wind speed and horizontal global solar radiation. One outdoor CO_2 concentration sensor has been installed after the retrofitting. The indoor sensors are also able to measure the brightness level, temperature, relative humidity and air quality (CO_2 concentration). Finally, the energy consumption of the heating systems is obtained, since the heating water flow rate, the flow temperature and the return temperature are measured for each floor. The distribution of the sensors installed inside the building is shown in Figure 44. On the other hand, it is also available the lighting electricity consumption by measuring the active power consumption in each floors' electrical board.

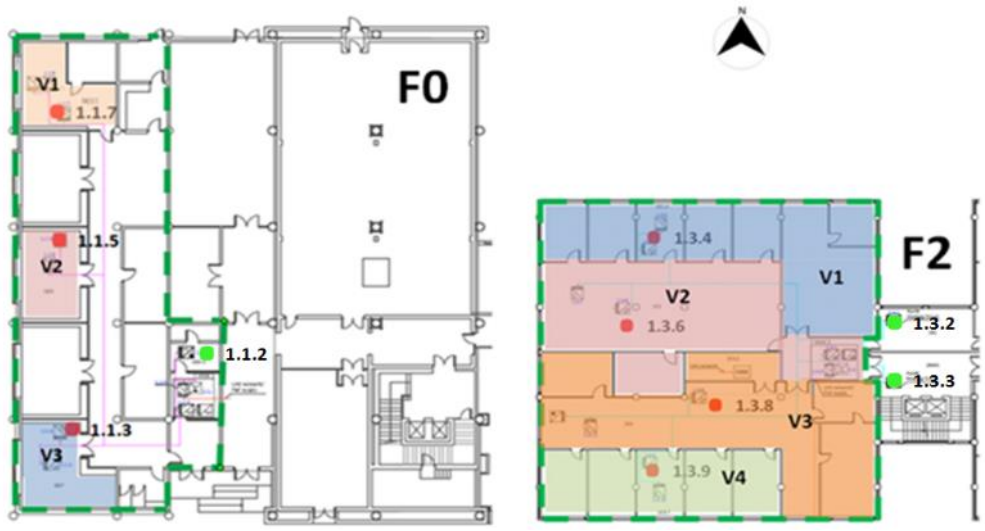

(a)

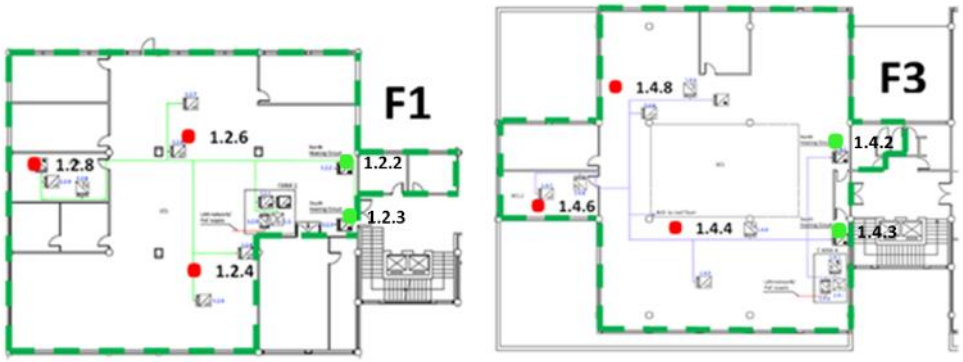

(b)

Figure 44. Distribution of monitoring devices within the considered thermal zones of the building for (a) F0 and F2 and (b) F1 and F3. RED DOT: locations where brightness level, air quality (CO_2 ppm), temperature and relative humidity have been measured. GREEN DOT: calorimeter positions. Representation of volume partitions considered in F0 and F2 for C_v calculation purposes are also highlighted in (a). [103, 104]

Total volumes of the monitored areas (see green contour line of Figure 44) are shown in Table 6.

	V_{ol_floor} [m^3]
FLOOR 0	1184.3
FLOOR 1	1700.2
FLOOR 2	1889.7
FLOOR 3	1619.3
BUILDING	**6393.5**

Table 6. Monitored total volumes for each thermal zone (floors in this case) and for the building.

Although most of the data has directly been obtained by the sensors, some parameters have been estimated for the HLC estimation. The estimated total window solar aperture of the building is S_a = 230.15 m² [103]. This values seem logical since the total south window area of the west block is 158.6 m², the east façade window area is 106.7 m² and the north façade window area is 195 m²; assuming 230.15 m² of solar aperture since a g-value of 0.5 is considered as already explained in section 2.1.1. The distribution of the solar aperture through the different floors has been done proportionally to the total window area of each floor: the ground floor has 16 %, the first floor has 36 %, the second floor has 23 % and the third floor has 25 % of the whole solar aperture. As shown in Table 7, the measured solar radiation is the global horizontal solar radiation (H_{sol}).

SENSOR	MEASUREMENT	DESCRIPTION	UNIT	UNCERTAINTY
Energy consumption	Heating system (Q) *7 Calorimeter: Kamstrup Multical 602 for heating; F0 1 calorimeter; F1, F2 and F3 2 calorimeters per floor*	Heating system	kW	ET ± (0.4 + 4/ΔT)% for the set sensors
	Lighting system ($K_{lighting}$) *4 Electricity Power Meter: 1 ABB EM/S 3.16.1 meter, 3 ABB A43 meters (1 per floor)*	Lighting system	kW	±2 % for all
Indoor Conditions	Illuminance (I_{in}) *13 Illuminance sensors: Siemens 5WG1 255-4AB12*	Illuminance	lux	-
	Air quality, temperature and relative humidity (AQ, T_{in} and RH) *13 Air quality, Temperature and Humidity Sensors: ARCUS SK04-S8-CO2-TF*	Air Quality	ppm CO_2	±1 % Measurement Error
		Temperature	°C	±0.5 °C
		Relative Humidity	%	±3 % RH
Weather	Illuminance, temperature, wind speed and rain (I_{in}, T_{out}, WS and RN) *1 Weather Station on roof: ELSNER 3595 Sun tracer KNX basic*	Illuminance	lux	±35 % at 0…150,000 lux
		Temperature	°C	±0.5 °C
		Wind Speed	m/s	±25 % at 0…15 m/s
		Rain	yes/no	-
	Temperature and relative humidity (T_{out} and RH) *1 Outdoors Temperature and Humidity Sensor on roof ARCUS SK01-TFK-AFF*	Temperature	°C	±0.5 °C
		Relative Humidity	%	±3 % RH
	Global Horizontal Solar Radiation (H_{sol}) *1 Pyranometer on roof: ARCUS SK08-GLBS*	Global Horizontal Solar Radiation	W/m²	±5 %
Ventilation system	Volumetric ventilation airflow rate ($\dot{V}_{air(vent)}$) *4 volumetric air flow rate sensors: TROX TR-EASY*	Volumetric ventilation airflow rate	m³/h	-

Table 7. Summary of the analysed building's sensors.

Therefore, in order to estimate the HLC of the in-use building, variables such as the indoor and outdoor air temperatures, the heating system, the lighting system and the solar radiation have been considered from Table 7 marked in blue. Moreover, in order to perform the HLC estimation as accurate as possible, the internal gains of the building have been estimated in order to consider the occupancy heat created by people's metabolic generation and the heat generated by the computers in the analysis. Heat gains due to people occupancy have been estimated assuming between 90 W to 215 W of metabolic heat generation per person during occupation. This estimation is based on chapter 8 (Thermal Comfort) of the [91] handbook where office activities generate between 55 W/m^2 (reading, seated) to 120 W/m^2 (lifting/packing) of metabolic heat depending on the office activity and where 1.8 m^2 is considered the average skin surface area of an adult. In the studied building, the main office activity is 'typing' (65 W/m^2, see [91]), making 117 W of metabolic heat generation per person. Moreover, a 150 W equipment heat generation have been estimated per person. There are 145 working places and 105 computers (with different timetables) in the studied building. This procedure is applied floor by floor, considering the people and computers working on each of them. The considered occupancy scheduled for each floor has been estimated by means of interviews and by analysing the measured lighting consumption data sets.

Apart from the mentioned variables, also the air quality of the building was measured. These measurements become this building the most appropriate building in order to apply the HLC decoupling process detailed in section 2.4. Therefore, within these comfort parameters, only the air quality (CO_2 concentration marked in green in Table 7) measuring sensor is indispensable for the estimation of the C_v. According to the ASTM D6245-18 guide and the Test Method ASTM E741-11 presented in section 2.4, in order to estimate the Air Change per Hour of a certain thermal zone, it is necessary to measure the CO_2 concentration in at least three points of the analysed thermal zones or floors. In this work three or four measurements points have been installed per analysed thermal zones (see Figure 44).

Data from weather measurements sensors located on the roof of the building were also available. Although a wide range of data was also measured in the roof for the estimation of the HLC, the only variables needed for this HLC decoupling study are the outdoor air

temperature and wind speed (also marked in green in Table 7). Then, despite these data are not used in the C_v calculation, they are still needed to filter the data or check the correlation between the estimated ACH values and wind speed. Moreover, for the analysis after the rehabilitation, also data measured inside the ventilation system has been used. There, the only required data measured for this analysis has been the ventilation volumetric airflow rate (marked in green in Table 7) on each floor heat recovery exchanger.

Finally, it must be commented, that all these variables and parameters presented in this section have been measured and estimated for four winter periods in a row, three of them before the retrofitting of the building (between November 2014 and March 2017) and one of them, after the retrofitting of the building (between November 2017 and March 2018). All data has been measured minutely.

3.3.4- Representation of the useful input data of the office building

Once all the data that is going to be used for the office building HLC analysis and its decoupling has been presented in section 3.3.3, it will be also shown graphically in order to study it before the methods are applied. Then, it is possible to filter the data and take some initial ideas. Therefore, the data measured and/or estimated for the HLC estimation is the indoor and the outdoor air temperature (shown in Figure 45, Figure 47, Figure 49 and Figure 51, together with their temperature difference), the heating system consumption, the internal heat gains and the solar gains (shown in Figure 46, Figure 48, Figure 50 and Figure 52). Thus, in order to estimate the most accurate HLC value, the total internal heat gains of the building must be considered. As commented in section 3.3.3, the occupancy heat created by people's metabolic generation and the heat generated by the computers is also included as internal heat gain ($K_{occupancy}$). Therefore, the total internal heat gains ($K= K_{lighting} + K_{occupancy}$) would include the occupancy heat created by people's metabolic generation, the heat generated by the computers and the lighting system electrical consumption. Moreover, the solar radiation would be multiplied by the solar aperture, in order to obtain the solar gains, and, as commented before, the results are shown, together with the heating system and the total internal heat gains, in the following Figure 46, Figure 48, Figure 50 and Figure 52. Note that the solar gains estimations are only valid in cloudy days where there is purely diffuse solar radiation. On those days

where there is only diffuse radiation, it can be considered that the radiation is similar in all the orientations of the building.

Moreover, despite in this section only the whole building variables and parameters are shown for each available winter period (each winter period starting from November 2014 to March 2018), it has been indispensable to repeat this process for each of the floors one by one. Due to the long and extensive monitorization carried out in this case study, there have been several problems with the sensors. There were periods where some data was not collected for some floors sensors while the data was correctly collected for the rest of them. Therefore, it has been very important to analyse accurately each floor data individually in order to obtain the useful periods where a proper estimation of HLC of each floor and consequently, also of the whole building could be carried out. However, in order to simplify this section, only the whole building data has been plotted here.

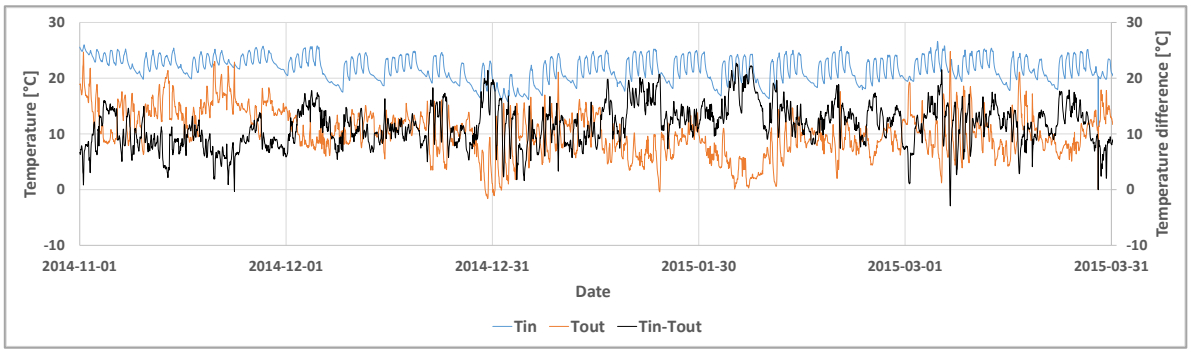

Figure 45. Indoor temperature (T_{in}), outdoor temperature (T_{out}) and temperature difference (T_{in}- T_{out}) for the in-use whole office building during winter 2014-2015 before the rehabilitation.

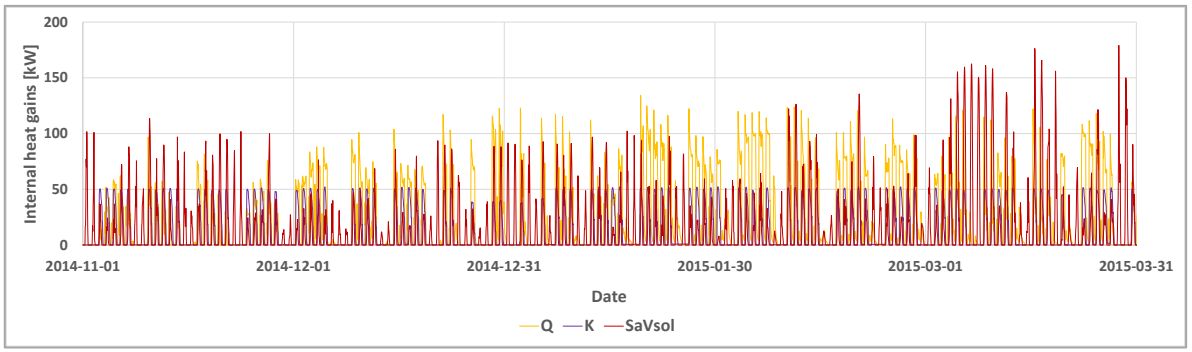

Figure 46. Space-heating systems' heat input (Q), total electricity consumption, including the occupancy heat created by people's metabolic generation and the heat generated by the computers (K), and solar gains (S_aV_{sol}) for the in-use whole office building during winter 2014-2015 before the rehabilitation.

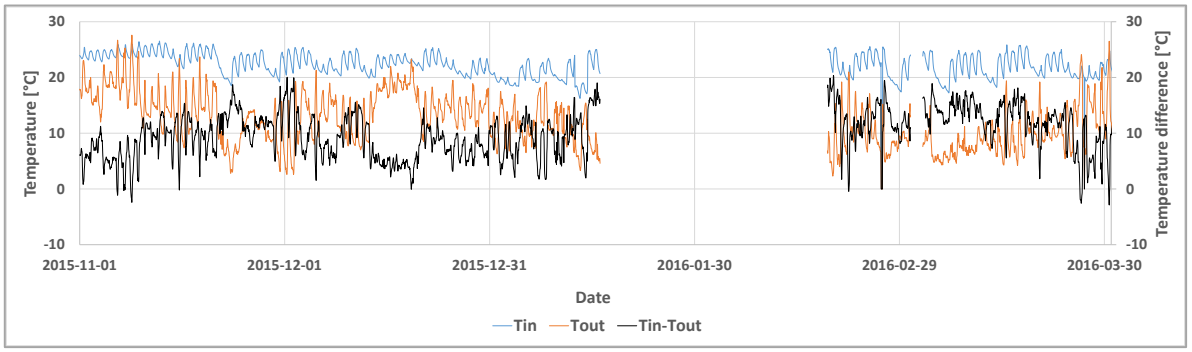

Figure 47. Indoor temperature (T_{in}), outdoor temperature (T_{out}) and temperature difference (T_{in}- T_{out}) for the in-use whole office building during winter 2015-2016 before the rehabilitation.

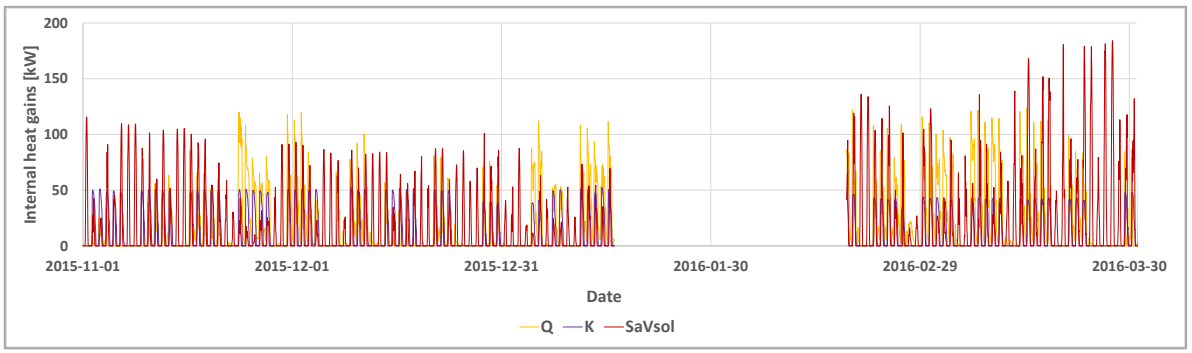

Figure 48. Space-heating systems' heat input (Q), total electricity consumption, including the occupancy heat created by people's metabolic generation and the heat generated by the computers (K), and solar gains (S_aV_{sol}) for the in-use whole office building during winter 2015-2016 before the rehabilitation.

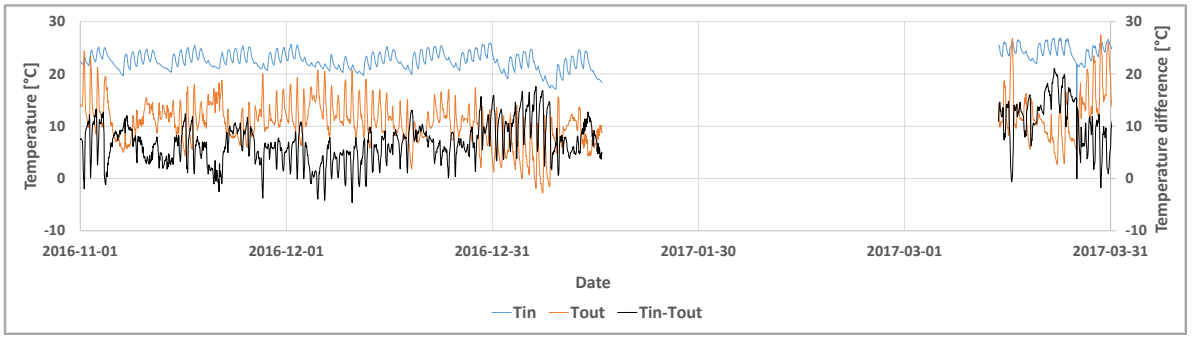

Figure 49. Indoor temperature (T_{in}), outdoor temperature (T_{out}) and temperature difference (T_{in}- T_{out}) for the in-use whole office building during winter 2016-2017 before the rehabilitation.

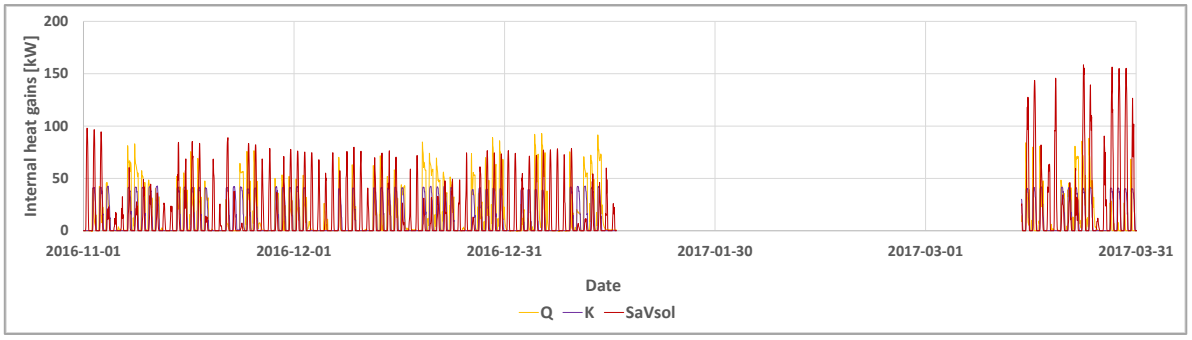

Figure 50. Space-heating systems' heat input (Q), total electricity consumption, including the occupancy heat created by people's metabolic generation and the heat generated by the computers (K), and solar gains (S_aV_{sol}) for the in-use whole office building during winter 2016-2017 before the rehabilitation.

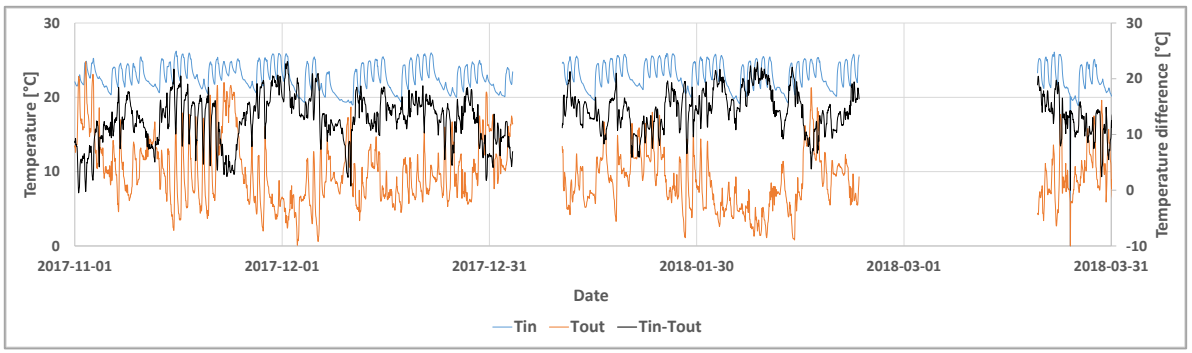

Figure 51. Indoor temperature (T_{in}), outdoor temperature (T_{out}) and temperature difference (T_{in}- T_{out}) for the in-use whole office building during winter 2017-2018 after the rehabilitation.

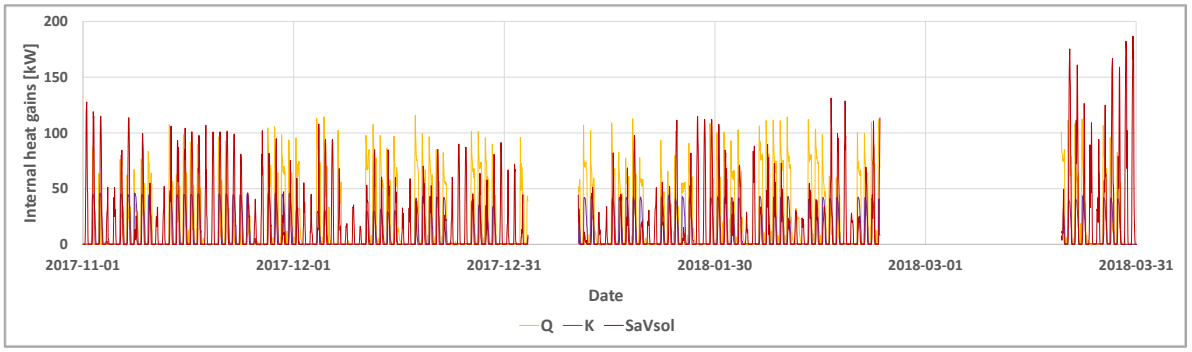

Figure 52. Space-heating systems' heat input (Q), total electricity consumption, including the occupancy heat created by people's metabolic generation and the heat generated by the computers (K), and solar gains (S_aV_{sol}) for the in-use whole office building during winter 2017-2018 after the rehabilitation.

Once all the whole buildings' data is plotted, it is possible to take some initial conclusion considering only the visual checking. As commented before, it is very important to also analyse each of the floors data individually in order to ensure a proper estimation of their HLC values. However, from these graphs as well as for the individual floor graphs, it is possible to find the temperature difference variations and consider the

periods where it takes the highest values. Moreover, the solar gains can also be compared with the rest of the internal gains and the heating system consumption (Q+K), in order to make an idea of where the solar gains could be low enough for the analysis. Moreover, several gaps can be found in the figures due to the failure of the sensors or acquisition systems of the whole building during some periods. Moreover, it must be commented that several data was missing when analysing the ground floor during the whole winter 2016-2017 period. In consequence, ground floor data has been removed from the graphs and thus, the shown result in Figure 49 and Figure 50 may show different results to the expected ones. This is more notorious in the Figure 50, when analysing the space heating data and the total internal heat gains. When they should show similar values to the values from winters 2014-2015 and 2015-2016, they show in general lower values. Moreover, if the internal heat gains before and after the rehabilitation are compared (excluding the winter 2016-2017), it can be seen that after the rehabilitation they are lower than before. This is mainly due to the replacement of old lighting system by a low energy consuming LED lighting system. Then, once an idea of the behavior of the data is obtained, the data is ready for been analysed with the average method developed in section 2.1 in order to estimate the HLC in this in-use building.

As an example of a suitable period fulfilling those requirements, the data from period 2 of winter 2014-2015 is analysed here (period from 2015-01-20 to 2015-01-23). This period's data is identified in Figure 45 and Figure 46 and marked in the new Figure 53(a) and Figure 54(a). Then, a zoom of period 2 is also plotted in Figure 53(b) and Figure 54(b).

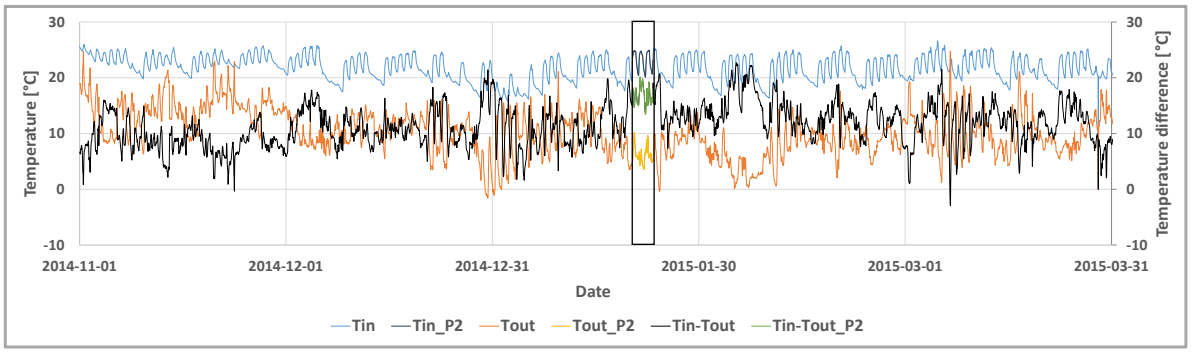

(a)

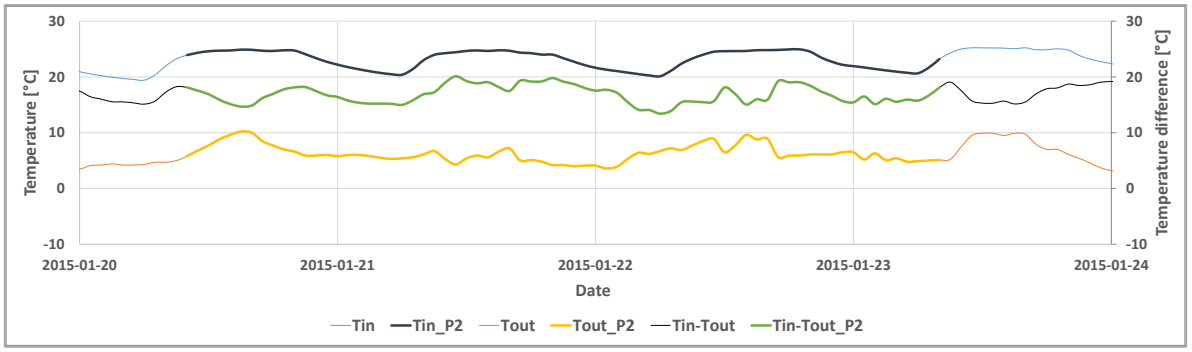

(b)

Figure 53. Indoor temperature (T_{in}), outdoor temperature (T_{out}) and temperature difference (T_{in}- T_{out}) for the office building during winter 2014-2015 before the rehabilitation for (a) the whole period, (b) for period 2.

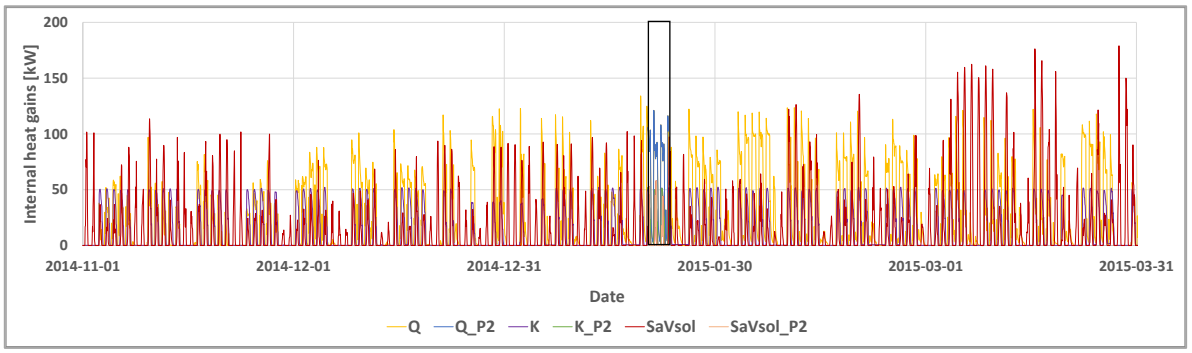

(a)

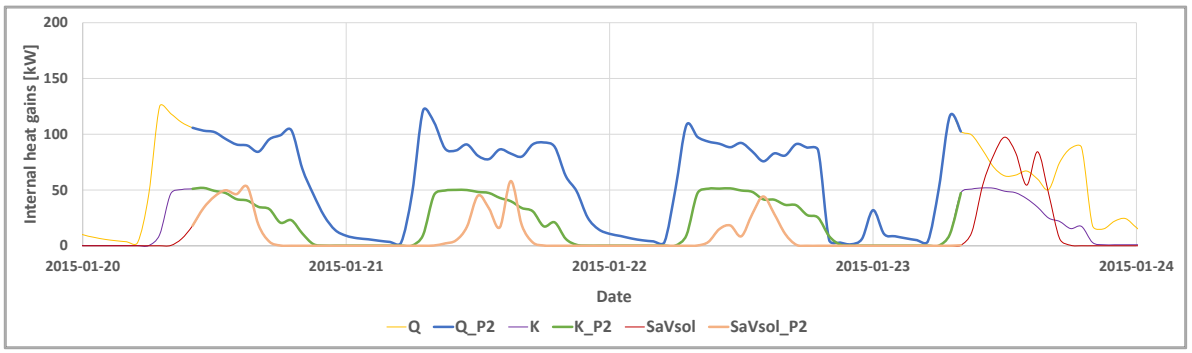

(b)

Figure 54. Space-heating systems' heat input (Q), total electricity consumption, including synthetic occupants' generation (K), and solar gains (S_aV_{sol}) for the office building during winter 2014-2015 before the rehabilitation for (a) the whole period, (b) for period 2.

Moreover, Table D.1 to Table D.4 from Appendix D show the average values of each of the main variables of all the selected periods. These values can be used directly to estimate the HLC values using the Eq. 50 (in this equation the variables are introduced as the average of the selected period). Thus, if the T_{out} column of Table D.1 and the S_aV_{sol} column of Table D.3 are observed, for the period 2 example, a low outdoor temperature (6.23 °C)

and low solar gains (8.76 kW) average values can be observed. These weather conditions permit the high indoor to outdoor temperature difference and the low solar gains conditions required by the average method to be fulfilled.

After the data for the HLC estimation is analysed, it is necessary to take a look to the useful data for the HLC decoupling process. Therefore, the CO_2 concentration, the outdoor temperature and the wind speed presented in Table 7, must be graphically represented for each of the winters in Figure 55-Figure 62.

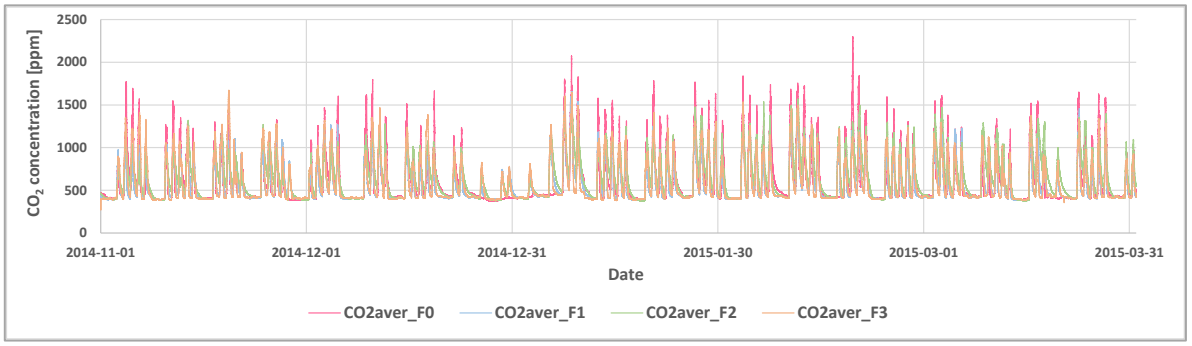

Figure 55. CO_2 concentration in the ground (CO_{2aver_F0}), first (CO_{2aver_F1}), second (CO_{2aver_F2}) and third (CO_{2aver_F3}) floor during winter 2014-2015.

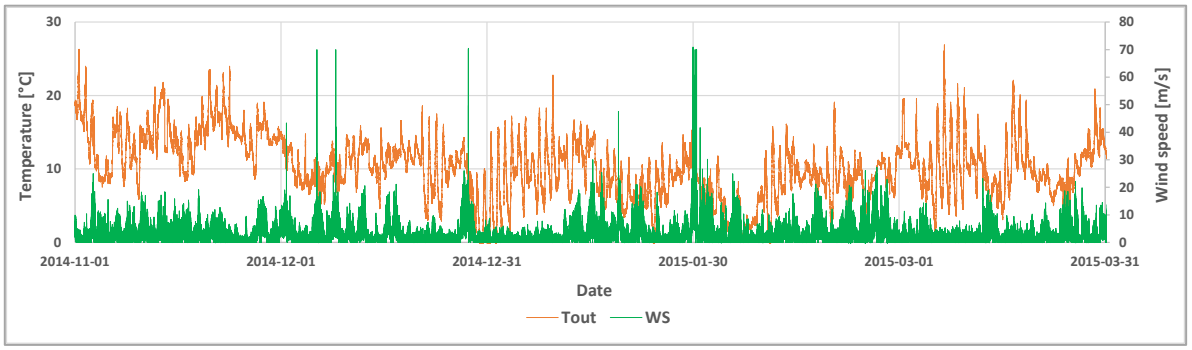

Figure 56. The outdoor temperature (T_{out}) and the wind speed (WS) during winter 2014-2015.

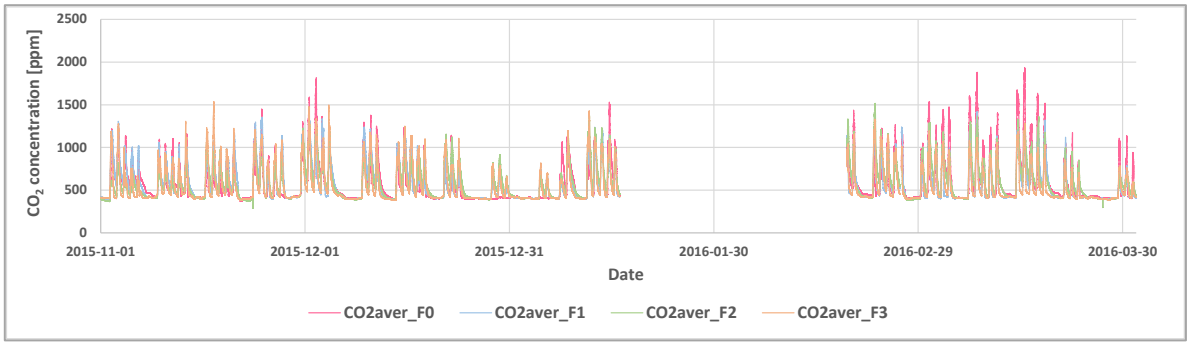

Figure 57. CO_2 concentration in the ground (CO_{2aver_F0}), first (CO_{2aver_F1}), second (CO_{2aver_F2}) and third (CO_{2aver_F3}) floor during winter 2015-2016.

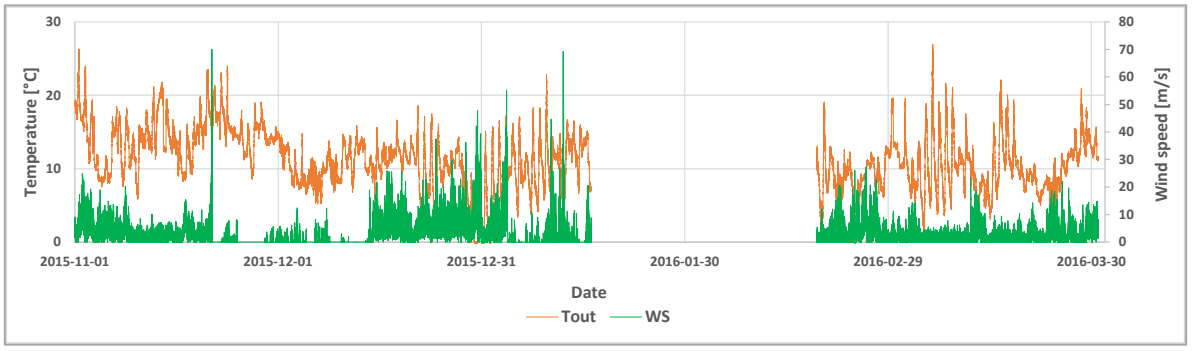

Figure 58. The outdoor temperature (T_{out}) and the wind speed (WS) during winter 2015-2016.

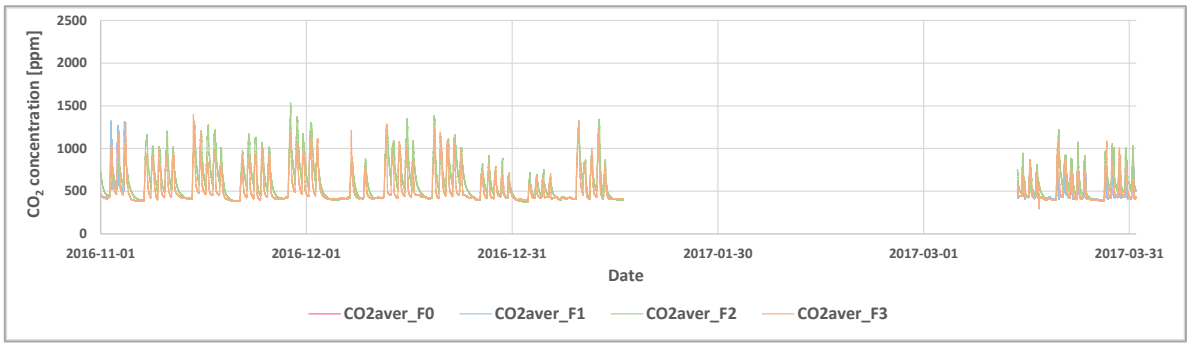

Figure 59. CO_2 concentration in the ground (CO_{2aver_F0}), first (CO_{2aver_F1}), second (CO_{2aver_F2}) and third (CO_{2aver_F3}) floor during winter 2016-2017.

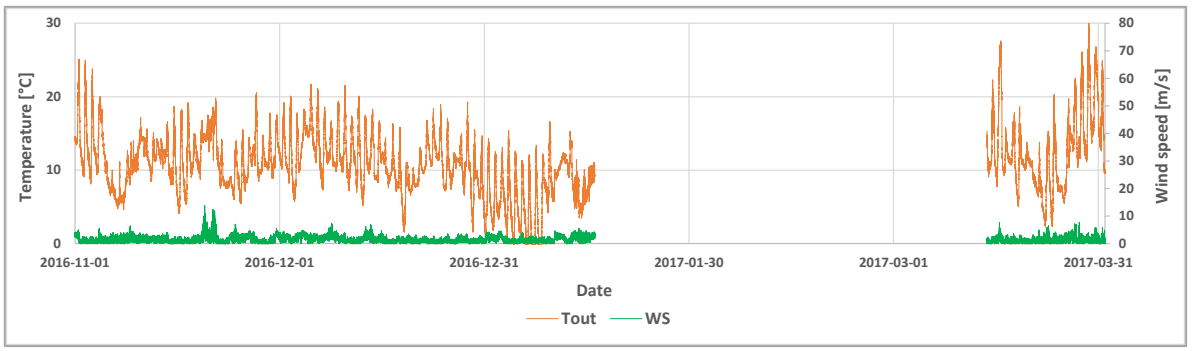

Figure 60. The outdoor temperature (T_{out}) and the wind speed (WS) during winter 2016-2017.

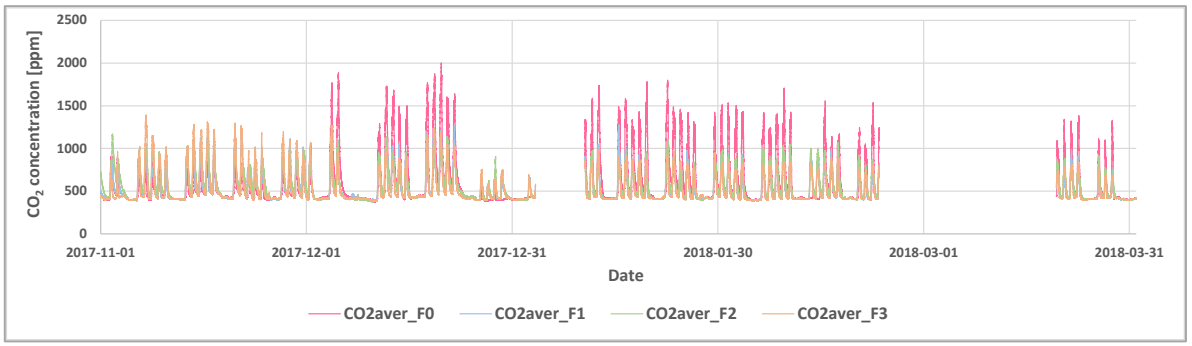

Figure 61. CO_2 concentration in the ground (CO_{2aver_F0}), first (CO_{2aver_F1}), second (CO_{2aver_F2}) and third (CO_{2aver_F3}) floor during winter 2017-2018.

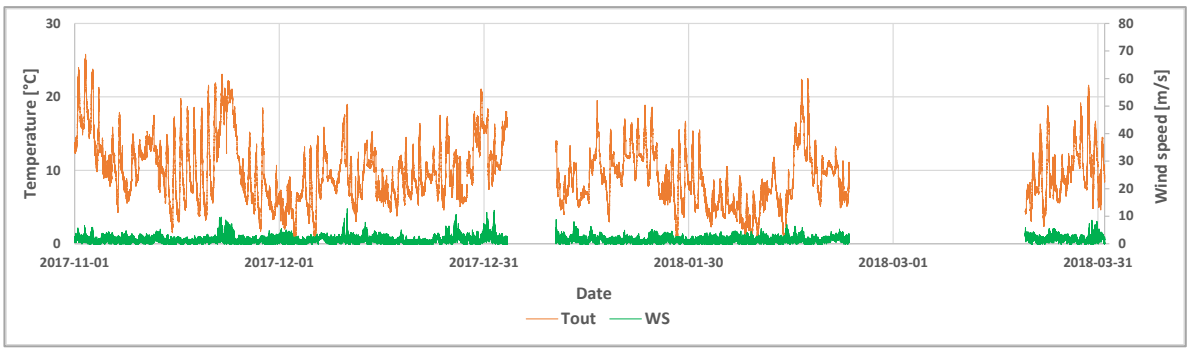

Figure 62. The outdoor temperature (T_{out}) and the wind speed (WS) during winter 2017-2018.

The figures shown above are able to provide very interesting information. For example, due to the missing data, the winter 2016-2017 must be discarded from the analysis. It can be seen that there are very long periods where no data is available, which limits considerably the possibility to estimate reliable results. Moreover, there was also some missing wind speed data during winter 2015-2016 (this cannot be distinguish clearly in the graphs since a long extension minutely data is plotted). However, since this is only a variable used for finding correlation with other parameters, the HLC decoupling analysis

can be carried out despite this data is missing. Finally, it is also possible to compare the data before the rehabilitation and after it, where a considerable drop can be observed in the CO_2 concentration in the majority of the floors. However, it can be assumed that something weird happens in the ground floor if Figure 61 is observed, since it is not reducing its concentration value as the rest of the floors are doing.

Moreover, after the rehabilitation, a ventilation system was installed in each floor of the building where a constant airflow rate was fixed for each of them. However, despite the ventilation volumetric airflow rates were measured for each of the floors, due to the illogical and unreliable values measured and provided in the dataset, they have not been plotted here. Then, from this issue can also be concluded that it is not possible to perform a suitable HLC decoupling process in the winter after the building rehabilitation.

Thus, once all the data is filtered and analysed, it is possible to apply the methods explained in section 2.4 for winters 2014-2015 and 2015-2016.

CHAPTER 4: RESULTS AND DISCUSSION

4. RESULTS AND DISCUSSION

In this chapter, the three different case studies already presented in section 3 have been analysed. However, as commented before, not all of them were useful for the application of all the methodologies detailed in section 2. Despite the average method has been applied to the three case studies in order to estimate the HLC, the solar gains analysis in opaque walls was only applied into the Round Robin Box presented in section 3.1 and the decoupling method, in the in-use office building presented in section 3.3.

Then, all the results obtained for each of the analysis are shown in the following section. First of all, all the results obtained for the Round Robin Box are presented in section 4.1. There, the section 4.1.1 shows the results obtained during the HLC estimation analysis while section 4.1.2 shows the results obtained for the solar gains analysis in opaque walls. Section 4.1.3 relates the results of the HLC analysis of the section 4.1.1 with the results of the solar gains analysis in opaque walls of section 4.1.2. Finally, section 4.1.4 contains the discussion of the previously obtained results in section 4.1.1, section 4.1.2 and section 4.1.3. Then, all the results obtained for the two residential buildings are shown in section 4.2. There, only the average method analysis has been carried out in order to estimate the heat loss coefficient for both residential buildings, the well insulated one in section 4.2.1 and the poorly insulated one in section 4.2.2. A discussion section 4.2.3 is also included for this case study. Finally, the four-story in-use office building is analysed in section 4.3. As done for the rest of the case studies, also the HLC is estimated applying the average method before and after the rehabilitation of the building in order to estimate the pre-retrofit and post-retrofit HLC in sections 4.3.1 and 4.3.2, respectively. Finally, these HLC values are decoupled into the transmission and infiltration and/or ventilation heat loss coefficient in section 4.3.3 before the rehabilitation and in section 4.3.4 after the rehabilitation. A general discussion is included for the four-story in-use office building in section 4.3.5.

4.1- The Round Robin Box results

4.1.1- HLC estimation results

In this section, the previously developed average method is applied to the simplest case study, the Round Robin Box. The method requirements have only permitted to find one

useful period for the HLC estimation between 6th December 2013 and 7th January 2014. This period starts the 18th of December at 21:00 and ends the 22nd of December at 5:00. In order to estimate this period HLC, after the first data analysis by visual checking done in section 3.1.3, the data has been studied mathematically in detail. There, the fulfilment of the requirements has been ensured and the obtained results are shown in the following Table 8.

PERIOD (Eq. 50)				HLC [W/K]
Period 1	2013-12-18 22:59	→	2013-12-22 4:59	4.1 ± 0.21

Table 8. HLC_{simple} and HLC estimation through the average method.

The obtained results have been compared with the results obtained with some simulation programs such as CTSM-R and LORD during the summer course of Dynastee [105]. [106] shows the results obtained with CTSM-R for the same dataset, where very similar HLC results are obtained applying the Grey Box modelling method.

Moreover, the obtained results are also compared with the design HLC value. There, the design value of the whole Round Robin Box is estimated to be 4.08 W/K. This value has been estimated assuming constant standard heat transfer coefficients for the inner and outer surface heat transfer coefficients. However, since in this case study a well-sealed test box is tested and the occupants behaviour is avoided since the Round Robin Box is not occupied, all the heat losses regarding infiltration and ventilation are avoided. Then, since in this case, the estimated HLC value is only considering the UA part, and this value barely changes after the building construction, the estimated HLC result using the average method is very close to the design value (it differs by only a 0.5%).

Once the HLC of the Round Robin Box has been estimated, the weight the not consideration of the solar gains through opaque elements could have respect to this performance indicator must be estimated, since this effect has not been considered when fixing the requirements of the average method. Therefore, it is first necessary to estimate the effect the solar gains through opaque walls have in the inner surface heat flux and then, transmit this weight to the estimated HLC value. The results obtained by applying this methodology are presented in the following section 4.1.2.

4.1.2- Results of the solar gain effect through opaque elements in the inner surface heat flux

Once the HLC has been estimated for the Round Robin Box, the analysis goes deeper in order to find the solar gains effect in the inner surface heat flux of the opaque walls of the Round Robin Box. Despite the average method is only applicable for winter period, the analysis has been performed for two different periods, one summer period and one winter period, as shown in Table 9.

PERIOD	SUMMER
Period 1	2013-06-18→ 2013-06-26
PERIOD	WINTER
Period 2	2013-12-19→ 2013-12-21

Table 9. Selected periods for summer and winter.

Obviously, the summer period will show higher solar radiation values than the winter period. Moreover, for the winter period, the period with the lowest solar radiation in a row has been consciously selected in order to test two extreme periods. Moreover, this winter period coincides with the period selected for applying the average method in the previous section. Thus, in the first instance, it could be considered that the effect this low solar radiation has on the opaque walls' inner surface heat flux would be low. Thus, most likely, disregarding this effect in the HLC value estimation would not be creating a considerable uncertainty in the final HLC result. However, unlike in the winter period, the effect the solar radiation could have in the inner surface heat flux of the opaque walls during the summer period could be considerable. Therefore, its percentage weight in the HLC value has also been estimated in this section.

4.1.2.1- Solar radiation estimated results

In section 2.2.2, the method used to estimate the missing global solar radiation was introduced. Then, the measured vertical south global solar radiation values have been compared with the results obtained from the proposed method in order to check their reliability. Once observed that the method was providing accurate results checking their RMSE, the estimated solar radiation values for east and west walls for the selected periods have been estimated and plotted in this section. They are shown in the following figures (Figure 63 and Figure 64) in order to show their meaningful behaviour.

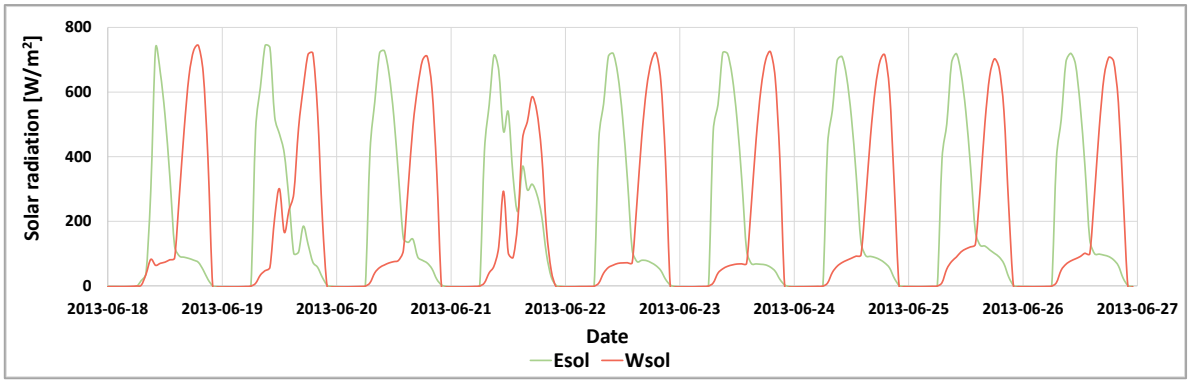

Figure 63. Vertical east and west global solar radiation results for period 1 (summer).

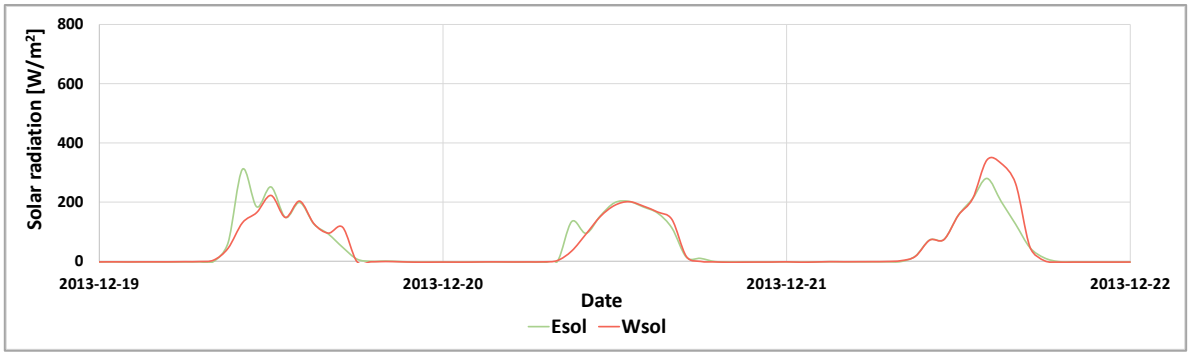

Figure 64. Vertical east and west global solar radiation results for period 2 (winter).

The vertical east and west global solar radiations estimated for both periods show logical, and thus reliable behaviour. During the summer morning, the vertical east global solar radiation increases and it decreases during the afternoon, while the vertical west global solar radiation shows just the opposite behaviour. However, during the winter period, both the vertical east global solar radiation and the vertical west global solar radiation show quite similar low results, since a very cloudy period has been selected and the solar radiation is almost purely diffuse and thus similar in all the orientations of the Round Robin Box.

4.1.2.2- Results of the validation of the models

As explained in section 2.2.3, in order to perform the best model selection, it has been necessary to carry out an exhaustive analysis of the residuals of the models and the U-value, together with the rest of the physical parameters (such as the solar absorptivity), estimated for each of the walls. Therefore, the first step of the model selection carried out has been the analysis of the model residuals through the RMSE. Since the inner surface

heat flux has been used as the output of all the models, the unit of all the presented RMSE values is [W/m^2]. All the obtained RMSE values for each of the models are presented in Table 10. All these values have been analysed one by one in order to find the lowest residual results.

RMSE	SUMMER							
	PERIOD 1							
WALL	M1	M2	M3	M4	M5	M6	M7	M8
Ceiling	0.53	2.62	1.61	2.92	2.04	1.09	0.94	**0.76**
Floor	0.40	1.27	0.60	0.72	**0.53**	0.60	0.60	**0.53**
East	0.44	2.09	0.65	1.32	0.63	**0.58**	0.73	**0.58**
North	0.30	0.81	0.49	1.26	0.49	**0.39**	0.49	**0.39**
West	-	2.03	0.38	1.02	**0.37**	0.38	0.58	**0.37**
RMSE	WINTER							
	PERIOD 2							
WALL	M1	M2	M3	M4	M5	M6	M7	M8
Ceiling	0.29	0.74	0.72	1.34	0.72	**0.45**	0.51	**0.41**
Floor	1.03	**0.97**	**0.97**	1.02	**0.96**	**0.97**	1.03	**0.97**
East	0.91	0.99	0.89	1.07	0.89	**0.86**	0.90	**0.86**
North	0.26	0.55	0.35	0.60	**0.34**	0.35	0.39	**0.34**
West	0.83	0.98	0.87	1.12	0.87	**0.86**	0.97	**0.86**

Table 10. The RMSE residual values for the corresponding model and wall for the selected periods in summer and winter.

As can be seen in Table 10, despite the difference in the obtained residual values between the models in general being low, the lowest residuals were obtained for the M8 model. However, in some of the walls, the same value obtained for Model 8 was also obtained for Model 5 or Model 6. Then, although it seems that several models can be considered suitable for the same wall, since Model 8 is the model representing the closest convective and radiative effects to reality occurring on the external surface of the wall, for this research, it is considered as the best approach. In other words, Model 8 is the model representing every detail occurring in reality, so it is considered as the best one.

However, in order to justify the fact that Model 8 is providing the closest values to reality, we have also included a comparison between the obtained physical parameters from the model fitting and the theoretical ones. So, it is necessary to compare the U-values estimated in each of the models with the theoretical values to carry out the model validation. However, as remarked in section 2.2.3.2, since the estimation in the models has been obtained between the inner surface temperature and the outdoor air

temperature, the estimated theoretical U-value will not be directly comparable to the value provided by LORD. So the thermal resistance (R) values are compared. If mathematically calculated, the obtained R_W value for the surface to surface wall is 1.93 m^2K/W. Moreover, the surface to outdoor air theoretical R_T value has been estimated and the obtained value is 1.97 m^2K/W. Therefore, all the thermal resistance values obtained for each of the models and their corresponding differences with respect to the theoretical value in percentages ($R_{\%}$) are shown in Table 11.

Thermal resistance	SUMMER															
PERIOD 1																
WALL	M1		M2		M3		M4		M5		M6		M7		M8	
	R_W	$R_{\%}$	R_W	$R_{\%}$	R_W	$R_{\%}$	R_W	$R_{\%}$	R_W	$R_{\%}$	R_W	$R_{\%}$	R_W	$R_{\%}$	R_W	$R_{\%}$
Ceiling	1.87	3.1	1.88	4.6	1.88	4.6	1.92	2.5	1.88	4.6	1.91	3.1	1.91	3.1	**1.89**	**4.1**
Floor	1.94	0.5	1.97	0.0	1.99	1.0	1.98	0.5	**1.96**	**0.5**	1.99	1.0	1.97	0.0	**1.96**	**0.5**
East	1.93	0.0	1.93	2.0	1.94	1.5	1.97	0.0	1.94	1.5	**1.96**	**0.5**	1.96	0.5	**1.95**	**1.0**
North	2.02	4.7	2.03	3.1	2.04	3.6	2.07	5.1	2.04	3.6	**2.05**	**4.1**	2.06	4.6	**2.05**	**4.1**
West	-*	-	1.97	0.0	1.92	2.5	1.93	2.0	**1.93**	**2.0**	1.94	1.5	1.92	2.5	**1.92**	**2.5**
Thermal resistance	WINTER															
PERIOD 2																
WALL	M1		M2		M3		M4		M5		M6		M7		M8	
	R_W	$R_{\%}$	R_W	$R_{\%}$	R_W	$R_{\%}$	R_W	$R_{\%}$	R_W	$R_{\%}$	R_W	$R_{\%}$	R_W	$R_{\%}$	R_W	$R_{\%}$
Ceiling	2.04	5.7	2.04	3.6	2.04	3.6	2.08	5.6	2.04	3.6	**2.07**	**5.1**	2.07	5.1	**2.05**	**4.1**
Floor	2.05	6.2	**2.27**	**15.2**	**2.26**	**14.7**	2.09	6.1	**2.18**	**10.7**	**2.26**	**14.7**	2.09	6.1	**2.13**	**8.1**
East	2.22	15.0	2.25	14.2	2.24	13.7	2.27	15.2	2.24	13.7	**2.27**	**15.2**	2.26	14.7	**2.27**	**15.2**
North	2.04	5.7	2.09	6.1	2.07	5.1	2.08	5.6	**2.05**	**4.1**	2.07	5.1	2.07	5.1	**2.06**	**4.6**
West	2.01	4.2	2.04	3.6	2.02	2.5	2.05	4.1	2.02	2.5	**2.02**	**2.5**	2.04	3.6	**2.03**	**3.1**

Table 11. The thermal resistance in [m^2K/W] values for the corresponding model and wall and their corresponding differences with respect to the theoretical value in percentages for the selected periods in summer and winter.

* Since there were no reliable outer surface temperature measurements for the west wall during the period of summer, it has been impossible to estimate the thermal resistance of the M1 case. However, it has been possible to estimate the rest of the values.

Therefore, the results of the models previously marked in Table 10 showing the lowest residuals are again in bold in Table 11. Interesting results are shown in this table. First of all, in general, the thermal resistance between all the models varies slightly, as happens with the residuals. Therefore, in some cases, it is quite complicated to select the best model based only on the thermal resistance value. As commented before, in order to fit all the models from M2 to M8 presented in section 2.2.3.1, the thermal resistances estimated in M1 have been fixed and LORD only needed to estimate the thermal resistances between the outer surface and the outdoor environment.

Having estimated the thermal resistances for each wall and model, it is now possible to estimate the corresponding U-values for each of them. Thus, using the inner surface to outdoor air thermal resistances estimated for each model in Table 11 and the standard inner surface thermal resistance [93], with a value of 0.13 m^2K/W, the air to air U-values shown in Table 12 are obtained.

U-value	SUMMER							
	PERIOD 1							
WALL	M1	M2	M3	M4	M5	M6	M7	M8
Ceiling	-	0.50	0.50	0.49	0.50	0.49	0.49	**0.50**
Floor	-	0.48	0.47	0.47	**0.48**	0.47	0.48	**0.48**
East	-	0.49	0.48	0.48	0.48	**0.48**	0.48	**0.48**
North	-	0.46	0.46	0.45	0.46	**0.46**	0.46	**0.46**
West	-	0.48	0.49	0.49	**0.49**	0.48	0.49	**0.49**
U-value	WINTER							
	PERIOD 2							
WALL	M1	M2	M3	M4	M5	M6	M7	M8
Ceiling	-	0.46	0.46	0.45	0.46	**0.45**	0.45	**0.46**
Floor	-	**0.42**	**0.42**	0.45	**0.43**	**0.42**	0.45	**0.44**
East	-	0.42	0.42	0.42	0.42	**0.42**	0.42	**0.42**
North	-	0.45	0.45	0.45	**0.46**	0.45	0.45	**0.46**
West	-	0.46	0.47	0.46	0.47	**0.47**	0.46	**0.46**

Table 12. The U-values in [W/m^2K] for the corresponding model and wall for the selected periods in summer and winter.

Then, considering all this information, it is possible to continue with the analysis of the model fits. Since the residuals were the lowest for Model 8 and the thermal resistance values (or U-value) obtained do not show irregularities, Model 8 can be selected as the best. However, it is also interesting to check the solar absorptivity provided by the model fit. Unfortunately, the theoretical solar absorptivity value of the walls' outermost material was not provided. However, considering that the outermost wall of the Round Robin Box is formed by fiber cement, it is possible to check the general properties of this material and find the solar absorptance reference value for it. In general, the solar absorptance of this material should be around 0.6 [92]. Therefore, this value can be used as reference to discard values that are too far from it. Moreover, in order to follow physical laws, it can be ensured that the estimated solar absorptivity values should not be too close to zero or one and that they should provide similar values in all the façades. Therefore, Table 13

shows the solar absorptivity values obtained for the selected bold models in the residual Table 10.

SURFACE	SUMMER		WINTER	
	PERIOD 1		PERIOD 2	
	A_5 for M5 or M6	A_5 for M8	A_5 for M5 or M6	A_5 for M7 or M8
Ceiling	-	**0.47**	0.48	**0.49**
Floor	0.34	**0.60**	-	**0.65**
East	0.56	**0.60**	0.34	**0.40**
North	0.54	**0.54**	0.87	**0.60**
West	0.31	**0.42**	0.97	**0.60**
AVERAGE	0.44	**0.52**	0.67	**0.55**

Table 13. The solar absorptivity in [-] values for the corresponding model and wall for the selected periods in summer and winter.

For the M8 ceiling case in summer, the obtained value is not too far from 0.6 and it is quite far from the limits, so it is directly considered as the best model. The same procedure must be followed with the rest of the models in summer. For example, in the case of the floor and the west walls, Model 8 is selected as the best, since the obtained solar absorptivity in this model is closer to the reference value as compared to the other models, as shown in Table 13. However, in the case of the east and the north, very similar results are obtained for both models 6 and 8. Therefore, as commented before, since Model 8 is the most detailed model and it provides good and logical results for all, Model 8 will be selected for all the walls for the rest of the calculations in the summer period.

However, if winter results are analysed, it can be seen that there is a considerable difference between the thermal resistance values in the floor results in Table 11. Therefore, although the best residuals were obtained for models 2, 3, 5, 6 and 8, the thermal resistance values obtained for these models, together with the solar absorptivity, were illogical. Therefore, since Model 7 was the only model providing thermal resistance and solar absorptivity results similar to the theoretical values and the obtained residuals are not far from the lowest residuals of the rest of the models of the wall, it has been selected as the best model. In the rest of the walls, the model selection has been performed considering the solar absorptivity value as reference. In other words, the models providing solar absorptivity values too close to the limits (0 as the lowest and 1 as the highest) were discarded. Once again, the selected best models are the most detailed ones, Models 7 and 8. Thus, it can be concluded that the most detailed models also show the

best residuals and the closest physical parameters to reality. Then, the finally selected model thermal resistance values are shown in the following Table 14. Moreover, further insights concerning the best-fitted models are graphically presented in Appendix E. There, the ceiling and north wall model cases are plotted as the most representative models (Figure E.1, Figure E.3, Figure E.5 and Figure E.7) showing the best fit obtained for each of the walls in the summer and winter periods and their RMSE values. The rest of the graphical model fits are also shown in Appendix E.

SURFACE	SUMMER	WINTER	
	PERIOD 1	PERIOD 2	
	R_T for M8 [m^2K/W]	R_T for M7 [m^2K/W]	R_T for M8 [m^2K/W]
Ceiling	1.89	-	2.05
Floor	1.96	2.09	-
East	1.95	-	2.27
North	2.05	-	2.06
West	1.92	-	2.03
AVERAGE	1.95	2.09	2.10

Table 14. The obtained thermal resistances (R values) for the selected periods in summer and winter.

Therefore, for the selected models, the estimated thermal resistance average for the summer period is 1.95 m^2K/W for M8. As can be seen, all values are very close to the theoretical value, 1.97 m^2K/W. Moreover, if the results are analysed independently, it can be observed that the lowest thermal resistance value is 1.89 m^2K/W and the highest is 2.05 m^2K/W. The lowest value is obtained from the surface most exposed to the sun, the ceiling of the Round Robin Box. However, the highest value is obtained in one of the walls least exposed to the sun, the north wall. Moreover, it is well known, as proven for example in [107] that the average temperature of the insulation layers of a wall can affect its thermal resistance value. It is proven that if the average temperature of the insulation layer increases, its thermal conductivity also increases. Thus, the thermal resistance will be reduced. Then, since the average temperature of the insulation layer can increase due to the direct effect of the solar radiation on the ceiling, the thermal resistance value can be reduced slightly. However, the opposite happens when analysing the north wall.

The same occurrence happening in this north wall can also be seen when analysing the winter results. The colder temperatures tend to cool down the average temperature of the

insulation layer of the wall. Thus, their insulation layer thermal conductivity is reduced slightly and, consequently, their thermal resistance value increases. However, the obtained results are very close to the theoretical estimated values, since the average value of the best estimates of the surface to air models is 2.10 m^2K/W.

4.1.2.3- Inner surface heat flux difference results

Having proven that the model selected as the best representation of reality for each of the walls for the summer and winter periods is able to provide a proper fit of the inner surface heat flux and a good validation of the thermal physical parameters, it is then possible to carry out the rest of the calculations mentioned in section 2.2.4. Thus, the models fitted and selected in the previous section 4.1.2.2 for each of the walls are taken and, once all the parameters are fixed, the solar radiation is removed from the model. Therefore, the model is then able to estimate the hypothetical inner surface heat flux ($\overline{\dot{q}'}$) without considering the solar radiation effect.

It has thus been possible to carry out a deeper analysis of the solar radiation effect on the inner surface heat flux. So, the total heat flux difference between the estimated heat flux considering the effect of the solar radiation and without considering its effect can be estimated. Moreover, the percentage of difference between them has also been estimated in order to see whether the solar radiation effect on the inner surface heat flux is negligible or not. Even if we have the real inner surface heat flux measurement, for this comparison, both inner surface heat fluxes have been obtained from the model, so any disturbance generated by the model will be identical in both heat fluxes and will not affect the difference calculation.

SURFACE	MEAN HEAT FLUX WITH SOLAR RADIATION [W/m²] $\bar{q}$	HYPOTHETICAL MEAN HEAT FLUX WITHOUT SOLAR RADIATION [W/m²] $\bar{q}'$	HEAT FLUX DIFFERENCE AVERAGE [W/m²] $\bar{q}_{dif} = (\bar{q}' - \bar{q})$	PERCENTAJES [%] $\dot{q}_{\%} = \frac{\bar{q}' - \bar{q}}{\bar{q}} \times 100$
SUMMER				
PERIOD 1				
Ceiling	8.51	11.33	2.82	33.1 %
Floor	7.76	8.42	0.66	8.5 %
East	7.56	9.25	1.69	22.4 %
North	8.20	8.82	0.62	7.6 %
West	7.20	8.76	1.56	21.7 %
WINTER				
PERIOD 2				
Ceiling	11.96	12.46	0.50	4.2 %
Floor	10.87	11.09	0.22	2.0 %
East	10.46	10.92	0.46	4.4 %
North	10.67	10.96	0.29	2.7 %
West	10.84	11.21	0.37	3.4 %

Table 15. The mean heat fluxes, the heat flux difference and the corresponding percentage results for the best models.

The first and the second columns of Table 15 show the analysed period mean heat flux both considering and not considering the solar radiation. In the first column, it can be seen that almost all the mean heat fluxes show similar results for the same period. In the case of period 1 in summer, all the average values are around 8 W/m². However, in the case of period 2 in winter, almost all of them are close to 10.5 W/m², except the ceiling model. This is slightly higher with a mean heat flux value of 11.96 W/m². However, in the second column, the ceiling shows a considerable difference if compared to the rest of the walls in summer. Nevertheless, during the winter period, the obtained mean value for the ceiling is slightly higher than the rest of the values, but the difference is not that considerable. This effect is mainly due to the low sky temperatures occurring during the clear nights in the test site during the summer period. These low night sky temperatures mainly affect the ceiling's outermost surface.

The third column shows the period averaged inner surface heat flux difference between the estimated average inner surface heat flux with and without considering the solar radiation. For the summer case, interesting conclusions can be taken from this table. As expected, since the ceiling is the most exposed to solar radiation, it is the model that

shows the highest heat flux difference due to this effect. After the ceiling, the east and west models show lower values which are quite similar to each other. Finally, the north wall and the floor are the least exposed to solar radiation; so, in consequence, the difference between considering or not the solar radiation is the smallest. The winter case is quite different compared to the case in summer. Since the sun's altitude is lower during winter, the difference between the ceiling, east and west models is very small. Furthermore, the selected winter period consists of cloudy days where mainly diffuse solar radiation is present. Remember that diffuse solar radiation can be considered similar for all orientations.

The last column shows the difference of the solar radiation effect on the inner surface heat flux during both the summer and winter in percentages. During summer, in walls such as the ceiling, the east and the west, the effect this solar radiation has on the inner surface heat flux is considerable. However, in the rest of the walls, the percentage shows quite low values. In general, this percentage is low in all the walls during winter. Figure F.1, Figure F.2, Figure F.3 and Figure F.4 of Appendix F graphically show the most representative model's inner surface heat flux evolution (with and without solar radiation) in order to see the difference visually. The inner surface evolution of the rest of the models are also shown in Appendix F.

Note that this percentage of the last column of Table 15 is directly proportional to the temperature difference between the outer and inner surfaces. If the temperature difference is reduced, the percentage effect of the solar radiation on the inner surface heat flux would increase. The inner surface heat flux, when considering the solar radiation, is estimated by $\bar{\dot{q}} = \frac{\overline{T_{Sin}} - \overline{T_{Sout}}}{R_{cond}}$, while the hypothetical inner surface heat flux, without considering the solar radiation, is estimated by $\overline{\dot{q}'} = \frac{\overline{T_{Sin}} - \overline{T_{Sout,nosolar}}}{R_{cond}}$. Here, due to the solar radiation effect, the T_{Sout} tends to be considerably higher than $T_{Sout,nosolar}$, which results in the $\overline{\dot{q}'}$ being higher than $\bar{\dot{q}}$, as already shown in Table 15. The rest of the parameters used in the equations (T_{Sin} and R_{cond}) are the same for both inner surface heat flux estimations. However, the variation of the inner surface temperature in both equations can result in the weight the solar radiation has in the inner surface heat flux varying considerably. An example will be performed to see this effect. If the inner surface average temperature of

the wall is 40 °C, the outer surface average temperature of the wall is 20 °C and the thermal resistance of the wall is 2 m²K/W, the obtained $\bar{\dot{q}}$ value would be 10 W/m². Then, if the $T_{Sout,nosolar}$ is 18 °C, the $\bar{\dot{q}}'$ value obtained would be 11 W/m². Thus, the weight the solar radiation would have in the inner surface heat flux, estimated using Eq. 82, is 10 %, since the $\bar{\dot{q}}' - \bar{\dot{q}}$ value is 1 W/m² and $\bar{\dot{q}}$ is 10 W/m². However, if the inner surface temperature is reduced to 30 °C, the temperature difference is also reduced, while the new $\bar{\dot{q}}$ and $\bar{\dot{q}}'$ are reduced to 5 W/m² and 6 W/m², respectively. Then, despite the $\bar{\dot{q}}' - \bar{\dot{q}}$ value still being 1 W/m², the $\bar{\dot{q}}$ is considerably reduced to 5 W/m², which results in the effect the solar radiation has on the inner surface heat flux increasing to 20 %, double the previous case. So, it is proved that the variation of the inner surface temperature has also a considerable influence on the solar radiation percentage effect in the inner surface heat flux.

4.1.2.4- g-value estimation results

Once the rest of the calculations had been carried out, it was possible to compare the g-value results of all the opaque walls using two different methods. As explained in section 2.2.5, one of the results is obtained directly from the software used for model fitting and simulation named LORD, while the other results are obtained from Eq. 69.

SURFACE	SUMMER PERIOD 1		WINTER PERIOD 2	
	LORD g-value [-]	Eq. 69 g-value [-]	LORD g-value [-]	Eq. 69 g-value [-]
Ceiling	0.010	0.008	0.010	0.009
Floor	0.016	0.013	0.033	0.030
East	0.009	0.009	0.009	0.009
North	0.007	0.006	0.014	0.013
West	0.009	0.009	0.007	0.007

Table 16. The obtained g-values for each of the periods using model M8 (LORD) and Eq. 69.

From Table 16, it can be concluded that, in general, the solar factor in the opaque elements seems quite low compared to the typical solar factor values obtained for such semi-transparent components as windows, where the solar factor is usually between 0.2 to 0.7. This has already been tested in [64]. For the winter case, in the floor, the g-value shows quite high values compared to the rest of the values. This alteration in the results

could be due to the extremely low solar radiation values striking the outermost surface of the floor, which means the results will be estimated with a considerably high uncertainty.

However, it has already been proven that despite the g-values being low, the effect the solar radiation has on the inner surface heat flux can be considerable for some of the cases. Finally, it must be mentioned that the results obtained using LORD and from Eq. 69 are very similar for all the selected models.

4.1.3- Results of the estimation of the effect of the solar gains through opaque walls in the HLC estimation

Through Eq. 84 and Eq. 85, it has been possible to quantify the weight the term $\frac{\sum(\bar{q}_{dif} \times A_W)}{(\overline{T_{in}} - \overline{T_{out}})}$ has in the Round Robin Box HLC estimation and the weight the solar gains through the opaque envelope have over the solar gains through the Round Robin Box window. These two figures are extremely important for HLC estimation methods, where the solar gains are not estimated with an identifiable constant value. As already commented, one cloudy, cold winter period and one sunny, warm summer period have been analysed.

For the winter period, for the Round Robin Box, it is estimated that the weight of the term $\frac{\sum(\bar{q}_{dif} \times A_W)}{(\overline{T_{in}} - \overline{T_{out}})}$ with respect to the estimated HLC term using the average method is of 1.7 % and the solar gains through the opaque envelope are 13.6 % with respect the solar gains through the window (estimated using the average method). If compared with the theoretical values, the results of the weights are 1.7 % and 11.3 % respectively, very similar to the weights values obtained respect to the estimated values. Thus, it is demonstrated that for methods such as the average method, where the energy balance was applied in cold and cloudy periods in order to estimate the HLC of in-use buildings, the effect of the solar gains through the opaque walls can be neglected in the calculation without generating a considerable error in the HLC estimates. For the Round Robin Box HLC estimation, in the analysed winter period, only considering the solar gains through the glazed part of the Round Robin Box, the error in the estimated HLC will be of just 1.7 %.

However, in the summer period, it is estimated that the weight of the term $\frac{\sum(\bar{q}_{dif} \times A_W)}{(\overline{T_{in}} - \overline{T_{out}})}$ with respect to the HLC term is 8.9 % and the solar gains through the opaque envelope are 37.2 % with respect to the solar gains through the window. As expected, the weight of the solar gains through the opaque envelope is considerably higher in sunny, summer periods than in cloudy, cold winter periods. So, it has been demonstrated that, for cases where the HLC is estimated in sunny periods without considering the solar gains through the opaque building envelope, the underestimation of the HLC could be considerable. To avoid this underestimation of the HLC estimate during sunny periods, the use of more complex methods that introduce the effect of the solar gains through the opaque walls by means of an identifiable constant solar aperture parameter should be used.

4.1.4- General discussion about obtained results

Once the HLC estimates and the solar gains effect through opaque walls results have been estimated, a general discussion is carried out in order to analyse them deeper. Therefore, the useful period obtained when applying the average method during December 2013 is first analysed. Using this period for the HLC estimation using the average method, as commented above, shows very similar results to the HLC values obtained applying different methods. For example, [106] presents the results obtained during the summer school using the same dataset for CTSM-R. During this analysis, two periods were analysed where the obtained results were 4.1 ± 0.11 W/K and 4.2 ± 0.09 W/K. As can be seen, they are very close to the value obtained with the average method 4.1 ± 0.21 W/K, which demonstrates the robustness of the developed average method. As also commented before, the obtained results are also similar to the design values provided in [64]. Since in this case, there are not infiltration and ventilation heat losses in the Round Robin Box, the obtained real and design HLC values show very similar results. Moreover, the accumulated average plot for the period is also shown in Figure A.1 of Appendix A, where the estimate HLC is stabilized within a ± 10 % band over all the last 24 testing hours.

However, as commented in section 2.1.1, the developed average method only considers the effect of the solar gains entering through the window. Apart from this, the period selected by this method only consider cloudy and cold days where the solar radiation in

all the orientations of the Round Robin Box can be considered purely diffuse and thus, similar in all orientations. Then, the uncertainties the solar radiation effect can create in the HLC estimated are very low. Therefore, by the analysis of the solar radiation effect through opaque walls, it has been proven that the effect is negligible in the HLC estimation in periods where the average method is applicable. In other words, since the solar radiation effect in the inner surface heat flux of opaque walls is very low for the winter periods selected by the average method, it has been demonstrated that not considering the solar radiation effect through opaque walls is creating a negligible uncertainty in the HLC estimation. Then, the HLC results obtained in the section 4.1.1 (and also the rest of the section 4.2.1, 4.2.2, 4.3.1 and 4.3.2, where the HLC is estimated using the average method) can be considered reliable despite the solar gains through opaque walls are not considered. However, during summer, the situation is quite different. In summer, not considering this effect can create a considerable error in the estimation of the HLC for these cases as demonstrated in section 4.1.3. Then, for the summer period, if a HLC value would be estimated through a method where an identifiable constant value is not used to estimate the solar gains, the HLC value could differ considerably from the real value.

4.2- Residential buildings results

In this section, the estimation of the HLC of the two residential buildings is performed. As previously commented in section 3.2.3, the two houses presented have not been monitored for the same data periods. The house in Loughborough [100] was only monitored from 16 February to 15 March 2014. Unfortunately, the electrical consumption data started to be collected on 25 February, which limits the opportunity to find a suitable period within the provided data. The house in Gainsborough was monitored from 1 November 2012 until 30 April 2015. Thus, since a longer monitoring period was provided, it was easier to find suitable periods to estimate the HLC that fulfil the average method requirements.

As explained in section 2.1.1, the average method is able to estimate the HLC of a building using short time periods (at least 72 h periods). However, due to all the requirements demanded by the average method from the periods for analysis, finding suitable periods when short data series are provided is not always possible. In this case, it was necessary to ease some of the method requirements, taking more flexible

limitations for the solar gains 10 % weight requirement, and this relaxation effect on the HLC estimation was analysed.

In the next two subsections 4.2.1 and 4.2.2, both building data series are analysed separately. In order to demonstrate the reliability of the method, several useful independent periods should be found during the study of each building's data sets. Thus, the individual results obtained for each period will be independent from each other and can then be compared for the same building. Then, an average HLC estimation value was calculated for each of the houses. Considering the characteristics of each house, the reliability of the results are also discussed.

4.2.1- HLC results of the highly insulated residential building

Since a large dataset was provided for the house in Gainsborough, three consecutive winters are available to find suitable cold and cloudy periods to apply the average method. Thus, six useful periods that fulfil most of the average method requirements were found, see Table 17 and Table 18.

WINTER	PERIOD			INPUT DATA						
				$\overline{T}_{out}$ [°C]	$\overline{T}_{in}$ [°C]	$\overline{T}_{in}$-$\overline{T}_{out}$ [°C]	$\overline{Q}$ [W]	$\overline{K}$ [W]	$\overline{Q+K}$ [W]	$\overline{S_a V_{sol}}$ [W]
2012-2013	Period 1	2012-12-03 18:02	→ 2012-12-07 19:02	2.6	21.2	18.6	1066.5	11.9	1078.4	491.7
	Period 2	2012-12-11 16:02	→ 2012-12-14 11:02	-0.4	16.9	17.3	767.9	22.6	790.5	380.9
	Period 3	2012-12-18 23:02	→ 2012-12-22 8:02	5.9	16.9	11.0	544.7	9.3	554.0	110.7
2013-2014	Period 4	2013-11-27 2:02	→ 2013-11-30 8:02	7.0	21.7	14.7	326.8	459.2	786	336.9
	Period 5	2013-12-13 21:02	→ 2013-12-17 3:02	9.5	21.7	12.2	393.8	453.7	847.5	282.0
2014-2015	Period 6	2014-11-26 3:02	→ 2014-11-30 8:02	8.7	21.9	13.2	322.7	353.8	676.5	139.4

Table 17. Necessary period averaged variable values to estimate the HLC_{simple} (simple Heat Loss Coefficient, Eq. 29) and HLC (Heat Loss Coefficient, Eq. 28) for Gainsborough. The variables included are the outdoor temperature (T_{out}), the indoor temperature (T_{in}), the temperature difference (T_{in}–T_{out}), the space heating heat input (Q), the electrical heat gains (K), the total internal heat gains (Q + K) and the solar gains (S_aV_{sol}). [102]

WINTER	PERIOD	OUTPUT DATA	
		HLC_{simple} [W/K]	**HLC** [W/K]
2012-2013	Period 1	57.9 ± 3.5	84.4 ± 8.5
	Period 2	45.9 ± 2.9	68.0 ± 7.2
	Period 3	50.2 ± 4.4	60.2 ± 6.6
2013-2014	Period 4	53.6 ± 3.8	76.6 ± 8.4
	Period 5	69.6 ± 5.7	92.7± 10.6
2014-2015	Period 6	51.4 ± 3.9	61.9 ± 6.1

Table 18. The HLC_{simple} (simple Heat Loss Coefficient, Eq. 29) and HLC (Heat Loss Coefficient, Eq. 28) estimated values for Gainsborough. [102]

The average value of the six HLC_{simple} estimations presented in Table 18 is 54.8 ± 4.1 W/K, and 74 ± 8.1 W/K for the HLC. As a comparison reference, the Annex 71 has provided a "theoretical HLC value" of 49.9 W/K. Note that the Gainsborough theoretical value only considers the envelope design transmittance values and design infiltration/ventilation characteristics, so it is not the "true" HLC value. However, as proven by [25], when design HLC values are compared to co-heating experimental HLC values, the co-heating HLC values are usually considerably higher than the design HLC values. These differences have been proven to be up to 100 % higher in the co-heating HLC when compared to the design HLC values. Thus, the obtained results follow this proven trend of having higher experimental HLC values when compared to the design HLC values.

In order to analyse the spread and reliability of the estimated in-use HLC results for Gainsborough, it is indispensable to carry out a more detailed study of the data. As explained in section 3.2.1.2, Gainsborough's gas consumption is not only providing space heating, but also DHW. Then, although a filter is developed to estimate the gas consumption for space heating and DHW production (see Table 19), this issue introduces an important uncertainty. The order of magnitude of the estimated energy dedicated to DHW is of the order of the estimated space heating requirements. However, periods 2 and 3 had no main water consumption and give very interesting information.

WINTER	PERIOD	INPUT DATA			
		$\overline{Q}$ [W]	$\overline{Q}_{DHW}$ [W]	$\overline{Q}_{Tot}$ [W]	$\%\overline{Q}_{DHW}$ [W]
2012-2013	Period 1	1066.5	406.0	1472.5	27.6
	Period 2	767.9	0.0	767.9	0.0
	Period 3	544.7	0.0	544.7	0.0
2013-2014	Period 4	326.8	404.7	731.6	55.3
	Period 5	393.8	431.6	825.5	52.3
2014-2015	Period 6	322.7	46.6	369.2	12.6

Table 19. Space heating (Q), DHW consumption (Q_{DHW}), total ($Q_{Tot} = Q + Q_{DHW}$) and corresponding DHW percentage of the total ($\%Q_{DHW}$) for the analysed periods in Gainsborough. [102]

If Table 19 is analysed, it can be seen how the second and third periods show null DHW consumption (actually they have null mains water consumption), while the space heating continues to work. Table 20 shows the individual indoor temperature measurements of the bedroom and lounge of the Gainsborough house.

WINTER	PERIOD	INPUT DATA				
		$\overline{T}_{out}$ [°C]	$\overline{T}_{in\text{-}bed}$ [°C]	$\overline{T}_{in\text{-}lounge}$ [°C]	$\overline{T}_{in\text{-}average}$ [°C]	$\overline{T}_{in}$-$\overline{T}_{out}$ [°C]
2012-2013	Period 1	2.6	21.2	21.3	21.2	18.6
	Period 2	-0.4	18.3	15.4	16.9	17.3
	Period 3	5.9	18.5	15.4	16.9	11.0
2013-2014	Period 4	7.0	21.3	22.1	21.7	14.7
	Period 5	9.5	21.5	21.9	21.7	12.2
2014-2015	Period 6	8.7	21.3	22.6	21.9	13.2

Table 20. Indoor temperature (bedroom, lounge and both average temperatures), outdoor temperature and temperature difference for the analysed periods in Gainsborough. [102]

From Table 20, for the second and third periods, the obtained indoor temperature is quite low in comparison to the rest of the indoor temperatures. Therefore, it can be concluded that the occupants are not at home during these two periods; this might provide accurate results of the HLC. Since there is no occupancy in the house during these two periods, it can be stated that there is no metabolic heat generation and no uncertainty in the space heating supply energy estimation due to DHW splitting, since 100 % is used for space heating purposes. During these two periods, the boiler is working for security reasons to avoid excessive cooling of the house while vacant.

Another issue to take into account is the low heating consumption (Q) in the well-insulated Gainsborough building. This leads to several difficulties when searching for valid periods to apply the average method. On the one hand, the internal heat gains (Q + K) of the house are probably underestimated since, when splitting the space heating and the DHW consumption, some space heating heat is probably not considered. Furthermore,

as shown in Table 17, for the last three periods, the heat generated by the electricity consumption is higher than the heat provided by the space heating. Note that period 1 has a very low electrical consumption for an occupied building. This phenomenon is not common in older, worse insulated buildings, since the space heating is usually the dominant internal heat gain in cold and cloudy periods. On the other hand, although cold and cloudy periods with low solar radiation have been selected, due to the low space heating requirements, the percentage of solar radiation as compared to the rest of the heat gains (Q + K) increased to an average of 35.1 % for all the periods (35.1 % × ($\overline{Q + K}$) = ($\overline{S_a V_{sol}}$)). It must be highlighted that none of the periods can provide values that fulfil the requirement of having just 10 % weight of solar gains as compared to the other internal heat gains (Q + K). However, periods 3 and 6 are the two closest to fulfilling the 10 % weight requirement, since both are around 20 % of weight.

There is a final issue to remark concerning the possible user behaviour regarding the ventilation system control and/or window opening. The individual HLC values estimated for the Gainsborough house in the unoccupied periods 2 and 3 and the occupied period 6 are very close to each other. While occupied periods 1, 4 and 5 have higher HLC values as compared to the unoccupied periods 2 and 3. It might be that the users were opening windows or increasing the ventilation system set points during periods 1, 4 and 5, thus increasing the ventilation rates and, consequently, the in-use HLC values during those periods. During period 6 (the one with the lowest weight of solar gains together with period 3), the building was also occupied, but the HLC is similar to the unoccupied periods 2 and 3.

Remember that the HLC of a building is the sum of two different coefficients (HLC = UA + C_v); the transmission heat loss coefficient (named the UA value), which considers the heat losses transmitted through the whole building envelope (including the thermal bridges), and the infiltration and ventilation heat loss coefficient (named C_v). The user behaviour can affect the part of the HLC term related to C_v by interfering in the ventilation system and/or by means of window opening. However, it cannot affect the UA value part, since the UA value can be considered constant throughout the life of the building, unless the building envelope is refurbished or the building envelope insulation layer is damaged

by mould growth, humidity problems, etc. Therefore, a considerable part of the HLC value will remain constant and could not be modified due to the users' behaviour.

Considering that the main issues for the Gainsborough house are related to the uncertainties created by the solar gains and the occupants of the building, the closest HLC result to the fulfilment of the original method is provided by period 3.

4.2.2- HLC results of the poorly insulated residential building

The Loughborough house provided shorter periods for the dataset. In this case, only one month's data was provided, so it was more difficult to find suitable periods that fulfil all the average method requirements. In this case, only two periods were found fulfilling almost every requirement (see Table 21 and Table 22).

WINTER	PERIOD			INPUT DATA						
				$\overline{T}_{out}$ [°C]	$\overline{T}_{in}$ [°C]	$\overline{T}_{in}$-$\overline{T}_{out}$ [°C]	$\overline{Q}$ [W]	$\overline{K}$ [W]	$\overline{Q+K}$ [W]	$\overline{S_aV_{sol}}$ [W]
2013-2014	Period 1	2014-02-27 23:59	→ 2014-03-03 7:59	3.5	16.8	13.3	2999.5	445.2	3444.7	1059.2
	Period 2	2014-03-05 22:59	→ 2014-03-09 0:59	7.9	17.7	9.8	2410.6	442.3	2852.9	1032.6

Table 21. Necessary period averaged variable values to estimate the HLC_{simple} (simple Heat Loss Coefficient, Eq. 29) and HLC (Heat Loss Coefficient, Eq. 28) for Loughborough. The variables included are the outdoor temperature (T_{out}), the indoor temperature (T_{in}), the temperature difference ($T_{in}-T_{out}$), the space heating heat input (Q), total electricity consumption, including synthetic occupants' generation (K), the total internal heat gains (Q + K) and the solar gains (S_aV_{sol}). [102]

WINTER	PERIOD	OUTPUT DATA	
		HLC_{simple} [W/K]	HLC [W/K]
2013-2014	Period 1	258.4 ± 14.4	337.9 ± 27.2
	Period 2	290.2 ± 21.4	395.2 ± 37.6

Table 22. The HLC_{simple} (simple Heat Loss Coefficient, Eq. 29) and HLC (Heat Loss Coefficient, Eq. 28) estimated values for Loughborough. [102]

The obtained average value for the HLC_{simple} is 274.3 ± 18.2 W/K, and for the HLC, 366.6 ± 32.9 W/K. The latter value is close to the HLC "theoretical value" given by Annex 71 of 382 W/K. Note that this theoretical value was obtained through the co-heating method. Since the analysed data for the Loughborough case has synthetic occupancy, and it is known that the windows have not been opened and no mechanical ventilation system is present, the co-heating HLC values and the average method HLC estimations are

performed with a very similar use of the building. Thus, the average method HLC and the co-heating method HLC should be comparable.

From Table 21, it can be concluded that none of the selected periods fulfil the requirement of having a lower solar gain weight than 10 % as compared with the rest of the internal gains (Q + K). In Loughborough, the solar gains are 30.75 % of (Q + K) for the first period and 36.19 % of (Q + K) for the second. Therefore, the average percentage for both periods is 33.47 %. If longer periods of data had been available, for example, a whole winter period, it is very possible, in northern areas such as Loughborough, to find two to four cloudy and cold periods per winter, where more suitable periods for the average method application could have been found.

4.2.3- General discussion about obtained results

In order to analyse the spread and reliability of the estimated HLC results, a detailed discussion has been developed for each of the residential buildings of section 4.2.1 and 4.2.2. Remember that the average method was developed for its application to an occupied office building and some of the original method requirements were eased to make it applicable to the two different tested residential buildings. Therefore, it was important to observe each house individually, since they are not affected by the same characteristics.

The analysis shows some variation between the individual HLC estimates of both buildings (see Table 18 and Table 22). For the Gainsborough building case, this variability is probably caused by the uncertainties due to the space heating estimations based on total gas consumption measurements, unknown metabolic heat generation of the occupants, unknown window opening behaviour, and/or ventilation system operation by the occupants and on the uncertainties related to the solar gains. For the Loughborough house; however, due to the availability of only one month's monitoring data, it was not possible to have proper cold and cloudy periods for analysis, so the main uncertainty comes from the uncertainty associated to the solar gains estimation. Then, the common main issue responsible for the spread between the individual HLC for both houses is probably the uncertainty related to the solar gains estimation.

The weight of the solar gains in the HLC estimates can be analysed in detail by comparing the HLC_{simple} against the HLC. For Gainsborough, not considering the solar gains in the HLC estimation leads to an average HLC_{simple} value of 54.8 ± 4.1 W/K; while the consideration of the solar gains increases the average HLC estimation to 74 ± 8.1 W/K. Although, in absolute values, the effect of considering the solar gains is just 19.2 W/K, in well-insulated buildings such as the Gainsborough case, not considering them leads to an approximate deviation over the HLC estimate of 26 %. In contrast, for Loughborough, not considering the solar gains in the HLC estimation leads to an average HLC_{simple} value of 274.3 ± 18.2 W/K; while the consideration of the solar gains increases the average HLC estimation to 366.6 ± 32.9 W/K. Although, in absolute values, the effect of considering the solar gains is much higher, 92.3 W/K; in poorly insulated buildings, such as the Loughborough case, it leads to a deviation of about 25 % over the HLC estimate. Note that, for the Loughborough case, the availability of longer monitoring periods could have provided periods for analysis with much lower solar gains and the latter deviations for the HLC due to solar gains would have been considerably lower.

Moreover, as commented before, it was impossible to ensure that the roughly estimated solar gains (S_aV_{sol}) are less than 10 % compared to the rest of the internal gains (Q + K) in the houses, even if the short periods with the lowest solar radiation were considered for analysis. Besides, considering that the weight of solar gains as compared to the rest of the heat gains (Q + K) were, on average, 35.1 % for Gainsborough and 33.47 % for Loughborough, it could be considered that the 10 % solar gains weight requirement in the HLC estimation should be extended to about 40 % for these two residential buildings. Since the accurate estimation of the solar gains is a hard task to perform, this extension on the solar gains weight requirement can increase the uncertainty and spread in the estimated HLC values.

However, despite the uncertainties created by several sources, interesting results were obtained. As commented in section 4.2.1, period 3 provided the most reliable results for Gainsborough, since it is not affected by the occupants behaviour, thus several uncertainty sources are avoided. The estimated HLC value for this period is 60.2 W/K, which is close but higher than the "theoretical value" 49.9 W/K provided by the Annex 71. These two values differ 17 %. However, as commented in the mentioned section, the "theoretical

value" only considers the design values, so it tends to underestimate the real in-use HLC. However, it can be used for comparison. Thus, the obtained value with the third period seems logical and promising. In the case of Loughborough, despite the solar gains, there are not any other uncertainty sources. Moreover, the provided "theoretical value" is estimated using the co-heating methods, so both HLC values are comparable. In this case, while the average estimated HLC value for both periods is 366.6 ± 32.9 W/K, the co-heating HLC value is 382 W/K. These two values only differ by 4 %, which means that, despite the non-fulfilment of the solar gains requirement, the difference between the two values remains low. Thus, these results can also be considered reliable.

Finally, it must be commented that the accumulated average graphs where the HLC estimates are stabilized within a ±10 % band over the last 24 testing hours are shown in Appendix B. The results for Gainsborough are plotted in Figure B.1 and the results for Loughborough in Figure B.2.

4.3- Rectorate in-use office building results

The presented in-use office building was monitored from November 2014 to March 2018; every November-March period has been studied. Within each of these four winter periods, useful data periods (at least 72h sub-periods) were identified in which the section 2.1.1 requirements are completely fulfilled. Once all these sub-periods had been detected, the proposed average method was applied floor by floor, and for the whole building, to all of them. Then, those values were compared to check the variation of the estimated HLCs and demonstrate the reliability of the method. If the method is valid, the HLC of the whole building should not vary much over time. Note that the estimated HLCs are independent of each other, since different periods of data are used within the same winter and, in the pre-retrofitting case, even the HLCs estimated in different winters are comparable.

In this section, the change of the Heat Loss Coefficient value for the pre- and post-retrofitting is also studied. Therefore, two different sections are presented for the estimation of the HLC in the building. There section 4.3.1 analyses the HLC of the public building before retrofitting. Thus, it can be checked whether the HLC values have been changing over time or whether they are similar, since the building did not undergo any

known improvement or deterioration during this period. Moreover, the section 4.3.2 studies how the HLC value has changed after the retrofitting of the building. The value is expected to decrease due to the improved insulation and new ventilation systems with heat recovery being installed in the building.

After the HLC estimation, its decoupling process has also been carried out. This decoupling analysis has been carried out using the same dataset used for the HLC estimation of the monitored in-use building between November 2014 and March 2018. There, the same four individual winter periods can be found, 2014-2015, 2015-2016 and 2016-2017, before the rehabilitation of the building and 2017-2018, after the rehabilitation. Unfortunately, due to the lack of data concerning monitoring problems, it has been impossible to analyse the winter 2016-2017. So, the minute by minute air quality data (CO_2 ppm) from December 2014 to March 2018 (without considering winter 2016-2017) of the metabolic CO_2 of the building's occupants is used to estimate air change rates by means of the CO_2 concentration decay analysis presented above.

Plotting and applying the linear regression to the tracer gas (in this case the indoor to outdoor CO_2 concentration in ppm) concentration decay over time in [h] (from 18:00 hours to 20:00 hours) on a natural logarithmic basis, the Air Change per Hour rates (ACH_{decay}) of each floor have been calculated for every day of the abovementioned period. Then, only the ACH_{decay} values of those days that fulfil the aforementioned requirements have been taken into consideration for the C_v estimation. Finally, for each winter period, the floor-by-floor estimated C_v values have been subtracted from the HLC estimates of each corresponding winter period to estimate each floor-by-floor transmission heat loss coefficient.

Then, this section will be divided into 5 subsection. Section 4.3.1 and 4.3.2 show the HLC estimated results for before and after the rehabilitation of the building. After that, section 4.3.3 and 4.3.4 show all the results obtained during the decoupling process in order to achieve the UA results for before and after the rehabilitation of the building. Finally, section 4.3.5 shows the final discussion of the in-use office building analysis.

4.3.1- HLC results of the building before retrofitting

The HLC results obtained for the valid sub-periods of the three winters between November 2014 and March 2017 are analysed in this section. In order to estimate the Heat Loss Coefficients of the building envelope before the retrofitting, Eq. 28 has been used to estimate the HLC, while Eq. 29 has been used to estimate the HLC_{simple}. In total, eight valid periods have been found for the three winters, as shown in Table 23 and Table 24, where estimated HLC_{simple} and HLC for each valid period are presented. Appendix D shows the mean value of each of the terms of Eq. 28 and Eq. 29 applied to each period, while Appendix C shows the ±10 % stabilization bands of all period's accumulated average plots with respect to the final HLC estimate. Moreover, the calculations have been done floor by floor and for the whole building. Thus, it is possible to compare the difference when estimating the HLC directly for the whole building's averaged data ($HLC_{building}$) or as a sum of the floor by floor HLCs (HLC_{sum}).

$HLC_{Simple} = \frac{\sum_{k=1}^{N}(Q_k + K_k)}{\sum_{k=1}^{N}(T_{in,k} - T_{out,k})}$ [kW/K] Eq. 29					TOTAL HOURS	FLOOR 0 Eq. 42	FLOOR 1 Eq. 42	FLOOR 2 Eq. 42	FLOOR 3 Eq. 42	HLC_{Sum} Eq. 30	$HLC_{Building}$ Eq. 49
WINTER	PERIOD					$HLC_{F0} \pm e_{HLC_{F0}}$	$HLC_{F1} \pm e_{HLC_{F1}}$	$HLC_{F2} \pm e_{HLC_{F2}}$	$HLC_{F3} \pm e_{HLC_{F3}}$	$HLC_{sum} \pm e_{HLC_{sum}}$	$HLC_{building} \pm e_{HLC_{building}}$
2014-2015	Period 1	2014-12-02 16:00	→	2014-12-05 20:00	77	0.82 ± 0.08	1.36 ± 0.12	0.97 ± 0.08	1.16 ± 0.10	4.32 ± 0.38	4.34 ± 0.38
	Period 2	2015-01-20 10:00	→	2015-01-23 8:00	70	0.95 ± 0.08	1.46 ± 0.12	1.06 ± 0.08	1.27 ± 0.10	4.74 ± 0.39	4.76 ± 0.39
	Period 3	2015-01-26 19:00	→	2015-01-30 20:00	99	1.06 ± 0.12	1.55 ± 0.17	1.05 ± 0.10	1.30 ± 0.13	4.96 ± 0.52	4.97 ± 0.52
	Period 4	2015-02-03 6:00	→	2015-02-07 1:00	93	0.97 ± 0.08	1.40 ± 0.11	0.98 ± 0.07	1.19 ± 0.09	4.53 ± 0.35	4.54 ± 0.34
2015-2016	Period 5	2015-11-24 19:00	→	2015-11-27 22:00	76	0.97 ± 0.13	1.60 ± 0.15	1.11 ± 0.11	1.34 ± 0.13	5.02 ± 0.51	5.10 ± 0.52
	Period 6	2016-01-06 20:00	→	2016-01-09 8:00	61	0.98 ± 0.17	1.44 ± 0.23	0.99 ± 0.16	1.30 ± 0.21	4.72 ± 0.77	4.75 ± 0.77
2016-2017	Period 7	2016-12-19 12:00	→	2016-12-22 6:00	67		1.34 ± 0.13	0.98 ± 0.09	1.20 ± 0.11	3.51 ± 0.34	3.51 ± 0.34
	Period 8	2017-01-09 18:00	→	2017-01-12 7:00	62		1.07 ± 0.13	0.91 ± 0.10	1.08 ± 0.13	3.05 ± 0.36	3.05 ± 0.36

Table 23. HLC_{simple} results before retrofitting. [85]

$HLC = \frac{\sum_{k=1}^{N}(Q_k + K_k + (S_a V_{sol})_k)}{\sum_{k=1}^{N}(T_{in,k} - T_{out,k})}$ [kW/K] Eq. 28					FLOOR 0 Eq. 43	FLOOR 1 Eq. 43	FLOOR 2 Eq. 43	FLOOR 3 Eq. 43	HLC_{Sum} Eq. 30	$HLC_{Building}$ Eq. 49
WINTER	PERIOD			TOTAL HOURS	$HLC_{F0} \pm e_{HLC_{F0}}$	$HLC_{F1} \pm e_{HLC_{F1}}$	$HLC_{F2} \pm e_{HLC_{F2}}$	$HLC_{F3} \pm e_{HLC_{F3}}$	$HLC_{sum} \pm e_{HLC_{sum}}$	$HLC_{building} \pm e_{HLC_{building}}$
2014-2015	Period 1	2014-12-02 16:00	→ 2014-12-05 20:00	77	0.91 ± 0.10	1.53 ± 0.16	1.08 ± 0.11	1.28 ± 0.12	4.80 ± 0.49	4.83 ± 0.49
	Period 2	2015-01-20 10:00	→ 2015-01-23 8:00	72	1.04 ± 0.09	1.64 ± 0.15	1.18 ± 0.09	1.39 ± 0.12	5.25 ± 0.45	5.28 ± 0.45
	Period 3	2015-01-26 19:00	→ 2015-01-30 20:00	99	1.14 ± 0.14	1.70 ± 0.20	1.14 ± 0.12	1.40 ± 0.16	5.38 ± 0.61	5.40 ± 0.60
	Period 4	2015-02-03 6:00	→ 2015-02-07 1:00	93	1.03 ± 0.08	1.54 ± 0.12	1.07 ± 0.08	1.28 ± 0.10	4.93 ± 0.38	4.94 ± 0.38
2015-2016	Period 5	2015-11-24 19:00	→ 2015-11-27 22:00	76	1.04 ± 0.14	1.73 ± 0.17	1.19 ± 0.12	1.42 ± 0.14	5.39 ± 0.66	5.47 ± 0.57
	Period 6	2016-01-06 20:00	→ 2016-01-09 8:00	61	1.06 ± 0.19	1.60 ± 0.27	1.09 ± 0.18	1.41 ± 0.24	5.17 ± 0.89	5.20 ± 0.90
2016-2017	Period 7	2016-12-19 12:00	→ 2016-12-22 6:00	67		1.49 ± 0.16	1.08 ± 0.11	1.31 ± 0.14	3.87 ± 0.42	3.87 ± 0.43
	Period 8	2017-01-09 18:00	→ 2017-01-12 7:00	62		1.13 ± 0.14	0.95 ± 0.11	1.12 ± 0.13	3.20 ± 0.36	3.19 ± 0.39

Table 24. HLC results before retrofitting. [85]

As expected, from the above tables, it can be concluded that the HLC value has barely changed during the independent periods considered in three consecutive winters, since all the estimated HLC_{simple} values are close to the average value 4.75 ± 0.49 kW/K with a standard deviation of 0.28 kW/K. For the HLC, the average value is 5.18 ± 0.56 kW/K with a standard deviation of 0.25 kW/K.

There is a lack of data on the ground floor during the winter of 2016-2017, which made it impossible to estimate its HLC during the two valid periods considered during this winter. However, the estimation has been carried out for the rest of the floors. Since the indoor average temperature of all the periods is similar on all the floors (see Appendix D), the floor-by-floor estimated HLC are considered physically meaningful. This means, that the HLC of the ground floor for winters 2014-2015 and 2015-2016 is only representing the HLC between the indoor and the outdoor. Since in winter 2016-2017, the indoor temperature is again similar in all the floors, it can be assumed that the HLCs of the ground floor are also representing the HLC between the indoor and the outdoor, and that the floor, is not affected by the heat exchanges with the rest of the thermal zones (or floors) of the building. Therefore, it is possible to estimate a HLC value for the ground floor for the winter of 2016-2017. The average value of 0.96 ± 0.11 kW/K for the HLC_{simple} and 1.04 ± 0.12 kW/K for the HLC of the ground floor is obtained by averaging the 6 available periods of the winters 2014-2016. Thus, an average value of the HLC_{sum} of 4.25 ± 0.46 W/K for the HLC_{simple} and 4.56 ± 0.53 kW/K for the HLC for the winter of 2016-2017

can be obtained. These are within the error bands of the total HLC average values obtained for the winters 2014-2016. However, the latter estimated values cannot be considered as completely reliable, since during the summer of 2016 the ground floor's false ceiling was insulated.

Obviously, the HLC values are higher than the HLC_{simple} values estimated without considering the solar gains. On the other hand, the difference is below 10 %, since low solar radiation periods have been considered to avoid a considerable error in the results due to roughly estimated solar gains, as detailed in section 2.1.1.

It should also be mentioned that the summed HLC (HLC_{sum} in Table 23 and Table 24) and the total HLC values ($HLC_{building}$ in Table 23 and Table 24) have similar values. Since the T_{in} is uniform on the different floors for all periods, the deviation between HLC_{sum} and $HLC_{building}$ is negligible. Nevertheless, since the measurements floor by floor can be obtained, the results obtained from these will always be more accurate than the result obtained for the whole building. Therefore, the HLC_{sum} value should be taken as reference.

To sum up, the HLC value of 5.18 ± 0.56 kW/K is considered the best estimate for the HLC of the building before the retrofitting.

4.3.2- HLC results of the building after retrofitting

The same procedure is followed to estimate the HLC_{simple} and the HLC for the winter of 2017-2018. These calculations have been carried out after the energy retrofitting of the public building. Since the building use has been kept identical in the post-retrofitting case, the same occupancy estimation as for section 4.3.1 has been assumed for occupancy heat gains. Thus, since the building has been insulated properly, the HLC should have decreased considerably. Appendix C also shows the ±10 % stabilization bands of all period's accumulated average plots with respect to the final HLC estimate for this winter period.

$HLC_{Simple} = \frac{\sum_{k=1}^{N}(Q_k + K_k)}{\sum_{k=1}^{N}(T_{in,k} - T_{out,k})}$ [kW/K] Eq. 29						FLOOR 0 Eq. 42	FLOOR 1 Eq. 42	FLOOR 2 Eq. 42	FLOOR 3 Eq. 42	HLC_{Sum} Eq. 30	$HLC_{Building}$ Eq. 49
WINTER	PERIOD				TOTAL HOURS	$HLC_{F0} \pm e_{HLC_{F0}}$	$HLC_{F1} \pm e_{HLC_{F1}}$	$HLC_{F2} \pm e_{HLC_{F2}}$	$HLC_{F3} \pm e_{HLC_{F3}}$	$HLC_{sum} \pm e_{HLC_{sum}}$	$HLC_{building} \pm e_{HLC_{building}}$
2017-2018	Period 1	2017-11-06 18:00	→	2017-11-10 9:00	88	0.60 ± 0.07	0.94 ± 0.09	0.64 ± 0.06	0.66 ± 0.08	2.83 ± 0.31	2.85 ± 0.30
	Period 2	2017-11-26 21:00	→	2017-12-02 12:00	136	0.60 ± 0.05	1.06 ± 0.09	0.63 ± 0.06	0.70 ± 0.07	2.99 ± 0.26	3.00 ± 0.27
	Period 3	2017-12-20 9:00	→	2017-12-23 9:00	73	0.62 ± 0.06	1.06 ± 0.10	0.63 ± 0.06	0.78 ± 0.08	3.10 ± 0.29	3.10 ± 0.29
	Period 4	2018-01-17 4:00	→	2018-01-20 6:00	75	0.63 ± 0.06	1.06 ± 0.10	0.69 ± 0.06	0.87 ± 0.08	3.25 ± 0.30	3.27 ± 0.30
	Period 5	2018-02-06 17:00	→	2018-02-10 7:00	87	0.57 ± 0.04	0.94 ± 0.08	0.64 ± 0.05	0.71 ± 0.06	2.86 ± 0.23	2.85 ± 0.23

Table 25. HLC_{simple} results after retrofitting. [85]

$HLC = \frac{\sum_{k=1}^{N}(Q_k + K_k + (S_a V_{sol})_k)}{\sum_{k=1}^{N}(T_{in,k} - T_{out,k})}$ [kW/K] Eq. 28						FLOOR 0 Eq. 43	FLOOR 1 Eq. 43	FLOOR 2 Eq. 43	FLOOR 3 Eq. 43	HLC_{Sum} Eq. 30	$HLC_{Building}$ Eq. 49
WINTER	PERIOD				TOTAL HOURS	$HLC_{F0} \pm e_{HLC_{F0}}$	$HLC_{F1} \pm e_{HLC_{F1}}$	$HLC_{F2} \pm e_{HLC_{F2}}$	$HLC_{F3} \pm e_{HLC_{F3}}$	$HLC_{sum} \pm e_{HLC_{sum}}$	$HLC_{building} \pm e_{HLC_{building}}$
2017-2018	Period 1	2017-11-06 18:00	→	2017-11-10 9:00	88	0.77 ± 0.09	1.29 ± 0.17	0.88 ± 0.11	0.96 ± 0.15	3.90 ± 0.52	3.92 ± 0.52
	Period 2	2017-11-26 21:00	→	2017-12-02 12:00	136	0.71 ± 0.06	1.28 ± 0.10	0.77 ± 0.06	0.86 ± 0.08	3.61 ± 0.30	3.62 ± 0.32
	Period 3	2017-12-20 9:00	→	2017-12-23 9:00	73	0.75 ± 0.08	1.32 ± 0.15	0.80 ± 0.09	0.97 ± 0.12	3.84 ± 0.44	3.85 ± 0.44
	Period 4	2018-01-17 4:00	→	2018-01-20 6:00	75	0.76 ± 0.08	1.33 ± 0.15	0.86 ± 0.10	1.07 ± 0.13	4.03 ± 0.46	4.04 ± 0.46
	Period 5	2018-02-06 17:00	→	2018-02-10 7:00	87	0.65 ± 0.05	1.11 ± 0.10	0.74 ± 0.07	0.83 ± 0.08	3.32 ± 0.30	3.32 ± 0.30

Table 26. HLC results after retrofitting. [85]

In section 4.3.1, the obtained average values were 4.75 ± 0.49 kW/K for the HLC_{simple} and 5.18 ± 0.56 kW/K for the HLC. On the other hand, the obtained average values during the winter 2017-2018 periods are 3.01 ± 0.27 kW/K for the HLC_{simple} with a standard deviation of 0.18 kW/K and 3.74 ± 0.41 kW/K for the HLC with a standard deviation of 0.28 kW/K. Thus, the reduction has been considerable for the HLC value, considering that the façade has been insulated and some of the windows changed, while the ventilation system with heat recovery has increased the ventilation rates. The combined effect is a reduction of 28 % in the HLC.

To sum up, the HLC value of 3.74 ± 0.41 kW/K is considered the best estimate for the HLC of the building after the retrofitting.

4.3.3- HLC decoupling results of the building before retrofitting

Once all the HLC values have been estimated for each winter (before and after the retrofitting of the building) floor-by-floor and for the whole building, it is possible to perform the decoupling process of the HLC values.

The first part of the decoupling analysis has been carried out using data provided from the monitored in-use building between November 2014 and March 2017. Three individual winter periods can be found, 2014-2015, 2015-2016 and 2016-2017, before the rehabilitation of the building. As previously mentioned in section 3.3.4, due to the lack of data concerning monitoring problems, it has been impossible to analyse the winter 2016-2017. So, the minute by minute air quality data (CO_2 ppm) from December 2014 to March 2016 of the metabolic CO_2 of the building's occupants is used to estimate air infiltration rates by means of the CO_2 concentration decay analysis presented in section 2.4.

4.3.3.1- Air Change per Hour (ACH) calculation

In Figure 14, the air quality data for each sensor has been plotted for F1 from 9th to 15th February 2015. In the example shown in Figure 14, the charging and discharging periods of CO_2 concentration can be clearly seen, with an exponential discharge coinciding with the end of the working day (about 17:00). This exponential discharge resembles a straight line when plotted on a logarithmic basis.

Table 27 shows an example of the calculations for the whole month of February 2015 for the first floor (F1). Non-working days (red lines) have very low indoor to outdoor concentrations because the building is empty from Friday afternoon until Monday morning. Thus, by Saturday 18:00 hours, there are already very similar CO_2 concentrations to the outdoor one and both the indoor to outdoor initial and final concentration values are very low and similar to each other. Of course, none of those non-working days fulfil the ASTM D6245-18 requirements and so are not considered in Table 29 for the later C_v estimations. Those days where the CO_2 concentration at any of the sensors (S1, S2 or S3, see Table 27 and Figure 44 for sensor codes) within the floor differs by more than 10 % of the average concentration in the floor at the beginning or end of the sampling period (grey lines) have been rejected. Again, none of those days fulfil the ASTM

D6245-18 requirements and are not considered in Table 29 for the later C_v estimations. In addition, those days where the initial value of the measured CO_2 concentration (C_I) of any of the sensors was less than [outdoors 400 ppm + 350 ppm] have also been discarded. Note that initial and final values of the concentrations of Table 27 show the difference between the indoor to outdoor concentrations.

		Initial CO_2 concentration (ppm)				Difference from the average (%)			Final CO2 concentration (ppm)				Difference from the average (%)		
Day	ACH decay	Aver.	S1 1.2.4	S2 1.2.6	S3 1.2.8	S1 1.2.4	S2 1.2.6	S3 1.2.8	Aver.	S1 1.2.4	S2 1.2.6	S3 1.2.8	S1 1.2.4	S2 1.2.6	S3 1.2.8
1	-0.07	9.2	10.0	7.0	10.5	9.1	-23.6	14.5	9.0	8.0	7.0	12.0	-11.1	-22.2	33.3
2	**0.19**	**704.7**	**669.0**	**706.0**	**739.0**	**-5.1**	**0.2**	**4.9**	**485.7**	**466.0**	**477.0**	**514.0**	**-4.0**	**-1.8**	**5.8**
3	0.20	701.3	648.0	653.0	803.0	-7.6	-6.9	14.5	479.7	452.0	458.0	529.0	-5.8	-4.5	10.3
4	0.59	355.3	372.0	336.0	358.0	4.7	-5.4	0.8	98.7	104.0	83.0	109.0	5.4	-15.9	10.5
5	0.41	263.0	264.0	257.0	268.0	0.4	-2.3	1.9	127.7	146.0	107.0	130.0	14.4	-16.2	1.8
6	**0.28**	**424.3**	**419.0**	**420.0**	**434.0**	**-1.3**	**-1.0**	**2.3**	**246.8**	**257.0**	**239.0**	**244.5**	**4.1**	**-3.2**	**-0.9**
7	0.00	27.8	30.5	24.0	29.0	9.6	-13.8	4.2	27.3	28.0	24.0	30.0	2.4	-12.2	9.8
8	0.03	17.7	20.0	14.0	19.0	13.2	-20.8	7.5	17.3	19.0	14.0	19.0	9.6	-19.2	9.6
9	0.12	564.0	598.0	608.0	486.0	6.0	7.8	-13.8	443.8	425.0	442.5	464.0	-4.2	-0.3	4.5
10	**0.15**	**694.3**	**635.0**	**710.0**	**738.0**	**-8.5**	**2.3**	**6.3**	**507.7**	**464.0**	**527.0**	**532.0**	**-8.6**	**3.8**	**4.8**
11	0.15	561.0	477.0	563.0	643.0	-15.0	0.4	14.6	403.0	376.0	404.0	429.0	-6.7	0.2	6.5
12	**0.18**	**712.3**	**674.0**	**724.0**	**739.0**	**-5.4**	**1.6**	**3.7**	**503.7**	**493.0**	**512.0**	**506.0**	**-2.1**	**1.7**	**0.5**
13	0.36	247.3	260.0	245.0	237.0	5.1	-0.9	-4.2	127.0	150.0	130.0	101.0	18.1	2.4	-20.5
14	-0.01	12.7	13.0	11.0	14.0	2.6	-13.2	10.5	12.0	13.0	11.0	12.0	8.3	-8.3	0.0
15	-0.05	12.2	11.0	11.0	14.5	-9.6	-9.6	19.2	14.7	16.0	14.0	14.0	9.1	-4.5	-4.5
16	0.71	471.2	500.0	484.5	429.0	6.1	2.8	-8.9	116.3	171.0	113.0	65.0	47.0	-2.9	-44.1
17	0.34	224.0	246.0	217.0	209.0	9.8	-3.1	-6.7	114.7	127.0	114.0	103.0	10.8	-0.6	-10.2
18	**0.18**	**614.0**	**604.0**	**642.0**	**596.0**	**-1.6**	**4.6**	**-2.9**	**436.0**	**436.0**	**450.0**	**422.0**	**0.0**	**3.2**	**-3.2**
19	**0.20**	**511.7**	**532.0**	**511.0**	**492.0**	**4.0**	**-0.1**	**-3.8**	**346.7**	**333.0**	**355.0**	**352.0**	**-3.9**	**2.4**	**1.5**
20	**0.19**	**366.3**	**342.0**	**388.0**	**369.0**	**-6.6**	**5.9**	**0.7**	**253.0**	**239.0**	**259.0**	**261.0**	**-5.5**	**2.4**	**3.2**
21	-0.04	4.3	4.0	3.0	6.0	-7.7	-30.8	38.5	4.0	5.0	1.0	6.0	25.0	-75.0	50.0
22	-0.35	0.3	2.0	-1.0	0.0	500.0	-400.0	-100.0	0.7	1.0	1.0	0.0	50.0	50.0	-100.0
23	0.41	315.0	413.0	370.0	162.0	31.1	17.5	-48.6	142.0	169.0	170.0	87.0	19.0	19.7	-38.7
24	0.71	214.3	264.0	229.0	150.0	23.2	6.8	-30.0	61.7	79.0	57.0	49.0	28.1	-7.6	-20.5
25	0.56	138.3	169.0	142.0	104.0	22.2	2.7	-24.8	46.2	55.5	45.0	38.0	20.2	-2.5	-17.7
26	0.47	449.0	474.0	483.0	390.0	5.6	7.6	-13.1	178.3	241.0	203.0	91.0	35.1	13.8	-49.0
27	0.27	107.7	135.0	111.0	77.0	25.4	3.1	-28.5	63.3	78.0	60.0	52.0	23.2	-5.3	-17.9
28	-0.07	11.0	12.0	10.0	11.0	9.1	-9.1	0.0	12.0	14.0	10.0	12.0	16.7	-16.7	0.0

Table 27. Data for the calculation of ACH_{decay} values that fulfil the ASTM D6245-18 requirements in February 2015 for the first floor. Note that the initial and final values of the concentrations show the difference between the indoor to outdoor concentrations.

Figure 65 shows a couple of examples of the ACH_{decay} values calculated for two of those days of February 2015 fulfilling the ASTM D6245-18 requirements for the first floor. Logarithmic concentration values have been used to obtain a linear relationship between the logarithm of the tracer gas concentration [LN(measured CO_2 ppm - outdoors CO_2 ppm)] and the time in [h]. Next, the ACH_{decay} of each day was calculated via linear regression analysis, since the ACH_{decay} value corresponds to the slope of the estimated straight line. The rest of the ACH_{decay} results, regression equations and R^2 values of the February 2015 days that fulfil the requirements are shown in Table 28.

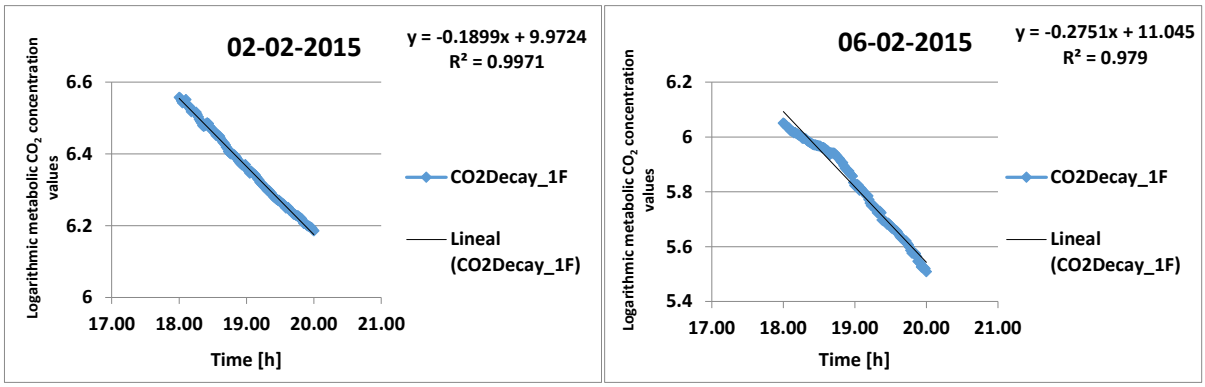

Figure 65. Two examples of the ACH_{decay} values obtained by linear regression for February 2015 fulfilling all ASTM D6245-18 requirements for the first floor. y-axis: Logarithmic metabolic CO_2 concentration values [LN(measured indoor CO_2 ppm - outdoors 400 CO_2 ppm)]; x-axis: time in [h].

Day	ACH	Regression equation	R^2
10	0.15	y= -0.1514x+9.2406	0.9858
12	0.18	y= -0.1770x+9.7566	0.9962
18	0.18	y= -0.1775x+9.6071	0.9924
19	0.20	y= -0.1952x+9.7323	0.9845
20	0.19	y= -0.1894x+9.3324	0.9877

Table 28. The rest of the ACH_{decay} results, regression equations and R^2 values of February 2015 fulfilling the ASTM D6245-18 requirements for the first floor.

FLOOR 1			FLOOR 3		
DATE	**ACH_{decay}**	**WS [m/s]**	**DATE**	**ACH_{decay}**	**WS [m/s]**
2014-12-04	0.19	0.59	2014-12-02	0.19	0.54
2014-12-11	0.18	0.58	2014-12-04	0.29	0.59
2014-12-15	0.23	0.30	2014-12-09	0.19	0.70
2015-01-08	0.24	0.34	2014-12-15	0.19	0.30
2015-01-09	0.21	0.55	2014-12-18	0.25	1.75
2015-01-12	0.20	3.86	2015-01-05	0.17	0.33
2015-01-15	0.23	1.45	2015-01-07	0.16	0.50
2015-02-02	0.19	1.01	2015-01-08	0.22	0.34
2015-02-06	0.28	2.57	2015-01-09	0.20	0.55
2015-02-10	0.15	0.75	2015-01-12	0.21	3.86
2015-02-12	0.18	0.94	2015-01-13	0.19	1.65
2015-02-18	0.18	0.50	2015-01-15	0.16	1.45
2015-02-19	0.20	0.41	2015-01-19	0.20	1.81
2015-02-20	0.19	3.83	2015-01-22	0.30	2.54
2015-03-02	0.13	1.25	2015-01-23	0.19	0.30
2015-03-05	0.19	1.36	2015-01-26	0.16	1.76
-	-	-	2015-01-27	0.23	1.72
-	-	-	2015-02-02	0.24	1.01
-	-	-	2015-02-06	0.24	2.57
-	-	-	2015-02-10	0.17	0.75
-	-	-	2015-02-11	0.20	2.40
-	-	-	2015-02-12	0.16	0.94
-	-	-	2015-02-17	0.27	4.02
-	-	-	2015-03-02	0.19	1.25
-	-	-	2015-03-03	0.11	0.18
-	-	-	2015-03-11	0.18	0.42
-	-	-	2015-03-16	0.25	2.83
-	-	-	2015-03-23	0.34	1.37
AVERAGE	**0.20 ±0.018 (ACH_{decay_aver})**	**-**	**AVERAGE**	**0.21 ±0.019 (ACH_{decay_aver})**	**-**

Table 29. The daily ACH_{decay} and average wind speed (WS [m/s]) values of all days fulfilling ASTM D6245-18 requirements for F1 and F3. The last row presents the average ACH_{decay_aver} values for F1 and F3 for the selected period (December 2014 – March 2015). 95 % confidence intervals are presented for the averaged values using the t-student distribution.

The average ACH_{decay_aver} for the first analysed winter (December 2014 - March 2015) of each floor is the average of all the ACH_{decay} values of those days that meet all the requirements presented in the previous section 2.4.2 (see Table 29). Now, the ACH_{decay} values of F1 and F3 of the second winter period analysed (December 2015 - March 2016) are presented in the following Table 30.

FLOOR 1			FLOOR 3		
DATE	**ACH_{decay}**	**WS [m/s]**	**DATE**	**ACH_{decay}**	**WS [m/s]**
2015-12-01	0.10	-	2015-12-04	0.36	-
2015-12-03	0.33	-	2015-12-14	0.25	-
2015-12-04	0.05	-	2016-01-08	0.16	-
2015-12-09	0.09	-	2016-01-12	0.34	-
2015-12-10	0.09	-	2016-01-13	0.34	-
2016-01-08	0.12	-	2016-02-23	0.13	-
2016-01-13	0.36	-	2016-02-25	0.20	-
2016-01-14	0.22	-	-	-	-
2016-02-22	0.36	-	-	-	-
2016-02-25	0.22	-	-	-	-
2016-03-01	0.17	-	-	-	-
2016-03-14	0.14	-	-	-	-
2016-03-15	0.12	-	-	-	-
2016-03-17	0.11	-	-	-	-
2016-03-18	0.12	-	-	-	-
AVERAGE	**0.17 ± 0.056 (ACH_{decay_aver})**	**-**	**AVERAGE**	**0.25 ± 0.086 (ACH_{decay_aver})**	**-**

Table 30. The daily ACH_{decay} and average wind speed (WS [m/s]) values of all days fulfilling ASTM D6245-18 requirements for F1 and F3. The last row presents the average ACH_{decay_aver} values for F1 and F3 for the selected period (December 2015 – March 2016). 95 % confidence intervals are presented for the averaged values using t-student distribution.

Only F1 and F3 have several winter days that completely fulfil the ASTM D6245-18 requirements. The uniformity requirement established by the Standard could not be fulfilled on any of the days in the analysed period on F0 and F2. However, as mentioned in section 2.4.2, the uniformity requirement has been substituted by a proposed one (maximum limit of 10 °C for the daily average outdoor temperature) in order to accept some daily ACH_{decay} values for these floors. Furthermore, as shown in Figure 44, each sensor on those floors has been assigned a portion of the total volume of each floor, while the infiltration heat loss coefficient (C_v) for each floor has been estimated using both Eq. 104 and Eq. 105. Note that in F0, the considered volume partitions do not complete the full volume. In this case, the C_v value obtained by Eq. 105 has been extrapolated to the complete volume of the floor (green contoured area in Figure 44).

Table 31 shows the ACH_{decay} values of each volume portion of both floors and the average ACH_{decay} values associated to each whole floor. The daily ACH_{decay_Vi} shown in Table 31 are calculated using the CO_2 ppm values measured by each independent sensor located in each of the considered sub-volumes of each floor. These ACH_{decay_Vi} values are then averaged per column (see last row of Table 31) and the $ACH_{decay\_aver\_Vi}$ values to be used in Eq. 105 are obtained. On the other hand, for F0 and F2 in Table 31, a column titled

'Daily ACH_{decay} Average' is also presented. These values are calculated daily, as for F1 and F3, using the averaged CO_2 concentration of the different sensors located in each floor. The last value of the column 'Daily ACH_{decay} Average' is the ACH_{decay_aver} to be used in Eq. 104, obtained by averaging all the values of this column, as done for F1 and F3.

		FLOOR 0				FLOOR 2					
DATE	**T_{out}**	**ACH decay_V1**	**ACH decay_V2**	**ACH decay_V3**	**Daily ACH_{decay} average**	**ACH decay_V1**	**ACH decay_V2**	**ACH decay_V3**	**ACH decay_V4**	**Daily ACH_{decay} average**	**WS [m/s]**
2014-12-03	8.88	-	-	-	-	0.04	0.06	0.29	0.37	0.20	0.44
2014-12-04	8.65	0.06	0.07	0.46	0.25	0.09	0.06	0.19	0.25	0.13	0.59
2014-12-05	8.35	0.26	0.31	0.47	0.37	-	-	-	-	-	3.22
2014-12-09	9.38	0.06	0.11	0.41	0.25	0.07	0.08	0.25	0.18	0.13	0.70
2014-12-15	10.06	-	-	-	-	0.08	0.08	0.21	0.24	0.11	0.30
2015-01-07	9.26	0.23	0.19	0.36	0.25	0.05	0.07	0.13	0.14	0.09	0.50
2015-01-08	9.65	0.21	0.30	0.40	0.29	0.06	0.06	0.07	0.03	0.06	0.34
2015-01-20	6.19	0.25	0.20	0.33	0.25	0.09	0.10	0.20	0.07	0.11	0.70
2015-01-22	6.56	0.14	0.34	0.59	0.43	0.13	0.09	0.24	0.22	0.16	2.54
2015-01-23	6.78	0.11	0.15	0.36	0.21	-	-	-	-	-	0.30
2015-01-26	7.92	0.08	0.07	0.40	0.21	0.08	0.09	0.14	0.10	0.09	1.76
2015-01-27	9.13	0.24	0.15	0.47	0.33	0.11	0.10	0.23	0.26	0.15	1.72
2015-01-30	8.88	0.12	0.10	0.33	0.19	-	-	-	-	-	0.92
2015-02-02	6.55	0.16	0.15	0.25	0.19	0.12	0.10	0.14	0.06	0.10	1.01
2015-02-03	4.49	-	-	-	-	0.12	0.09	0.25	0.13	0.13	4.23
2015-02-06	1.51	0.19	0.16	0.42	0.29	-	-	-	-	-	2.57
2015-02-10	6.33	0.25	0.27	0.39	0.29	0.08	0.08	0.19	0.07	0.09	0.75
2015-02-17	8.78	-	-	-	-	0.15	0.13	0.20	0.23	0.17	4.02
2015-02-18	8.30	-	-	-	-	0.09	0.06	0.32	0.17	0.13	0.50
2015-02-19	8.32	-	-	-	-	0.06	0.08	0.28	0.33	0.16	0.41
2015-03-05	8.84	-	-	-	-	0.02	0.04	0.09	0.17	0.08	1.36
2015-03-16	8.71	0.33	0.28	0.41	0.33	0.06	0.07	0.09	0.17	0.09	2.83
2015-03-23	6.38	-	-	-	-	0.12	0.06	0.29	0.36	0.16	1.37
2015-03-24	7.71	-	-	-	-	0.19	0.18	0.48	0.21	0.22	3.05
Average	**-**	**0.18 ± 0.046 ($ACH_{decay\_aver\_V1}$)**	**0.19 ± 0.050 ($ACH_{decay\_aver\_V2}$)**	**0.40 ± 0.043 ($ACH_{decay\_aver\_V3}$)**	**0.28 ± 0.038 (ACH_{decay_aver})**	**0.09 ± 0.019 ($ACH_{decay\_aver\_V1}$)**	**0.08 ± 0.014 ($ACH_{decay\_aver\_V2}$)**	**0.21 ± 0.045 ($ACH_{decay\_aver\_V3}$)**	**0.19 ± 0.046 ($ACH_{decay\_aver\_V4}$)**	**0.13 ± 0.019 (ACH_{decay_aver})**	**-**

Table 31. ACH_{decay} values of each volume portion and average wind speed (WS [m/s]) of F0 and F2, and the average ACH_{decay} values associated to each whole floor for the selected period (December 2014 – March 2015). 95 % confidence intervals are presented for the averaged values using the t-student distribution.

Moreover, the Daily ACH_{decay} average values of F0 and F2 of the second winter period (December 2015 - March 2016) can be seen in the following Table 32. There, only the ACH_{decay_aver} has been estimated, as done in F1 and F3. As shown in the following section, for the winter period 2014-2015, there was not a wide difference between the C_v values estimated using Eq. 104 and Eq. 105. Then, the simplest case is used for the rest of the winter analysis, only using Eq. 104 for the C_v estimation.

		FLOOR 0		FLOOR 2	
DATE	**T_{out}**	**Daily ACH_{decay} average**	**WS [m/s]**	**Daily ACH_{decay} average**	**WS [m/s]**
2015-12-01	7.37	-	-	0.14	-
2015-12-02	9.00	0.15	-	-	-
2016-01-11	10.92	-	-	0.18	-
2016-01-12	7.98	-	-	0.12	-
2016-01-13	8.35	-	-	0.16	-
2016-01-14	10.58	0.18	-	-	-
2016-02-25	9.48	0.33	-	0.14	-
2016-03-07	6.20	-	-	0.18	-
2016-03-08	6.99	0.34	-	0.27	-
2016-03-11	8.67	0.20	-	-	-
2016-03-14	8.22	0.23	-	0.10	-
2016-03-15	10.13	0.27	-	0.10	-
Average		**0.24 ± 0.069 (ACH_{decay_aver})**	**-**	**0.16 ± 0.040 (ACH_{decay_aver})**	**-**

Table 32. The "daily ACH_{decay} average" and average wind speed (WS [m/s]) of F0 and F2. Last row presents the average ACH_{decay_aver} values for F0 and F2 for the selected period (December 2015 – March 2016). 95 % confidence intervals are presented for the averaged values using the t-student distribution.

Finally, it must be commented that the daily ACH_{decay} values and average wind speed in the same period (18:00 hours to 20:00 hours) of those days fulfilling the ASTM D6245-18 requirements are correlated. The ACH_{decay} values depend on the indoor to outdoor temperature difference and on wind direction, but mainly on wind speed. In general, from Table 29 and Table 31, it can be concluded that the higher the average wind speed, the higher the ACH_{decay} values. Unfortunately, from Table 30 and Table 32 can be concluded, that despite there was some wind speed measured data for this winter as shown in Figure 58, when analysing the data accurately it could be observed that there was excessive missing data to perform an accurate analysis. Then, it has been impossible to find a correlation between the ACH and the wind speed for this winter period.

4.3.3.2- Infiltration heat loss coefficient ($C_{v\text{-}inf}$) calculation

Once the ACH_{decay} values for the days fulfilling the ASTM D6245-18 requirements have been estimated, it is possible to estimate the corresponding C_v (or $C_{v\text{-}inf}$ in this case) values for each of those days, as shown in Table 33 and Table 34. Moreover, using the averaged ACH_{decay_aver} values in the last row from Table 29 to Table 32, the infiltration heat loss coefficients of each floor can be estimated for the whole winter. Then, using Eq. 104 for F1 and F3 and both Eq. 104 and Eq. 105 (only for the winter of 2014-2015) for F0 and F2, it is possible to estimate the infiltration heat loss coefficient for each floor, as shown in the last row of Table 33 and Table 34.

FLOOR 1		FLOOR 3		FLOOR 0		FLOOR 2	
DATE	**C_v [kW/K]**	**DATE**	**C_v [kW/K]**	**DATE**	**C_v [kW/K]**	**DATE**	**C_v [kW/K]**
2014-12-04	0.11	2014-12-02	0.10	2014-12-04	0.10	2014-12-03	0.13
2014-12-11	0.10	2014-12-04	0.16	2014-12-05	0.15	2014-12-04	0.08
2014-12-15	0.13	2014-12-09	0.10	2014-12-09	0.10	2014-12-09	0.08
2015-01-08	0.14	2014-12-15	0.10	2015-01-07	0.10	2014-12-15	0.07
2015-01-09	0.12	2014-12-18	0.14	2015-01-08	0.11	2015-01-07	0.06
2015-01-12	0.11	2015-01-05	0.09	2015-01-20	0.10	2015-01-08	0.03
2015-01-15	0.13	2015-01-07	0.09	2015-01-22	0.17	2015-01-20	0.07
2015-02-02	0.11	2015-01-08	0.12	2015-01-23	0.08	2015-01-22	0.10
2015-02-06	0.16	2015-01-09	0.11	2015-01-26	0.08	2015-01-26	0.06
2015-02-10	0.09	2015-01-12	0.11	2015-01-27	0.13	2015-01-27	0.09
2015-02-12	0.10	2015-01-13	0.10	2015-01-30	0.08	2015-02-02	0.07
2015-02-18	0.10	2015-01-15	0.09	2015-02-02	0.08	2015-02-03	0.08
2015-02-19	0.11	2015-01-19	0.11	2015-02-06	0.11	2015-02-10	0.06
2015-02-20	0.11	2015-01-22	0.16	2015-02-10	0.11	2015-02-17	0.11
2015-03-02	0.08	2015-01-23	0.10	2015-03-16	0.13	2015-02-18	0.08
2015-03-05	0.11	2015-01-26	0.09	-	-	2015-02-19	0.10
-	-	2015-01-27	0.12	-	-	2015-03-05	0.05
-	-	2015-02-02	0.13	-	-	2015-03-16	0.06
-	-	2015-02-06	0.13	-	-	2015-03-23	0.10
-	-	2015-02-10	0.09	-	-	2015-03-24	0.14
-	-	2015-02-11	0.11	-	-	-	-
-	-	2015-02-12	0.09	-	-	-	-
-	-	2015-02-17	0.15	-	-	-	-
-	-	2015-03-02	0.10	-	-	-	-
-	-	2015-03-03	0.06	-	-	-	-
-	-	2015-03-11	0.10	-	-	-	-
-	-	2015-03-16	0.14	-	-	-	-
-	-	2015-03-23	0.19	-	-	-	-
AVERAGE	**0.11 ±0.010 (C_{v_aver})**	**AVERAGE**	**0.11 ±0.011 (C_{v_aver})**	**AVERAGE**	**0.11 ±0.015 (C_{v_aver})**	**AVERAGE**	**0.08 ±0.012 (C_{v_aver})**

Table 33. The daily C_v values estimated using Eq. 104 for all the floors. The last row presents the average C_{v_aver} values for all floors for the selected period (December 2014 – March 2015). 95 % confidence intervals are presented for the averaged values using the t-student distribution.

FLOOR 1		FLOOR 3		FLOOR 0		FLOOR 2	
DATE	**C_v [kW/K]**	**DATE**	**C_v [kW/K]**	**DATE**	**C_v [kW/K]**	**DATE**	**C_v [kW/K]**
2015-12-01	0.06	2015-12-04	0.19	2015-12-02	0.06	2015-12-01	0.09
2015-12-03	0.19	2015-12-14	0.13	2016-01-14	0.07	2016-01-11	0.11
2015-12-04	0.03	2016-01-08	0.09	2016-02-25	0.13	2016-01-12	0.08
2015-12-09	0.05	2016-01-12	0.18	2016-03-08	0.13	2016-01-13	0.10
2015-12-10	0.05	2016-01-13	0.18	2016-03-11	0.08	2016-02-25	0.09
2016-01-08	0.07	2016-02-23	0.07	2016-03-14	0.09	2016-03-07	0.12
2016-01-13	0.20	2016-02-25	0.11	2016-03-15	0.11	2016-03-08	0.17
2016-01-14	0.12	-	-	-	-	2016-03-14	0.07
2016-02-22	0.20	-	-	-	-	2016-03-15	0.07
2016-02-25	0.13	-	-	-	-	-	-
2016-03-01	0.10	-	-	-	-	-	-
2016-03-14	0.08	-	-	-	-	-	-
2016-03-15	0.07	-	-	-	-	-	-
2016-03-17	0.06	-	-	-	-	-	-
2016-03-18	0.07	-	-	-	-	-	-
AVERAGE	**0.10 ± 0.032 ($C_{v\ aver}$)**	**AVERAGE**	**0.14 ± 0.047 ($C_{v\ aver}$)**	**AVERAGE**	**0.10 ± 0.027 ($C_{v\ aver}$)**	**AVERAGE**	**0.10 ± 0.025 ($C_{v\ aver}$)**

Table 34. The daily C_v values estimated using Eq. 104 for all the floors. The last row presents the average C_{v_aver} values for all floors for the selected period (December 2015 – March 2016). 95 % confidence intervals are presented for the averaged values using the t-student distribution.

As commented before in section 2.1.2, considering the building as a thermodynamic system, the HLC value is an extensive property of the system; thus, the sum of the individual HLC values of all floors is the HLC of the building. The same happening with the HLC happens also with the C_v. Then, the building infiltration and/or ventilation heat loss coefficient could also be precisely estimated by summing all the C_v values of all the thermal zones of the building. As proven in section 2.4.1, when estimating the building C_v as the sum of the C_v values of the different thermal zones of the building, the effects of the mass exchanges due to infiltration through the walls/floors/ceilings between the different thermal zones are cancelled out in the summation process. Nevertheless, unless the analysed thermal zones are completely airtight between them in the whole building, the individual C_v values estimated for each thermal zone (floors in this case) have no physical meaning, since they are also considering the mass transmission between the floors. However, since for this analysed building, the thermal zones were different floors separated by continuous concrete slabs, the infiltration exchanges between floors can be considered to be very low, which means that the considered individual thermal zone C_v values are mainly due to the indoor to outdoor infiltration effects. Furthermore, the indoor temperature is homogeneous between floors, making internal heat exchange

effects low compared to the indoor to outdoor heat exchanges, thus also making the individual thermal zones HLC, C_v and UA value estimates meaningful.

Table 35 shows that similar C_{v_aver} values are obtained by means of both equations for F0 and F2. Although using Eq. 105 is a better approach for F0 and F2, using and programming Eq. 104 is easier in practice.

Winter 2014-2015	FLOOR 0	FLOOR 1	FLOOR 2	FLOOR 3	BUILDING
C_{v_aver} [kW/K] Eq. 104	0.11 ± 0.015	0.11 ± 0.010	0.08 ± 0.012	0.11 ± 0.011	**0.41 ± 0.048**
C_{v_aver} [kW/K] Eq. 105	0.10 ± 0.013	-	0.08 ± 0.014	-	-

Table 35. C_{v_aver} values for each floor by means of both Eq. 104 and Eq. 105 and the whole building C_{v_aver} value for the winter of 2014-2015.

As commented before, since the difference is negligible for this case, only Eq. 104 values are considered for the second winter analysed in this work, as presented in Table 36.

Winter 2015-2016	FLOOR 0	FLOOR 1	FLOOR 2	FLOOR 3	BUILDING
C_{v_aver} [kW/K] Eq. 104	0.10 ± 0.027	0.10 ± 0.032	0.10 ± 0.025	0.14 ± 0.047	**0.44 ± 0.131**

Table 36. C_{v_aver} values for each floor by means of Eq. 104 and the whole building C_{v_aver} value for the winter of 2015-2016.

Although the obtained C_{v_aver} results do not differ greatly between the two different winter periods, it can be seen that the confidence intervals are wider for the winter of 2015-2016. This is due to the higher variability between the daily estimated ACH_{decay} values in the second winter and due to a lower number of daily estimates within the winter. These daily ACH_{decay} values could be affected by the wind speed effects. However, as commented in section 4.3.3.1, since there are no enough measured values for wind speed during this second winter period, it cannot be proved.

4.3.3.3- Transmission heat loss coefficient (UA) calculation

In Table 37, decoupled UA and C_v (or C_{v_aver}) values are shown for each floor and for the whole building for the two analysed winters. Once the floor-by-floor HLC and C_v have been estimated, the decoupling of the HLC is carried out by applying Eq. 111. The measurement errors were propagated until the UA values have been obtained. In Table 37, the HLC, UA and C_v values are calculated and, in Table 38, the values per floor area have also been estimated.

		FLOOR 0	FLOOR 1	FLOOR 2	FLOOR 3	BUILDING
Winter 2014-2015	**HLC [kW/K]**	1.03 ± 0.102	1.60 ± 0.158	1.12 ± 0.100	1.34 ± 0.124	**5.09 ± 0.484**
	C_v [kW/K]	0.11 ± 0.015 (10.7%)	0.11 ± 0.010 (6.9%)	0.08 ± 0.012 (7.1%)	0.11 ± 0.011 (8.2%)	**0.41 ± 0.048 (8.1%)**
	UA [kW/K]	0.92 ± 0.087 (89.3%)	1.49 ± 0.148 (93.1%)	1.04 ± 0.088 (92.9%)	1.23 ± 0.113 (91.8%)	**4.68 ± 0.436 (91.9%)**
Winter 2015-2016	**HLC [kW/K]**	1.05 ± 0.164	1.66 ± 0.221	1.14 ± 0.148	1.42 ± 0.191	**5.27 ± 0.724**
	C_v [kW/K]	0.10 ± 0.027 (9.5%)	0.10 ± 0.032 (6.0%)	0.10 ± 0.025 (8.8%)	0.14 ± 0.047 (9.9%)	**0.44 ± 0.131 (8.3%)**
	UA [kW/K]	0.95 ± 0.137 (90.5%)	1.56 ± 0.189 (94%)	1.04 ± 0.123 (91.2%)	1.28 ± 0.144 (90.1%)	**4.83 ± 0.593 (91.5%)**

Table 37. HLC, C_v and UA values for each floor and for the whole building for the two winters. The error was propagated until the UA values have been estimated. The percentage of the weight of the UA and C_v on the HLC are also presented.

		Area [m^2]	HLC [W/Km^2]	C_v [W/Km^2]	UA [W/Km^2]
Winter 2014-2015	FLOOR 0	391.65	2.63	0.28	2.35
	FLOOR 1	456.32	3.51	0.24	3.27
	FLOOR 2	604.61	1.85	0.13	1.72
	FLOOR 3	458.51	2.92	0.24	2.68
	BUILDING	**1911.09**	**2.66**	**0.21**	**2.45**
Winter 2015-2016	FLOOR 0	391.65	2.68	0.26	2.43
	FLOOR 1	456.32	3.64	0.22	3.42
	FLOOR 2	604.61	1.89	0.17	1.72
	FLOOR 3	458.51	3.10	0.31	2.79
	BUILDING	**1911.09**	**2.76**	**0.23**	**2.53**

Table 38. HLC, C_v and UA values per unit floor area for each floor and for the whole building. For clarity, errors have not been included.

4.3.4- HLC decoupling results of the building after retrofitting

The second part of the decoupling analysis has been carried out using data provided from the monitored in-use building between November 2017 and March 2018, after the rehabilitation of the building.

4.3.4.1- Air Change per Hour (ACH) calculation

The same procedure applied in section 4.3.3.1 has been also used in this section. However, as commented in section 2.4.2, due to the ventilation system installed in the building after the retrofitting, the concentration of CO_2 in the building is considerably lower than the CO_2 concentration analysed in section 4.3.3.1. This can be seen in Figure 15 in section 2.4.2. The ventilation system is working with a constant airflow during the whole winter period and, in consequence, the CO_2 concentration barely reaches the

minimum fixed value in the requirements since the building is ventilated during the whole day. Therefore, it is quite complicate to fulfil the requirement 9.3.4 of section 2.4.2, since only a few days during the whole winter period achieve the difference concentration of CO_2 to be higher than the minimum fixed value of 350 ppm.

Apart from this, the rest of the requirements are easily fulfilled as in section 4.3.3.1. The ACH_{decay_aver} values obtained for this data set for all the floors can be seen in Table 39 (F1 and F3) and Table 40 (F0 and F2).

FLOOR 1		FLOOR 3	
DATE	**ACH_{decay}**	**DATE**	**ACH_{decay}**
2018-01-15	0.32	-	-
AVERAGE	**0.32 (ACH_{decay_aver})**	**AVERAGE**	**- (ACH_{decay_aver})**

Table 39. The daily ACH_{decay} of all days fulfilling ASTM D6245-18 requirements for F1 and F3. Last row presents the average ACH_{decay_aver} value for F1 and F3 for the selected period (December 2017– March 2018).

Then, also the ACH_{decay_aver} values for F0 and F2 are estimated for this winter period after rehabilitation. In this case, also the "Daily ACH_{decay} average" has been estimated directly as done in winter 2015-2016.

		FLOOR 0	FLOOR 2
DATE	**T_{out}**	**Daily ACH_{decay} average**	**Daily ACH_{decay} average**
2018-01-10	-	0.36	-
2018-01-11	6.49	0.48	-
2018-01-12	8.53	0.26	-
2018-01-15	8.78	0.31	-
2018-01-16	13.30	0.24	-
2018-01-19	10.10	0.34	-
2018-01-22	12.15	0.21	0.27
2018-01-25	9.50	0.27	-
2018-01-30	8.81	-	0.28
2018-02-01	6.22	0.37	-
2018-02-02	4.61	0.40	-
2018-02-05	4.76	-	0.42
2018-02-14	11.32	0.27	-
2018-02-16	13.48	0.23	-
2018-02-23	-	0.32	-
2018-02-26	-	0.31	0.27
2018-02-27	-	0.32	-
2018-03-01	-	0.32	-
Average		**0.32 ± 0.04 (ACH_{decay_aver})**	**0.31 ± 0.16 (ACH_{decay_aver})**

Table 40. The "daily ACH_{decay} average" of F0 and F2. Last row presents the average ACH_{decay_aver} value for F0 and F2 for the selected period (December 2017– March 2018). 95 % confidence intervals are presented for the averaged values using t-student distribution.

Due to the low number of ACH_{decay} values obtained, the estimation of the average airflow rate cannot be considered a representative value. For example, as shown in Table 39, there is not any valid day for the third floor fulfilling all the requirements fixed by the ASTM D6245-18 guide for the whole winter period. Moreover, there is only one valid day for the first floor. The rest of the floors are able to provide some extra results, but not as much as before the rehabilitation.

Then, in order to obtain some extra ACH_{decay} results, the requirement 9.3.4 has been modified. Therefore, using Eq. 102 and Eq. 103 of the procedure carried out to fix the minimum indoor to outdoor concentration value in section 2.4.2, it has been reduced to the minimum value as far as the method permits with the given sensor uncertainty. From this analysis can be concluded that it is possible to reduce the initial minimum indoor to outdoor concentration difference value from 350 ppm to 300 ppm for the first and the third floor in order to obtain some extra valid results without overcoming the permitted maximum concentration measurement uncertainty. The obtained extra values can be seen in Table 41 (F1 and F3) and Table 42 (F0 and F2) in italics typing.

FLOOR 1		**FLOOR 3**	
DATE	**ACH_{decay}**	**DATE**	**ACH_{decay}**
2018-01-15	0.32	-	-
2018-01-23	*0.22*	-	-
2018-01-29	*0.31*	-	-
AVERAGE	**0.28 ± 0.14 (ACH_{decay_aver})**	**AVERAGE**	**- (ACH_{decay_aver})**

Table 41. The daily ACH_{decay} of all days fulfilling ASTM D6245-18 requirements for F1 and F3, where the minimum initial CO_2 concentration difference value has been reduced to 300 ppm. Last row presents the average ACH_{decay_aver} value for F1 and F3 for the selected period (December 2017– March 2018). 95 % confidence intervals are presented for the averaged values using t-student distribution.

Then, the same procedure is also performed for estimating the ACH_{decay} values for F0 and F2 in this winter period after rehabilitation.

		FLOOR 0	FLOOR 2
DATE	**T_{out}**	**Daily ACH_{decay} average**	**Daily ACH_{decay} average**
2018-01-10	-	0.36	-
2018-01-11	6.49	0.48	-
2018-01-12	8.53	0.26	-
2018-01-15	8.78	0.31	-
2018-01-16	13.30	0.24	*0.24*
2018-01-19	10.10	0.34	-
2018-01-22	12.15	0.21	0.27
2018-01-25	9.50	0.27	-
2018-01-30	8.81	-	0.28
2018-02-01	6.22	0.37	*0.29*
2018-02-02	4.61	0.40	-
2018-02-05	4.76	-	0.42
2018-02-12	*4.21*	-	*0.28*
2018-02-14	11.32	0.27	-
2018-02-16	13.48	0.23	-
2018-02-23	-	0.32	-
2018-02-26	-	0.31	0.27
2018-02-27	-	0.32	-
2018-03-01	-	0.32	-
Average		**0.31 ± 0.04 (ACH_{decay_aver})**	**0.29 ± 0.07 (ACH_{decay_aver})**

Table 42. The "daily ACH_{decay} average" of F0 and F2, where the minimum initial CO_2 concentration difference value has been reduced to 300 ppm. Last row presents the average ACH_{decay_aver} value for F0 and F2 for the selected period (December 2017– March 2018). 95 % confidence intervals are presented for the averaged values using t-student distribution.

Thus, it has been possible to obtain two new ACH_{decay} values for the first floor and three new values for the second floor. This can facilitate the estimation of the total volumetric airflow rate, and in consequence, the estimation of the total C_v value in some of the floors. However, when using this method, the number of estimated ACH_{decay} values is still very low for some of the floors, as for example, the first and the third floor. Then, the use of ACH_{decay_aver} estimated value of the first floor in this case, could provide erroneous C_v results in the decoupling process. Despite that, the obtained average ACH_{decay_aver} values are shown in Table 43.

Winter 2017-2018	FLOOR 0	FLOOR 1	FLOOR 2	FLOOR 3
ACH_{decay_aver} [h^{-1}]	0.31 ± 0.040	0.28 ± 0.143	0.29 ± 0.070	-

Table 43. Average ACH_{decay_aver} values for each floor for winter 2017-2018.

Another way to test the methods' applicability in the winter after the rehabilitation is through the reduction of each decay test duration. In section 4.3.3.1, it has been proven that a two hour testing period fixed in the requirement 9.3.1 is a proper decay period length for the ACH_{decay} estimation for the winters before the building rehabilitation, where no ventilation system was installed in each floor of the building. However, this section has

demonstrated that the decay testing period length of two hours is too long once a ventilation system has been installed in each floor of the building. Then, the same test has been performed reducing the daily test duration to one hour (from 18:00 to 19:00) instead of two hours (from 18:00 to 20:00). Moreover, in order to obtain some extra ACH_{decay} results, the ASTM D6245-18 requirement 9.3.4 has been again modified. Once again, using Eq. 102 and Eq. 103 of the procedure carried out to fix the minimum indoor to outdoor concentration value in section 2.4.2, it has been reduced to the minimum value as far as the method permits with the uncertainty of the sensors used in this research. In this case, it has been possible to reduce the initial minimum indoor to outdoor concentration difference value from 350 ppm to 200 ppm for the ground, first and second floors. However, due to higher ventilation/infiltration rates, it has been reduced from 350 ppm to 250 ppm for the third floor. For all the floors, the reduction has been performed without overcoming the permitted maximum concentration measurement uncertainty. The obtained new results can be seen in the following Table 44 (F1 and F3) and Table 45 (F0 and F2).

FLOOR 1		**FLOOR 3**	
DATE	**ACH_{decay}**	**DATE**	**ACH_{decay}**
2018-01-11	0.49	2018-01-11	0.64
2018-01-12	0.24	2018-01-16	0.33
2018-01-15	0.35	2018-01-23	0.32
2018-01-16	0.31	2018-01-29	0.41
2018-01-17	0.25	2018-02-08	0.43
2018-01-23	0.35	2018-02-12	0.48
2018-01-24	0.38	2018-02-14	0.25
2018-01-29	0.32	2018-02-15	0.37
2018-02-01	0.41	-	-
2018-02-05	0.57	-	-
2018-02-07	0.33	-	-
2018-02-12	0.32	-	-
2018-02-26	0.29	-	-
2018-02-27	0.29	-	-
2018-03-22	0.31	-	-
AVERAGE	**0.35 ± 0.05 (ACH_{decay_aver})**	**AVERAGE**	**0.40 ± 0.10 (ACH_{decay_aver})**

Table 44. The daily ACH_{decay} in a reduced decay testing period of one hour of all days fulfilling ASTM D6245-18 requirements for F1 and F3, where the minimum initial CO_2 concentration difference value has been reduced to 200 ppm in the first floor and to 250 ppm in the third floor. Last row presents the average ACH_{decay_aver} value for F1 and F3 for the selected period (December 2017– March 2018). 95 % confidence intervals are presented for the averaged values using t-student distribution.

		FLOOR 0	FLOOR 2
DATE	**T_{out}**	**Daily ACH_{decay} average**	**Daily ACH_{decay} average**
2018-01-10	-	0.41	-
2018-01-11	6.49	0.51	0.46
2018-01-12	8.53	0.29	-
2018-01-15	8.78	0.35	-
2018-01-16	13.30	0.29	0.15
2018-01-17	9.22	0.46	-
2018-01-18	8.78	0.30	-
2018-01-19	10.10	0.29	-
2018-01-22	12.15	0.31	0.24
2018-01-23	13.16	0.65	0.32
2018-01-24	12.16	0.43	-
2018-01-25	9.50	0.28	-
2018-01-26	7.46	0.78	-
2018-01-30	8.81	-	0.24
2018-01-31	8.22	0.67	-
2018-02-01	6.22	0.33	0.24
2018-02-02	4.61	0.39	-
2018-02-05	4.76	0.61	0.35
2018-02-06	4.70	0.41	-
2018-02-07	2.82	0.46	0.23
2018-02-08	3.16	0.36	0.27
2018-02-12	4.21	-	0.30
2018-02-13	5.18	-	0.28
2018-02-14	11.32	0.39	-
2018-02-19	10.35	0.66	0.30
2018-02-21	7.25	0.47	-
2018-02-22	-	0.53	-
2018-02-23	-	0.33	-
2018-02-26	-	0.37	0.23
2018-02-27	-	0.38	-
2018-03-01	-	0.33	0.24
2018-03-05	-		0.25
2018-03-19	-	0.40	-
2018-03-22	9.08	-	0.23
Average		**0.43 ± 0.05 (ACH_{decay_aver})**	**0.27 ± 0.04 (ACH_{decay_aver})**

Table 45. The "daily ACH_{decay} average" in a reduced decay testing period of one hour of F0 and F2, where the minimum initial CO_2 concentration difference value has been reduced to 200 ppm. Last row presents the average ACH_{decay_aver} value for F0 and F2 for the selected period (December 2017– March 2018). 95 % confidence intervals are presented for the averaged values using t-student distribution.

As can be seen in Table 44 and Table 45, the quantity of the obtained ACH_{decay} values has increased considerably when reducing the testing period length. While for a testing period of two hours, the obtained ACH_{decay} values where only three for the first floor and zero for the third period, they have increased until fifteen and eight values respectively applying this testing period reduction. Moreover, in general, the obtained average ACH_{decay_aver} values seem reasonable, since they are around double the ACH_{decay_aver} values obtained before the rehabilitation for each corresponding floor. This results seem logical since the installation of the mechanical ventilation systems has increased the air renovation inside the building, and then, the ACH_{decay} results have increased considerably.

Unfortunately, the obtained results are not fulfilling the ACH_{decay} values requirements established in the ASTM E741-11 method guide. The guide stablishes that for the test duration of 1 hour, the obtained ACH_{decay} values should be around 1 h^{-1}. Since in this case, the mean ACH_{decay} value of every floor is closer to 0.5 h^{-1}, it means that the testing period duration should be of 2 hours. Then, despite the reasonable results obtained, the method is not applicable to these data with the uncertainty provided by the sensors used in this research. Despite that, the obtained ACH_{decay_aver} values are shown in Table 46.

Winter 2017-2018	FLOOR 0	FLOOR 1	FLOOR 2	FLOOR 3
ACH_{decay_aver} [h^{-1}]	0.43 ± 0.05	0.35 ± 0.05	0.27 ± 0.04	0.40 ± 0.10

Table 46. Average ACH_{decay_aver} values for each floor for winter 2017-2018 for a reduced decay testing period of 1 hour length.

4.3.4.2- Infiltration and ventilation heat loss coefficient (C_v) calculation

Once all the average ACH_{decay_aver} values have been estimated in Table 46 for every floor, considering the above mentioned issues with the uncertainty of the C_v estimation, it is possible to estimate their corresponding total average volumetric airflow rate using Eq. 106. These results are shown in the following Table 47.

Winter 2017-2018	FLOOR 0	FLOOR 1	FLOOR 2	FLOOR 3
$\dot{V}_{air\ (total)}$ $[m^3/h]$	506.42	590.95	512.93	652.91

Table 47. Total average volumetric airflow rate values for each floor for winter 2017-2018.

Unfortunately, despite the estimation of the total volumetric airflow rate could have been performed correctly, there was not reliable ventilation system airflow rate data measured for any of the floors. During this winter, despite the sensors were installed and the ventilation systems were working with a constant airflow rate, the measured data from these sensors was not providing proper results. Then, it has been impossible to estimate the infiltration volumetric airflow rate subtracting the measured ventilation volumetric airflow rate from the estimated total volumetric airflow rate. In other words, despite the results obtained in section 4.3.4.1 would have been reliable, the ventilation air flow rates were not measured correctly. In consequence, anyway, it would be impossible to estimate the corresponding C_v value for each of the losses, ventilation and infiltration, for this winter period.

4.3.4.3- Transmission heat loss coefficient (UA) calculation

Since due to several reasons, the estimation of the infiltration and ventilation heat loss coefficient was not possible after the rehabilitation, it has been impossible to estimate the corresponding UA value for each floor and the whole building.

4.3.5- General discussion about obtained results

Once the HLC estimates and the decoupling results have been obtained for both cases, before and after the rehabilitation, a general discussion is carried out in order to analyse them deeply. Therefore, the whole building's HLC results are firstly plotted in the following figures from Figure 66 to Figure 69 and then discussed.

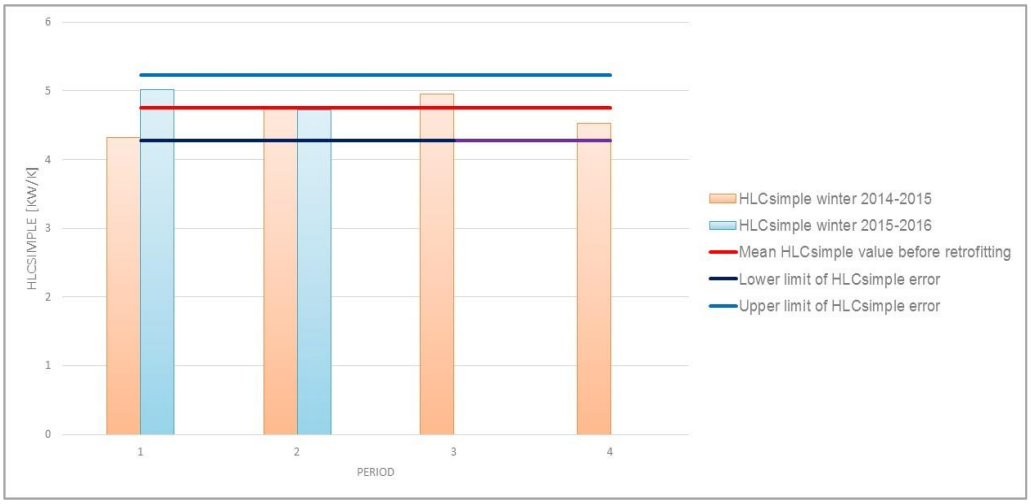

Figure 66. HLC_{simple} values before retrofitting (winter 2014-2015 and winter 2015-2016). [85]

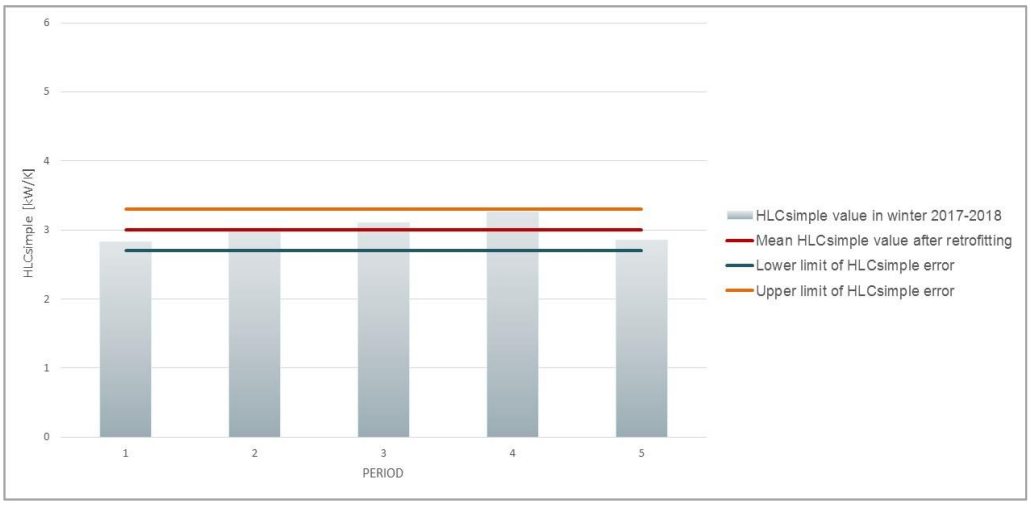

Figure 67. HLC_{simple} values after retrofitting (winter 2017-2018). [85]

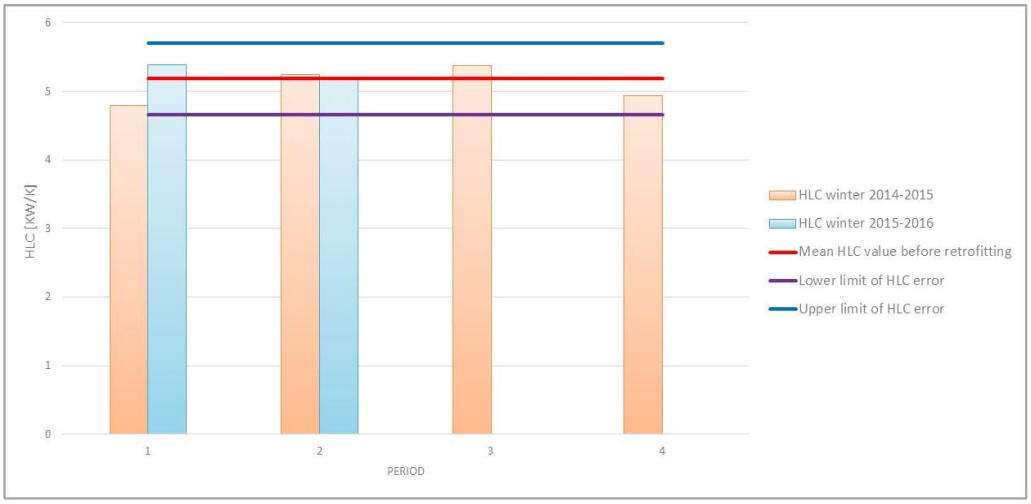

Figure 68. HLC values before retrofitting (winter 2014-2015 and winter 2015-2016). [85]

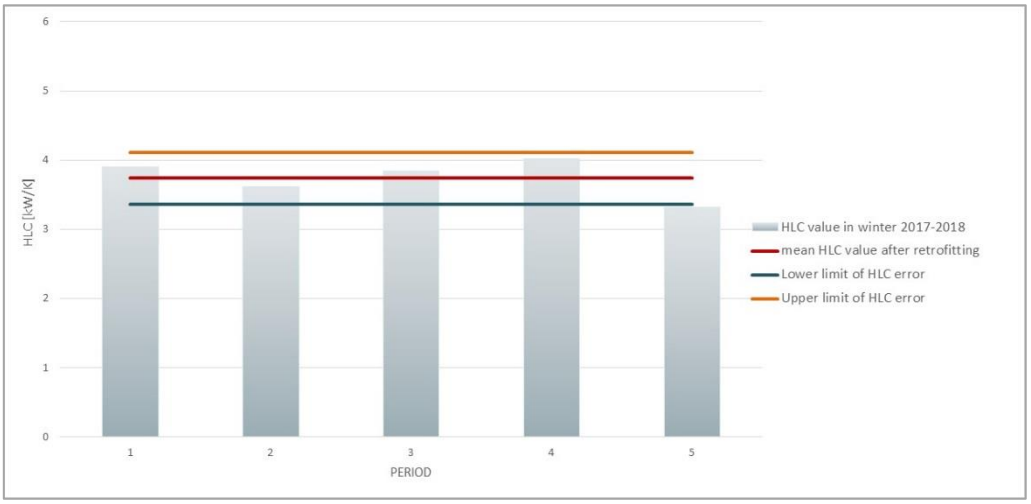

Figure 69. HLC values after retrofitting (winter 2017-2018). [85]

As commented in the sections 4.3.1 and 4.3.2, several conclusions can be drawn from the graphics. First of all, it is important to check that all the periods, before and after retrofitting, show similar results. From these figures, it can be concluded that almost all the individual HLC_{simple} or HLC estimates are within the corresponding average value, plus or minus the error band.

Only the fifth period of winter 2017-2018 (Figure 69) was not able to reach the error band limits of the estimated HLC average value. However, this estimate is not differing considerably from the rest of the values since the lower error limit is 3.36 kW/K while the fifth period HLC estimate is 3.32 kW/K.

Moreover, the values obtained by estimating the HLC with and without considering the solar radiation do not differ by much. While the average value for the pre-retrofit HLC_{simple}

was 4.75 kW/K, the HLC value considering solar radiation increases to 5.18 kW/K. These two results only differ by 8.3 % thanks to the proposed data period selection procedure described in section 2.1.1. It is very difficult to estimate the real solar gains entering the building due to the unmeasurable effects of such elements as blinds or curtains located in windows, which are the main obstacle when making an estimation of solar gains. Therefore, by selecting cloudy and cold days, the unreliable in-use solar gain effect on the HLC estimate can be limited to below 10 %, which would be the limiting case of not considering the solar gains effect, as in Eq. 29. By using Eq. 28, although roughly estimating the solar gains, the uncertainty effect on the HLC will be below 10 %. However, solar gains effects in the post-retrofitted HLC estimation are higher, while the HLC_{simple} value was 3.01 kW/K, the HLC increased until 3.74 kW/K. These two values differ by 20 %. As expected, for correctly insulated buildings, the solar gains effect on the HLC is greater. In insulated buildings, the heating demand decreases and thus, the same amount of solar gains will produce a bigger difference between the HLC_{simple} and the HLC.

When estimating the HLC before and after the retrofitting, a considerable drop can be observed. If all valid period average HLC_{sum} values are compared, it can be seen that the HLC has decreased by 1.44 kW/K (28%).

In order to verify the results, it was in mind the possibility to compare the average method results with the results of an established method. Therefore, it was considered that the co-heating method [27] could play an important role in this comparison. However, due to the size and the geometry of the building, it has been unfeasible to apply the co-heating method in the analysed building. Furthermore, since winter period is not a holyday period, it was inviable to empty the whole building during one month in any of the studied winters for applying the co-heating method. However, this average method has been previously tested in section 4.1.1, 4.2.1 and 4.2.2 and compared to “theoretical values”. Since the rest of the cases have been able to provide reliable and logical results, it can be concluded that the results obtained in this section so are.

Note that, as detailed in section 2.1.1, the HLC = UA + C_v and thus it considers: transmission (UA) plus infiltration (C_v as in Eq. 5) for the periods considered in the pre-retrofitting case; while for the post-retrofitting case, the HLC considers the transmission effects (UA) plus infiltration plus ventilation with heat recovery effects (C_v as in Eq. 13)

for the post-retrofitted case. Then, in order to find the main responsible of the heat losses of the in-use office building, the decoupling of the already estimated HLC values is performed winter by winter for each floor and for the whole building.

As commented along the section 4.3.3 and 4.3.4, several aspects of this method and the corresponding results in the tables can be discussed. For example, Table 29 and Table 31 for the winter of 2014-2015, as well as the Table 30 and Table 32 for the winter of 2015-2016 and Table 44 and Table 45 for the winter of 2017-2018 show a large variation in the daily ACH_{decay} values, depending on the day. In other words, the in-use HLC is not constant over time, since the C_v part can vary greatly from day to day. It is important to remark that these C_v values have been obtained based on the ACH_{decay} values estimated by means of the application of the ASTM D6245-18 guide, so they generally fulfil the reliability criteria stated in the guide. Then, converting the ACH_{decay} values to C_v values before the rehabilitation of the building, only requires them to be multiplied by the volume of the corresponding floor, the density of the air and the constant pressure specific heat of the air. Thus, the C_v values can be considered as reliable as the calculated ACH_{decay} values that fulfil the ASTM D6245-18 guide. However, once the ventilation system has been installed, apart from the infiltration heat losses considered before in the C_v, also the ventilation heat losses need to be considered. Unfortunately, as shown in Table 44 and Table 45 for the winter of 2017-2018, the method was not able to obtain reliable enough ACH_{decay} values after the rehabilitation. Since during the rehabilitation, the building was dotted with a ventilation system in each of the floors, the CO_2 concentration has decreased considerably in the whole building. Then, it has been complicated to find days fulfilling the minimum indoor concentration requirement. Therefore, due to the low quantity of valid ACH_{decay} values obtained in some of the floors when applying the decay testing period duration of two hours as before the rehabilitation, the obtained results cannot be considered reliable enough. Moreover, after applying the same method reducing the testing period length from two hours to one hour, it was impossible to fulfil the final ACH_{decay} value requirement according to the guide ASTM E741-11. Then, the obtained results of this analysis can neither be considered reliable enough. Hence, it is concluded that the metabolic CO_2 decay method, with the typical sensor accuracy of CO_2 concentration sensors used in the building sector, is not valid to apply to well mechanically ventilated buildings. Using more accurate CO_2 sensors could permit the correct application of the ASTM E741-11guide,

however, finding CO_2 sensors with a better accuracy than a 1 % of the measure is not easy unless laboratory quality sensors are used for the measures.

Therefore, before the rehabilitation, the ACH_{decay} estimations for F1 and F3 are reliable, since they completely fulfil the ASTM D6245-18 guide. However, since not all the building floors where structured equally, not all the requirements were fulfilled in F0 and F2. For F0 and F2, the 10 % uniformity criteria has not been fulfilled and has been replaced by a no window opening criteria, according to an outdoor low temperature criteria and visual checking of disturbances in the CO_2 concentration measurements. If we analyse the ACH_{decay} values for F0 in Table 31, it can be seen that V_1 and V_2 have very similar behaviour, while V_3 has nearly double the ACH_{decay} values compared to V_1 and V_2. If V_1 and V_2 (those volumes are close to each other) have similar ACH_{decay} values, it means that the CO_2 decay was not due to air exchanges between them. On the other hand, the V_3 of F0 has an old door that permits the children in the nursery to go out to the garden. This door is probably responsible for the much higher infiltration rates of V_3.

If the F2 ACH_{decay} rates are analysed in detail, two different behaviours can clearly be observed. V_1 and V_2 represent the north face offices and common north space that are connected by doors. If $ACH_{decay\_aver\_V1}$ and $ACH_{decay\_aver\_V2}$ are compared, they are very close, meaning that this subspace of F2 made up of V_1 plus V_2 has a similar ACH_{decay} behaviour. The same happens if $ACH_{decay\_aver\_V3}$ and $ACH_{decay\_aver\_V4}$ are analysed. In fact, there is a continuous brick wall separating both subspaces (north and south) and, logically, they have different behaviour. Since $V_1 + V_2 \sim V_3 + V_4$, if those two subspaces were treated separately, the C_v value calculated by Eq. 105 of Table 35 would be obtained. In this work, two options have been calculated for F0 and F2, as shown in Table 35, but since the difference is very small compared to the uncertainties we are working with, the easier to program Eq. 104 has been used for the decoupling calculations. Although the uncertainties associated to the estimations of the ACH_{decay} values of F0 and F2 might be bigger as they do not fulfil the 10 % uniformity criteria, after the above analysis and after checking the results, we consider them reliable enough to carry out the decoupling process of the HLC.

Despite it has been concluded that the metabolic CO_2 decay method, with the accuracy of the CO_2 concentration sensors used in this research, is not valid for the ACH estimation

in buildings with high ventilation and/or infiltrations, the obtained ACH_{decay} results after the rehabilitation will be analysed. Then, regarding the ACH_{decay} analysis carried out with the data after the retrofitting, it must be commented that despite it has been complicate to find days where the CO_2 concentration difference between the interior and the exterior was higher than 350 ppm at the beginning of the decay analysis, in general, the rest of the requirements have been successfully and easily fulfilled as done with data sets before retrofitting. However, for some of the floors, it has been possible to reduce this CO_2 concentration minimum difference limit to 300 ppm fulfilling the requirement of maintaining the concentration measurement accuracy lower than 5 %. This provided some extra results for the first and second floor of the building. However, they are still quite limited for considering them reliable enough. Therefore, in order to obtain more values, the same method has been applied and tested again but instead of using a two hour length decay testing period, reducing it to only one hour. Despite in this case, the quantity of the obtained ACH_{decay} results has increased considerably, the results are not fulfilling one of the requirements established in the guide ASTM E741-11. The guide says that for a testing period of 1 hour length, the obtained ACH_{decay} results should show similar values to 1 h^{-1}. However, it can be concluded that despite the ACH_{decay_aver} results obtained after the rehabilitation reducing the testing period length are not reliable enough, they make sense if compared against the results before rehabilitation. For this analysis, while the average ACH_{decay_aver} value for all the floors before retrofitting is 0.20 ± 0.04 [h^{-1}], the average ACH_{decay_aver} value for all the floors after retrofitting is 0.36 ± 0.06 [h^{-1}]. Since after the rehabilitation of the building, maintaining the same occupation patterns as before rehabilitation, the CO_2 concentration is considerably reduced, it means that the ventilation has increased in the building. Due to the installed mechanical ventilation system in each floor of the building, the CO_2 concentrations after the rehabilitation does not reach the same CO_2 concertation levels as before the rehabilitation. A 50 % increase of the volumetric airflow rate has been enough to reduce the CO_2 concentration inside the building to values below 950 ppm. Then, it was not necessary to increase too much the ACH_{decay} values to improve the air quality of the building. Moreover, after the rehabilitation, probably part of the infiltrations that were present in the building before rehabilitation have been fixed and avoided. However, despite the obtained results seems logical, as commented previously, due to the limited ACH_{decay} results obtained after the

rehabilitation or the not fulfilment of the guide requirement when reducing the testing period, more accurate CO_2 concentration sensors should be used or another method should be found to reliably perform the HLC decoupling process in buildings where properly working mechanical ventilation system are installed based on CO_2 concentration measurements.

Therefore, as concluded from section 4.3.3 and section 4.3.4, the reliable estimation of the C_v value has only been possible for data before rehabilitation. However, the two winters analysed before the rehabilitation have shown very interesting C_v results. In general, the third floor should be the one that shows the highest C_v results, since it is the floor most exposed to the wind. Moreover, it is logical that the floors that have distributions with big open spaces connecting internally north and south façades, such as F1 and F3, should have bigger C_v values, since it is easier for the air to enter, for example, from the north face and exit through the south face. This effect is usually lower for such floor distributions as F0 and F2, where there are many partition walls that hinder the indoor movement of the air. If the results are observed, it can be seen that the third floor is the one providing the highest C_v values. This effect can be more clearly seen in Table 38 where the C_v values are presented per floor area.

Furthermore, the results shown from Table 33 to Table 36 lead to very interesting conclusions. If the individual daily C_v results are observed in Table 33 and Table 34, it is possible to find a considerable variation between the results obtained for the same floor. However, if the average C_v results are compared from Table 35 and Table 36 for the two winter periods for the whole building, the results only differ by 7 %. So it can be concluded that, despite the variability of the obtained daily results, the final obtained values for the whole winters are stable and similar between the two winters.

Finally, regarding the HLC decoupling, if the results of Table 37 are observed, it can be seen that, floor by floor, the infiltration losses range is between 6.0 % and 10.7 % of the total heat losses for both winters. Thus, transmission losses range between 89.3 % and 94 %. This table provides highly valuable information about the effect of the retrofitting of the studied building. It is clear that, for this building, more than 90 % of heat losses are transmission losses, which suggests that the building should be better insulated to reduce the UA value. Moreover, Table 38 also shows very interesting results. From the results per

unit area, it can be demonstrated that since the second floor is the one with the least wall area exposed to the exterior, the loss results obtained per floor square meter are the lowest. If the ground floor did not have a ventilated false ceiling, the first floor would have shown similar results as the second floor. However, due to the heat losses created by this ventilated false ceiling located between the ground floor and the first floor, the first floor shows the highest total losses, followed by the third floor, the floor most exposed to the wind effect.

CHAPTER 5: CONCLUSIONS AND FUTURE WORK

5. CONCLUSIONS AND FUTURE WORK

5.1- Conclusions about the average method

This Thesis proves the validity of the proposed average method to estimate the HLC of in-use buildings by developing it from the First Law of Thermodynamics in order to provide the method with the suitable assumptions to work with in-use buildings. The method has been tested from the simplest to the most complex case studies in order to demonstrate its applicability in buildings considering different characteristics and behaviours. This Thesis shows that the results obtained for the Round Robin Box, the two residential buildings and the four-storey in-use office building are reliable. However, despite that, each of them has provided individual conclusions, from which some general conclusions can also be drawn.

The Round Robin Box was the first case study to be tested in this work and the conclusions taken for this simplest case study are set out below:

- In this case study, it has been impossible to obtain more than one valid period due to the limited data provided (only one month's data from one winter period).
- Despite that, the results obtained are reliable, since they have been compared to other results obtained by applying other methods and with the theoretically known HLC value. The obtained HLC result is 4.1 ± 0.21 W/K (very close to the theoretical value, 4.08 W/K).
- The method was directly applicable to the data provided. In other words, no adjustment to any requirement of the method was necessary to obtain the HLC estimate.
- This case study was not a real building as in the rest of the cases. Therefore, it is a well sealed miniature building that completely avoids heat losses due to infiltrations. Moreover, the Round Robin Box was unoccupied and there was no ventilation system installed inside, so the heat losses regarding ventilation were also avoided. Thus, the obtained HLC value can be assumed to be equal to the UA value of the Round Robin Box. As commented previously, this value is maintained constant after the building's construction, so both the theoretical and estimated values must show very similar results, as happens in this case study.

The second case study to be tested were the two residential buildings showing completely different characteristics. For these two cases, a common conclusion drawn is that it was necessary to ease one of the requirements of the average method. Despite that, promising results could be obtained for both buildings. So the individual conclusions from each of the houses are noted below:

The main conclusions for the Gainsborough house analysis are:

- Since the house is a well-insulated building, the reduced space heating consumption inside the building, due to the proper insulation, reduces the possibilities of finding periods with a solar radiation weight below 10 % of the other measurable internal gains.
- Despite the wide range of the results obtained in the Gainsborough building, the best HLC estimate value is considered to be 60.2 ± 6.6 W/K of period 3. However, some of the results obtained for this house do not differ considerably from this value, such as periods 2 and 6, which are the two periods least affected by the uncertainties. However, the HLC estimates of periods 1, 4 and 6 differ by more than 20 % from the period 3 HLC estimate, affected mainly by the occupants' behaviour and the solar gains effect.
- The theoretical HLC value based on design data is 49.9 W/K. Usually, as commented before, the HLC theoretical value tends to show lower HLC values than the real HLC values, as also happens in this case study. So it can be concluded that the obtained HLC result seems logical.

The main conclusions taken for the Loughborough house are:

- The house is a poorly insulated building, so the estimated HLC results are considerably higher than in Gainsborough.
- The results obtained for Loughborough in the two periods where the HLC has been estimated are very similar and the average HLC result of both HLC values is quite similar to the "theoretical value" estimated with the co-heating method. The average HLC estimate value for both periods is 366.6 ± 32.9 W/K, while the HLC estimated using the co-heating method is 382 W/K.

- Due to the bad insulation, the accurately measurable space heating needs are high in order to keep the house warm, which makes the average method more insensitive to the uncertainties associated to the method. Moreover, this building considers synthetic profiles to simulate the occupants' behaviour, so occupancy heat gains inside the building can be estimated accurately. Thus, it has been easier to provide good HLC estimation results for the two analysed periods identified for the average method's application.
- However, due to the short period of monitoring data provided (only one month's winter data were available), it was not possible to find more suitable periods that fulfilled all the average method requirements. The latter would have permitted the uncertainty of the solar gains in the Loughborough HLC estimations to be reduced.

The developed method was finally applied to the last case study; the four-storey office building, both before and after its rehabilitation. The conclusions taken from this case study are presented below:

- Following the method's indications, a successful estimation of the Heat Loss Coefficient has been achieved for both the pre-retrofitted building and the post-retrofitted building. The averaged HLC result obtained before the rehabilitation was 5.18 ± 0.56 kW/K. However, a considerable drop can be observed in the HLC after the rehabilitation, since the value attained was 3.74 ± 0.41 kW/K. The values considered most reliable are those obtained from the floor by floor HLC sum (HLC_{sum}), since they consider more accurate data, rather than a single estimated HLC value for the whole building ($HLC_{building}$). Hence, the HLC has decreased 28 % after the retrofitting from the pre-retrofit case of 5.18 kW/K to the post-retrofitted case of 3.74 kW/K.
- All the individual HLC estimates were similar for the different periods considered in both winters before retrofitting. A similar behaviour has been found for all individual estimates of the HLC after the retrofitting. Note that each individual period within a winter estimates an independent HLC. The method itself is able to provide accurate results without the requirement of a physical model of the building.

Then, from these individual conclusions taken for each of the case studies, several general conclusions can be highlighted. Even if the method only seems applicable to northern countries, it has been proven that the method is also applicable in northern areas of such countries as Spain where the weather is, in general, warmer than in northern countries. Therefore, it must be concluded that the majority of countries in Europe would be able to fulfil the weather related requirements of the presented method, excluding solely the southern areas of Mediterranean countries. Despite the fact that the method was applied to the Round Robin Box in Almeria, it must be remarked that in real building conditions it would not be applicable, since the winter periods in this area do not provide sufficiently low temperatures as those required for the method's application. So it is complicated to fulfil the minimum temperature difference requirement. Moreover, the low solar radiation requirement would also be complicated to fulfil. However, in this case, since the Round Robin Box was heated up to a considerably high indoor temperature (during the tests the box's indoor air temperature reached 40 °C), it was possible to obtain a suitable period.

Moreover, this research has also shown that the application to buildings with considerably low space heating and internal electric/occupation gains (Q + K), such as the very well insulated Gainsborough residential building, makes it hard to find suitable periods for HLC estimation. However, even using periods with a higher weight of solar gains than 10 % of (Q + K) has provided some HLC estimates within a decidedly narrow range for different independent periods. Furthermore, it is obvious that the better insulated the residential building is, the harder it will be to obtain periods where the solar gains become negligible as compared to (Q + K), since the space heating (Q) will be very low, even in cold and cloudy periods. Thus, the need to accurately measure and/or estimate the other internal heat gains (K) and solar gains (S_aV_{sol}) will become crucial for accurate HLC estimation using the average method in well-insulated buildings. Once a method for accurate solar gains estimation has been developed, the 10 % criteria for the solar gains could be made more flexible, to the extent that the accuracy of the solar gains estimation techniques permit. Accurate metabolic heat generation estimation techniques, based on anthropogenic CO_2 decay analysis, or artificial vision techniques, will also help to improve the accuracy of the average method to a great extent.

Moreover, it must be stated that the need to measure the real space heating provided to the house is also a major issue regarding the method's accuracy. If only gas consumption is available, too many assumptions regarding the efficiency of the boiler and the percentage of heat used for space heating versus DHW have to be applied. Calorimeters in the head of the space heating circuit could be a good option to accurately measure the real space heating provided to the house.

Another factor that considerably eases the application of the average method is the length of the dataset provided. If a longer dataset had been provided for a case study such as the Loughborough house, it would certainly be possible to find more valid periods to estimate the HLC that fulfil all the average method requirements.

Furthermore, it can be concluded that the proposed method can be applied to different building types. In this case, the method has been able to provide promising results for a test Round Robin Box, two residential buildings and an occupied office building. Despite the complexity of each of the case studies, the method has been adapted to each of them, analysing them as a unique zone (as in the Round Robin Box and the two residential buildings) and as in both cases, the individual analysis of the floors together with the unique zone analysis (as in the office building). Although the requirements were eased in some cases, all the cases were able to provide logical HLC estimates. Nevertheless, for some cases, the variation between the individual HLC estimates should be reduced to make the average method robust enough to be able to energetically certify the in-use behaviour of building envelopes.

Furthermore, it is also important to remark how the occupant's behaviour and the weather conditions affect the real HLC results. Unlike in the rest of the cases of the study, in the Round Robin Box there were no occupants and the box was well sealed. So it has been possible to obtain very similar results to the design HLC. However, in real buildings such as the two residential building and the office building, the obtained real HLC results show considerably higher values than the design values when these are provided.

Finally, it can be concluded that during this work it has been possible to develop a simple average method that can make considerably accurate estimates of HLC results for in-use buildings without the necessity of an extensive monitoring system. During its

development, the main uncertainty sources found have been identified and limited successfully, in order to minimize the uncertainty they could create in the final HLC estimates of in-use buildings. Within the considerations of these uncertainty sources, the effect of the metabolic heat generation, the heat accumulated in the building, the uniformity of the indoor temperature within the building and the ground temperature, have all been studied and limited whenever possible. Moreover, another assumption also considered was the solar gains effect through windows. However, the effect of the solar gains through opaque walls in the HLC value is not considered within the average method. Therefore, although it could be assumed that their effect will be low, the method has been developed further in order to estimate the uncertainty that the avoidance of the estimation of these solar gains could have in the HLC value and the final conclusions drawn are presented in the following section 5.2.

5.2- Conclusions about the solar gains effect through opaque walls and its relation to the HLC estimation method

The conclusions taken from the average method analysis led us to analyse in depth one of the main uncertainty sources of the HLC; the solar gains. Despite the average method developed in the work having already considered the effect of the solar gains through the windows, the solar gains through opaque walls were neglected. Since the application of the average method requires periods formed by cloudy and cold days, it was assumed that the solar gains through opaque building envelope elements would not have a considerable effect on the estimated HLC; however, an estimate of their effect on the inner surface heat flux of opaque elements and the transmission of their weight to the HLC value has not yet been demonstrated. So this research also proves the validity of the proposed experimental method to estimate the solar radiation effect on the inner surface heat flux and the g-value estimation of opaque building envelope elements by an application to a real case. This real case is the opaque elements of a carefully monitored Round Robin Box that represents a building on a small scale. Furthermore, this inner surface heat flux reduction effect (or solar gains through the building envelope opaque elements) has been transferred to the estimation techniques of the Heat Loss Coefficient of in-use buildings, where the solar gains effect through opaque walls in buildings is not taken into account.

During the analysis of the Round Robin Box's opaque walls, roof and floor, two very different periods have been tested. The first started on 18th June 2013 and ended on 26th June 2013. As expected, the solar radiation was high during this summer period. However, the second period started on 19th December 2013 and ended on 21th December 2013. This period was selected consciously so as to be able to consider a cloudy period with the lowest possible solar radiation. Thus, it could be ensured that the solar radiation was almost purely diffuse and similar in all orientations, as in the periods selected to apply the average method. In other words, two extreme periods were selected. Then, despite the average method only being applicable to cloudy and cold winter periods, the effect of the solar gains through opaque walls has also been estimated for HLC estimation methods not considering the solar gains through opaque walls during sunny periods. Thus, the difference between these two extreme cases can be compared.

To estimate the effect of the solar radiation on the inner surface of the analysed opaque elements, thermal resistance-capacitance models of each of the analysed envelope opaque elements have been fitted using monitored data. Once the models had been validated, they were run without the consideration of the solar radiation and the hypothetical inner surface heat flux was obtained. The difference between the inner surface heat flux, with the solar radiation effect, and the hypothetical inner surface heat flux, without the solar radiation effect, has been considered as the solar gains through the analysed opaque building elements.

If the g-values obtained for the summer period are observed, it can be seen that the results are very low compared to the typical solar factors estimated for windows. However, if the effect of the solar radiation on the inner surface heat flux is observed, it can be concluded that its effect cannot be neglected for some of the opaque envelope elements. In the case of the Round Robin Box's ceiling, the reduction of the inner surface heat flux due to solar radiation was 33.1 %. Moreover, the obtained effect on the east and west walls is also considerable, with 22.4 % and 21.7 %, respectively. As the north wall and the floor are the least exposed to solar radiation, the effect in these is considerably lower.

However, in the case of the winter period, the results are completely different if compared to the summer case. Despite the g-values obtained also being low, as in the

summer period, the effect of the solar radiation on the inner surface heat flux is considerably lower. In this case, the effect obtained in winter for the ceiling is of 4.2 %, very similar to the east and west wall results, 4.4 % and 3.4 %, respectively. In this case, the lowest values are also obtained for the floor and the north wall, with effects of around 2 %.

If the effect of the solar radiation on the inner surface heat flux is significant, as happens in some opaque envelope elements during the summer period, not considering the blocking effect of the outwards heat flux leads to an underestimation of the Heat Loss Coefficients estimated by methods where the solar gains are not estimated as an identifiable constant value. Then, it has been quantified that the Round Robin Box HLC would be underestimated by 1.7 % if the solar gains through the opaque building envelope were not considered in the analysed cold and cloudy period. On the other hand, in the analysed sunny summer period, the HLC would be underestimated by 8.9 % if the solar gains through the opaque building envelope were not considered.

Finally, when comparing the weight of the solar gains through the opaque building envelope of the analysed Round Robin Box with respect to the theoretical solar gains through the window of the Round Robin Box, they represent 11.3 % in the analysed winter period, and 37.2 % in the sunny, summer period. Thus, the weight of the solar gains through the opaque building envelope in the analysed sunny, summer period are significant when compared to the theoretical solar gains through the window of the Round Robin Box. It can therefore be concluded that not considering the solar gains effect through the opaque walls in cold and cloudy periods can be considered negligible in the estimation of the HLC through the average method. However, this is not true for sunny periods.

To sum up, it must be remarked that although the solar gains through opaque walls could create a considerable error in the estimation of the HLC when the solar radiation is high, this is not happening when it can be assumed that only purely diffuse solar radiation affects the building envelope. Then, the estimated HLC value using the average method could be reliable enough, since it would barely be affected by this issue.

However, when working with real in-use buildings, as demonstrated for some case studies such as Gainsborough, the obtained HLC values using the average method tend to

show higher values if compared with the estimated theoretical ones based on the design values. In order to understand the gap between these two values, this work has also carried out the decoupling of the in-use office building's HLC values and the final conclusions are shown in the next section 5.3.

5.3- Conclusions about the HLC decoupling into the transmission (UA) and infiltration and/or ventilation (C_v) heat loss coefficients

Having proved that the estimated HLC values were reliable enough, since the solar gains through opaque walls barely affect them, the last part of the research was carried out; the in-use HLC decoupling process. This last part tests the internal validity of the decoupling of previously estimated floor-by-floor HLC values into their transmission heat loss coefficients (UA) and infiltration and/or ventilation heat loss coefficients (C_v) by using the occupants' metabolic CO_2 concentration decay analysis to estimate the C_v. Then, since HLC = UA + C_v, obtaining the value of the UA is straightforward once the HLC and the C_v are known. The method proposed in this work has been tested in an in-use office building, but it can also be considered valid for residential buildings. However, in that case, the CO_2 decay analysis should probably be done in the morning when the residential buildings have just been vacated by their occupants.

The proposed method is considered much more appropriate and suitable for this analysis than the blower door test, since the ACH_{decay} values are calculated in many different short testing periods over a long period and under real operating conditions. Unlike the blower door test, this method only needs the installation of simple air quality sensors (ppm of CO_2).

The decoupling analysis has only been performed for the in-use office building. The air quality sensors were distributed in different rooms of each floor, making it possible to estimate the infiltration and/or ventilation heat loss coefficients of the different thermal zones of the building. Last but not least, since the tracer gas is CO_2, it is not necessary to inject any gas into the building, which makes the method considerably more affordable in comparison to the blower door test or using other tracer gases.

The study was conducted using winter period data, when windows are usually closed (minimal air infiltrations). Thus, analysing the occupational CO_2 decay curves, the in-use

infiltration Air Change per Hour (ACH_{decay}) rates have been estimated before the rehabilitation and the in-use infiltration and ventilation Air Change per Hour (ACH_{decay}) rates after the rehabilitation. These ACH_{decay} values have been used to calculate the C_v values for each floor and for the whole building, making it possible to obtain the building envelope UA value using the following expression: $UA = HLC - C_v$.

Although the objective of the ASTM D6245-18 Standard is not to decouple the HLC into its UA and C_v parts, it provides a proven method to estimate the ACH_{decay} values of an occupied volume by means of metabolic CO_2 concentration measurements. As proven in this work, these ACH_{decay} values allow the C_v value of the studied volumes or thermal zones to be calculated before the rehabilitation of the analysed in-use office building. Depending on the distribution of the studied area, it is not easy to fulfil all the requirements established in the ASTM D6245-18 guide, in particular, those concerning the concentration uniformity throughout the whole studied area. However, analysing the floor-by-floor characteristics, acceptable ACH_{decay} results could be ensured, as proven in the calculation section, only for the pre-rehabilitation case.

However, after the rehabilitation, apart from the infiltration heat losses considered before, the ventilation heat losses also needed to be estimated. This means that the ventilation and infiltration heat loss coefficients cannot be directly estimated by the estimated ACH_{decay} values. Nevertheless, due to the low quantity of ACH_{decay} values estimated using the metabolic CO_2 decay method for some of the floors, the method with the actual typical building sector air quality sensor accuracy, in its current form cannot be considered a suitable method for ACH value estimation when the building is well ventilated using a mechanical ventilation system. Then, in order to increase the quantity of ACH_{decay} values estimated using the metabolic CO_2 decay method, the method has been modified for analysing the data after rehabilitation. In this case, instead of using a decay testing period of two hours, the testing period has been reduced to only one hour. Unfortunately, the obtained ACH_{decay} results were far from the period length corresponding reference value established in the guide ASTM E741-11. Thus, the results can neither be considered reliable enough. Therefore, higher accuracy air quality sensors or a new method should be proposed for future work for buildings where the ventilation and infiltration rates are high. Hence, using typical accuracy of the air quality sensors used

in the building sector, the proposed metabolic CO_2 decay method would only be suitable for buildings where the infiltration and/or ventilation rates are low, such as buildings without mechanical ventilation systems installed.

Finally, together with the average method, this HLC decoupling method, when applicable, can provide the in-use HLC, UA and C_v values that could be used to obtain energy certificates for buildings in a more realistic approach. Then, the theoretical UA value of the building could be compared against the in-use UA value in order to know whether the construction has been carried out as designed. A similar comparison could be made between the in-use C_v value and the design C_v value. If the method is correctly integrated in the building´s automation systems, it could be a cheap and non-disturbing method for the building users to understand the real behaviour of their building envelopes. In addition, once the in-use HLC (and both UA and C_v values) are available, decisions on where and how to optimally improve the building's energy performance can be made. This energy characterization of the building is a key point for the retrofitting process of existing buildings, since it allows the retrofitting needs to be evaluated, while still being aware of the impact of the retrofitting actions, and finally evaluating the savings and improvements obtained once the retrofitting has been accomplished. If the in-use HLC infiltration and/or the ventilation part (C_v) is too high, the window frames could be checked and improved if necessary, ventilation patterns could be optimized and window opening and closing patterns defined. If the UA must be reduced, optimized energy retrofitting strategies of the building envelope can be performed.

To sum up, through this Thesis, it has been possible to develop a method that could help to identify the real origin of the heat losses of in-use buildings. In the analysed in-use office building case, it could be seen that the main heat losses of the building were created by the building envelope transmittance. However, they could not be compared with the design UA value. Since the analysed building is old, the thermal characteristics of the building envelope were not available. However, should the design UA and C_v values have been available, it would have been possible to understand the HLC performance gap through the comparison between the real and the design value. Moreover, if the design transmission and infiltration and/or ventilation heat losses had also been available for

the building after its retrofitting, whether the retrofitting has been performed as designed could have been analysed.

5.4- Future work

Although much work has been developed during this Thesis, much more research can be done in the future to strengthen the work presented here. Therefore, several proposals are mentioned in this section relating to the different methods developed and presented within this study.

The first proposed future work is related to the HLC analysis of the four-storey in-use office building. After the retrofitting, some extra sensors were installed in the building. One was the total electricity consumption measurer per floor. This means that it is currently possible to measure the total electricity demand (computers, electrical devices…). However, it is still necessary to estimate the person's metabolic heat generation, since it is hard to measure this on site. Therefore, the proposal for further research is to estimate the Heat Loss Coefficient using the measured total electricity consumption and to compare the final results with those obtained in this Thesis. The difference is expected to be small, since the weight of the occupancy heat gains is small during the cold and cloudy periods considered in this work for HLC estimations, where heating demands are dominant.

Moreover, related to the estimation of the HLC of in-use buildings, it would also be interesting to analyse the same case studies with other methods, such as a simple or multiple regression method or a more complex method, such as the grey box modelling. Then, the results could be compared and their validity justified, if possible.

Moreover, with respect to the solar gains analysis through opaque walls, it would be interesting to apply the same methodology in a different fitting-simulation program. During the Thesis, the same procedure has also been followed using CTSM-R software. However, due to lack of time, it has been impossible to obtain as good results as with the LORD software. Then, the continuation of this work is also proposed for the future.

The last proposal concerns the decoupling of the in-use HLC of the study. Unfortunately, as proven during the Thesis, the proposed metabolic CO_2 decay method, which has provided very interesting results when applied to the building before

rehabilitation, is not fully valid once the building has been rehabilitated using the air quality sensors selected for this research. Due to the low quantity of valid ACH_{decay} values obtained from some of the floors, the results cannot be considered reliable enough. Moreover, despite modifying the method in order to increase the quantity of ACH_{decay} values by reducing the method's decay test duration, the obtained results can neither be considered reliable enough. Then, for buildings where a high infiltration and/or ventilation rate is found, air quality sensors with higher accuracy than the typical one used in the building sector or new method should be applied for the total ACH estimation. This method would also be based on the metabolic CO_2 data analysis. However, a different CO_2 analysis method should be used, which must be combined with an accurate occupancy estimation method, together with the building user's metabolic activity information. Therefore, it would be interesting to analyse the artificial intelligence, artificial vision, counting… techniques in order to accurately estimate the occupancy of the building. Once the number of occupants of the building and their metabolic rates are known, it is possible to estimate the total CO_2 that the occupants of the building generate. From this data, an accurate metabolic CO_2 balance could be performed. Through this balance, the total (ventilation plus infiltration) rates could be estimated for a longer period of time than the period analysed using the metabolic CO_2 decay method. Moreover, if the ventilation rates are well measured, it would be possible to perform the infiltration and ventilation ACH estimation correctly and to estimate reliable C_v results using the procedure presented in section 2.4.4. Thus, it would also be possible to estimate the UA values for the post-rehabilitation winter and compare them with the UA values before the rehabilitation in order to estimate the reduction created due to the better insulation of the building.

Finally, it would also be interesting to implement this work in another building where the average method and the HLC decoupling process could be implemented and also where the UA and C_v design values were available. Then, apart from the identification of the heat loss origin, it would also be possible to find which of them is further from the design value.

CHAPTER 6: CONTRIBUTIONS

6. CONTRIBUTIONS

6.1- Research papers of this thesis

1. I. Uriarte, A. Erkoreka, C. Giraldo-Soto, K. Martin, A. Uriarte and P. Eguia, **Mathematical development of an average method for estimating the reduction of the Heat Loss Coefficient of an energetically retrofitted occupied office building**, *Energy and Buildings*, vol. 192, p. 101-122, (March 2019). //doi.org/10.1016/j.enbuild.2019.03.006. (Published)
2. I. Uriarte, A. Erkoreka, P. Eguia, E. Granada and K. Martin-Escudero, **Estimation of the Heat Loss Coefficient of Two Occupied Residential Buildings through an Average Method**, *Energies*, vol. 13, no. 21, p. 5724, (November 2020). (Published)
3. I. Uriarte, A. Erkoreka, A. Legorburu, K. Martin-Escudero, C. Giraldo-Soto and M. Odriozola-Maritorena, **Decoupling the Heat Loss Coefficient of an in-use office building into its Transmission and Infiltration heat loss coefficients**, *Journal of building engineering*. (Accepted)

6.2- Research papers related to this thesis work

1. C. Giraldo-Soto, A. Erkoreka, L. Mora, I. Uriarte and L. Del Portillo, **Monitoring system analysis for evaluating a building's envelope energy performance through estimation of its heat lost coefficient**, *Sensors,* vol. 18, no. 7, p. 2360, (July 2018). DOI: 10.3390/s18072360. (Published)

6.3- International conferences

1. I. Uriarte, C. Giraldo-Soto, K. Martin, L. Del Portillo and A. Erkoreka, **Estimating the Heat Loss Coefficient of an in-use office building, floor by floor and as a whole, through basic monitoring and modelling,** *10CNIT-XX-2017: X National and I International Engineering Thermodynamics Congress,* 28th – 30th June 2017 (Lleida, Spain).
2. I. Uriarte, C. Giraldo, A. Erkoreka, E. Pérez and E. Granada, **Estimating the Heat Loss Coefficient of an in-use office building through basic monitoring and accumulated averaging techniques,** *8th European Congress on Energy Efficiency and Sustainability in Architecture and Urbanism (EESAP 8) and 1th International Congress on Advanced Construction (CICA 1),* 5th – 7th July 2017 (Donostia-San Sebastián, Spain).

3. I. Uriarte, A. Erkoreka, P. Eguia, E. Granada and K. Martin, **Estimation of the heat loss coefficient for two houses through an average method,** *11CNIT-XX-2019: XI National and II International Engineering Thermodynamics Congress,* 12th – 14th June 2019 (Albacete, Spain).

4. I. Uriarte, C. Giraldo-Soto, K. Martin, P. Eguia and A. Erkoreka, **Quantification of the reduction of the heat loss coefficient of the envelope of an energy-rehabilitated office building,** *11th European Congress on Energy Efficiency and Sustainability in Architecture and Urbanism (EESAP 11) and 4th International Congress on Advanced Construction (CICA 4),* 1st – 2nd December 2020 (Online).

6.4- Contributions to the IEA-EBC Annex 71 expert meetings

1. I. Uriarte and A. Erkoreka, **Loughborough house analysis through the modified average method,** *IEA-EBC Annex 71 expert meeting: Building Energy Performance Assessment Based On In-Situ Measurements (4th meeting),* 9th - 11th April 2018 (Brussels, Belgium).

2. I. Uriarte and A. Erkoreka, **Gainsborough and Loughborough house analysis through an average method,** *IEA-EBC Annex 71 expert meeting: Building Energy Performance Assessment Based On In-Situ Measurements (5th meeting),* 17th - 19th October 2018 (Innsbruck, Austria).

3. I. Uriarte and A. Erkoreka, **Analysis of the solar radiation effect in Gainsborough and Loughborough houses through an average method,** *IEA-EBC Annex 71 expert meeting: Building Energy Performance Assessment Based On In-Situ Measurements (6th meeting),* 8th - 10th April 2019 (Bilbao, Spain).

REFERENCES

7. REFERENCES

[1] Kyoto Protocol, United Nations framework convention on climate change. 19 (1997), 497.

[2] Paris Agreement, Paris agreement. Report of the Conference of the Parties to the United Nations Framework Convention on Climate Change. 4 (2015).

[3] H2020 EeB, H2020 Energy Efficient Buildings (EeB), https://ec.europa.eu/commission/presscorner/detail/en/fs_19_6725 (2020).

[4] European Parliament, Directive 2018/844/EU of the European Parliament and of the council of 19 June 2018 on the energy performance of buildings (recast), Official Journal of the European Communities. 61 (2018); 75-91.

[5] European Parliament, Directive 2010/31/EU of the European Parliament and of the Council of 19 May 2010 on the energy performance of buildings (recast), Official Journal of the European Union. 18 (2010).

[6] European Parliament, Directive 2012/27/EU of the European Parliament and of the Council of 25 October 2012 on energy efficiency, amending Directives 2009/125/EC and 2010/30/EU and repealing Directives 2004/8/EC and 2006/32, Official Journal, L. 315 (2012); 1-56.

[7] EU Buildings Factsheets, https://ec.europa.eu/energy/en/eu-buildings-factsheets (2020).

[8] E. Burman, D. Mumovic, J. Kimpian, Towards measurement and verification of energy performance under the framework of the European directive for energy performance of buildings, Energy. 77 (2014), 153-163 //doi.org/10.1016/j.energy.2014.05.102.

[9] Buildings Performance Institute Europe (BPIE), http://bpie.eu/ (2020).

[10] International Energy Agency's Energy in Buildings and Communities Programme, http://www.iea-ebc.org/projects/project?AnnexID=71 (2020).

[11] "Intelligent Energy-Europe", Implementing of the Energy Performance of Buildings directive (EPBD), Co-funded under the Intelligent Energy-Europe Programme of the European Union (2015).

[12] A.J. Summerfield, T. Oreszczyn, I.G. Hamilton, D. Shipworth, G.M. Huebner, R.J. Lowe, P. Ruyssevelt, Empirical variation in 24-h profiles of delivered power for a sample of UK dwellings: Implications for evaluating energy savings, Energy Build. 88 (2015), 193-202 //doi.org/10.1016/j.enbuild.2014.11.075.

[13] P.X.W. Zou, X. Xu, J. Sanjayan, J. Wang, Review of 10 years research on building energy performance gap: Life-cycle and stakeholder perspectives, Energy Build. 178 (2018); 165-181. //doi.org/10.1016/j.enbuild.2018.08.040.

[14] X. Xu, P.X. Zou, Analysis of factors and their hierarchical relationships influencing building energy performance using interpretive structural modelling (ISM) approach, J. Clean. Prod. 272 (2020); 122650.

[15] B. Bordass, A. Leaman, P. Ruyssevelt, Assessing building performance in use 5: Conclusions and implications, Build. Res. Inf. 29 (2001); 144-157. 10.1080/09613210010008054.

[16] A.C. Menezes, A. Cripps, D. Bouchlaghem, R. Buswell, Predicted vs. actual energy performance of non-domestic buildings: Using post-occupancy evaluation data to reduce the performance gap, Appl. Energy. 97 (2012); 355-364. //doi.org/10.1016/j.apenergy.2011.11.075.

[17] C. Mitterer, H.M. Künzel, S. Herkel, A. Holm, Optimizing energy efficiency and occupant comfort with climate specific design of the building, Front. Archit. Res. 1 (2012); 229-235. //doi.org/10.1016/j.foar.2012.06.002.

[18] Y. Zhu, X. Fan, C. Wang, G. Sang, Analysis of heat transfer and thermal environment in a rural residential building for addressing energy poverty, Appl. Sci. 8 (2018); 2077. //doi.org/10.3390/app8112077.

[19] T.L. Hemsath, K. Alagheband Bandhosseini, Sensitivity analysis evaluating basic building geometry's effect on energy use, Renew. Energ. 76 (2015); 526-538. //doi.org/10.1016/j.renene.2014.11.044.

[20] H. Montazeri, B. Blocken, D. Derome, J. Carmeliet, J.L.M. Hensen, CFD analysis of forced convective heat transfer coefficients at windward building facades: Influence of building geometry, J. Wind. Eng. Ind. Aerodyn. 146 (2015); 102-116. //doi.org/10.1016/j.jweia.2015.07.007.

[21] K. Ahn, C. Park, Correlation between occupants and energy consumption, Energy Build. 116 (2016); 420-433.

[22] I. Gaetani, P. Hoes, J.L. Hensen, Occupant behavior in building energy simulation: Towards a fit-for-purpose modeling strategy, Energy Build. 121 (2016); 188-204.

[23] B. Sun, P.B. Luh, Q. Jia, Z. Jiang, F. Wang, C. Song, Building energy management: Integrated control of active and passive heating, cooling, lighting, shading, and ventilation systems, IEEE Trans. Autom. Sci. Eng. 10 (2012); 588-602.

[24] S. Baldi, T. Le Quang, O. Holub, P. Endel, Real-time monitoring energy efficiency and performance degradation of condensing boilers, Energy Convers. Manag. 136 (2017); 329-339.

[25] D. Johnston, D. Miles-Shenton, D. Farmer, Quantifying the domestic building fabric 'performance gap', Build Serv Eng Res Technol. 36 (2015); 614-627. 10.1177/0143624415570344.

[26] A. Marshall, R. Fitton, W. Swan, D. Farmer, D. Johnston, M. Benjaber, Y. Ji, Domestic building fabric performance: Closing the gap between the in situ measured and modelled performance, Energy Build. 150 (2017); 307-317.

[27] D. Butler, A. Dengel, Review of co-heating test methodologies: Primary research (2013).

[28] M. Li, D. Allinson, K. Lomas, Estimation of building heat transfer coefficients from in-use data, Int. J. Build. Pathol. Adapt. (2019).

[29] K. Chávez, D.P. Ruiz, M.J. Jiménez, Dynamic integrated method applied to assessing the in-situ thermal performance of walls and whole buildings. Robustness analysis supported by a benchmark set-up, Appl. Therm. Eng. 152 (2019); 287-307.

[30] O. Mejri, E.P. Del Barrio, N. Ghrab-Morcos, Energy performance assessment of occupied buildings using model identification techniques, Energy Build. 43 (2011); 285-299.

[31] Y. Li, Y. Rezgui, A novel concept to measure envelope thermal transmittance and air infiltration using a combined simulation and experimental approach, Energy Build. 140 (2017); 380-387.

[32] M.H. Sherman, W.R. Chan, Building air tightness: research and practice, Building Ventilation: the state of the Art (2006); 137-162.

[33] A.K. Persily, Field measurement of ventilation rates, Indoor Air. 26 (2016); 97-111.

[34] J.F. Belmonte, R. Barbosa, M.G. Almeida, CO2 concentrations in a multifamily building in Porto, Portugal: Occupants' exposure and differential performance of mechanical ventilation control strategies, J. Build. Eng. 23 (2019); 114-126.

[35] W. Lin, L. Li, X. Liu, T. Zhang, On-site measurement and numerical investigation of the airflow characteristics in an aquatics center, J. Build. Eng (2020); 101968.

[36] Y. Liu, P.K. Misztal, J. Xiong, Y. Tian, C. Arata, W.W. Nazaroff, A.H. Goldstein, Detailed investigation of ventilation rates and airflow patterns in a northern California residence, Indoor Air. 28 (2018); 572-584.

[37] A. Meiss, J. Feijó-Muñoz, The energy impact of infiltration: a study on buildings located in north central Spain, Energy Effic. 8 (2015); 51-64.

[38] A. Bhatia, Heat Loss Calculations and Principles, M04-003 Continuing Education and Devekopment, NY (2013).

[39] C. Younes, C.A. Shdid, G. Bitsuamlak, Air infiltration through building envelopes: A review, J. Build. Phys. 35 (2012); 267-302.

[40] P.H. Baker, A Retrofit of a Victorian Terrace House in New Bolsover: A Whole House Thermal Performance Assessment, Historic England & Glasgow Caledonian University: Glasgow, UK (2015).

[41] T.E. Kuhn, State of the art of advanced solar control devices for buildings, Sol Energy. 154 (2017); 112-133.

[42] Y. Cascone, V. Corrado, V. Serra, Calculation procedure of the shading factor under complex boundary conditions, Sol Energy. 85 (2011); 2524-2539.

[43] C. Rasmussen, L. Frölke, P. Bacher, H. Madsen, C. Rode, Semi-parametric modelling of sun position dependent solar gain using B-splines in grey-box models, Sol Energy. 195 (2020); 249-258. https://doi.org/10.1016/j.solener.2019.11.023.

[44] M.J. Jiménez, M.R. Heras, Application of multi-output ARX models for estimation of the U and g values of building components in outdoor testing, Sol Energy. 79 (2005); 302-310. //doi.org/10.1016/j.solener.2004.10.008.

[45] M.J. Jiménez, B. Porcar, M.R. Heras, Estimation of building component UA and gA from outdoor tests in warm and moderate weather conditions, Sol Energy. 82 (2008), 573-587 //doi.org/10.1016/j.solener.2008.02.013.

[46] M. Senave, G. Reynders, P. Bacher, S. Roels, S. Verbeke, D. Saelens, Towards the characterization of the heat loss coefficient via on-board monitoring: Physical interpretation of ARX model coefficients, Energy Build. 195 (2019); 180-194.

[47] K.K. Andersen, H. Madsen, L.H. Hansen, Modelling the heat dynamics of a building using stochastic differential equations, Energy Build. 31 (2000), 13-24 //doi.org/10.1016/S0378-7788(98)00069-3.

[48] P. Bacher, H. Madsen, Identifying suitable models for the heat dynamics of buildings, Energy Build. 43 (2011); 1511-1522. //doi.org/10.1016/j.enbuild.2011.02.005.

[49] N.R. Kristensen, H. Madsen, S.B. Jørgensen, Parameter estimation in stochastic grey-box models, Automatica. 40 (2004), 225-237 //doi.org/10.1016/j.automatica.2003.10.001.

[50] S. Roels, P. Bacher, G. Bauwens, H. Madsen, M.J. Jiménez, Characterising the Actual Thermal Performance of Buildings: Current Results of Common Exercises Performed in the Framework of the IEA EBC Annex 58-Project, Energy Procedia. 78 (2015); 3282-3287. //doi.org/10.1016/j.egypro.2015.11.726.

[51] X. Lü, T. Lu, C.J. Kibert, M. Viljanen, Modeling and forecasting energy consumption for heterogeneous buildings using a physical–statistical approach, Appl. Energy. 144 (2015); 261-275.

[52] G. Bauwens, S. Roels, Co-heating test: A state-of-the-art, Energy Build. 82 (2014); 163-172. //doi.org/10.1016/j.enbuild.2014.04.0390378-7788.

[53] S. Danov, J. Carbonell, J. Cipriano, J. Martí-Herrero, Approaches to evaluate building energy performance from daily consumption data considering dynamic and solar gain effects, Energy Build. 57 (2013); 110-118. //doi.org/10.1016/j.enbuild.2012.10.050.

[54] M. Senave, S. Roels, G. Reynders, S. Verbeke, D. Saelens, Assessment of data analysis methods to identify the heat loss coefficient from on-board monitoring data, Energy Build. 209 (2020); 109706.

[55] D. Farmer, C. Gorse, W. Swan, R. Fitton, M. Brooke-Peat, D. Miles-Shenton, D. Johnston, Measuring thermal performance in steady-state conditions at each stage of a full fabric retrofit to a solid wall dwelling, Energy Build. 156 (2017); 404-414. https://doi.org/10.1016/j.enbuild.2017.09.086.

[56] S. Stamp, R. Lowe, H. Altamirano-Medina, An investigation into the role of thermal mass on the accuracy of co-heating tests through simulations & field results (2013), 25-28.

[57] S. Stamp, H. Altamirano-Medina, R. Lowe, Measuring and accounting for solar gains in steady state whole building heat loss measurements, Energy Build. 153 (2017); 168-178.

[58] H. Li, K. Zhong, J. Yu, Y. Kang, Z.J. Zhai, Solar energy absorption effect of buildings in hot summer and cold winter climate zone, China, Sol Energy. 198 (2020); 519-528.

[59] P.A. Strachan, L. Vandaele, Case studies of outdoor testing and analysis of building components, Build. Environ. 43 (2008); 129-142.

[60] R. Jack, D. Loveday, D. Allinson, K. Lomas, First evidence for the reliability of building co-heating tests, Build. Res. Inf. 46 (2018); 383-401.

[61] L. Castillo, R. Enríquez, M.J. Jiménez, M.R. Heras, Dynamic integrated method based on regression and averages, applied to estimate the thermal parameters of a room in an occupied office building in Madrid, Energy Build. 81 (2014); 337-362.

[62] H.P. Díaz-Hernández, P.R. Torres-Hernández, K.M. Aguilar-Castro, E.V. Macias-Melo, M.J. Jiménez, Data-Based RC Dynamic Modelling Incorporating Physical Criteria to Obtain the HLC of In-Use Buildings: Application to a Case Study, Energies. 13 (2020); 313.

[63] Y. Olazo-Gómez, H. Herrada, S. Castaño, J. Arce, J.P. Xamán, M.J. Jiménez, Data-Based RC Dynamic Modelling to Assessing the In-Situ Thermal Performance of Buildings. Analysis of Several Key Aspects in a Simplified Reference Case toward the Application at On-Board Monitoring Level, Energies. 13 (2020); 4800.

[64] M.J. Jiménez, EBC Annex 58- Reliable building energy performance characterisation based on full scale dynamic measurements, Report of Subtask 3, part 1: Thermal performance characterization based on full scale testing – description of the common exercises and physical guidelines, International Energy Agency (2016).

[65] R. Claude-Alain, F. Foradini, Simple and cheap air change rate measurement using CO2 concentration decays, Int. J. Vent. 1 (2002); 39-44.

[66] A. Sfakianaki, K. Pavlou, M. Santamouris, I. Livada, M. Assimakopoulos, P. Mantas, A. Christakopoulos, Air tightness measurements of residential houses in Athens, Greece, Build Environ. 43 (2008); 398-405.

[67] A. Hayati, M. Mattsson, M. Sandberg, Single-sided ventilation through external doors: Measurements and model evaluation in five historical churches, Energy Build. 141 (2017); 114-124.

[68] G. Hong, B.S. Kim, Field measurements of infiltration rate in high rise residential buildings using the constant concentration method, Build Environ. 97 (2016); 48-54.

[69] A. Kabirikopaei, J. Lau, Uncertainty analysis of various CO2-Based tracer-gas methods for estimating seasonal ventilation rates in classrooms with different mechanical systems, Build Environ (2020); 107003.

[70] C.Y. Chao, M.P. Wan, A.K. Law, Ventilation performance measurement using constant concentration dosing strategy, Build Environ. 39 (2004); 1277-1288.

[71] J.T. Reardon, M.R. Atif, S. Chia-yu, Tracer gas measurements for ventilation, air movement and air infiltration in a four-sided atrium office building, Int. J. Vent. 1 (2002); 13-22.

[72] C.J. Ghazi, J.S. Marshall, A CO2 tracer-gas method for local air leakage detection and characterization, Flow Meas Instrum. 38 (2014); 72-81.

[73] E. Zender–Świercz, Improvement of indoor air quality by way of using decentralised ventilation, J. Build. Eng. 32 (2020); 101663.

[74] S. Cui, M. Cohen, P. Stabat, D. Marchio, CO2 tracer gas concentration decay method for measuring air change rate, Build Environ. 84 (2015); 162-169.

[75] S. Guillén-Lambea, B. Rodríguez-Soria, J.M. Marín, Air infiltrations and energy demand for residential low energy buildings in warm climates, Renew. Sust. Energ. Rev. 116 (2019); 109469.

[76] B. Khemet, R. Richman, An empirical approach to improving preconstruction airtightness estimates in light framed, detached homes in Canada, J. Build. Eng. 33; 101433.

[77] K. Ghoreishi, A. Fernández-Gutiérrez, F. Fernández-Hernández, L. Parras, Retrofit planning and execution of a Mediterranean villa using on-site measurements and simulations, J. Build. Eng (2020); 102083.

[78] S. Roels, P. Bacher, G. Bauwens, S. Castaño, M.J. Jiménez, H. Madsen, On site characterisation of the overall heat loss coefficient: Comparison of different assessment methods by a blind validation exercise on a round robin test box, Energy Build. 153 (2017), 179-189 https://doi.org/10.1016/j.enbuild.2017.08.006.

[79] F. Alzetto, D. Farmer, R. Fitton, T. Hughes, W. Swan, Comparison of whole house heat loss test methods under controlled conditions in six distinct retrofit scenarios, Energy Build. 168 (2018); 35-41.

[80] J. Parker, D. Farmer, D. Johnston, M. Fletcher, F. Thomas, C. Gorse, S. Stenlund, Measuring and modelling retrofit fabric performance in solid wall conjoined dwellings, Energy Build. 185 (2019), 49-65 https://doi.org/10.1016/j.enbuild.2018.12.010.

[81] O. Gutschker, LORD 3.2. Logical R- Determination User Guide, Angewandte Pysik, BTU Cottbus (2003).

[82] O. Gutschker, Parameter identification with the software package LORD, Build. Environ. 43 (2008); 163-169.

[83] ASTM D6245-18, Standard guide for using indoor carbon dioxide concentrations to evaluate indoor air quality and ventilation, West Conshohocken, PA (2018).

[84] M.J. Moran, H.N. Shapiro, D.D. Boettner, M.B. Bailey, Fundamentals of engineering thermodynamics, John Wiley & Sons, 2010.

[85] I. Uriarte, A. Erkoreka, C. Giraldo-Soto, K. Martin, A. Uriarte, P. Eguia, Mathematical development of an average method for estimating the reduction of the Heat Loss Coefficient of an energetically retrofitted occupied office building, Energy Build. 192 (2019); 101-122. //doi.org/10.1016/j.enbuild.2019.03.006.

[86] J.A. Duffie, W.A. Beckman, Solar engineering of thermal processes, John Wiley & Sons, 2013.

[87] John Carmody, Stephen Selkowitz, Dariush Arasteh, Lisa Heschong, Residential windows: a guide to new technologies and energy performance, Ringgold Inc, Portland, 2007.

[88] ISO 9869-1:2014, Thermal insulation — Building elements — In-situ measurement of thermal resistance and thermal transmittance — Part 1: Heat flow meter method (2014).

[89] J.R. Taylor, Error analysis, Univ.Science Books, Sausalito, California (1997).

[90] A.R. Day, T.G. Karayiannis, Degree-days: comparison of calculation methods, Building Services Engineering Research and Technology. 19 (1998); 7-13.

[91] ASHRAE Handbook, Thermal Comfort Chapter: Fundamentals Volume of the ASHRAE Handbook , Inc. Atlanta, GA (2005).

[92] Y. Cengel, Heat and mass transfer: fundamentals and applications, McGraw-Hill Higher Education, 2014.

[93] ISO 6946:2017, Building components and building elements–Thermal resistance and thermal transmittance–Calculation method (2017).

[94] J.H. Watmuff, W. Charters, D. Proctor, Solar and wind induced external coefficients-solar collectors, Cooperation Mediterraneenne pour l'Energie Solaire (1977); 56.

[95] S. Van Buggenhout, T.Z. Desta, A. Van Brecht, E. Vranken, S. Quanten, W. Van Malcot, D. Berckmans, Data-based mechanistic modelling approach to determine the age of air in a ventilated space, Build Environ. 41 (2006); 557-567.

[96] ASTM E741-11: Standard Test Method for Determining Air Change in a Single Zone by Means of a Tracer Gas Dilution, (2017).

[97] H. Van Dijk, Van der Linden, G P, The PASSYS method for testing passive solar components, Build. Environ. 28 (1993); 115-126.

[98] IEA-EBC Annex 71 "Building energy performance assessment based on in-situ measurements", https://www.kuleuven.be/bwf/projects/annex71/ (2020).

[99] B. Sodagar, D. Starkey, The monitored performance of four social houses certified to the Code for Sustainable Homes Level 5, Energy Build. 110 (2016); 245-256. //doi.org/10.1016/j.enbuild.2015.11.016.

[100] A. Beizaee, D. Allinson, K.J. Lomas, E. Foda, D.L. Loveday, Measuring the potential of zonal space heating controls to reduce energy use in UK homes: The case of un-furbished 1930s dwellings, Energy Build. 92 (2015); 29-44. //doi.org/10.1016/j.enbuild.2015.01.040.

[101] SAP, The government's standard assessment procedure for energy rating of dwellings, Building Research Establishment, (2009).

[102] I. Uriarte, A. Erkoreka, P. Eguia, E. Granada, K. Martin-Escudero, Estimation of the Heat Loss Coefficient of Two Occupied Residential Buildings through an Average Method, Energies. 13 (2020); 5724.

[103] A. Erkoreka, E. Garcia, K. Martin, J. Teres-Zubiaga, L. Del Portillo, In-use office building energy characterization through basic monitoring and modelling, Energy Build. 119 (2016); 256-266. //doi.org/10.1016/j.enbuild.2016.03.030.

[104] C. Giraldo-Soto, I. Uriarte, A. Erkoreka, J.M. Sala, P.E. Oller, Desacoplamiento del Coeficiente de Perdida de Calor de un edificio en uso aplicando el método de decaimiento del CO2,.

[105] Dynastee, DYNamic Analysis Simulation and Testing applied to the Energy and Environmental performance of buildings, https://dynastee.info/ (2020).

[106] Dynastee, Dynastee On-Line Training Webinar Series: "Dynamic Calculation Methods for Building Energy Performance Assessment" – Recordings and Slides now available, https://dynastee.info/introduction-to-dynastee-on-line-training-webinar-series-dynamic-calculation-methods-for-building-energy-performance-assessment-recordings-and-slides-now-available/ (2020).

[107] A. Erkoreka, Modelling and testing of green roof using the PASLINK methodology for characterization of its energy behaviour (2012).

APPENDIX

I. APPENDIX A

In order to fulfil all the requirements of the average method, it must be ensured that the accumulated average HLC value of the selected period is inside the ±10 % stabilization band during the last 24 hours of the period. Then, the accumulated HLC graph of the selected period has been plotted in the following Figure A.1.

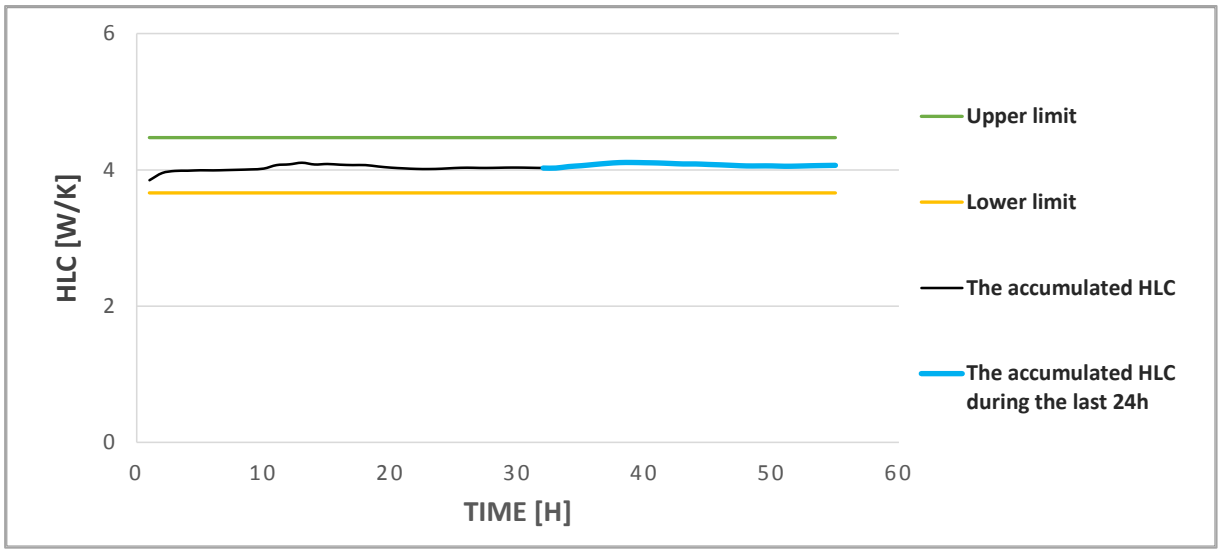

Figure A.1. Evolution of the accumulated average of the Heat Loss Coefficient for the whole Round Robin Box.

As shown in previous Figure A.1, the accumulated average HLC value barely changes during the whole period. Therefore, it can be assumed that despite the period is shorter than the period length proposed in the section 2.1.1, the obtained final HLC result can be considered stable and reliable.

II. APPENDIX B

In order to justify the stabilization band requirement of the average method, where the estimated HLC value should be within a 10 % error band in the accumulated average plots over the last 24 hours of the selected periods, all the graphs have been plotted in Figure B.1 for Gainsborough and Figure B.2 for Loughborough.

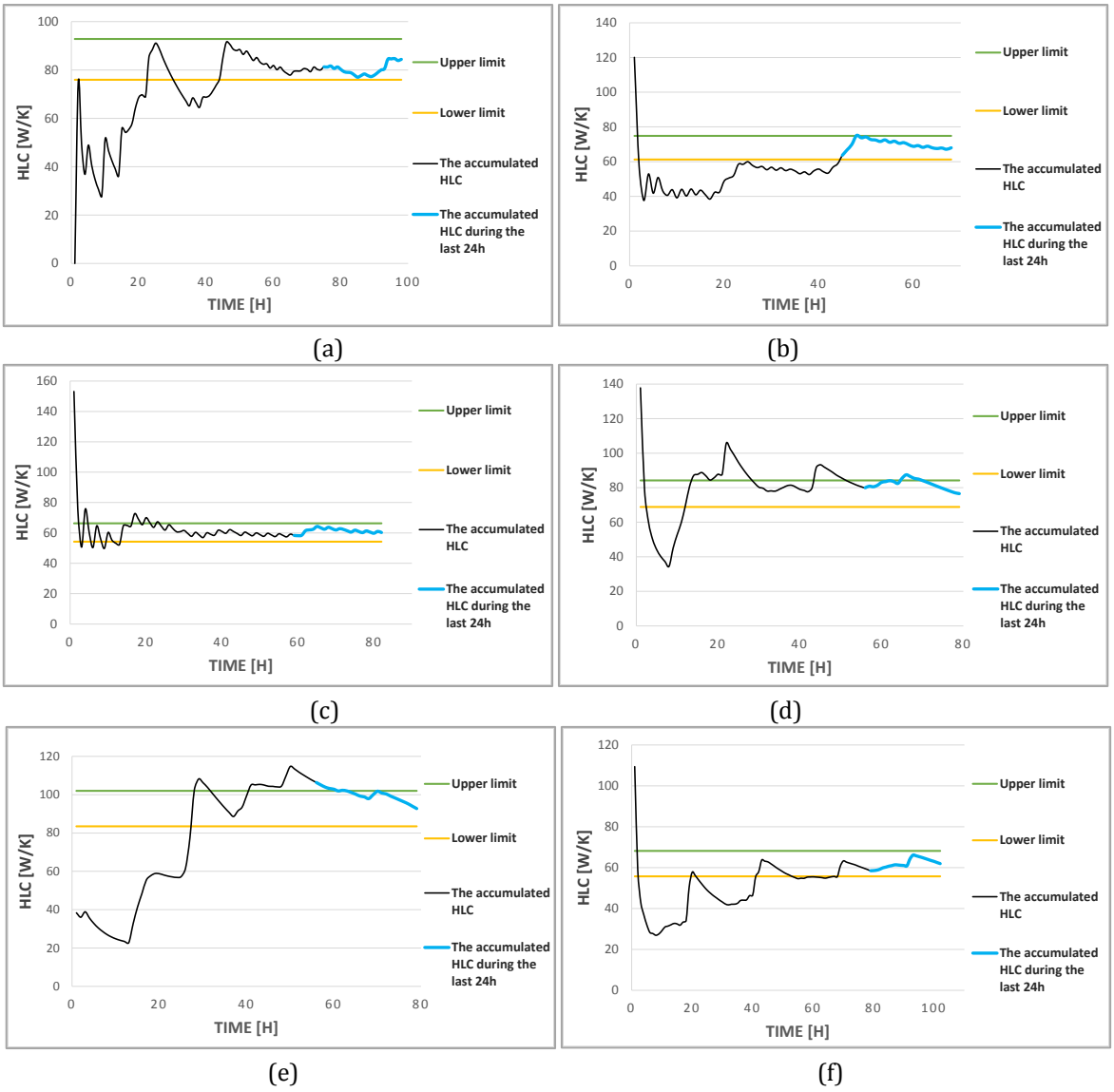

Figure B.1. Evolution of the accumulated average of the Heat Loss Coefficient for (a) period 1, (b) period 2, (c) period 3, (d) period 4, (e) period 5 and (f) period 6 in Gainsborough. [102]

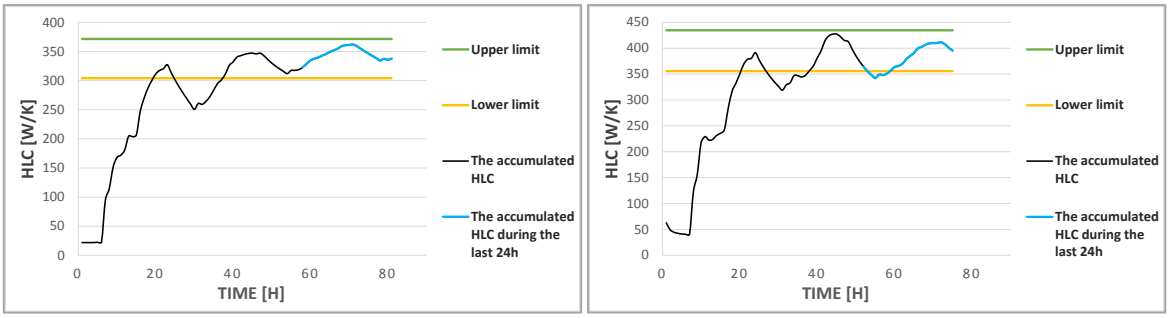

(a) (b)

Figure B.2. Evolution of the accumulated average of the Heat Loss Coefficient for (a) period 1 and (b) period 2 in Loughborough. [102]

III. APPENDIX C

Since one of the method requirements is that the stabilization band of the selected periods in the accumulated average plots should be ±10 % as compared to the HLC estimate during the last 24 hours of the period, the accumulated HLC graphs have been plotted for all floors and for the whole building in all the analysed periods. All the cases have been plotted below:

Winter 2014-2015

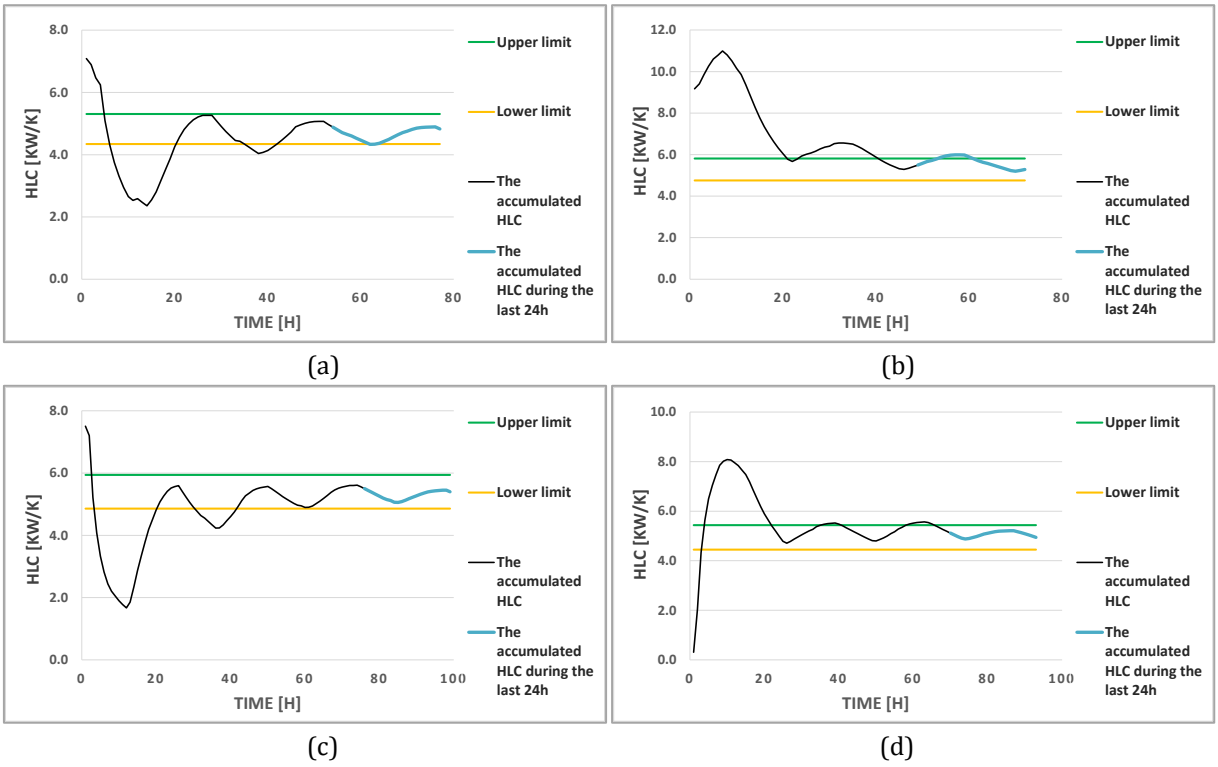

Figure C.1. Evolution of the accumulated average of the Heat Loss Coefficient for (a) period 1, (b) period 2, (c) period 3 and (d) period 4 for the whole building for all periods in 2014-2015. [85]

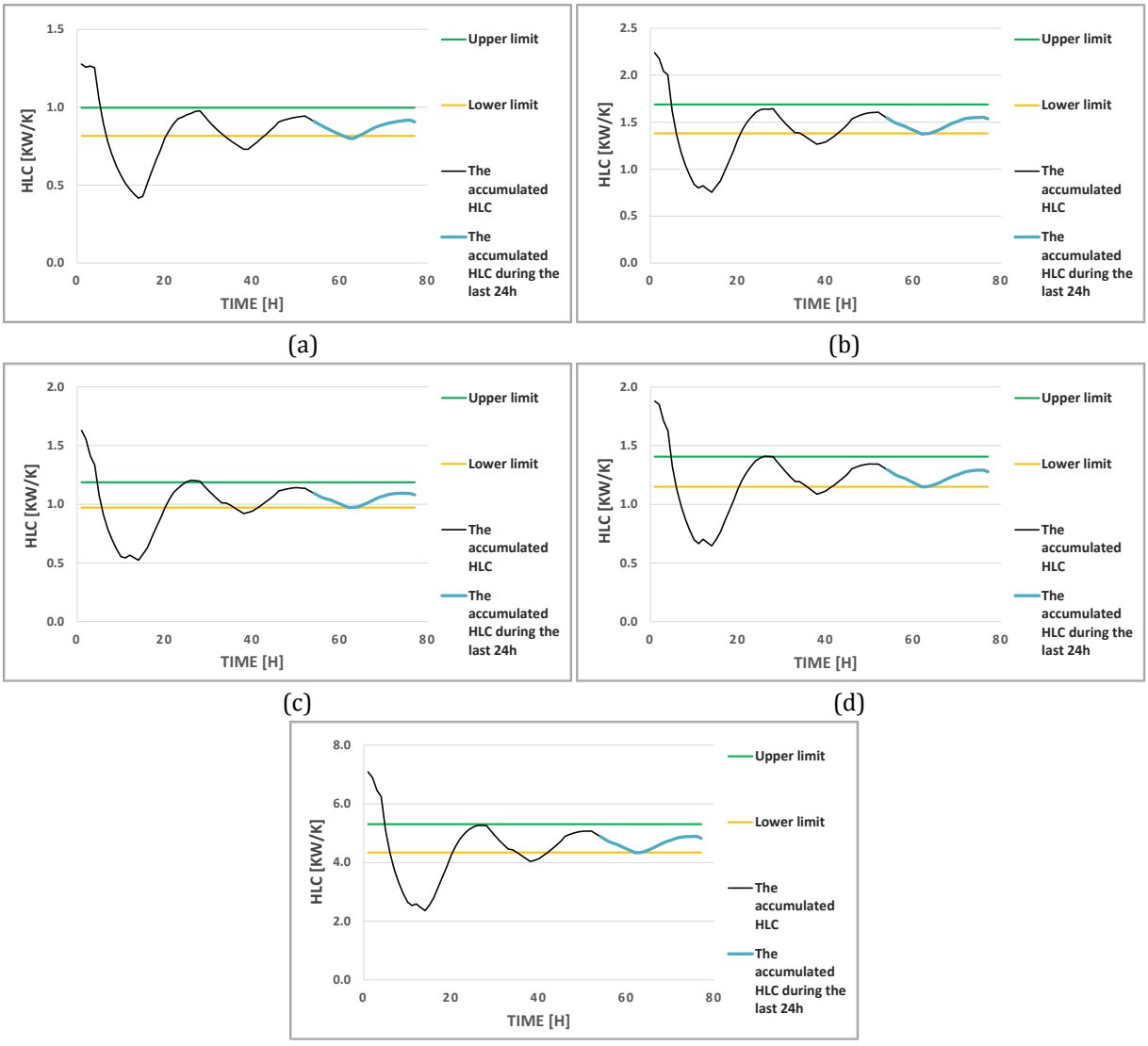

Figure C.2. Evolution of the accumulated average of the Heat Loss Coefficient for (a) ground floor, (b) floor 1, (c) floor 2, (d) floor 3 and (e) the whole building for period one in 2014-2015. [85]

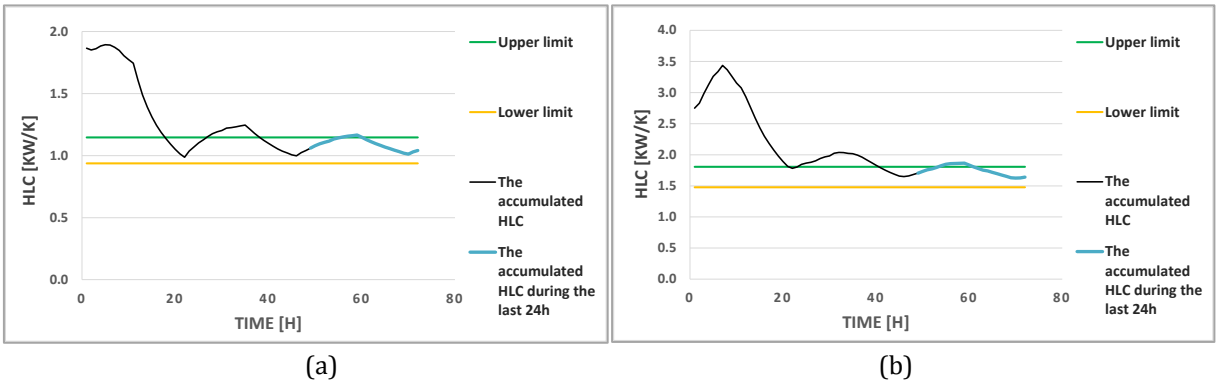

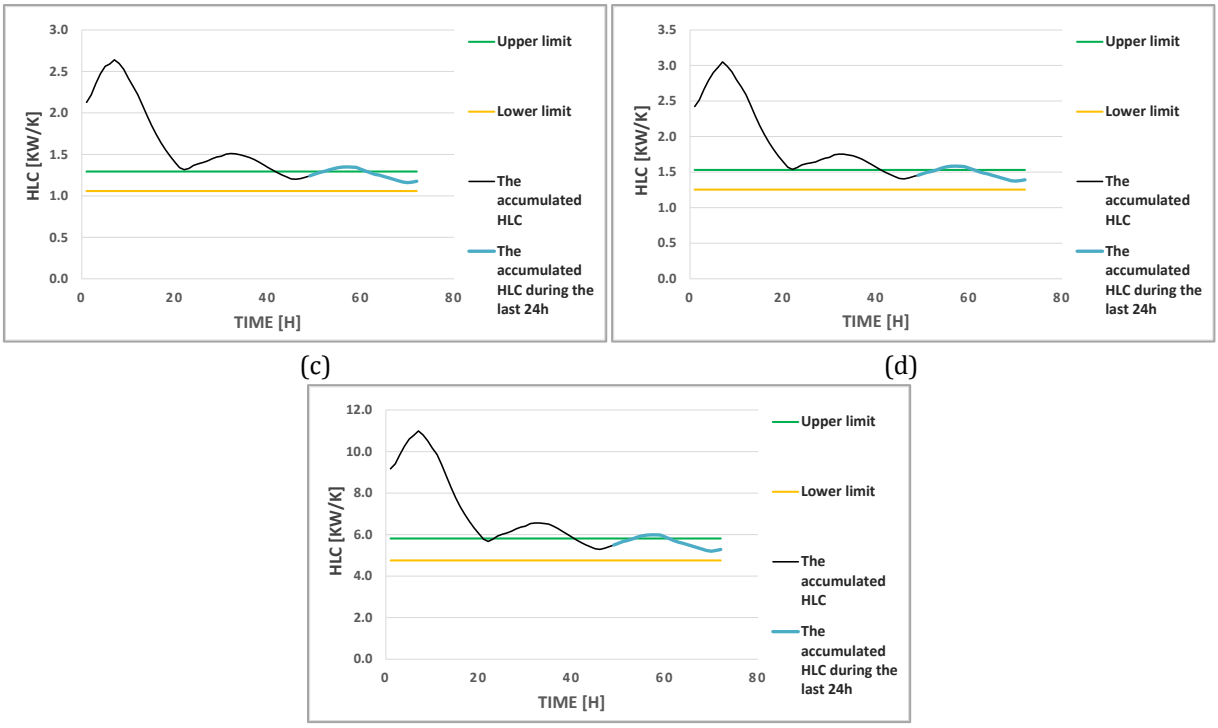

(c) (d)

(e)

Figure C.3. Evolution of the accumulated average of the Heat Loss Coefficient for (a) ground floor, (b) floor 1, (c) floor 2, (d) floor 3 and (e) the whole building for period two in 2014-2015.

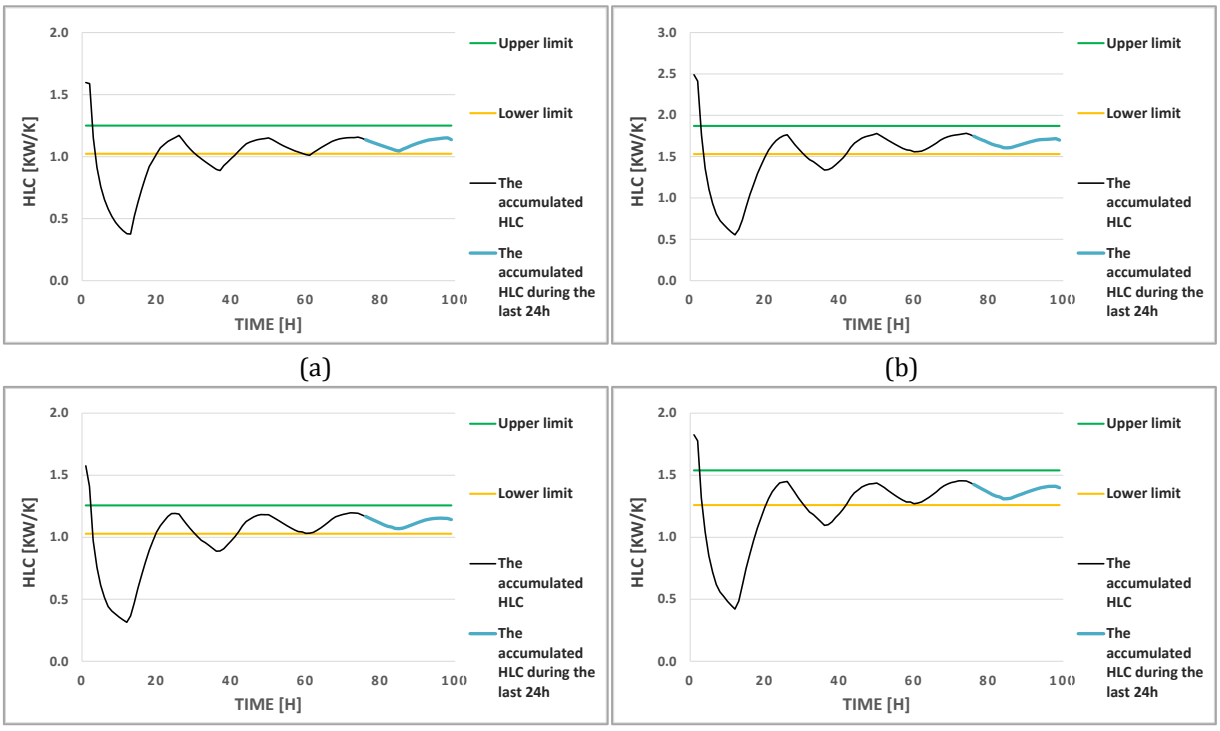

(a) (b)

(c) (d)

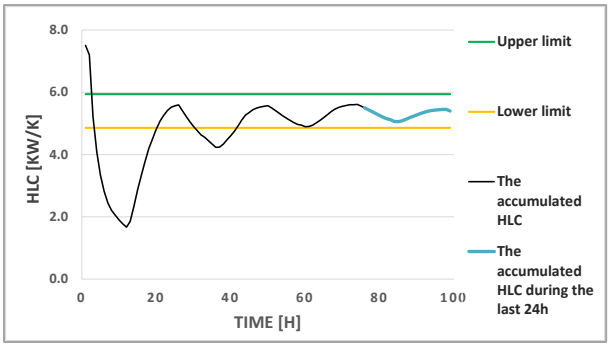

(e)

Figure C.4. Evolution of the accumulated average of the Heat Loss Coefficient for (a) ground floor, (b) floor 1, (c) floor 2, (d) floor 3 and (e) the whole building for period three in 2014-2015.

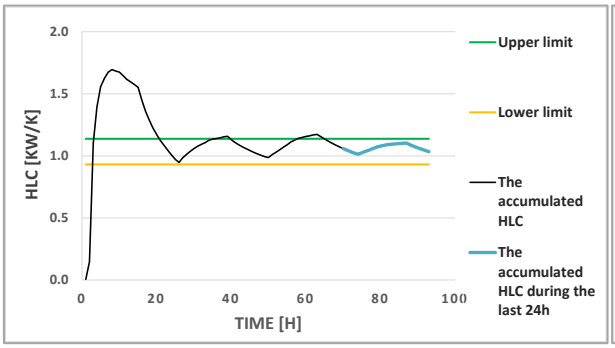

(a)

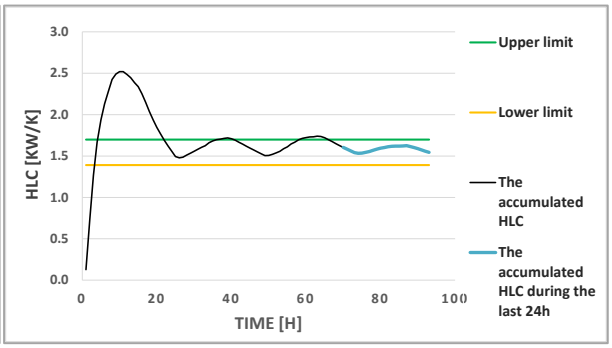

(b)

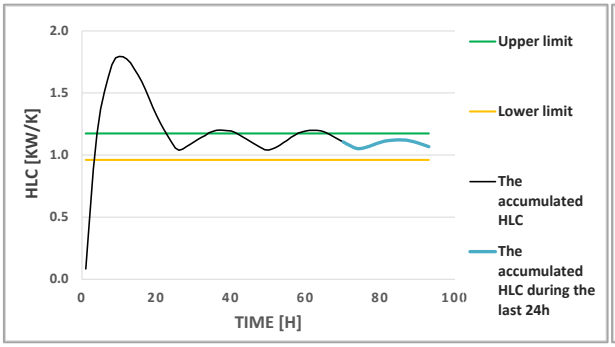

(c)

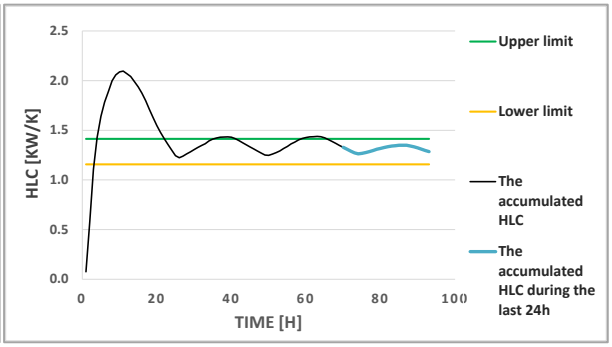

(d)

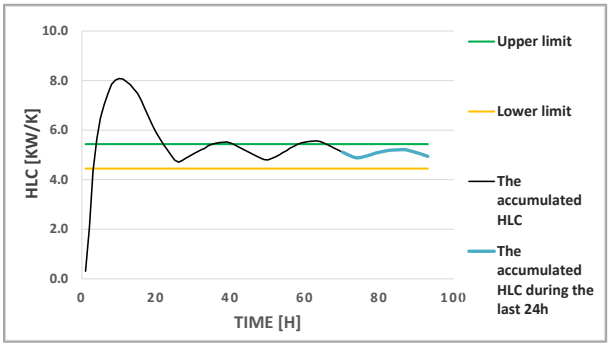

(e)

Figure C.5. Evolution of the accumulated average of the Heat Loss Coefficient for (a) ground floor, (b) floor 1, (c) floor 2, (d) floor 3 and (e) the whole building for period four in 2014-2015.

Winter 2015-2016

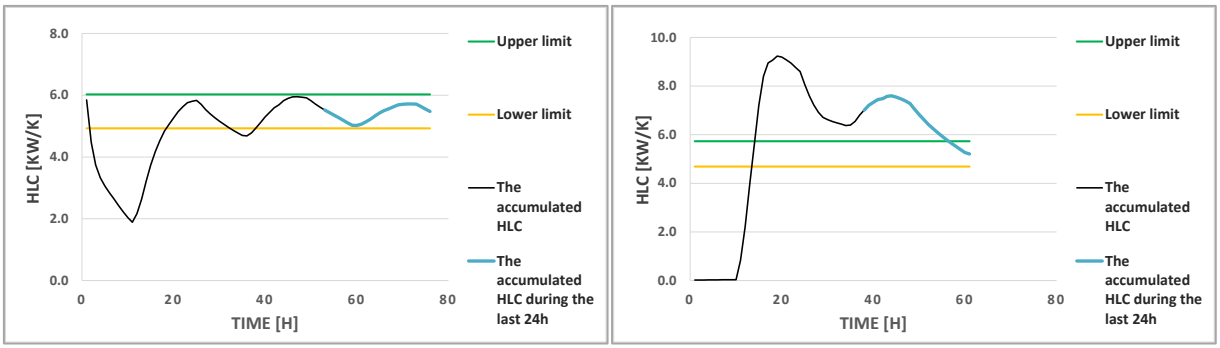

(a) (b)

Figure C.6. Evolution of the accumulated average of the Heat Loss Coefficient for (a) period 1 and (b) period 2 for the whole building for all periods in 2015-2016. [85]

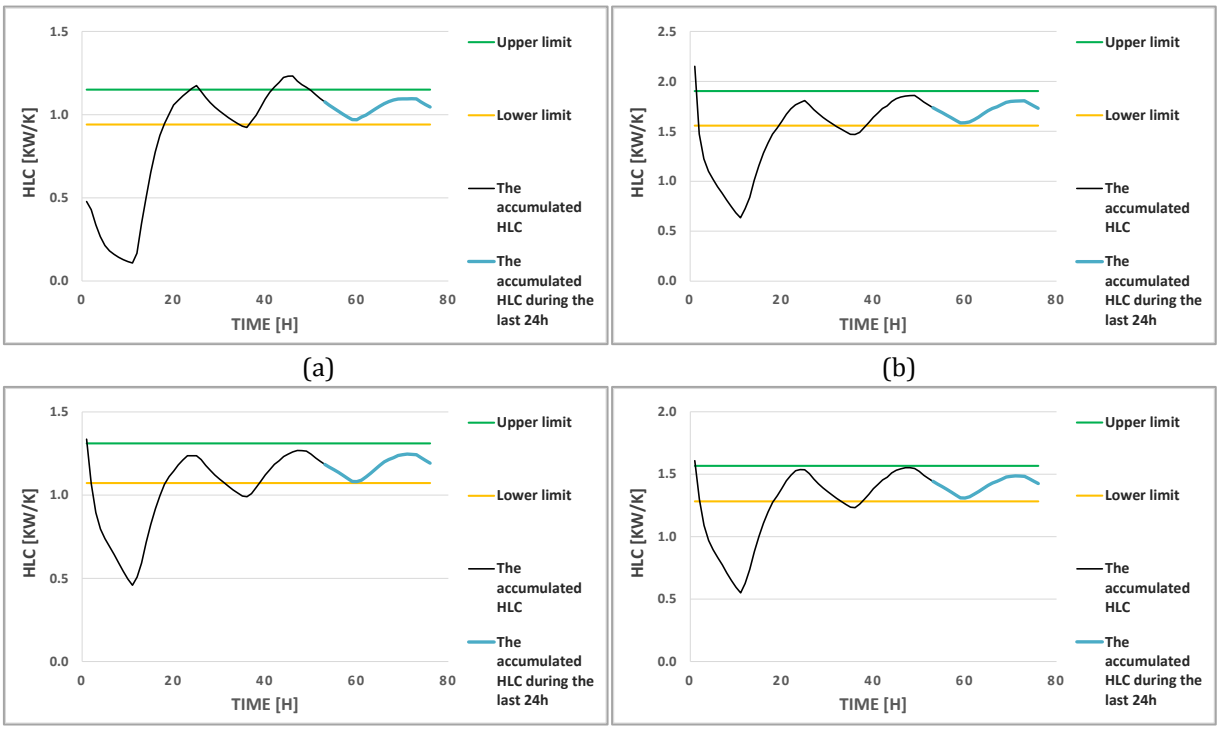

(a) (b)

(c) (d)

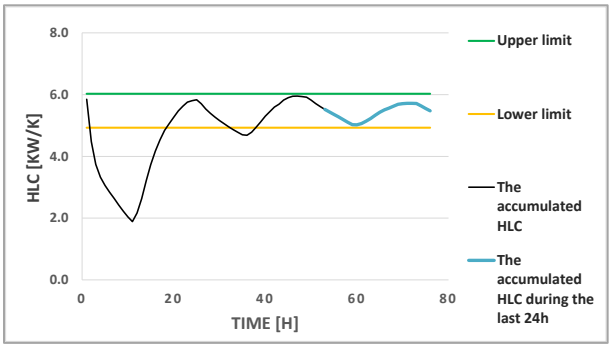

(e)

Figure C.7. Evolution of the accumulated average of the Heat Loss Coefficient for (a) ground floor, (b) floor 1, (c) floor 2, (d) floor 3 and (e) the whole building for period one in 2015-2016.

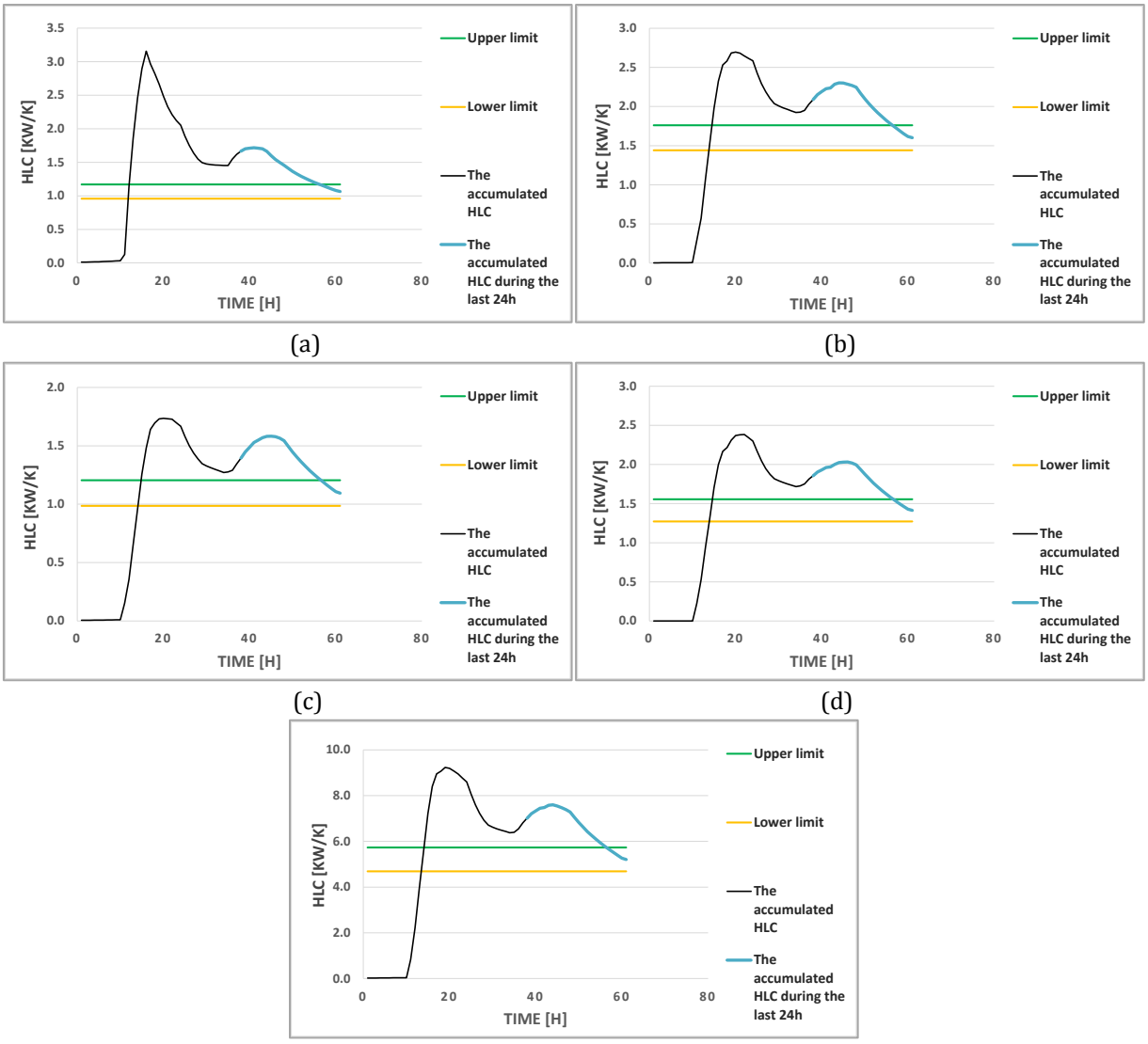

Figure C.8. Evolution of the accumulated average of the Heat Loss Coefficient for (a) ground floor, (b) floor 1, (c) floor 2, (d) floor 3 and (e) the whole building for period two in 2015-2016. [85]

Winter 2016-2017

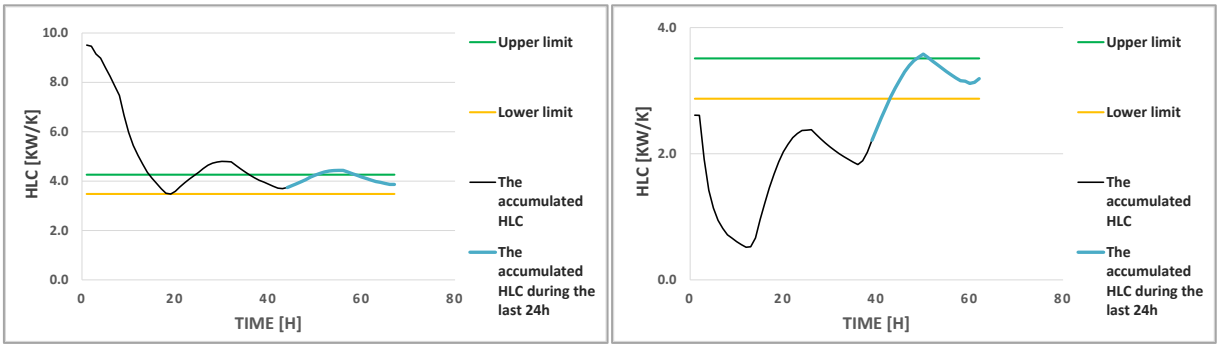

(a) (b)

Figure C.9. Evolution of the accumulated average of the Heat Loss Coefficient for (a) period 1 and (b) period 2 for the whole building for all periods in 2016-2017. [85]

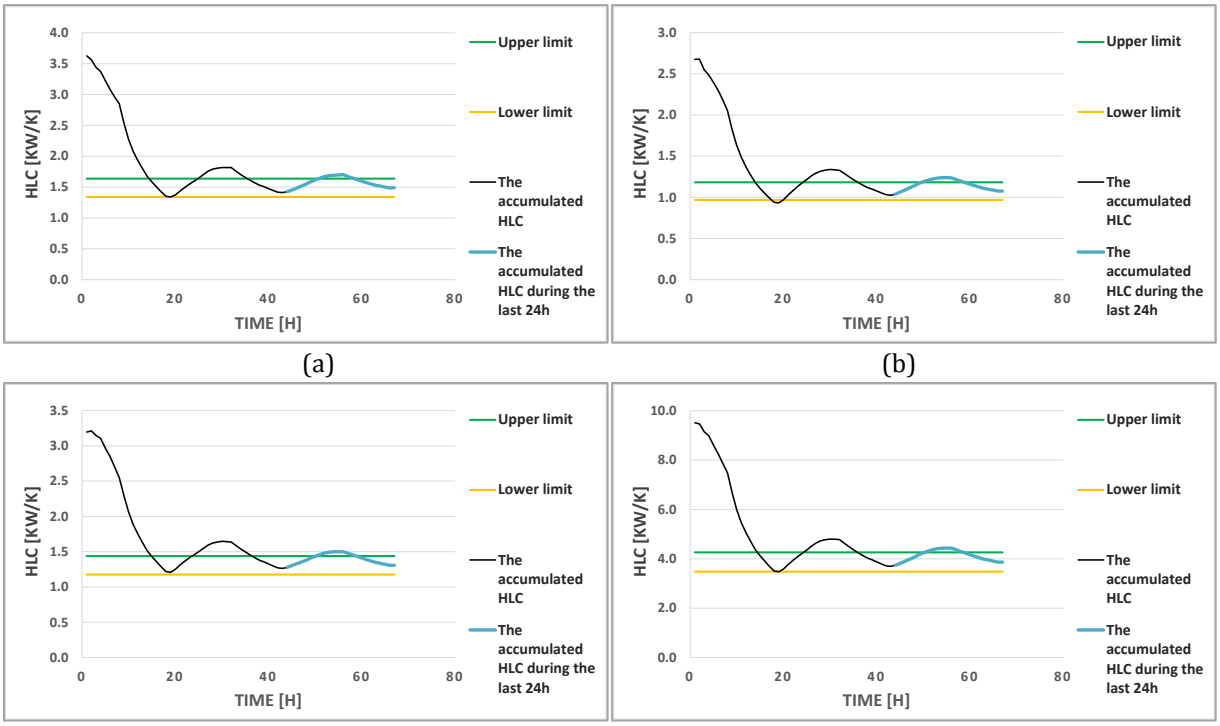

(a) (b)

(c) (d)

Figure C.10. Evolution of the accumulated average of the Heat Loss Coefficient for (a) floor 1, (b) floor 2, (c) floor 3 and (d) the whole building for period one in 2016-2017.

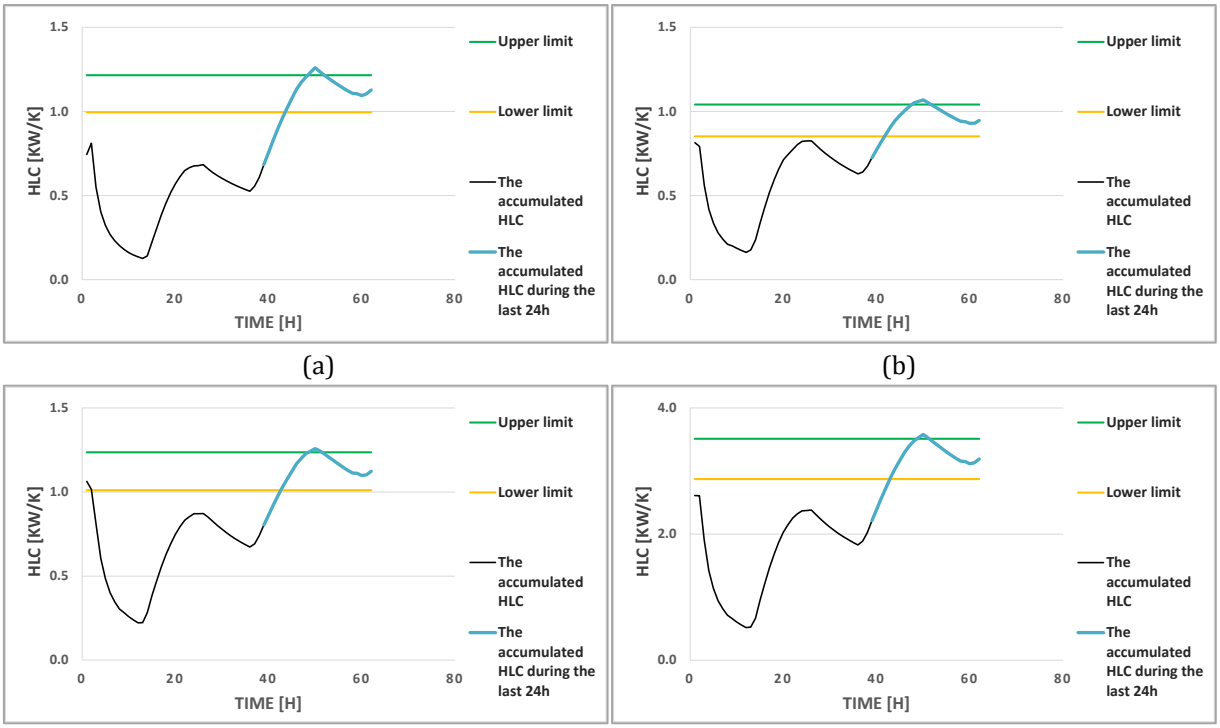

Figure C.11. Evolution of the accumulated average of the Heat Loss Coefficient for (a) floor 1, (b) floor 2, (c) floor 3 and (d) the whole building for period two in 2016-2017.

Winter 2017-2018

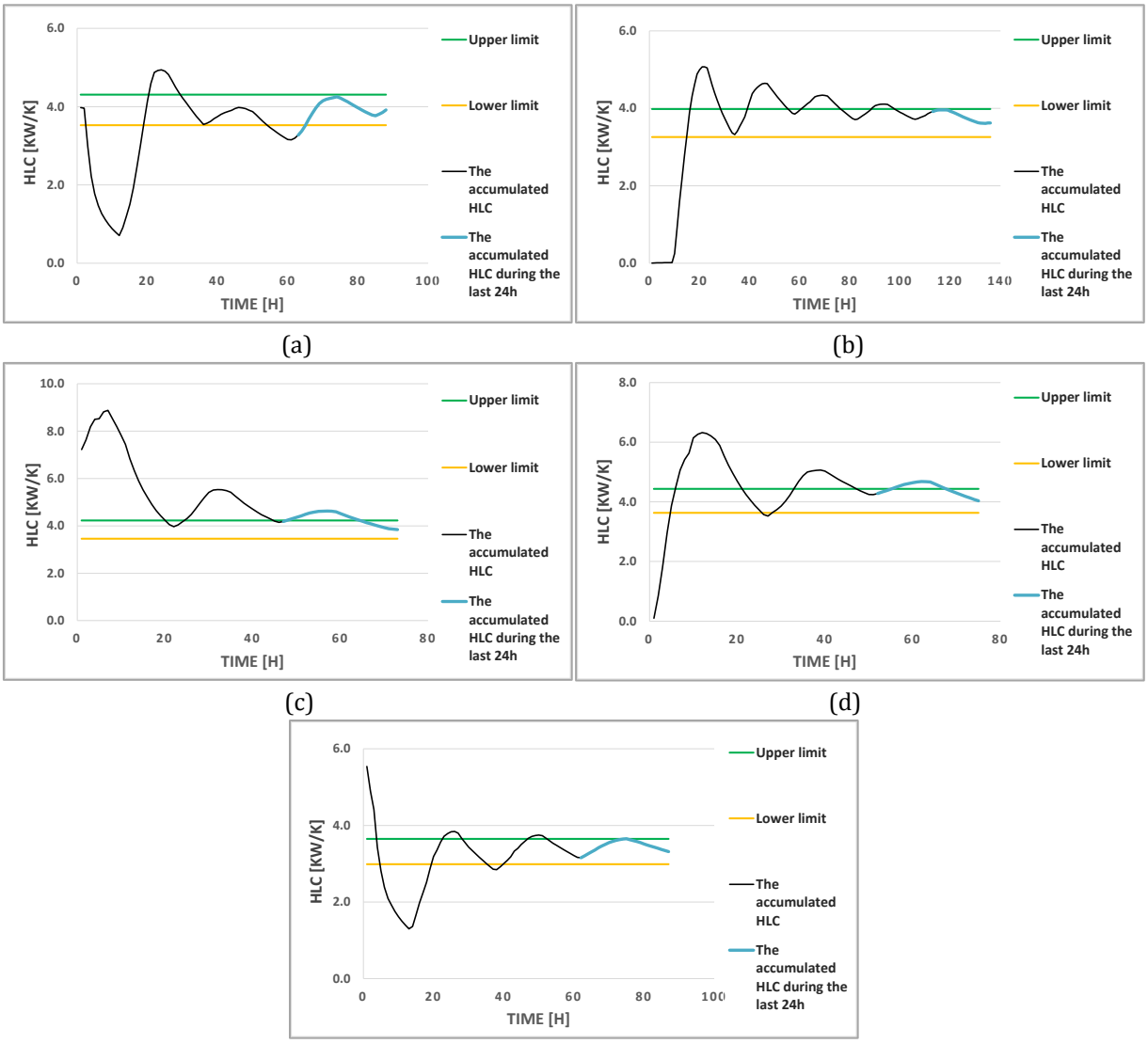

Figure C.12. Evolution of the accumulated average of the Heat Loss Coefficient for (a) period 1, (b) period 2, (c) period 3, (d) period 4 and (e) period 5 for the whole building for all periods in 2017-2018. [85]

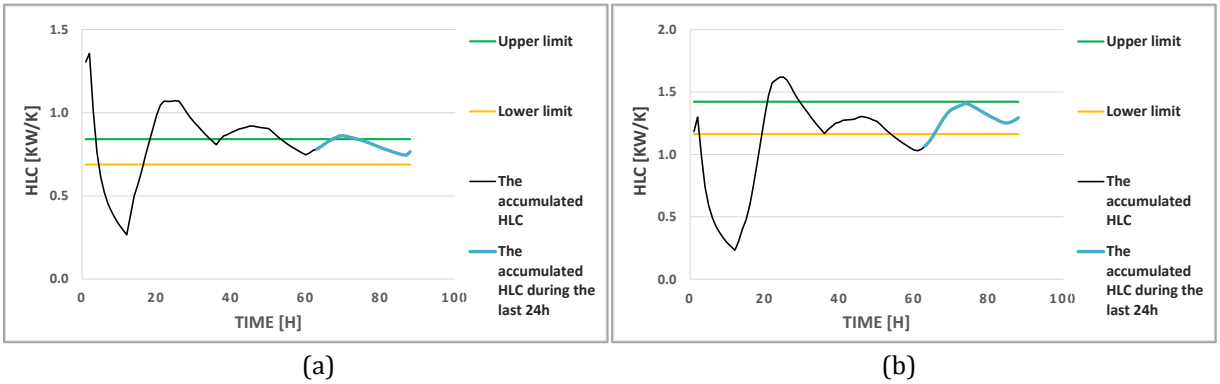

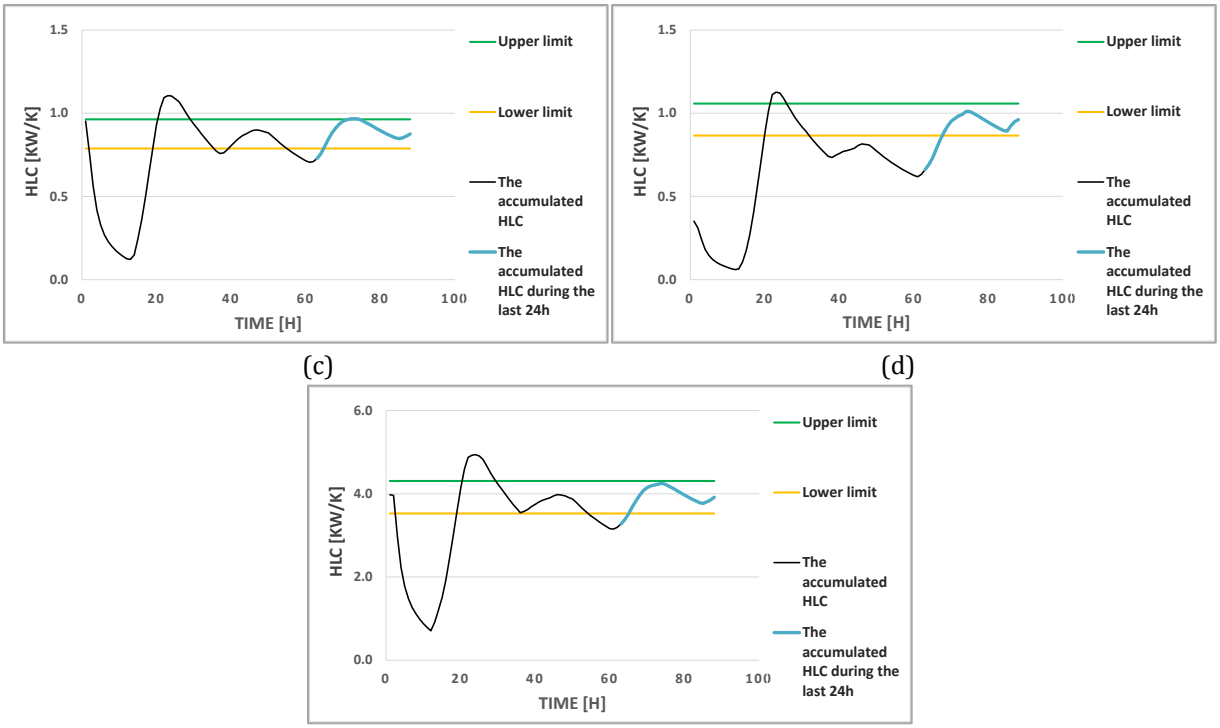

(c) (d)

(e)

Figure C.13. Evolution of the accumulated average of the Heat Loss Coefficient for (a) ground floor, (b) floor 1, (c) floor 2, (d) floor 3 and (e) the whole building for period one in 2017-2018.

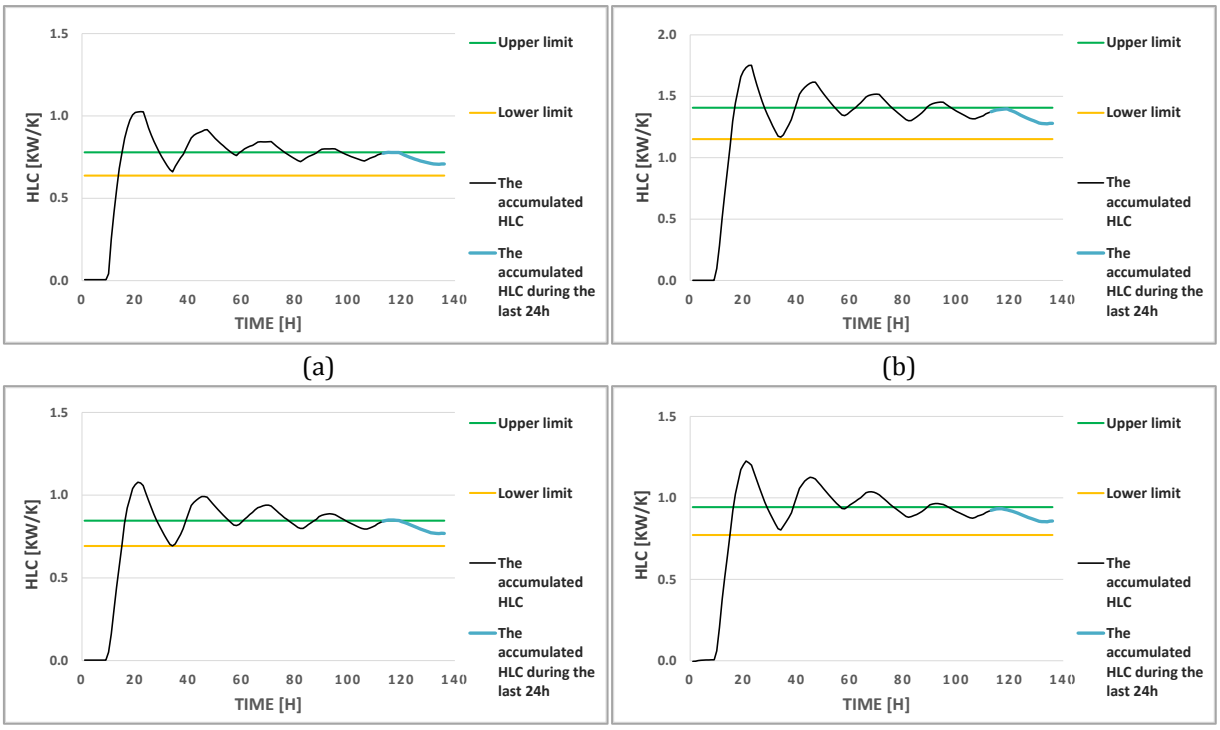

(a) (b)

(c) (d)

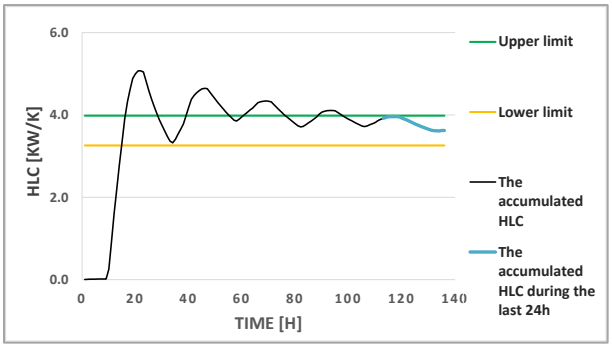

(e)

Figure C.14. Evolution of the accumulated average of the Heat Loss Coefficient for (a) ground floor, (b) floor 1, (c) floor 2, (d) floor 3 and (e) the whole building for period two in 2017-2018. [85]

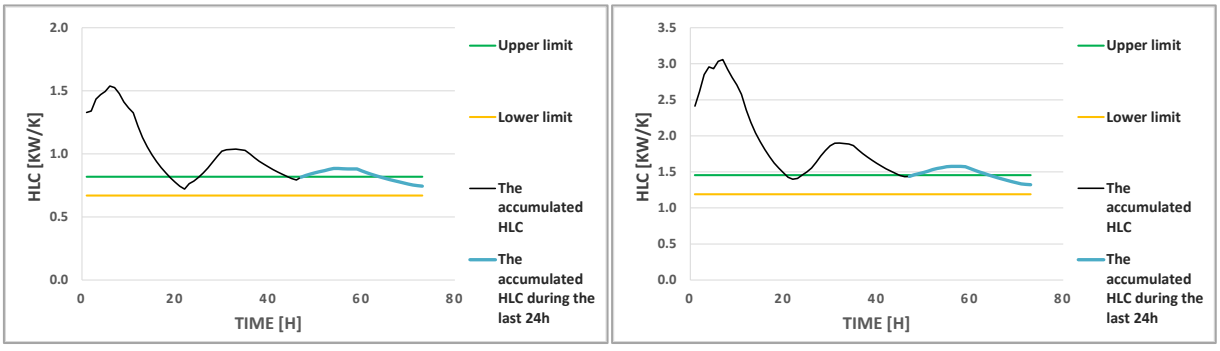

(a) (b)

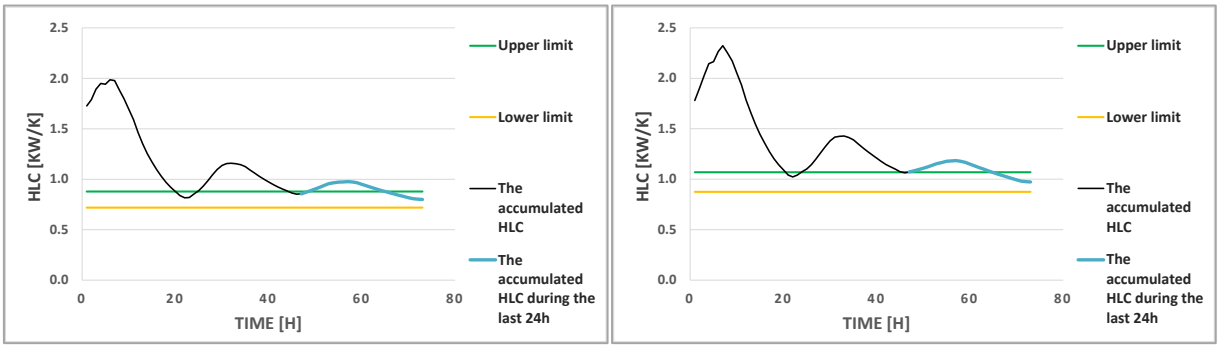

(c) (d)

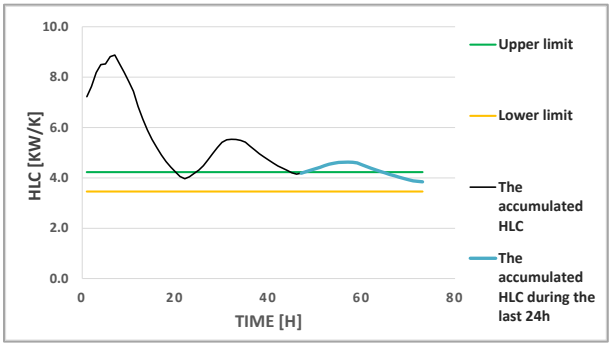

(e)

Figure C.15. Evolution of the accumulated average of the Heat Loss Coefficient for (a) ground floor, (b) floor 1, (c) floor 2, (d) floor 3 and (e) the whole building for period three in 2017-2018.

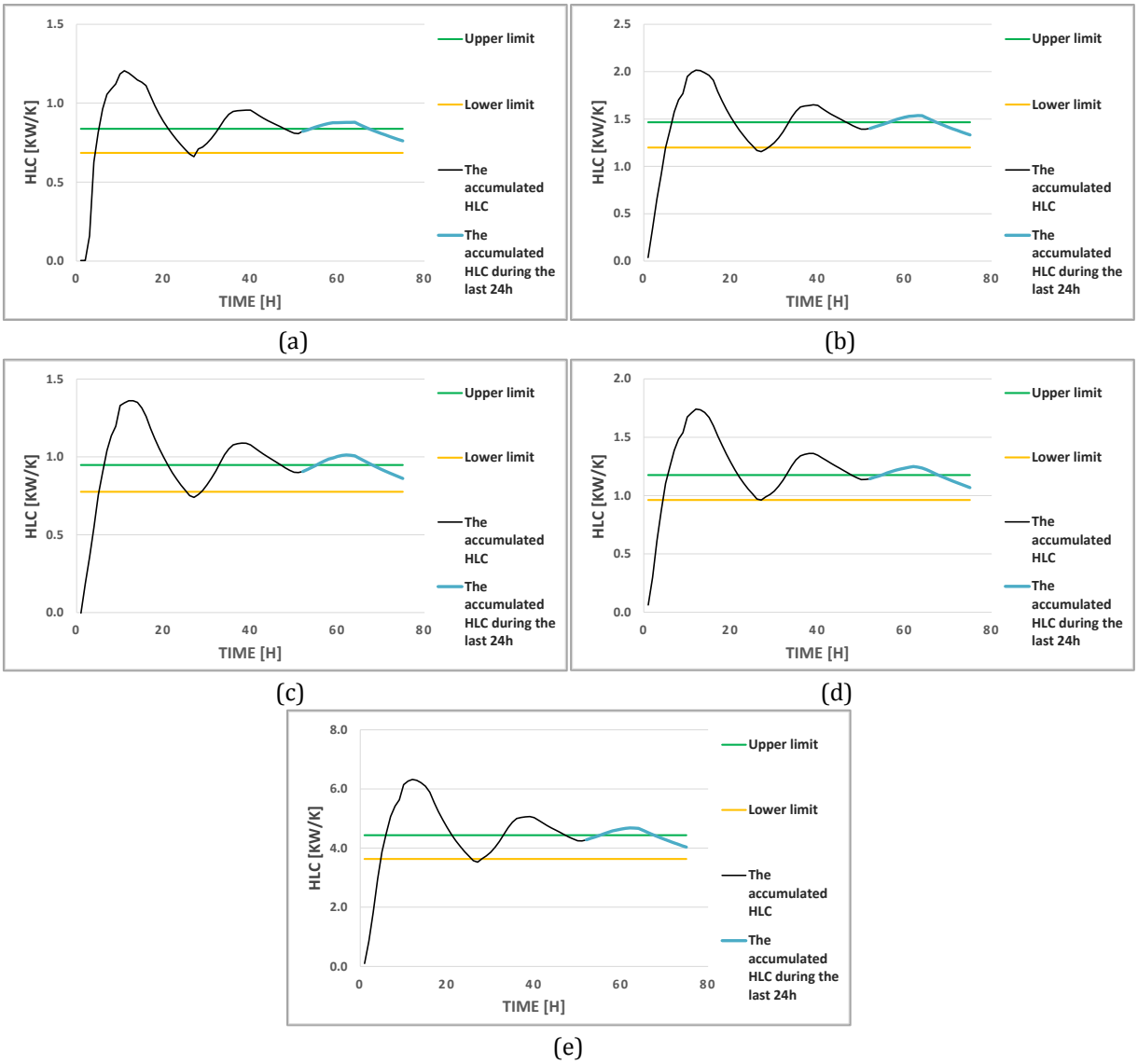

Figure C.16. Evolution of the accumulated average of the Heat Loss Coefficient for (a) ground floor, (b) floor 1, (c) floor 2, (d) floor 3 and (e) the whole building for period four in 2017-2018.

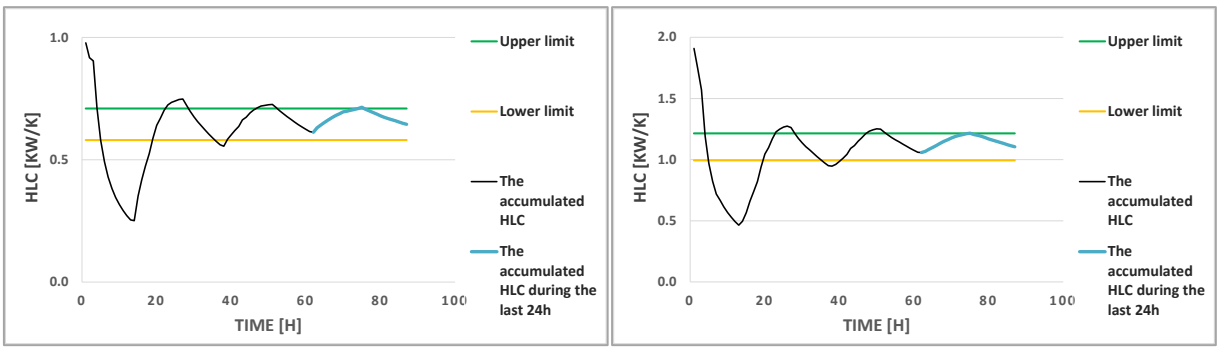

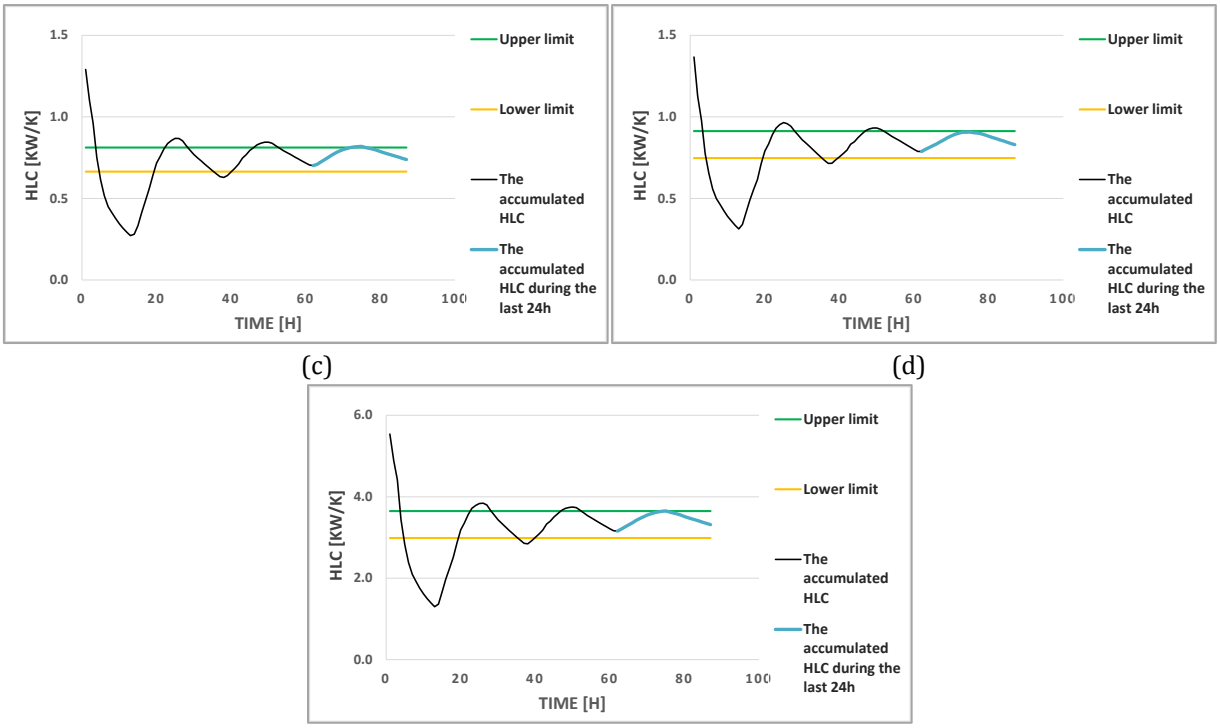

Figure C.17. Evolution of the accumulated average of the Heat Loss Coefficient for (a) ground floor, (b) floor 1, (c) floor 2, (d) floor 3 and (e) the whole building for period five in 2017-2018.

As shown in previous figures, the variation of the accumulated average HLC is considerable until it reaches the last 24 hours. Therefore, it is important to consider only long periods where the accumulated average HLC value is stable during the last 24 hours. A proof of this conclusion can be clearly seen in Figure C.8, where the estimated period is shorter than 72h and not long enough to be stabilized during the last 24 hours. However, during this analysis, the obtained HLC value is considered correct, since it is really close to the HLC values obtained with other periods and it is very close to the minimum period length requirement of 72 hours. On the other hand, the rest of the periods do not show noteworthy issues.

IV. APPENDIX D

The average values of all the required variables over the analysed periods have been calculated as in Eq. 50 and Eq. 52. The considered uncertainty of each variable is shown in section 3.3.3. Moreover, the obtained results have been collected and reported in the following tables, floor by floor, for each period:

Before Retrofitting				Out	FLOOR 0		FLOOR 1		FLOOR 2		FLOOR 3		Building	
WINTER	PERIOD			T_{out} [°C]	T_{in} [°C]	T_{in}-T_{out} [K]	T_{in} [°C]	T_{in}-T_{out} [K]	T_{in} [°C]	T_{in}-T_{out} [K]	T_{in} [°C]	T_{in}-T_{out} [K]	T_{in} [°C]	T_{in}-T_{out} [K]
2014-2015	Period 1	2014-12-2 16:00 →	2014-12-5 20:00	8.7	22.3	13.6	24.4	15.7	24.7	15.9	24.8	16.1	24.1	15.3
	Period 2	2015-1-20 10:00 →	2015-1-23 8:00	6.2	21.6	15.4	23.5	17.2	23.6	17.4	23.7	17.2	23.1	16.9
	Period 3	2015-1-26 19:00 →	2015-1-30 20:00	9.9	21.6	11.6	23.1	13.2	23.5	13.6	23.7	13.8	23	13.0
	Period 4	2015-2-3 6:00 →	2015-2-7 1:00	3.0	20.9	17.8	22.6	19.5	22.8	19.7	22.8	19.8	22.3	19.2
2015-2016	Period 5	2015-11-24 19:00 →	2015-11-27 22:00	12.3	20.9	8.5	24.0	11.7	24.2	11.8	23.8	11.5	23.2	10.9
	Period 6	2016-1-6 20:00 →	2016-1-9 8:00	13.7	20.5	6.8	21.7	8.0	21.6	7.9	21.4	8.0	21.3	7.6
2016-2017	Period 7	2016-12-19 12:00 →	2016-12-22 6:00	9.0			23.2	14.1	23.4	14.3	23.3	14.2	23.3	14.2
	Period 8	2017-1-9 18:00 →	2017-1-12 7:00	10.1			21.1	11.2	21.6	11.7	21.1	11.2	21.3	11.4

Table D.1. Average temperatures of each analysed period for winters 2014-2015, 2015-2016 and 2016-2017 before retrofitting.

Before Retrofitting				Out	FLOOR 0		FLOOR 1		FLOOR 2		FLOOR 3		Building	
WINTER	PERIOD			T_{out} [°C]	T_{in} [°C]	T_{in}-T_{out} [K]	T_{in} [°C]	T_{in}-T_{out} [K]	T_{in} [°C]	T_{in}-T_{out} [K]	T_{in} [°C]	T_{in}-T_{out} [K]	T_{in} [°C]	T_{in}-T_{out} [K]
2014-2015	Period 1	2017-11-6 18:00 →	2017-11-10 9:00	9.5	23.3	13.7	24.2	14.7	23.7	14.1	21.3	11.8	23.1	13.6
	Period 2	2017-11-26 21:00 →	2017-12-2 12:00	6.2	23.2	17	24.1	17.9	24.5	18.3	23.5	17.3	23.8	17.6
	Period 3	2017-12-20 9:00 →	2017-12-23 9:00	9.0	23.9	14.9	24.6	15.6	24.9	15.9	24.1	15.1	24.4	15.4
	Period 4	2018-1-17 4:00 →	2018-1-20 6:00	9.2	23.6	14.4	24.5	15.3	24.7	15.5	23.9	14.7	24.2	15
	Period 5	2018-2-6 17:00 →	2018-2-10 7:00	3.8	23.3	19.5	23.6	19.8	24.3	20.5	22.8	19	23.5	19.7

Table D.2. Average temperatures of each analysed period for winter 2017-2018 after retrofitting.

Winter	Before Retrofitting		Q [kW]	K [kW]	Q+K [kW]	SaVsol ~ SaHsol [kW]	Tin-Tout [K]	HLC [kW/K]
2014 - 2015	Period 1 2014-12-02 16:00 - 2014-12-05 20:00	Floor 0	8.1	3.0	11.1	1.2	13.6	0.9
		Floor 1	13.4	7.9	21.4	2.7	15.7	1.5
		Floor 2	11.2	4.3	15.5	1.7	15.9	1.1
		Floor 3	13.4	5.3	18.6	1.9	16.0	1.3
		HLC_{sum}	46.1	20.5	66.6	7.5	15.3	4.8
		$HLC_{building}$	46.1	20.5	66.6	7.5	15.3	4.8
	Period 2 2015-01-20 10:00 - 2015-01-23 8:00	Floor 0	11.6	3.1	14.6	1.4	15.4	1.0
		Floor 1	16.7	8.4	25.1	3.2	17.2	1.6
		Floor 2	14.0	4.4	18.4	2.0	17.4	1.3
		Floor 3	16.6	5.4	22.2	2.2	17.2	1.4
		HLC_{sum}	58.9	21.3	80.3	8.8	16.8	5.3
		$HLC_{building}$	58.9	21.3	80.3	8.8	16.9	5.3
	Period 3 2015-01-26 19:00 - 2015-01-30 20:00	Floor 0	9.3	3.1	12.4	0.9	11.6	1.1
		Floor 1	11.9	8.5	20.4	2.0	13.2	1.7
		Floor 2	10.0	4.3	14.2	1.3	13.6	1.2
		Floor 3	12.4	5.3	17.9	1.4	13.8	1.4
		HLC_{sum}	43.6	21.2	64.9	5.6	13.0	5.4
		$HLC_{building}$	43.6	21.2	64.9	5.6	13.0	5.4
	Period 4 2015-02-03 6:00 - 2015-02-07 1:00	Floor 0	14.1	3.1	17.2	1.1	17.8	1.0
		Floor 1	18.8	8.5	27.4	2.5	19.5	1.5
		Floor 2	15.0	4.4	19.3	1.6	19.7	1.1
		Floor 3	18.0	5.5	23.5	1.7	19.8	1.3
		HLC_{sum}	65.9	21.5	87.4	6.9	19.2	4.9
		$HLC_{building}$	65.9	21.5	87.4	6.9	19.2	4.9
2015 - 2016	Period 1 2015-11-24 19:00 - 2015-11-27 22:00	Floor 0	5.8	2.4	8.3	0.5	8.5	1.1
		Floor 1	11.2	7.6	18.7	1.1	11.7	1.7
		Floor 2	9.2	4.0	13.2	0.7	11.8	1.2
		Floor 3	10.4	4.9	15.3	0.6	11.5	1.4
		HLC_{sum}	36.6	18.9	55.5	2.9	10.9	5.4
		$HLC_{building}$	36.6	18.9	55.5	2.9	10.9	5.5
	Period 2 2016-01-06 20:00 - 2016-01-09 8:00	Floor 0	4.3	2.4	6.7	0.5	6.8	1.1
		Floor 1	5.7	5.8	11.6	1.3	8.0	1.6
		Floor 2	4.8	3.1	7.9	0.8	7.9	1.1
		Floor 3	5.7	4.3	10.0	0.9	8.0	1.4
		HLC_{sum}	20.5	15.6	36.2	3.5	7.7	5.2
		$HLC_{building}$	20.5	15.6	36.2	3.5	7.6	5.2
2016 - 2017	Period 1 2016-12-19 12:00:00 - 2016-12-22 6:00:00	Floor 0						
		Floor 1	11.7	7.2	18.9	1.7	14.1	1.5
		Floor 2	9.9	4.1	14.0	1.1	14.3	1.1
		Floor 3	12.0	5.0	17.0	1.3	14.2	1.3
		HLC_{sum}	33.6	16.3	49.9	4.1	14.2	3.9
		$HLC_{building}$	33.6	16.3	49.9	4.1	14.2	3.9
	Period 2 17-01-09 18:00:00 - 17-01-12 7:00:00	Floor 0						
		Floor 1	5.6	6.4	11.9	0.8	11.2	1.1
		Floor 2	6.9	3.7	10.6	0.5	11.7	1.0
		Floor 3	7.6	4.5	12.2	0.5	11.2	1.1
		HLC_{sum}	20.1	14.6	34.7	1.8	11.4	3.2
		$HLC_{building}$	20.1	14.6	34.7	1.8	11.4	3.2

Table D.3. Main variables period averaged values for winters 2014-2015, 2015-2016 and 2016-2017 before retrofitting.

Winter	After Retrofitting		Q [kW]	K [kW]	Q+K [kW]	SaVsol ~ SaHsol [kW]	Tin-Tout [K]	HLC [kW/K]
2017 - 2018	Period 1 2017-11-06 18:00- 2017-11-10 9:00	Floor 0	6.2	2.0	8.2	2.3	13.7	0.8
		Floor 1	7.6	6.1	13.8	5.2	14.7	1.3
		Floor 2	5.5	3.6	9.0	3.3	14.1	0.9
		Floor 3	3.1	4.6	7.7	3.6	11.8	0.9
		HLC_{sum}	22.4	16.3	38.7	14.4	13.6	3.9
		$HLC_{building}$	22.4	16.3	38.7	14.4	13.6	3.9
	Period 2 2017-11-26 21:00- 2017-12-02 12:00	Floor 0	8.1	2.0	10.3	1.8	17.0	0.7
		Floor 1	12.8	6.2	18.9	4.0	17.9	1.3
		Floor 2	7.8	3.8	11.5	2.5	18.3	0.8
		Floor 3	7.2	4.9	12.1	2.8	17.4	0.8
		HLC_{sum}	35.9	16.9	52.8	11.1	17.7	3.6
		$HLC_{building}$	35.9	16.9	52.8	11.1	17.7	3.6
	Period 3 2017-12-20- 9:00 - 2017-12-23- 9:00	Floor 0	6.9	2.3	9.3	1.8	14.9	0.8
		Floor 1	10.9	5.7	16.6	4.1	15.6	1.3
		Floor 2	6.5	3.6	10.1	2.6	15.9	0.8
		Floor 3	6.6	5.2	11.7	2.9	15.0	0.9
		HLC_{sum}	30.9	16.8	47.7	11.4	15.4	3.8
		$HLC_{building}$	30.9	16.8	47.7	11.4	15.4	3.9
	Period 4 2018-1-17- 4:00 - 2018-1-20- 6:00	Floor 0	7.0	2.2	9.2	1.8	14.4	0.8
		Floor 1	10.7	5.6	16.3	4.1	15.3	1.3
		Floor 2	7.4	3.3	10.7	2.6	15.5	0.9
		Floor 3	8.0	4.8	12.8	2.9	14.7	1.0
		HLC_{sum}	33.1	15.9	49	11.4	15.0	4.0
		$HLC_{building}$	33.1	15.9	49	11.4	15.0	4.0
	Period 5 2018-2-6- 17:00- 2018-2-10- 7:00	Floor 0	6.9	2.3	9.3	1.8	14.9	0.8
		Floor 1	10.9	5.7	16.6	4.1	15.6	1.3
		Floor 2	6.5	3.6	10.0	2.6	15.9	0.8
		Floor 3	6.6	5.2	11.8	2.9	15.1	0.9
		HLC_{sum}	30.9	16.8	47.7	11.4	15.4	3.8
		$HLC_{building}$	30.9	16.8	47.7	11.4	15.4	3.9

Table D.4. Main variables period averaged values for winter 2017-2018 after retrofitting.

As can be seen, the period averaged solar gain values are quite low in comparison with the rest of the heat gains inside the building (Q+K). During the last winter, the solar gains weight increased in comparison with the rest of the heat gain inside the building. The method was also able, however, to provide suitable results. Moreover, it can also be seen that, when checking the temperature difference between the interior and the exterior, the obtained value is usually around 15 °C.

V. APPENDIX E

As explained in section 2.2.3.1, several models have been tested. These models have been used to analyse two periods (one in summer and one in winter) in order to estimate which is able to best fit the inner surface heat flux measured signal and represent the reality the outermost surface of the Round Robin Box is suffering. Therefore, the software LORD was used to fit the models. Thus, all the models from M1 to M8 have been tested for the period in summer and the period in winter and some of the results are shown below. Since there are plenty of models, first, the most representative ones are shown and explained in this section. Among them, the ceiling models, which are the most affected by all the analysed phenomena due to its exposition to them, and the north wall models, which is one of the least exposed walls to the solar radiation, are presented. Moreover, the corresponding input inner surface temperature, outer surface temperature, outdoor air temperature, sky or surrounding temperature and the global solar radiation signals are plotted for each of the most representative walls in the selected periods.

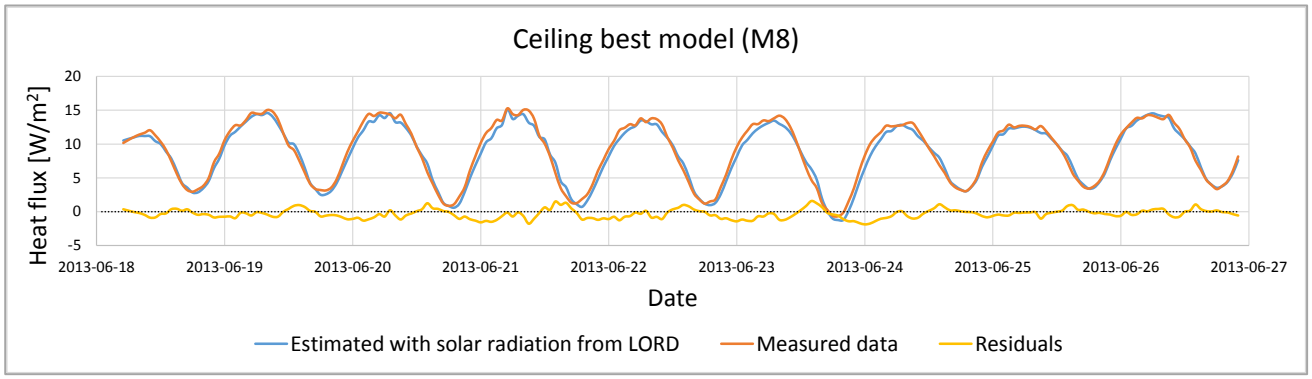

Figure E.1. The best ceiling model fit for the inner surface heat flux considering the solar radiation in period 1 (summer). The fit residuals are also present.

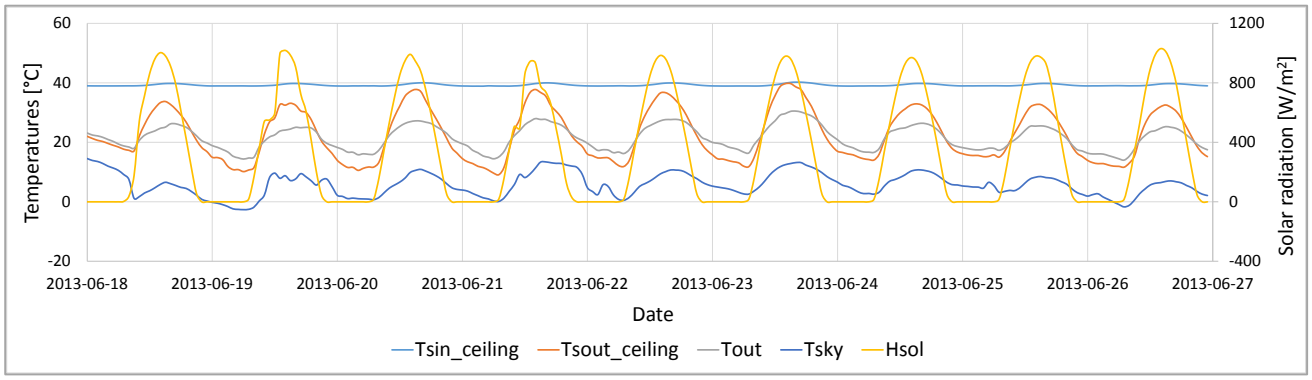

Figure E.2. The best ceiling model's inner surface temperature, outer surface temperature, outdoor air temperature, sky temperature and horizontal global solar radiation signals in period 1 (summer).

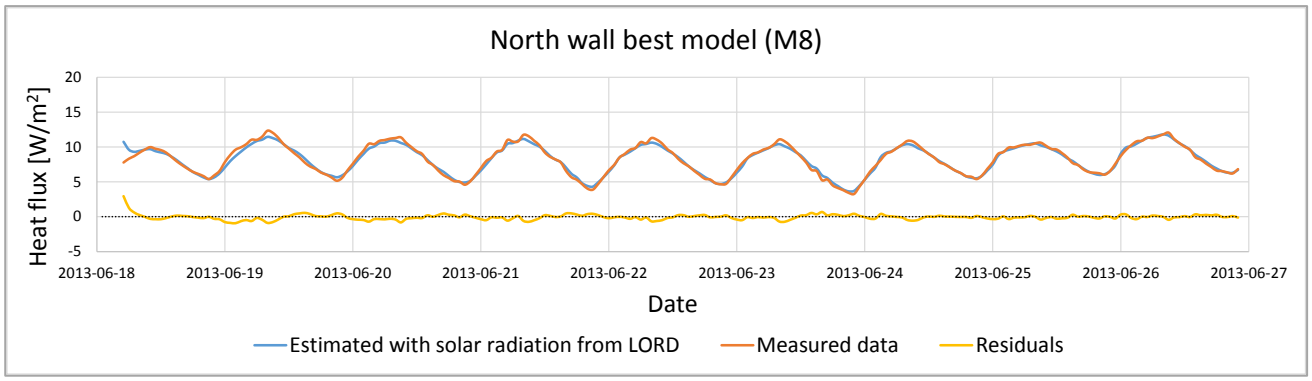

Figure E.3. The best north wall model fit for the inner surface heat flux considering the solar radiation in period 1 (summer). The fit residuals are also present.

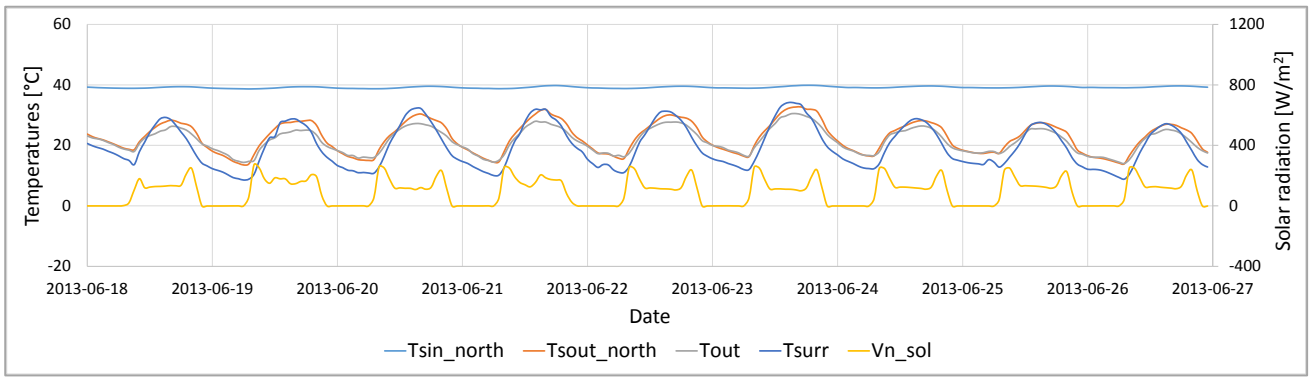

Figure E.4. The best north model's inner surface temperature, outer surface temperature, outdoor air temperature, surrounding temperature and vertical north global solar radiation signals in period 1 (summer).

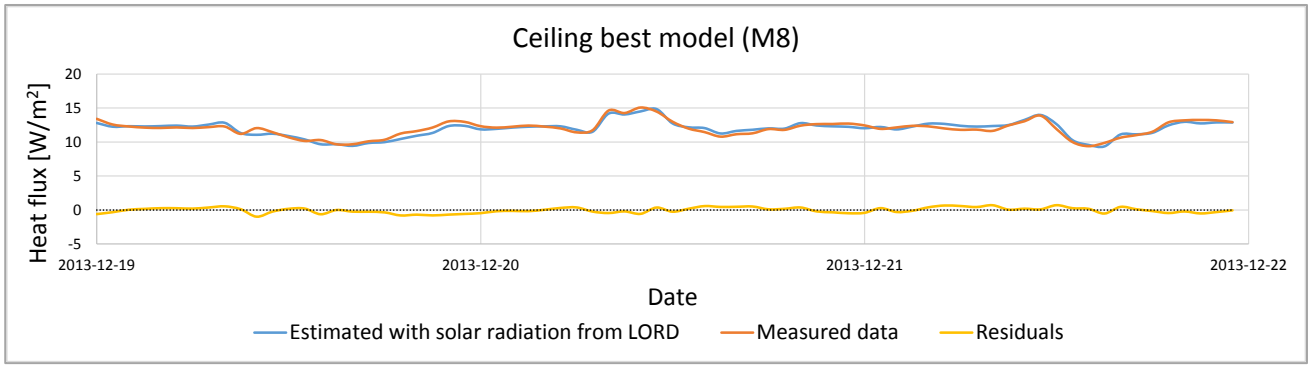

Figure E.5. The best ceiling model fit for the inner surface heat flux considering the solar radiation in period 2 (winter). The fit residuals are also present.

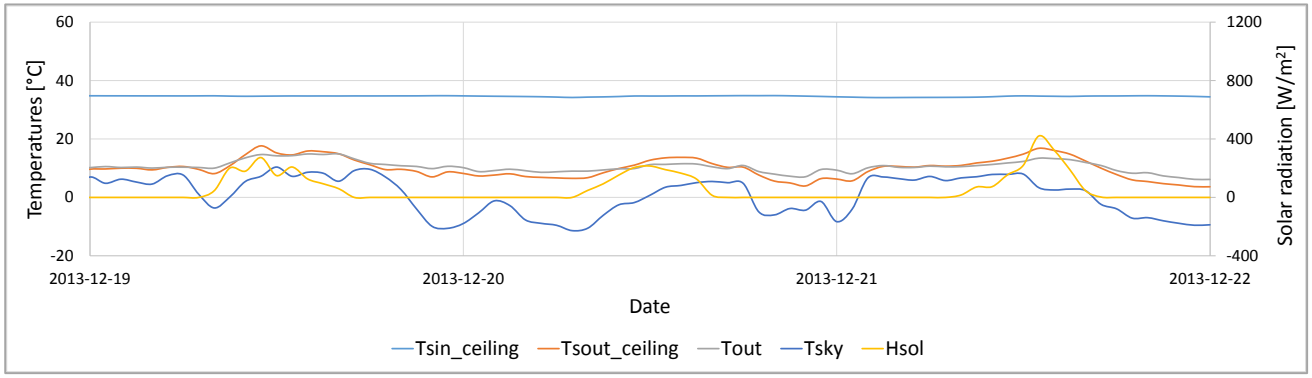

Figure E.6. The best ceiling model's inner surface temperature, outer surface temperature, outdoor air temperature, sky temperature and horizontal global solar radiation signals in period 2 (winter).

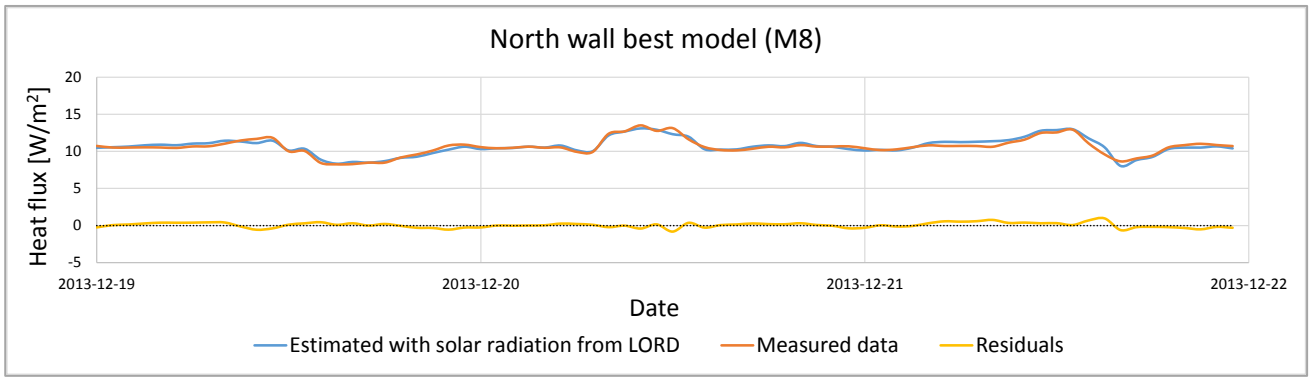

Figure E.7. The best north wall model fit for the inner surface heat flux considering the solar radiation in period 2 (winter). The fit residuals are also present.

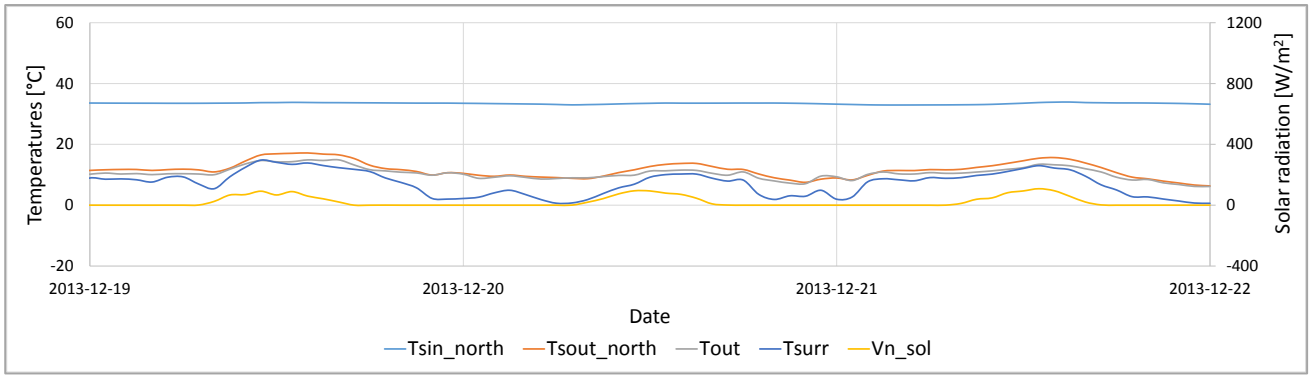

Figure E.8. The best north model's inner surface temperature, outer surface temperature, outdoor air temperature, surrounding temperature and vertical north global solar radiation signals in period 2 (winter).

The model selection has been carried out by the estimation of the RMSE of the residuals. Then, the fits with the lowest RMSE value and logical physical validation results (the thermal resistance and the solar absorptivity) have been selected as the best models. In this case, Figure E.1 shows the best fit for the ceiling case for the period in summer where the estimated RMSE value was 0.76 W/m^2. Figure E.3 shows the best fit obtained for the north wall case in summer with an RMSE value of 0.39 W/m^2. The same procedure is also followed to estimate the best models for the winter period. In this case, the corresponding best fits are Figure E.5 for the ceiling case and Figure E.7 for the north wall case. The obtained RMSE values are 0.41 W/m^2 for the ceiling and 0.34 W/m^2 for the north wall. The rest of the RMSE values for the rest of the walls and models are shown in Table 10.

Moreover, Figure E.2, Figure E.4, Figure E.6 and Figure E.8 show the corresponding input inner surface temperature, outer surface temperature, outdoor air temperature, sky or surrounding temperature and the global solar radiation signals for each of the extreme behaving walls in the selected periods. As previously shown in section 3.1.3, there can be seen that the period average outdoor air temperature and the period average surrounding temperature are quite close for the period in Figure E.4 (21.5 °C vs. 19.6 °C) and Figure E.8 (10.2 °C vs. 7 °C). However, this is not happening when the sky temperature and the ground temperature are compared. If the sky temperature is checked in Figure E.2 and Figure E.6, there can be seen that the period average outdoor air temperature and the period average sky temperature are quite far for the period in Figure E.2 (21.5 °C vs. 5.8 °C) and Figure E.6 (10.2 °C vs. -1 °C). Then, even though the effect of the long wave radiation can be not so notorious during the day due to the high solar radiation effect on

the outermost horizontal surface of the Round Robin Box, its effect can be considerable during the night period. Therefore, when implementing the models, it is important to consider these heat exchanges due to the long wave radiation, mainly on the outer horizontal surface of the wall, together with the outdoor air temperature effect, in order to obtain the most accurate fits.

The fits of the rest of the models for summer and winter are also shown in the following figures. The obtained corresponding residuals have also been calculated using the RMSE and can be seen in Table 10.

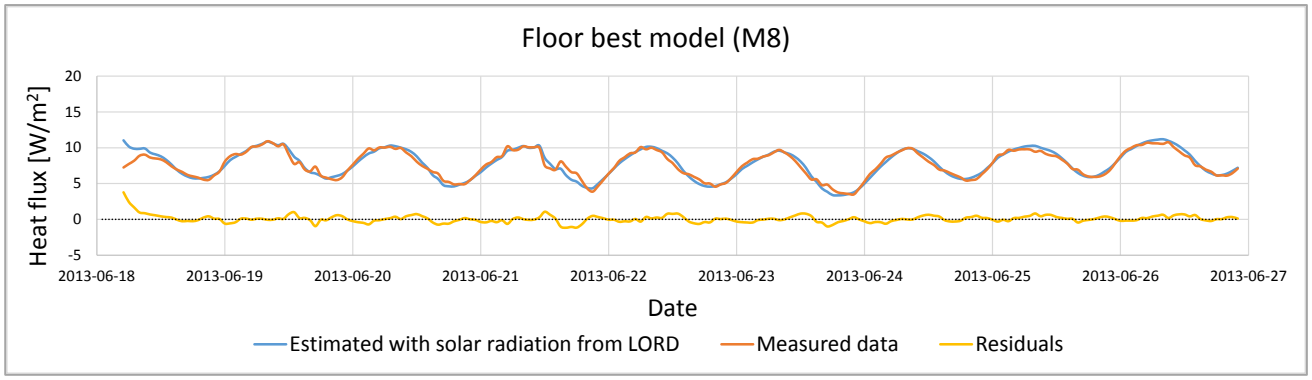

Figure E.9. The best floor model fit for the inner surface heat flux considering the solar radiation in period 1 (summer). The fit residuals are also present.

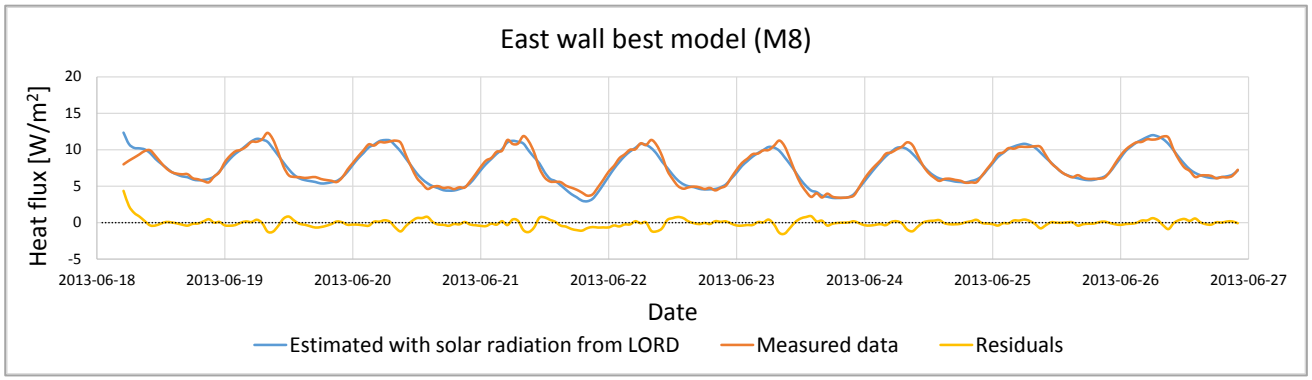

Figure E.10. The best east wall model fit for the inner surface heat flux considering the solar radiation in period 1 (summer). The fit residuals are also present.

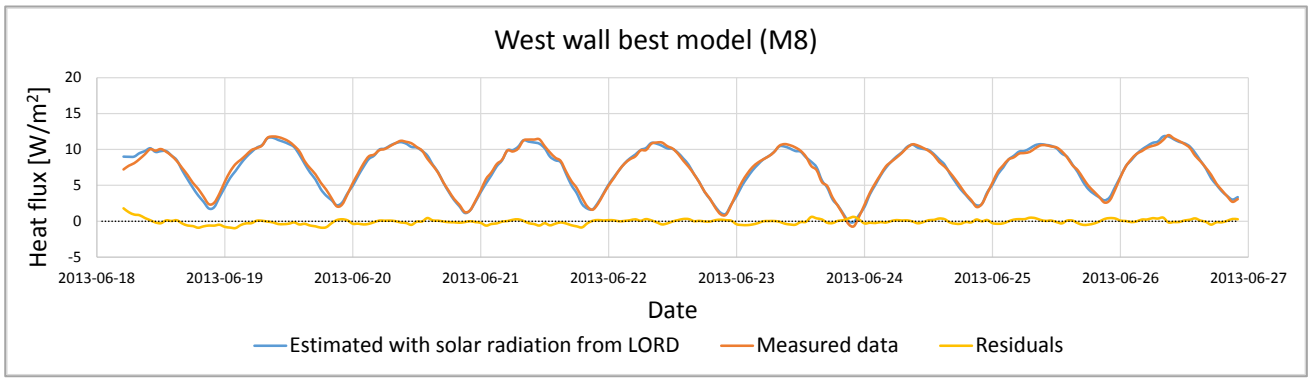

Figure E.11. The best west wall model fit for the inner surface heat flux considering the solar radiation in period 1 (summer). The fit residuals are also present.

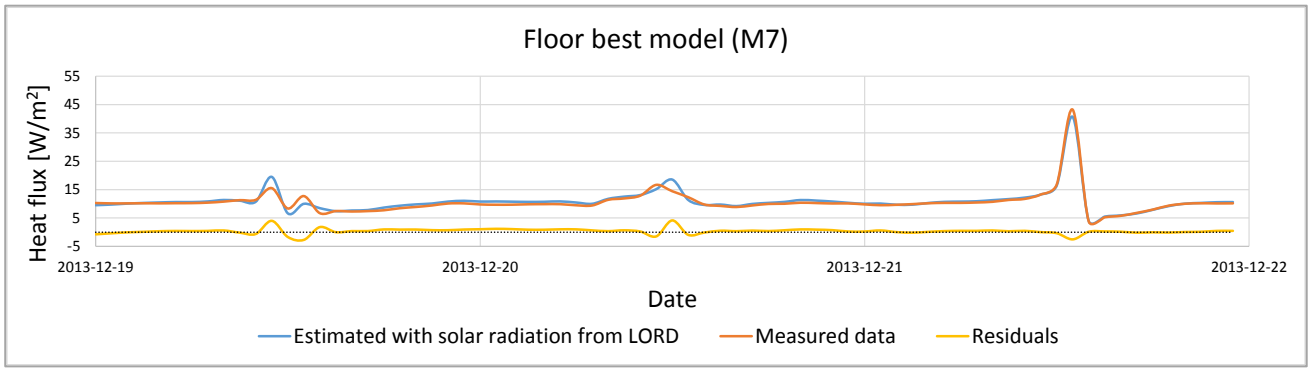

Figure E.12. The best floor model fit for the inner surface heat flux considering the solar radiation in period 2 (winter). The fit residuals are also present.

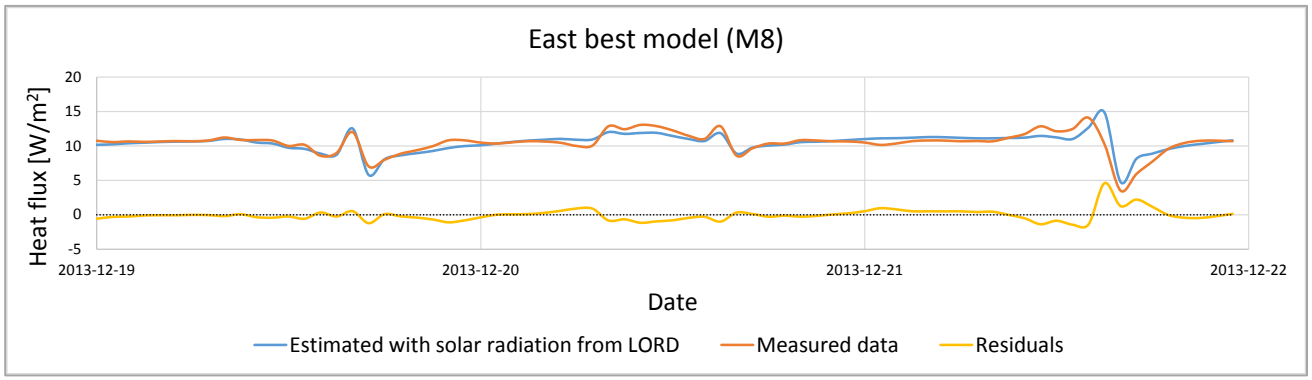

Figure E.13. The best east wall model fit for the inner surface heat flux considering the solar radiation in period 2 (winter). The fit residuals are also present.

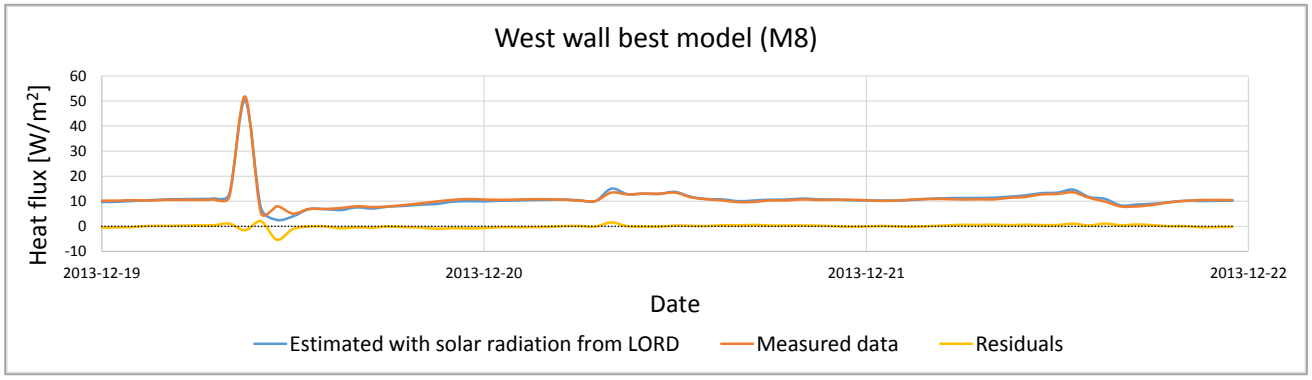

Figure E.14. The best west wall model fit for the inner surface heat flux considering the solar radiation in period 2 (winter). The fit residuals are also present.

VI. APPENDIX F

As explained in section 2.2.4, once the best fits have been selected and the models validated, it is possible to analyse the effect the solar radiation has in the inner surface heat flux. Therefore, the best fits are selected and, once every parameter is fixed, the solar radiation is removed from the model. Then, the software is able to obtain the hypothetical inner surface heat flux the model would have if there was no solar radiation. All the numerical results have already been summarised in section 4.1.2.3. However, in order to show them graphically, the same representative models selected in Appendix E are also plotted here in order to show the difference between the inner surface heat flux estimated by the software considering the solar radiation effect and the inner surface heat flux estimated by the software without considering the solar radiation effect.

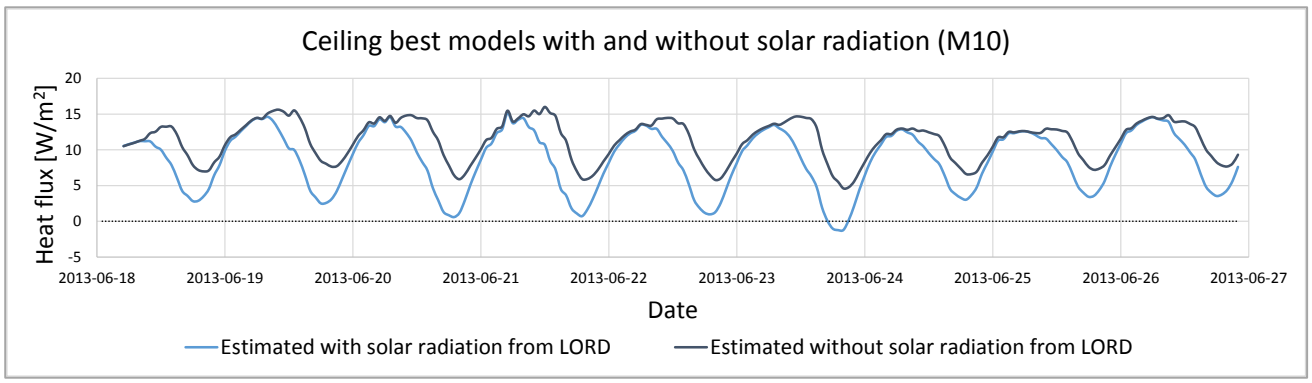

Figure F.1. Inner surface heat flux simulation with the best model fit with and without solar radiation for the ceiling in the summer period.

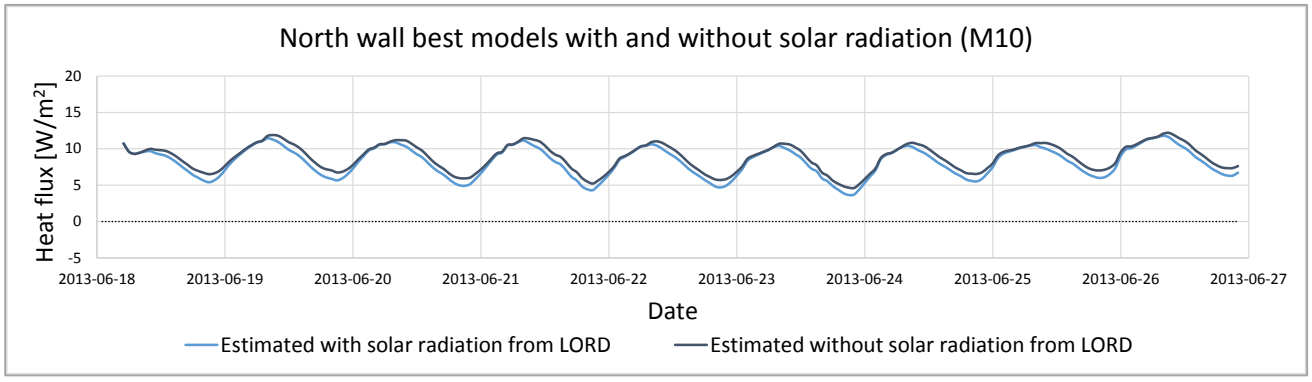

Figure F.2. Inner surface heat flux simulation with the best model fit with and without solar radiation for the north wall in the summer period.

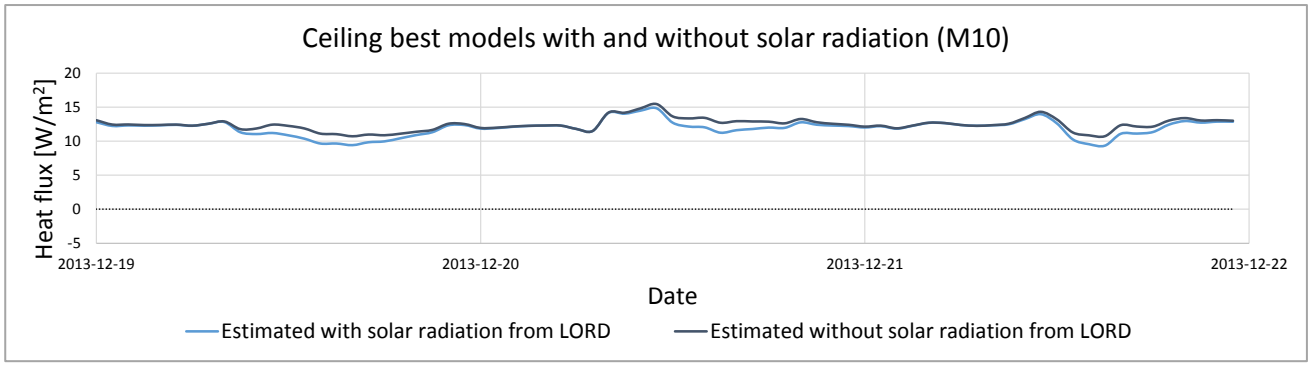

Figure F.3. Inner surface heat flux simulation with the best model fit with and without solar radiation for the ceiling in the winter period.

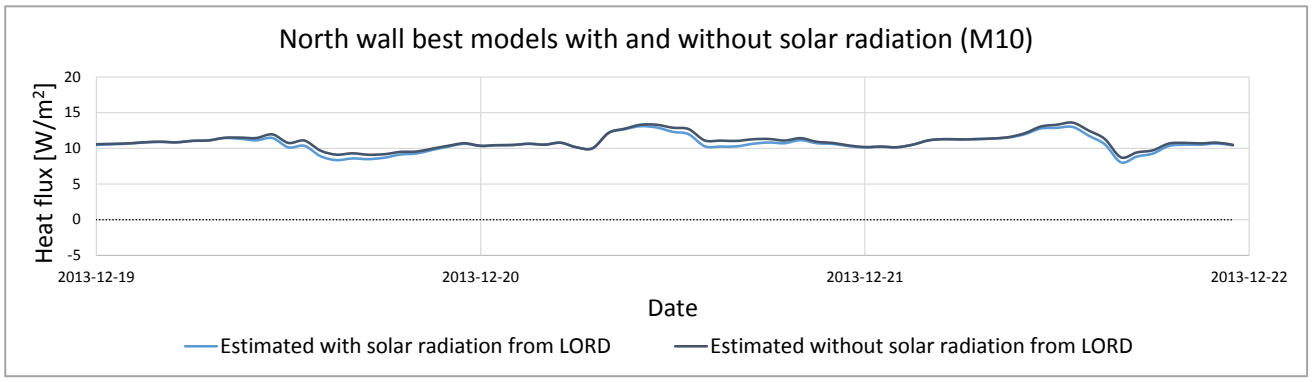

Figure F.4. Inner surface heat flux simulation with the best model fit with and without solar radiation for the north wall in the winter period.

As concluded in section 4.1.2.3, it is now possible to see graphically how notorious the effect of the solar radiation is in the ceiling case during summer in Figure F.1. However, the effect decreases considerably for the north wall in summer in Figure F.2. Despite the effect of the ceiling case in winter in Figure F.3 being slightly higher than the effect of the north wall in the Figure F.4, it is by far much lower than the difference between the ceiling case in summer and winter. Thus, this visual check helps to corroborate the results obtained in section 4.1.2.3 and to justify the discussion explained there. Moreover, the rest of the wall graphs are shown below:

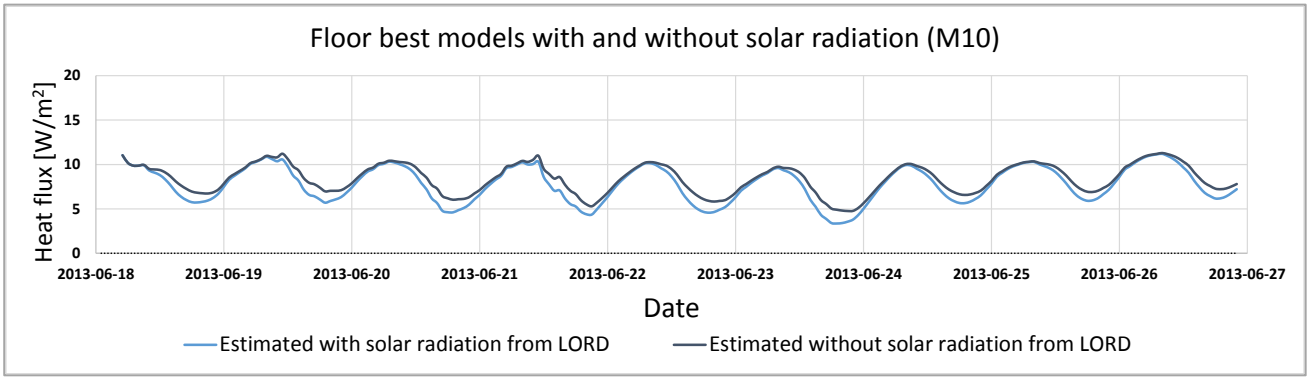

Figure F.5. Inner surface heat flux simulation with the best model fit with and without solar radiation for the floor in summer period.

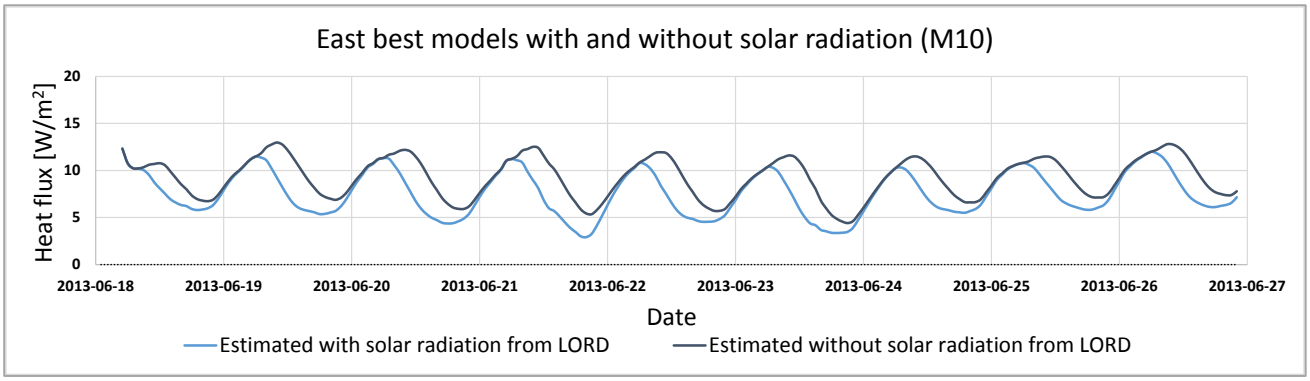

Figure F.6. Inner surface heat flux simulation with the best model fit with and without solar radiation for the east wall in summer period.

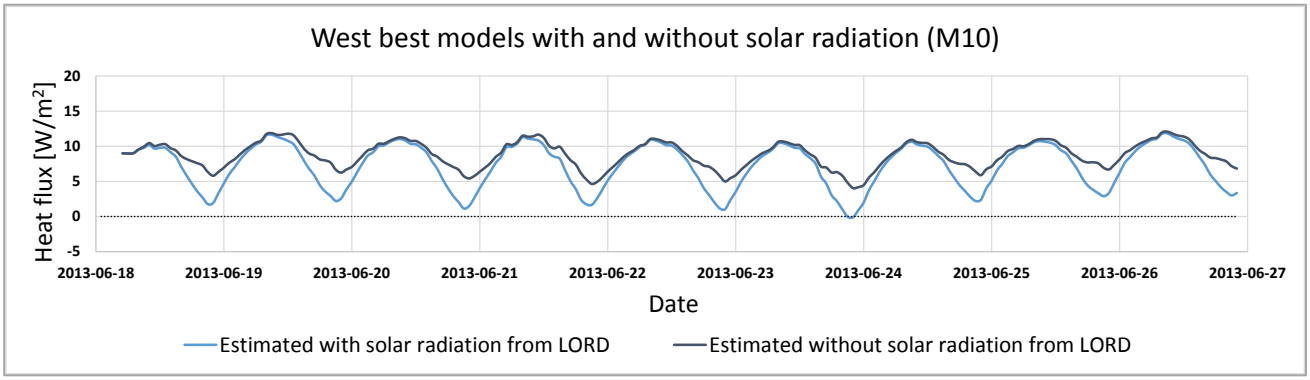

Figure F.7. Inner surface heat flux simulation with the best model fit with and without solar radiation for the west wall in summer period.

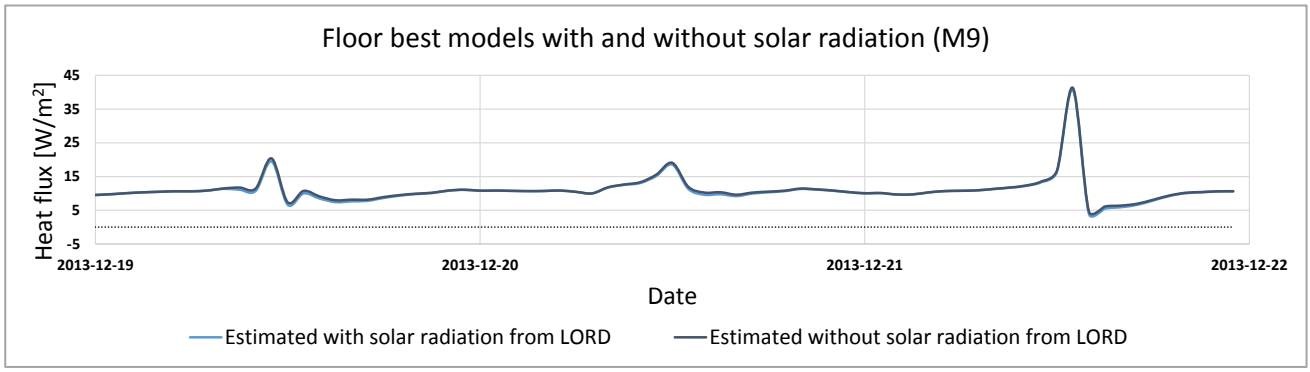

Figure F.8. Inner surface heat flux simulation with the best model fit with and without solar radiation for the floor in winter period.

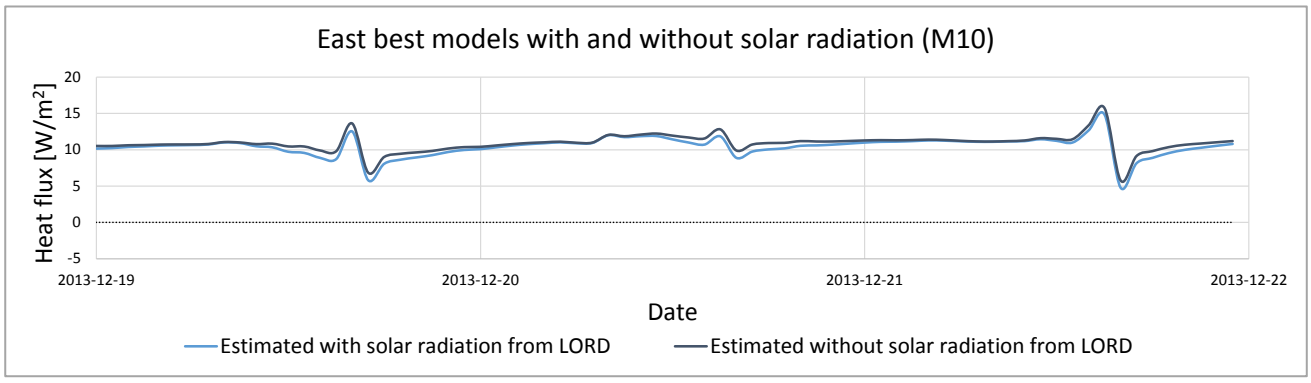

Figure F.9. Inner surface heat flux simulation with the best model fit with and without solar radiation for the east wall in winter period.

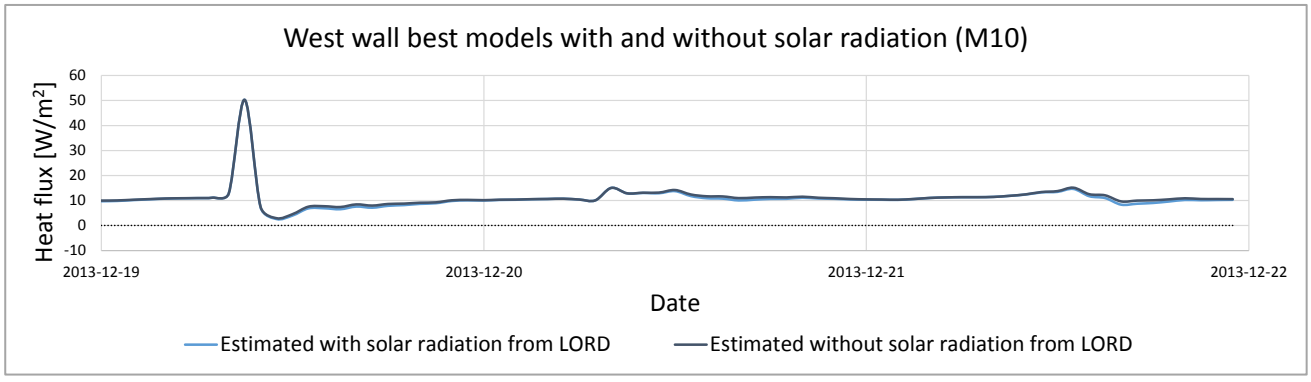

Figure F.10. Inner surface heat flux simulation with the best model fit with and without solar radiation for the west wall in winter period.

Doctoral Thesis

enedi

eman ta zabal zazu

Universidad del País Vasco

Euskal Herriko Unibertsitatea

FACULTY OF ENGINEERING BILBAO

UNIVERSITY OF THE BASQUE COUNTRY